THE EFFECT OF COAL COMPOSITION, MOISTURE CONTENT, AND PORE VOLUME DISTRIBUTION UPON SINGLE AND BINARY GAS EQUILIBRIUM AND NONEQUILIBRIUM ADSORPTION: IMPLICATIONS FOR GAS CONTENT DETERMINATION

By

CHRISTOPHER RAYMOND CLARKSON

B.A.Sc, The University of British Columbia, 1992
M.A.Sc. The University of British Columbia, 1994

A THESIS SUBMITTED IN PARTIAL FULFILLMENT OF

THE REQUIREMENTS FOR THE DEGREE OF

DOCTOR OF PHILOSOPHY

in

THE FACULTY OF GRADUATE STUDIES
Department of Earth and Ocean Sciences

We accept this thesis as conforming
to the required standard

THE UNIVERSITY OF BRITISH COLUMBIA

MAY, 1998

In presenting this thesis in partial fulfilment of the requirements for an advanced degree at the University of British Columbia, I agree that the Library shall make it freely available for reference and study. I further agree that permission for extensive copying of this thesis for scholarly purposes may be granted by the head of my department or by his or her representatives. It is understood that copying or publication of this thesis for financial gain shall not be allowed without my written permission.

Department of Earth and Ocean Sciences

The University of British Columbia
Vancouver, Canada

Date 09/30/98

ABSTRACT

An experimental and modeling study was undertaken to determine the effect of coal composition, moisture content, and pore structure, upon natural gas adsorption and matrix transport. A volumetric high-pressure (up to 17 MPa) adsorption apparatus was constructed for the collection of single and multicomponent adsorption equilibrium and non-equilibrium adsorption data. A variety of equilibrium and non-equilibrium adsorption models were applied to determine which provided the best fits to the data. Coals selected for study included medium volatile bituminous coals of the Gates Formation, Northeastern B.C. Canada, and a suite of coals from the Sydney and Bowen Basins of Australia.

Coal composition affects pore volume distribution, which in turn dictates the equilibrium and non-equilibrium adsorption characteristics of coals. Bright and banded bright coals have a greater amount of microporosity than dull coals, and hence have larger methane and carbon dioxide adsorption capacities. Dull coals have less microporosity but a greater amount of mesoporosity. Pore volume distributions in turn affect the adsorption rate behaviour of coals; bright coals have a uniform microporous structure and are adequately modeled using unipore diffusion models whereas dull and banded coals require models that account for a multimodal pore volume distribution.

Coal composition also affects binary gas total adsorption isotherms, but has little effect upon carbon dioxide gas selectivity over methane. Coal moisture content appears to have a greater effect upon selective adsorption, but this requires further investigation.

New numerical models, which account for bimodal pore volume distributions and non-linear adsorption characteristics, provide an adequate fit to adsorption rate data of the

Gates coals. A bidisperse analytical model also provides excellent fits to the data, but does not account for non-linear adsorption. Models that do not account for non-linear adsorption yield optimized methane diffusivities that increase with pressure. The numerical model diffusivities decrease with an increase in pressure, possibly reflecting a bulk gaseous diffusion mechanism. Carbon dioxide diffusivities obtained from all models are larger than methane diffusivities. Methane diffusivities obtained using moisture-equilibrated coal data are smaller than those determined for dry coal.

The Dubinin-Astakhov and Dubinin-Radushkevich isotherm equations provide better fits than the Langmuir equation to equilibrium methane and carbon dioxide adsorption data. The Dubinin models, which are based upon pore volume filling/adsorption potential theory, also have general validity in their application to supercritical methane-coal systems. Binary gas equilibrium predictions vary depending on whether the IAS or extended Langmuir model is used. The IAS theory, used in conjunction with the Dubinin-Astakhov equation, provides the best fit to CH_4/CO_2 adsorption data collected during this study.

TABLE OF CONTENTS

LIST OF FIGURES

LIST OF TABLES

ACKNOWLEDGEMENTS

This thesis could not have been successfully completed without the help and support of a number of people. Firstly, I gratefully acknowledge Dr. R. Marc Bustin for his assistance and advice during this project. He has been a great inspiration to me, and has provided me with the best possible work environment. Thanks also to my supervisory committee whose expertise and support have been instrumental. I would particularly like to thank Dr. R. Beckie from whom I have learned a great deal. The technical staff at the Department of Earth and Ocean Sciences/Geology have aided me greatly in the construction of experimental equipment for my research. John Levy of CSIRO (Australia) helped me early on in my thesis project with adsorption isotherm equipment and experimental procedures. Assistance in the laboratory was provided by: J. Houston, M. St. Pierre, Y. Bayani, and R. Deol. Thank you all for your help!

This research was supported by graduate fellowships from the University of British Columbia and the Natural Sciences and Engineering Research Council of Canada. NSERC research grants provided to R. Marc Bustin also provided financial assistance.

Finally, thanks to my family and friends who had faith in me. You were there when I needed you! Special thanks to my girlfriend, Andrea Tan, whose patience is greatly appreciated.

CHAPTER 1

INTRODUCTION

1.1 INTRODUCTORY STATEMENTS

Natural gas in coal seams, or "coalbed methane", has become a viable alternative fuel source, particularly in the United States. Production of coalbed methane in the U.S. went from nearly zero in 1982[1] to approximately 24 Bm^3 (851 Bcf) in 1994[2] and currently represents about 6 percent of the U.S. natural gas reserves[3]. Coalbed methane exploration and development is in its infancy in Canada; an estimated 19 Tm^3 (672 Tcf) of total reserves potential exists in the Alberta plains of the Western Canadian Sedimentary Basin[4]. Interest in coalbed methane development is also increasing in Australia[5], Eastern Europe and Asia[6].

In addition to being a source of fuel, coal seams may be an important repository for the storage of greenhouse gases. The injection of anthropogenic carbon dioxide into coal seams and subsequent recovery of stored methane in an effort to reduce greenhouse emissions has been proposed recently[7]. The study of natural gas storage and transport mechanisms in coal is important for the evaluation of gas recovery and injection operations.

Coal is unique in that it acts as both a source rock and reservoir to natural gas. The storage and transport mechanisms of coal seams differ from conventional reservoirs in several important ways. Unlike conventional reservoirs, coalbed gas is mainly stored in coal in the adsorbed state[8] (> 90%), but also exists as free gas (unadsorbed) in coal porosity, or as a solute in groundwater. The amount of gas stored depends upon a variety

of coal properties and environmental conditions including: coal rank, ash (inorganic) content, coal organic composition, gas composition, coal seam temperature and pressure[9,10].

Gas is transported through coal seams via the dual mechanisms of laminar flow through the natural fracture system (cleat) and diffusion through the coal matrix bounded by cleat[11-12]. The flow through cleat is pressure-driven and may be modeled using Darcy's Law, whereas flow through the matrix is assumed to be concentration-driven and is modeled using Fick's Law. Gas production from coal is assumed to follow a three-stage process[13] : 1) flow through the natural fracture (cleat) system to the well bore; 2) desorption from the surfaces of the cleat; and 3) diffusion of gas through the coal matrix pore structure to the cleat system. Gas transport through the coal seam fracture system, which is dependent upon permeability, is considered to be a greater control upon gas production than matrix diffusion transport[14]. Matrix diffusion, however, is an important control upon gas content estimates and may be an important control upon the ultimate gas recovery in low permeability reservoirs or coal mine gob zones.

The primary methods for determining coal gas contents and matrix transport parameters are the determination of adsorption isotherms, and desorption canister testing. The adsorption isotherm expresses the equilibrium relationship between adsorbed and free gas phases and has utility in determination of maximum gas storage capacity of coal; the estimation of the actual gas-in-place if the coal is fully gas-saturated; and the estimation of gas recovery as a function of pressure[10]. Comparison of gas contents estimates obtained from desorption canisters, and from the adsorption isotherm, gives an indication of the degree of gas saturation in a coal[10]. In-situ coal gas contents are often

estimated through measurement of the amount of gas released from core or drill cuttings, which are retrieved from the coal reservoir[6]. The recovered coal sample is placed into a canister, and gas is released as the canister pressure drops from reservoir pressure to atmospheric pressure. One of the problems associated with gas content determination is that some gas is lost during the retrieval of sample prior to placement in a canister. The amount of gas lost, which is controlled by the matrix transport properties of the coal, is determined from the extrapolation of the measured desorbed gas volumes versus time to the time at which desorption began. Lost gas calculations often assume a simplified model for gas diffusion[6] through the coal matrix and do not properly account for coal properties such as matrix pore structure and adsorption.

The accurate determination of gas-in-place is of critical importance for the proper economic assessment of coal gas reserves and for production forecasting. The factors that affect gas-in-place are still under investigation. Little is known about the effect of coal physical properties, such as composition and pore volume distribution, upon gas content and transport, although some studies have been conducted. For example, organic composition and organic content have been determined to be an important control upon pure gas adsorption[9,10] and therefore the gas adsorption capacity of a coal may vary greatly within a particular coal seam or between a succession of seams. Natural gas in coal seams, however, is usually a mixture of methane and other contaminants, and little is currently known about the effect of coal composition upon component adsorption in gas mixtures. Coal composition is also known to be an important control upon matrix porosity and pore volume distribution[15]. Knowledge of the effect of coal composition, and hence pore structure, upon matrix gas transport is potentially important for the

accurate determination of gas contents of heterogeneous reservoirs, and for gas production forecasting.

1.2 STATEMENT OF PROBLEM

Proper characterization of coal gas reservoirs must account for variations in physical properties, which affect the storage and transport of gas. Coal compositional heterogeneity, which imparts heterogeneity in other coal properties, is expressed at all scales, from the molecular to the seam scale[9]. An understanding of how heterogeneity in coal affects gas storage and transport is important for the proper economic evaluation of a coalbed methane resource. Further, refinement of mathematical models used for gas content determination are required for accurate economic assessment. The following questions are addressed in this thesis:

1) What is the effect of coal physical properties, such as coal composition and moisture content, upon multicomponent adsorption?
2) What is the effect of coal pore structure and gas adsorption upon matrix gas transport?
3) Are the current popular equilibrium and non-equilibrium adsorption models accurate for coals of varying composition and moisture contents?

A systematic investigation of the effect of coal composition, moisture content and pore structure upon gas adsorption and matrix transport was therefore undertaken to address these questions.

The current study is concerned with both equilibrium and non-equilbrium adsorption in coal. A volumetric adsorption apparatus was built for the collection of single and multicomponent adsorption equilibrium and non-equilibrium adsorption data.

This study extends previous studies, which have evaluated the effect of coal moisture content[16-17, 5], and composition[9] upon pure gas, usually methane, equilibrium adsorption. Because coal gas is usually composed of gas mixtures, the effect of coal properties such as moisture content and composition upon the selective adsorption of different gas components is investigated. Various models for equilibrium single and multicomponent adsorption were also evaluated against experimental data. The results of this study have important implications for gas content determination and reservoir characterization, which in turn affect economic forecasting.

The effect of coal pore structure, moisture and adsorption upon non-equilibrium gas adsorption is also investigated. New numerical models, which properly account for coal pore structure and adsorption characteristics, are described and applied to methane and carbon dioxide adsorption rate data. This study has important implications for understanding gas transport and for the determination of lost gas calculations for gas content determination.

1.3 STRUCTURE OF THESIS

This thesis contains four research papers, divided into chapters, which address

the questions outlined above. Chapter 2 is concerned with the application of some popular single-component adsorption isotherm equations to Australian coal isotherm data. The validity of mono/multilayer and adsorption potential theories is tested, and isotherm curve-fits for the models are compared. The results of this study are also used in Chapter 5, which examines multicomponent gas adsorption.

Chapter 3 is part one of a two-part study that examines the effect of composition, pore structure, and adsorption characteristics upon the matrix transport properties of coal. The purpose of Chapter 3 is to determine the (equilibrium) adsorption/desorption properties and pore volume distributions of four coal lithotypes from the Cretaceous Gates Formation of Northeast B.C. in order to assess the effect of these properties upon adsorption rate behaviour (subject of Chapter 4).

Chapter 4 examines the effect of coal pore structure and adsorption characteristics upon methane and carbon dioxide gas adsorption rate behaviour for the four Gates Formation lithotypes. A new numerical model for matrix gas diffusion/adsorption is developed and applied to adsorption rate data. The new model accounts for coal properties such as non-linear adsorption in coal microporosity, and a bimodal pore volume distribution.

Chapter 5 investigates the effect of coal moisture content and composition upon methane/carbon dioxide mixed gas adsorption characteristics of Gates coals. Two popular multicomponent adsorption models are evaluated against experimental data.

Some repetition of subject matter occurs due to the adoption of the current dissertation format. While regrettable, the inclusion of some repetitious material is required in each paper; your patience on this matter is appreciated.

1.4 REFERENCES

1. Schraufnagel, R.A., and Schafer, P.S. In 'A Guide to Coalbed Methane Reservoir Engineering' (Eds J.L. Saulsberry, P.S. Schafer, and R.A. Schraufnagel), Gas Research Institute Report No. GRI-94/0397, Chicago, Illinois, 1996, pp. 1.1-1.10

2. Scott, A.R., Nance, H.S., and Beltran, M.Z. In Proceedings of the 1997 International Coalbed Methane Symposium, Tuscaloosa, May 12-17, 1997, pp. 213-223

3. Energy Information Administration, 1995 *as cited in* Scott, A.R., Nance, H.S., and Beltran, M.Z. In Proceedings of the 1997 International Coalbed Methane Symposium, Tuscaloosa, May 12-17, 1997, pp. 213-223

4. Sinclair, K.G., and J.R. Cranstone. In Proceedings of the 1997 International Coalbed Methane Symposium, Tuscaloosa, May 12-17, 1997, pp. 115-119

5. Levy, J.H., Day, S.J., and Killingley, J.S. *Fuel* 1997, **74**, 1

6. McLennan, J.D., Schafer, P.S., and Pratt, T.J. 'A Guide to Determining Coalbed Gas Content', Gas Research Institute Report No. GRI-94/0396, Chicago, Illinois,

7. Gunter, W.D., Gentzis, T., Rottenfusser, B.A., and Richardson, R.J.H. Paper Presented at the Third International Conference on Carbon Dioxide Removal, Massachusetts Institute of Technology, Sept. 9-11, 1996

8. Gray, I. *SPE Reservoir Engineering* (February,1987), 28

9. Lamberson, M.N., and Bustin, R.M. *AAPG Bull.* 1993, 77, 2062

10. D. Yee, J.P. Seidle, and W.B. Hanson, In 'Hydrocarbons from Coal', AAPG Studies in Geology #38 (Eds B.E. Law and D.D. Rice), 1993, pp. 203-218

11. King, G.R., Ertekin, T., and Schwerer, F.C. *SPE Formation Evaluation* 1986, 165

12. Kolesar, J.E., and Ertekin, T. In Proceedings of the Society of Petroleum Engineers Unconventional Gas Technology Symposium, Louisville, Kentucky, May 18-21, 1986, Houston, Texas, pp. 289-314

13. Zuber, M.D. In 'A Guide to Coalbed Methane Reservoir Engineering' (Eds J.L. Saulsberry, P.S. Schafer, and R.A. Schraufnagel), Gas Research Institute Report No. GRI-94/0397, Chicago, Illinois, 1996, pp. 3.1-3.33

14. Mavor, M.J. In 'A Guide to Coalbed Methane Reservoir Engineering' (Eds J.L. Saulsberry, P.S. Schafer, and R.A. Schraufnagel), Gas Research Institute Report No. GRI-94/0397, Chicago, Illinois, 1996, pp. 4.1-4.58

15. Clarkson, C.R. and Bustin, R.M. *Fuel* 1996, **75**, 1483

16. Joubert, J.I., Grein, C.T., and Bienstock, D. *Fuel* 1973, **52**, 181

17. Joubert, J.I., Grein, C.T., and Bienstock, D. *Fuel* 1974, **53**, 186

CHAPTER 2

APPLICATION OF THE MONO/MULTILAYER AND ADSORPTION POTENTIAL THEORIES TO COAL METHANE ADSORPTION ISOTHERMS AT ELEVATED TEMPERATURE AND PRESSURE

2.1 ABSTRACT

Accurate estimates of gas-in-place and prediction of gas production from coal reservoirs require reasonable estimates of gas contents. Equations based on pore volume filling/potential theory provide a better fit than the Langmuir equation to both high-pressure (up to 10 MPa), high-temperature (> 1.5 Tc) methane isotherm data and low-pressure (< .127 MPa) carbon dioxide isotherm data for 13 Australian coals. The assumption of an energetically homogeneous surface as proposed by Langmuir theory is not true for coal. Application of potential theory to the methane-coal system results in temperature-invariant methane characteristic curves, obtained with the assumption of liquid molar volume of the adsorbate and extrapolated vapour pressures. Temperature-invariant characteristic curves are obtained for carbon dioxide, although further testing is required. The application of isotherms equations based upon pore volume filling/potential theory, in particular the Dubinin-Astakhov equation, have general validity in their application to high-pressure supercritical methane-coal systems as well as providing a better fit to isotherm data.

2.2 INTRODUCTION

Recent interest in both recovery of natural gas from coal seams and in outburst hazards related to coal mining has led to extensive study of gas adsorption in coal. The accurate prediction of coal gas capacities is important in gas reserve estimates and for input to production simulators. To simulate reservoir conditions, laboratory adsorption isotherm data are generally collected at elevated temperature, usually between 0 and 50°C, and elevated pressure (up to 100 MPa). Methane gas adsorption isotherms in coal, commonly Type I[1] in nature, are most often modeled using the Langmuir isotherm[2] and less frequently the Freundlich[3] or linear[4] isotherms. A study performed by Hall *et al.* [5] compared the Langmuir model with various two-dimensional equations of state, the ideal adsorbed solution model, and loading ratio correlations for the adsorption of various gases and their mixtures on moisture-equilibrated coal. Only limited attention has been focused upon the application of adsorption potential theories to the description of methane adsorption isotherms collected for coals at elevated temperature and pressure[2]. Both the Dubinin-Radushkevich (D-R) and Dubinin-Astakhov (D-A) equations have been used to model Type I isotherms[1]. These isotherm equations are based upon the potential theory developed by Polanyi[6].

Ruppel *et al.*[2] applied the Langmuir and Polanyi adsorption models to methane adsorption isotherms collected for coals at temperatures ranging from 0 to 50°C and pressures from 10 to 150 atm (1 - 15 MPa). The Ruppel *et al.* study is the first detailing the application of adsorption-potential theory to methane adsorption on dry coal at elevated temperature and pressure, although the model had previously been applied to

other porous media under various conditions[7-10]. Ruppel *et al.*[2] found that the coal-methane adsorption system was well described by the Langmuir model, but the Polanyi theory did not accurately describe the system for all coals. It should be noted that thermal expansion of the adsorbate was not accounted for by Ruppel *et al.*, which, as shown in the case of activated carbons, may lead to the failure of one of the fundamental postulates of potential theory[11].

More recent studies[11,12] have applied Dubinin's volume filling theory, an adaptation of the original potential theory developed by Polanyi, to the high-pressure adsorption of various gases on activated carbon, in particular methane, above the critical point. These studies[11,12] outline the difficulties of applying the Dubinin postulates to supercritical fluids, such as the attainment of saturation vapour pressures and adsorbate densities. Agarwal and Schwartz[11] and Yang[13] provide a summary of the different approaches used to obtain these parameters. The desirability of using potential theory for the description of supercritical gas adsorption is that a single characteristic curve may be used to describe gas adsorption at a variety of temperatures.

The adsorption of methane in coal is generally believed to be due to physical adsorption. This is demonstrated by the small heats of adsorption[1,14] and that methane isotherms are reversible[15,16]. It is therefore reasonable to apply theories based on physical adsorption to the problem of methane adsorption in coal. In particular, Dubinin-Polanyi potential theory may be applied to the current problem, if properly validated.

The purpose of the current study is to apply the Brunauer, Emmett and Teller (BET), Dubinin-Radushkevich (D-R) and Dubinin-Astakhov (D-A) equations to methane/moisture-equilibrated coal isotherm data at elevated temperature and pressure,

above the critical point for methane (T > 1.5Tc), and compare the results to isotherms obtained by the more commonly applied Langmuir equation. The BET, D-R, and D-A equations contain either two or three parameters that are easily determined from experimental isotherm data. The goal of this research is to determine the optimum equation to be applied to adsorption isotherm data. In addition, the general validity of the monolayer and pore volume filling theories is tested for methane-coal systems. The conceptual model of pore-filling is different for these theories, and therefore the current study will have important implications for the modeling of equilibrium isotherm data in coal.

2.2.1 Background

2.2.1.1 Langmuir (Monolayer) and BET (Multilayer) Theory

The most commonly applied adsorption isotherm model for coal at elevated temperature and pressure is the Langmuir model[17], from which the Langmuir equation is obtained. The Langmuir equation is written in the following form for plotting purposes:

$$\frac{P}{V} = \frac{1}{BV_m} + \frac{P}{V_m} \tag{1}$$

where P is the equilibrium gas or vapour pressure; V is the volume of gas adsorbed, commonly reported at standard temperature and pressure (STP), per unit mass of coal, V_m is the Langmuir monolayer volume, and B is an empirical constant.

The Langmuir model is based upon the assumption that a state of dynamic equilibrium exists (at constant T and P) between adsorbed and non-adsorbed species and

that adsorption is restricted to a single monolayer[1]. In addition, the adsorbent surface is assumed to be energetically homogeneous with respect to adsorption. In many cases, a plot of P/V versus P yields a straight line whose slope yields V_m. The Langmuir model has frequently been applied to the description of Type I isotherms obtained for microporous solids such as activated carbons. Several studies of methane adsorption on coal have shown that the Langmuir equation fits well over the range of temperatures and pressures applied[2,14,15,18].

The BET model is an extension of the Langmuir model that accounts for the formation of multilayers[19]. The model was developed for the interpretation of Type II isotherms and the reversible part of Type IV isotherms. The BET equation has the following form:

$$\frac{1}{V(P_o / P - 1)} = \frac{1}{V_m C} + \frac{C-1}{V_m C}\frac{P}{P_o} \qquad (2)$$

where P/P_o is the relative pressure, and C is a constant related to the net heat of adsorption. A plot of the left-hand side of equation (2) versus relative pressure should yield a straight line in the relative pressure range $0.05 < P/P_0 < 0.35$[20]. The application of the BET equation to supercritical fluid adsorption cannot be justified physically as multilayer formation is considered unlikely[14].

2.2.1.2 Dubinin Theory of Adsorption of Vapours in Micropores

Dubinin theory has commonly been applied to the description of Type I isotherms[21]. A fundamental difference between the Dubinin and Langmuir theories of

adsorption is in the postulated mechanism of pore filling. In the Langmuir theory, the sorbed phase is assumed to occupy a monolayer on the adsorbent surface, which is in turn assumed to be homogeneous. Dubinin[21,22] theory, however, assumes that, in micropores, the adsorbate fills the adsorption space via the mechanism of volume filling and hence does not form discrete monolayers in the pores. Dubinin[21] showed that, for several vapours, the ratio of limiting adsorption values on two varieties of zeolite crystals is essentially constant and equal to the ratio of void volumes calculated from X-ray data. The ratio was, however, not equal to the ratio of the geometric surface area of the zeolites. This observation was given as proof of the volume filling mechanism of micropores with radii less than .6 - .7 nm.

Two equations developed by Dubinin and his coworkers are the Dubinin-Radushkevich (D-R) equation[22,13,23]:

$$W = W_o \exp\left\{-\left(\frac{RT}{\beta E}\ln\frac{P_o}{P}\right)^2\right\} \tag{3}$$

and the Dubinin-Astakhov (D-A) equation:

$$W = W_o \exp\left\{-\left(\frac{RT}{\beta E}\ln\frac{P_o}{P}\right)^n\right\} \tag{4}$$

where W is the volume of adsorbate adsorbed at equilibrium, W_o is the micropore volume, β is a sorbate affinity coefficient, E is the characteristic energy, R is the universal gas

constant, T is temperature, P_o is the saturation vapour pressure for the adsorbate, P is the equilibrium vapour pressure, and n is a small integer (1-4) and is related to the distribution of pore sizes. These equations have been applied to a variety of microporous solid-adsorbate systems, including activated carbons. The D-A equation is a general form of the D-R equation in which the coefficient n may be optimized. For plotting purposes, equations (3) and (4) may be written in the following form:

$$\log W = \log W_o - D\left(\log P_o / P\right)^n \tag{5}$$

where n is equal to *2* for the D-R equation, and is optimized for the D-A equation. A plot of $\log W$ versus $\left(\log P_o / P\right)^n$ should yield a straight line. P and P_o may be replaced by f and f_o, the equilibrium and saturation fugacities, to account for non-ideality.

The Dubinin equations are valid for a particular adsorbate-adsorbent system only if certain fundamental postulates of the Dubinin theory are adhered to. An important postulate is that characteristic curves, which are plots of the degree of filling $\theta\,(W/W_o)$ versus the parameter $A = RT \ln P_o / P$, defined as the differential molar work of adsorption by Dubinin[21], are invariant with temperature for a particular adsorbate-adsorbent system. This may be expressed analytically as $\left(\frac{\partial A}{\partial T}\right)_\theta = 0$. Dubinin demonstrated this to be the case for a variety of systems[21]. Bering *et al.*[24] give the thermodynamic limits for which temperature invariance holds. Dubinin[22] states that temperature invariance of the characteristic curve is not a necessary requirement for all microporous systems, but simply that for many systems it appears to be true. Deviations

of the characteristic curve from temperature independence reflect the temperature dependence of the work of adsorption.

The Dubinin equations (3) and (4) were mainly developed for the adsorption of vapours below the critical point but may also be modified for gases above the critical point. Several authors[2,7-12,25,26] have extrapolated the Polanyi adsorption-potential theory, upon which the Dubinin equations are based, to the supercritical region for methane in various adsorption systems. Recent work has focused upon the application of this theory to the adsorption of gases above their critical point[11,12] upon activated carbons. Two important problems associated with the application of potential theories are: 1) the determination of a suitable molar volume of the adsorbate at a given temperature and a pseudo-saturation pressure (above critical temperature) value; and 2) the form of the temperature-invariant characteristic curve to be utilized. Several approaches to these problems have been used[11,13].

2.3 METHODS

2.3.1 Sample Collection and Preparation

Seven lithotypes of Upper Permian coal were collected from the Appin mine (Bulli seam) and five from the Wongawilli mine (Wongawilli seam) in New South Wales, Australia[27]. In addition, one sample (GHA1-09) was obtained from the Bowen Basin. Each sample was prepared for petrographic (maceral and mineral) analysis and proximate analysis according to procedures discussed in Bustin *et al.*[28]. High-pressure methane isotherm analysis sample preparation was performed according to procedures

described in Mavor *et al.*[15]. A split of each sample was also taken for low-pressure carbon dioxide analysis.

2.3.2 Isotherm Analysis

High-pressure methane adsorption isotherms at 30°C were collected using a volumetric apparatus constructed by the CSIRO of Lucas Heights, Australia. In addition, one sample (GHA1-09) was run at 25, 30, and 50°C on a similar apparatus at The University of British Columbia, Earth and Ocean Sciences Department. The instrument is described in Levy *et al.*[29]. Instrument design is based on the volumetric adsorption apparatus described by Mavor *et al.*[15]. Samples were equilibrated with moisture (96-97 % relative humididty) prior to isotherm analysis using the following procedure: samples were placed in a vacuum type desiccator containing a saturated solution of K_2SO_4; the desiccator was evacuated and placed in an oven set at 30°C; at least 48 hours were allowed for equilibrium prior to isotherm analysis. Ten or 11 pressure points were collected during isotherm analysis up to a pressure of about 10 MPa (absolute) for each sample. Equilibrium at each point is assumed to have been achieved if the pressure reading is constant (ΔP=0.000 MPa) over a 40 minute interval. Volumes of gas adsorbed are calculated using the Real Gas Law, and the void volume of the system, determined through helium expansion, is corrected for gas adsorbed at each pressure step, assuming liquid density of the adsorbate. Precision of isotherm runs, determined by repeated anayses, is about $\pm$ 1%.

Low-pressure (< .127 MPa) carbon dioxide isotherms at 0°C were performed on dry (evacuated) coal samples on a Micromeritics ASAP 2010® automated volumetric gas

adsorption apparatus. In addition, the GHA1-09 sample was run at 25°C. Coal samples were evacuated at 100°C overnight to a pressure of < .25 Pa prior to analysis. No non-ideality correction was made for carbon dioxide at these low pressures. A saturation vapour pressure of 3.48 MPa was used for carbon dioxide at 273 K and 6.42 MPa at 298 K. Precision of isotherm runs for coal is about $\pm$ 1%. The instrument is periodically calibrated against a zeolite standard to check for systematic error.

2.3.3 Langmuir, BET, D-R, and D-A Regression Analysis

The Langmuir isotherm was fit to the methane and carbon dioxide experimental data through the following procedure:

1) A linear regression was performed for P/V versus P plots (referred to as Langmuir plots) and the Langmuir constants (B and Vm) were calculated from the slope and intercept.
2) The calculated Langmuir sorbed volumes were obtained from the Langmuir equation in the usual form: $V = \frac{V_m BP}{1 + BP}$
3) The Langmuir isotherm, plotted for 0.1 MPa pressure increments, was superimposed upon the experimental data.
4) A similar procedure was followed for the BET analysis except a linear regression was performed upon $\frac{1}{V(P_o / P - 1)}$ versus relative pressure plots (BET plots).

The saturation vapour pressure (or pseudo-saturation pressure) for the high-pressure/temperature methane analysis was obtained from the extrapolation of the log of vapour pressure, obtained from the CRC handbook[30], versus reciprocal of absolute

temperature to the temperature of actual analysis. A similar procedure was used by Grant *et al.*[9]. This approach is compared against other methods in a later section. The values obtained from this extrapolation method agree most closely with values obtained from the use of the reduced Kirchoff equation as utilized by Kapoor *et al.*[23].

Dubinin regression analysis was performed in the following fashion:

1) $\log V$ is plotted against $\left(\log P_o / P\right)^n$ (D-R or D-A transformed plots) and a least squares fit performed. For the D-R equation, the value of n is equal to *2* but for the D-A equation, the value of n is optimized by recalculating the linear regression until the standard error of the Y-intercept is minimized. The value of n is optimized to within 10^{-4}.
2) The micropore capacity (V_o) is obtained from the Y-intercept.
3) The calculated volumes adsorbed are obtained from equation (4). The Dubinin isotherms are then plotted for 0.1 MPa increments and superimposed upon the experimental data.

Although conventional linearized unweighted regression models[2,15,31,32] were used to obtain fit parameters for the four isotherm equations, more refined and statistically rigorous regression models were also considered. Non-linear and non-linear weighted ordinary least squares (OLS) *V on P*, and non-linear weighted OLS *P on V* regression models were also applied to representative samples. These regression models more rigorously accommodate the proportional measurement error observed in pressure and volume adsorbed measurements. They have unbiased V residuals (see below), as opposed to the linearized regression model, which biases the V residual plots during transformation. Furthermore, comparison of the *V on P* and *P on V* non-linear weighted

regression results allow determination of whether a regression model accommodating errors in both P and V variables is required.

Results from the various regressions were insignificantly different. This is a consequence of the relatively high degree of fit of all isotherm regression models. The average relative error (see below) averaged over all samples is less than 4.2, 2.1, 1.6 and 0.4 % for the Langmuir, BET, D-R, and D-A equations, respectively, regardless of the regression model applied. Results did not reorder the relative quality of fit for the four isotherm models (discussed below) and demonstrate that an "error in both variables" regression model is not required. Thus, although the non-linear weighted V-P regression model is the most consistent with the nature of the data and their errors, the conventionally applied linearized regression results are presented below in order to allow comparison with previous isotherm results.

2.4 RESULTS

2.4.1 Petrographic and Proximate Analysis

The results of petrographic (maceral), presented on a mineral matter-free (mmf) basis, and proximate analysis are given in Table 2-1. Fixed carbon content of the Bulli seam samples range from 71 to 77 % (dry, ash-free basis) whereas the Wongawilli seam values range from 64 to 76 %[27]. Samples are composed mainly of the vitrinite macerals telocollinite and desmocollinite, and inertinite macerals fusinite and semifusinite as well as mineral matter. Liptinite is rare.

Table 2-1. Maceral composition (vol %, mmf) and proximate analysis of samples studied.

Sample	Tc	Dc	Sf	F	Id	Moisture (%)	Volatiles (%)	Fixed C (%)	Ash (%)
B1	9	24	34	33	-	0.9	20.3	68.6	10.2
B2	11	37	24	28	-	0.8	22.0	67.6	9.6
B3	10	39	37	14	-	0.7	21.8	68.9	8.6
B4	16	39	24	22	-	0.8	25.1	66.6	7.5
B5	30	36	20	15	-	0.7	25.4	64.1	9.8
B6	39	37	12	11	-	0.6	26.8	69.2	3.4
B7	90	0	1	9	-	0.7	21.8	67.7	9.8
W1	7	40	41	12	-	0.8	18.3	58.6	22.3
W2	13	54	18	15	-	0.6	24.6	59.4	15.4
W3	41	38	13	9	-	0.8	23.8	43.0	32.4
W4	62	31	4	3	-	1.0	21.7	58.0	19.3
W5	79	16	3	2	-	0.9	25.0	63.3	10.8
GHA1-09	13	48	24	1	14	1.4	24.1	67.0	7.5

Tc = Telocollinite
Dc = Desmocollinite
Sf = Semifusinite
F = Fusinite
Id = Inertodetrinite

2.4.2 Langmuir Correlations

Correlation coefficients (r^2) calculated from linear regression analysis of the Langmuir plots (*P/V vs. P*) are greater than 99% for all coals, and range from 99.06 % (W1) to 99.85 % (B4).

The calculated Langmuir isotherms (solid line) for the coals with the worst (W1) and best (B4) Langmuir correlations are shown in Figure 2-1 along with the experimental high-pressure methane isotherms. The adsorbed volumes are presented on a dry, ash-free basis (daf) and are corrected to standard temperature and pressure. The Langmuir isotherm calculated for W1 and B4 underestimates the volumes adsorbed at low (< 2 MPa) and high pressure (> 7 MPa) and overestimates the volume adsorbed in the mid-region of the isotherm (2-7 MPa). Although data for only two samples are shown here, the Langmuir isotherm breaks down in the same pressure region for all samples analyzed.

Langmuir isotherms are plotted for the low-pressure carbon dioxide analyses at 273 K (Figure 2-2). The Langmuir plot r^2 values (not shown) are around 99%, and the correlation for B4 (99.17%) is better than for W1 (98.50%).

A plot of the residuals, the difference between experimentally-determined and calculated adsorbed volumes of methane for the Langmuir fit, is shown in Figure 2-3 for samples B4 and W1. The same trend is apparent for the low-pressure carbon dioxide analyses (Figure 2-4), despite the difference in experimental conditions. It is important to note, however, that these plots may not be compared directly with the methane results as the isotherms for methane and carbon dioxide were run over much different relative pressure ranges (~ .001 - .3 for methane, and .002 - .035 for carbon dioxide).

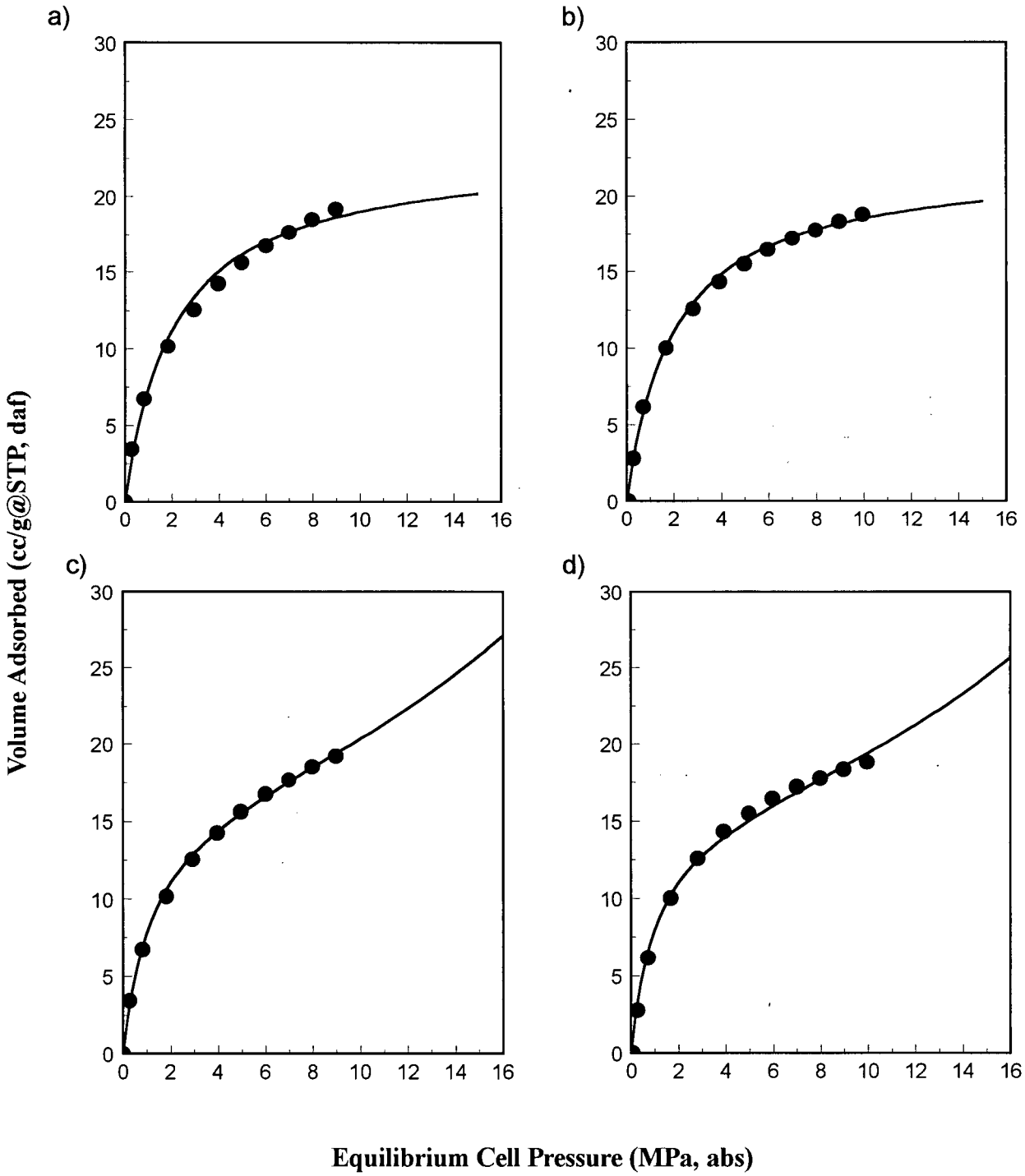

Figure 2-1. Langmuir (a,b) and BET (c,d) curve fits to methane isotherm data for samples W1 (a,c) and B4 (b,d). Solid line is curve fit.

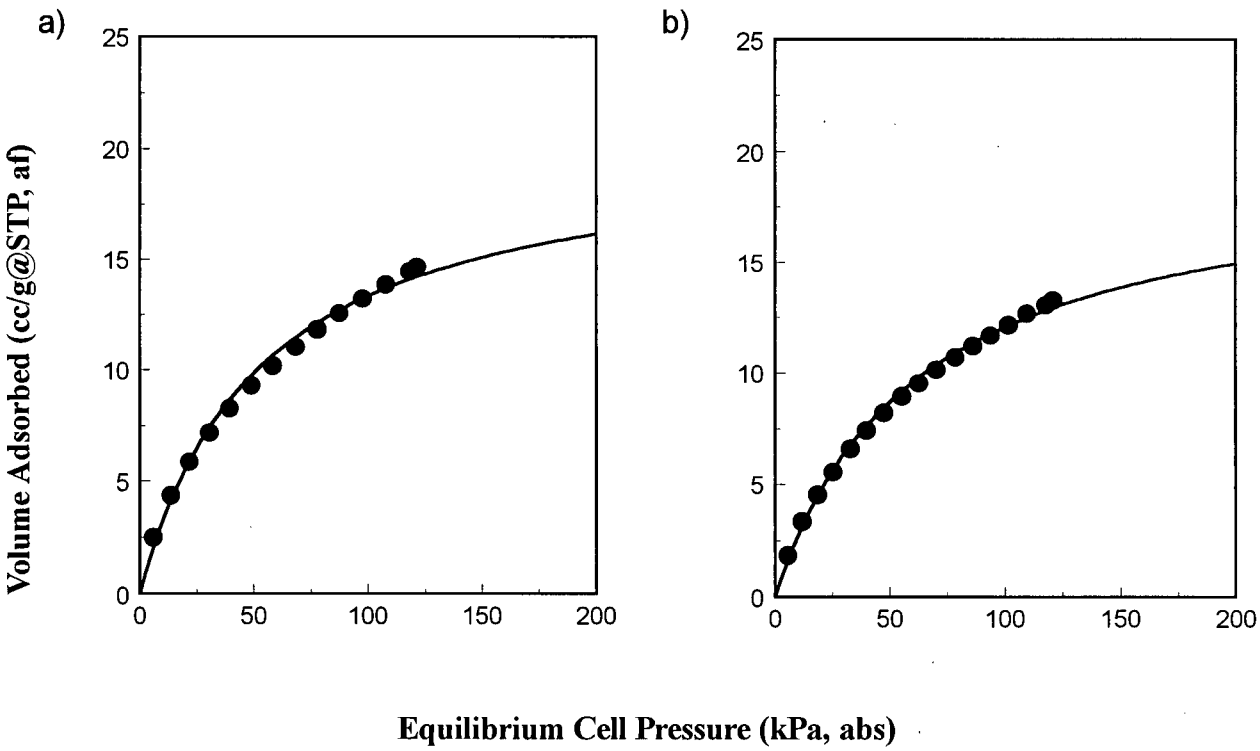

Figure 2-2. Langmuir curve fits for samples W1 (a) and B4 (b). Solid lines are curve fit.

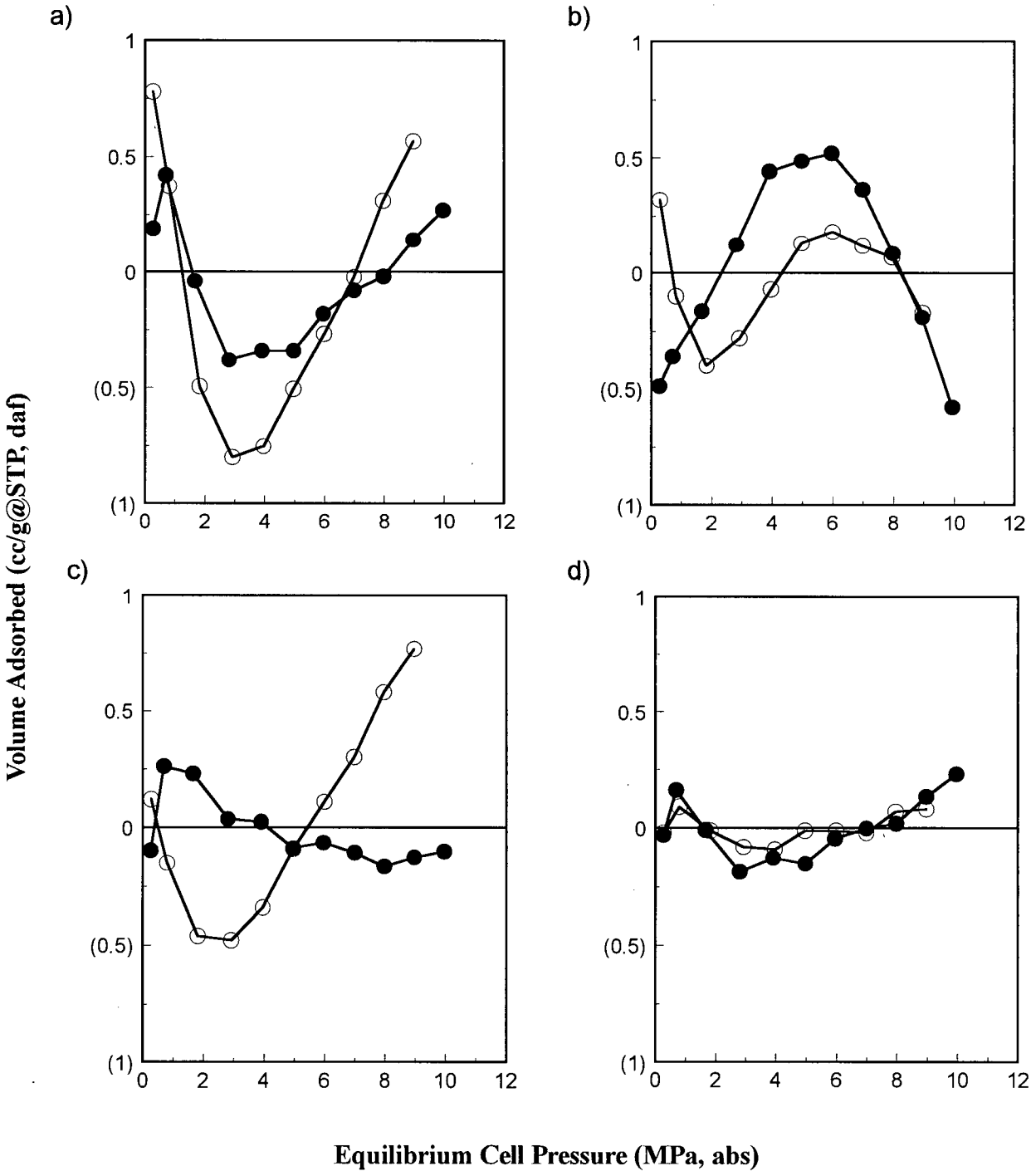

Figure 2-3. Plots of residuals for Langmuir (a), BET (b), D-R (c) and D-A (d) curve fits. Samples are W1 (open circles) and B4 (solid circles).

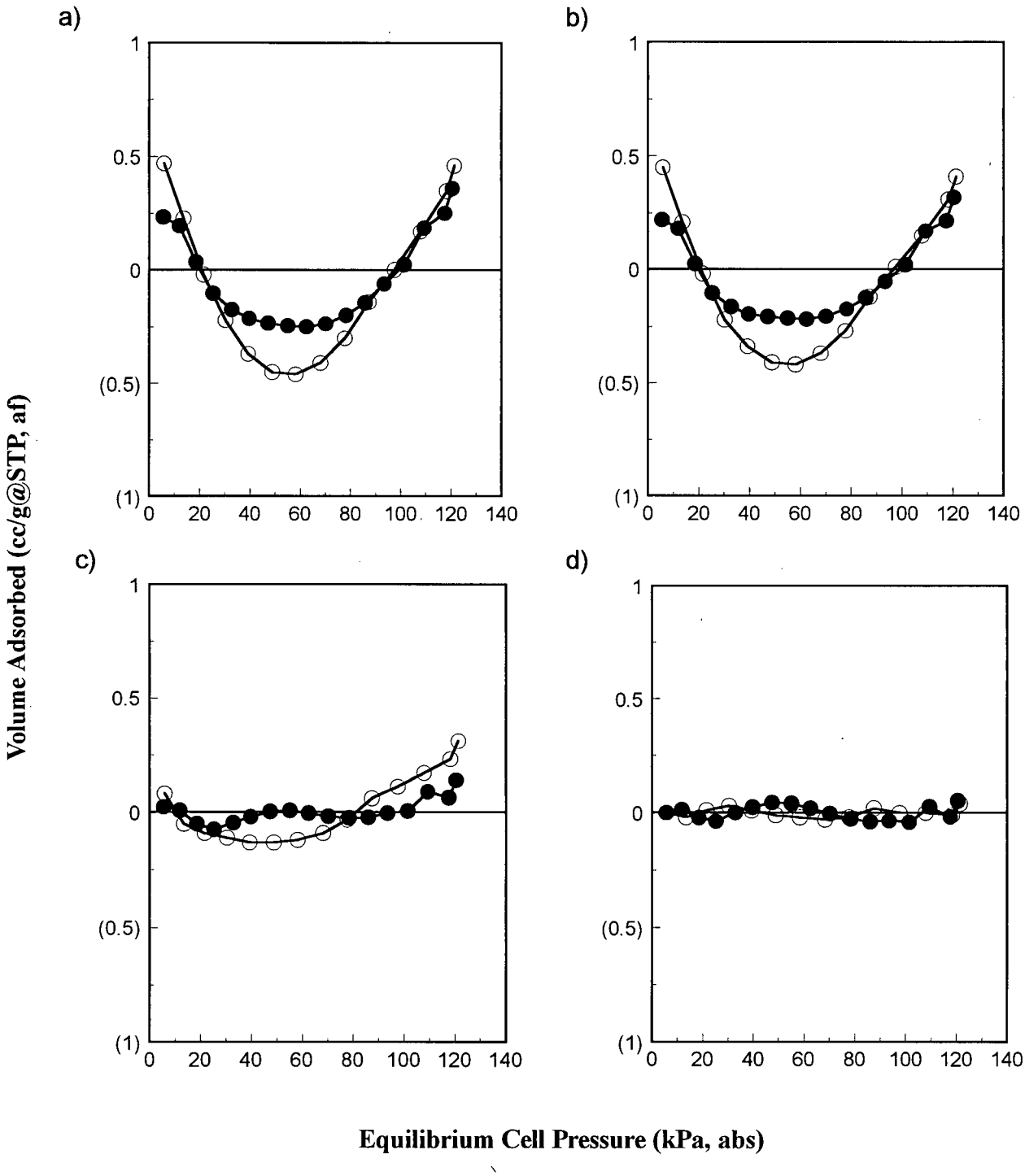

Figure 2-4. Plots of residuals for Langmuir (a), BET (b), D-R (c) and D-A (d) curve fits. Samples are W1 (open circles) and B4 (solid circles).

In order to quantify the curve-fit for all samples, the average relative errors (r.e.) between the calculated and experimental adsorbed volumes of methane were determined (Table 2-2). In addition, the Langmuir monolayer volume is given. The mean average relative errors for all samples tested is about 4.2% for the Langmuir correlation.

2.4.3 BET Correlations

BET isotherms for sample W1 and B4 are shown in Figure 2-1. BET plot (not shown) r^2 values are greater than 99% (99.71 - 99.92%), and are on average greater than the Langmuir values. The BET isotherm better fits the experimental data for sample W1 than the Langmuir isotherm (2.1% r.e. versus 5.0%), but not for B4 (3.8% versus 2.3%). In general, however, the BET isotherm provides a better fit to the high-pressure methane experimental data (Table 2-2).

A plot of the BET residuals for samples W1 and B4 is shown in Figure 2-3. The opposite trend is observed than for the Langmuir residuals: the BET isotherm underestimates the volumes adsorbed in the middle region of the isotherm and overestimates at the low and high-pressure ends. This trend is obeyed for all samples studied. The same plot for carbon dioxide analyses (Figure 2-4) illustrates that the BET residual trend is very similar to the Langmuir trend.

2.4.4 D-R Correlations

D-R plots for the Australian coals are linear (not shown) and correlations are greater than 99% (99.66 - 99.98%) for all samples. The mean average relative error for the D-R fit for all samples is slightly lower than the BET fit (1.6 versus 2.1%). The D-R

Table 2-2. Relative error calculations for isotherm fits

	Average Relative Error				Vo (Monolayer Vol. / Micropore Cap.)			
Sample	Langmuir	BET	D-R	D-A	Lang	BET	D-R	D-A
	%	%	%	%	cc/g, daf	cc/g, daf	cc/g, daf	cc/g, daf
B1	3.05	1.82	0.67	0.67	21.4	15.1	20.8	20.7
B2	3.99	1.65	1.01	0.15	21.7	15.5	21.1	22.2
B3	3.93	2.65	1.14	0.36	21.7	15.0	20.9	21.9
B4	2.32	3.83	1.29	0.86	22.3	15.3	21.9	20.8
B5	4.18	1.48	1.06	0.47	22.3	15.9	21.7	22.6
B6	4.01	2.57	1.10	0.25	22.7	15.8	22.0	23.1
B7	4.29	1.63	1.18	0.62	21.4	15.2	20.7	21.9
W1	5.44	2.12	2.65	0.41	23.1	16.2	21.6	25.0
W2	4.86	1.95	2.49	0.37	24.8	17.3	23.1	26.3
W3	5.02	2.21	2.71	0.25	22.1	15.4	20.5	23.9
W4	5.31	1.78	2.31	0.77	23.9	16.8	22.5	25.4
W5	4.82	1.94	2.28	0.30	24.7	17.3	23.2	26.2
GHA1-09	2.71	2.19	0.86	0.31	23.2	15.6	21.7	22.6
Avg %	4.15	2.14	1.60	0.45				

Average Relative Error = (100/N)Sum(abs(Vcal-Vexp)/Vexp) %

isotherm fit (Figure 2-5) is better for sample B4 than for W1 and the residual plot trends (Figure 2-3) for sample W1 is similar to that for the Langmuir fit. Residual plots are also shown for the carbon dioxide analyses (Figure 2-4).

2.4.5 D-A Correlations

The D-A equation yielded the highest correlations for the experimental data (99.96 - 100%); the mean average relative error for all samples is around 0.5%. Residual plots for samples W1 and B4 show no distinct trend (Figure 2-3), which indicates an excellent fit to the data.

2.5 DISCUSSION

In general, for the coals studied, the isotherm equations based upon adsorption potential theory (D-R, and D-A) yield a better curve-fit to the experimental data than those based upon the mono/multi-layer pore filling models (Langmuir and BET). Three equations are two-parameter models (Langmuir, BET, and D-R) while the fourth is a three-parameter model (D-A). Both the BET and D-R equations yield better fits to the data than the Langmuir equation for all coals, except sample B4. Although all the isotherm equations applied yield a reasonable approximation to the experimental data, the validity of the underlying theories requires testing.

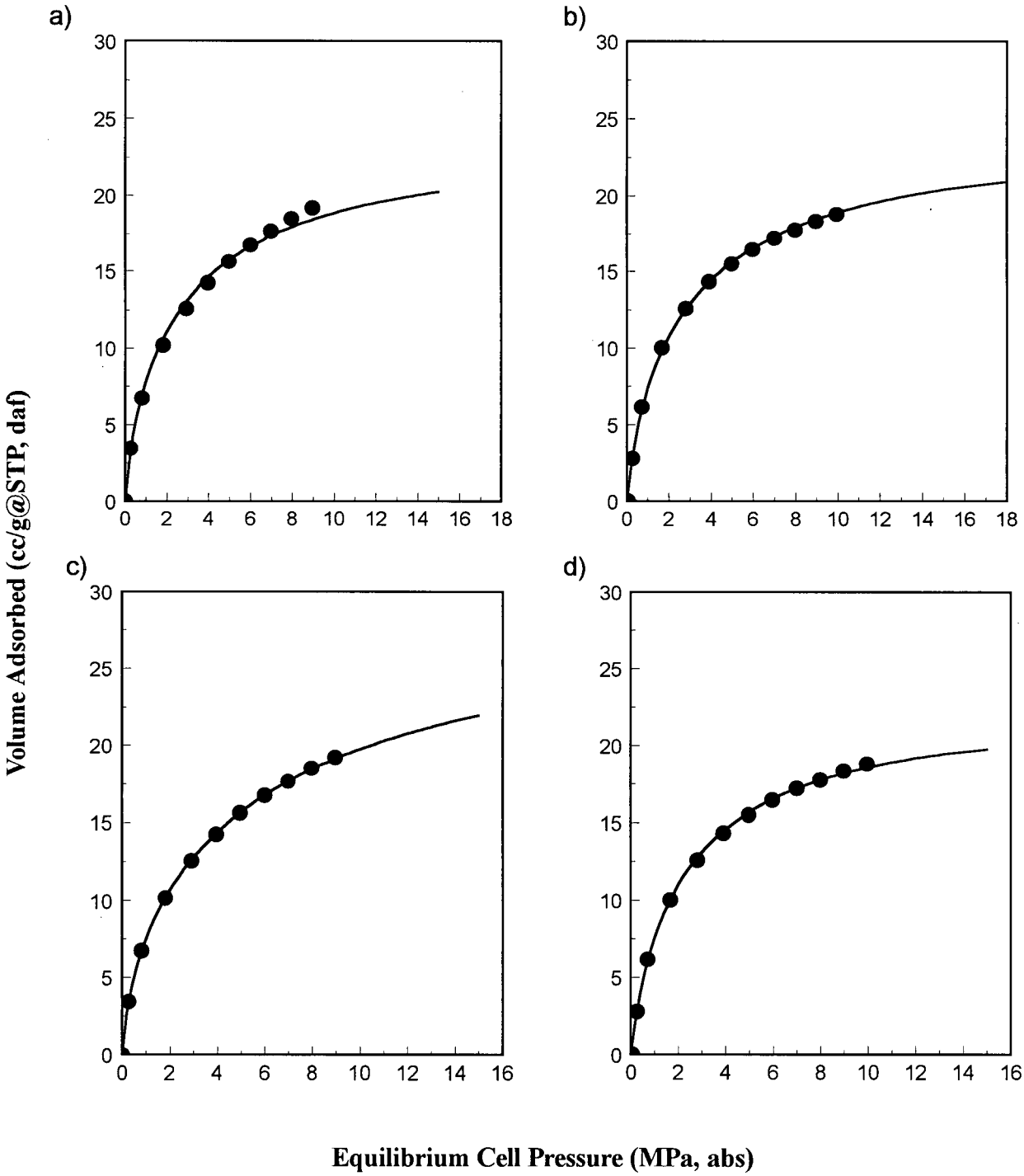

Figure 2-5. D-R (a,b) and D-A (c,d) curve fits to methane isotherm data for samples W1 (a,c) and B4 (b,d). Solid line is curve fit.

2.5.1 Langmuir Theory

The basic assumptions of the Langmuir model are[13]:

1) Adsorbed molecules are held at well-defined localized sites.
2) Only one adsorbed molecule can be held at each site.
3) All adsorption sites are energetically equivalent and there is no interaction between adsorbates on neighbouring sites.

As outlined by Koresh[34], the Langmuir model, as applied to physisorption on microporous adsorbents, has been criticised for the following reasons:

1) The slope of the linearized Langmuir isotherm and the intercept are not constant in various ranges of adsorption.
2) The monolayer amount varies with temperature.

Brunauer[33] showed that the Langmuir plot may not have a constant slope for the complete range of relative pressures, but may be subdivided into linear subsegments. This behaviour was attributed to surface heterogeneity. Several studies have shown that the monolayer amounts vary with temperature, but, as stated by Koresh[34], these experiments were performed at the same pressure range at different temperatures, and hence at higher temperatures, the isotherms represent less surface coverage. The consequent lower determined monolayer amounts may therefore be attributed to surface heterogeneity, as stated above. In this study, as with Koresh[34], criticisms 1) and 2) will be considered as one.

Figure 2-6 shows the Langmuir plot (303 K isotherm data) for sample W1, along with a plot of the residuals. A line fit to the low-pressure data (< 3MPa) would yield a larger slope of the Langmuir plot compared to that at higher pressures, resulting in a

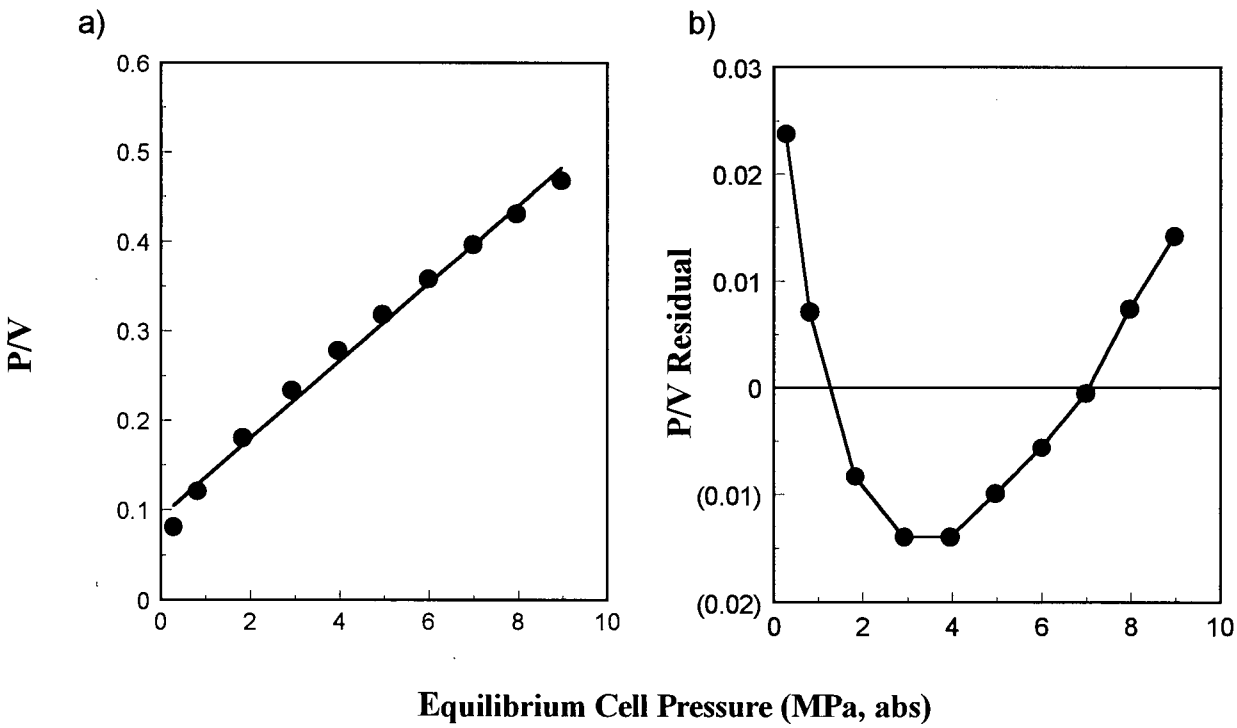

Figure 2-6. Langmuir plot (a) and plot of residuals (b) for W1.

smaller predicted monolayer volume at the lower pressures. In addition, the *B* constant would be larger. If the first three points of Langmuir plot are used to calculate the monolayer volume, a value of 15.8 cc/g (daf) is obtained, which is about 32% smaller than the value obtained from the entire range of pressure (23.1 cc/g). Note that although sample W1 is an extreme case of the failure of the Langmuir model in this regard, all the samples studied show a similar trend to varying degrees.

Ruppel *et al.*[2] found that correcting for the change in dead space volume with gas adsorption actually introduced curvature into the Langmuir plot. In the current study, Langmuir plots were generated for uncorrected (no dead space correction) adsorbed volumes, and the curvature in the plots still existed (not shown). Correction for dead space error is therefore not the cause of curvature in the Langmuir plots shown.

A plot of the parameter *B* versus temperature should be exponential in form[2] and this was demonstrated for sample GHA1-09 (not shown). Langmuir isotherms were recalculated by fitting a linear relationship between the (natural) logarithm of the experimentally-derived *B* parameter and the reciprocal temperature. These isotherms are shown in Figure 2-7 along with the original experimentally determined isotherms. The fit to the original data is good with a relative error of around 2-3%. The Langmuir volumes determined from the Langmuir fit to each of the three isotherms separately were used in the recalculated Langmuir isotherms.

2.5.2 Dubinin Theory

The thermal equation for adsorption may be written in the following form[22]:

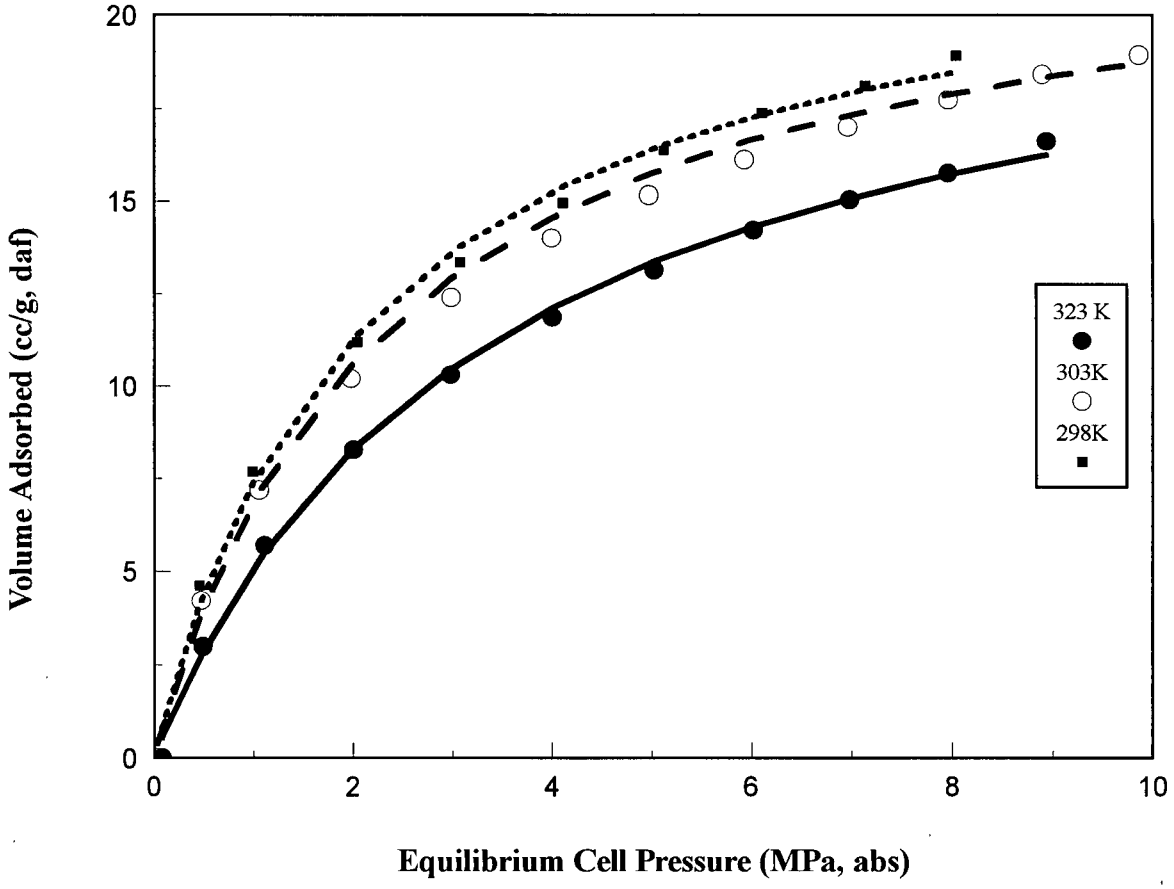

Figure 2-7. Recalculated Langmuir isotherms for GHA1-09.

$$\theta = F(A / E, n)$$

where θ is the degree of filling of the adsorption space, A is as defined previously (for vapours), E is the characteristic energy, which is equal to A at a particular value of θ, and n is a constant parameter. The function F is a distribution function of θ with respect A; in the case of the D-A equation, the distribution adopted is that due to Weibull[35]. If E and n are temperature invariant parameters of this distribution, then the characteristic curve defined by the relationship $A=E\varphi(\theta, n)$ should also be temperature invariant.

Methane adsorption characteristic curves for sample GHA1-09 at 298, 303, and 323 K were calculated to determine the effect of using several techniques for the determination of saturation pressure; adsorbed phase volume; differential molar work of adsorption (A) as well as for the correction for gas non-ideality. Table 2-3 outlines the various techniques utilized to obtain these parameters.

Figure 2-8 shows the characteristic plots for the case of no correction for gas non-ideality (pressure instead of fugacity), the assumption of liquid molar volume of the adsorbate at boiling point (2-8a), and the calculated adsorbate molar volume using Dubinin's technique (2-8b), which corrects for the thermal expansion of the adsorbate. For plots 2-8a) and 2-8b), the pseudo-saturation pressure was calculated using the extrapolation procedure discussed above. For the two plots, the maximum deviations from the characteristic curve are around $\pm$2%. Deviations are defined as the maximum deviation of adsorbed volume at a particular value of A divided by the maximum adsorption volume (x100)[11]. The correction for the thermal expansion of the adsorbate does not appear to have a significant effect upon the characteristic curve.

Table 2-3. Summary of the various methods used for the attainment of pseudo-saturation pressure and molar volume of the adsorbate.

Pseudo-Saturation Pressure	Molar Volume of Adsorbate
$Ps = (T/Tc)^2 Pc$ From reduced Kirchoff ***Extrapolated Log vp versus 1/T plot	* $V = Vs(Tb)$ **$V = Vs(Tb)\exp(\Omega(T-Tb))$

* Vs(Tb) = liquid molar volume of the adsorbate at normal boiling point.

** Ω = thermal expansion coefficient of the adsorbate[10], taken as .0016.

*** vp = vapour pressure

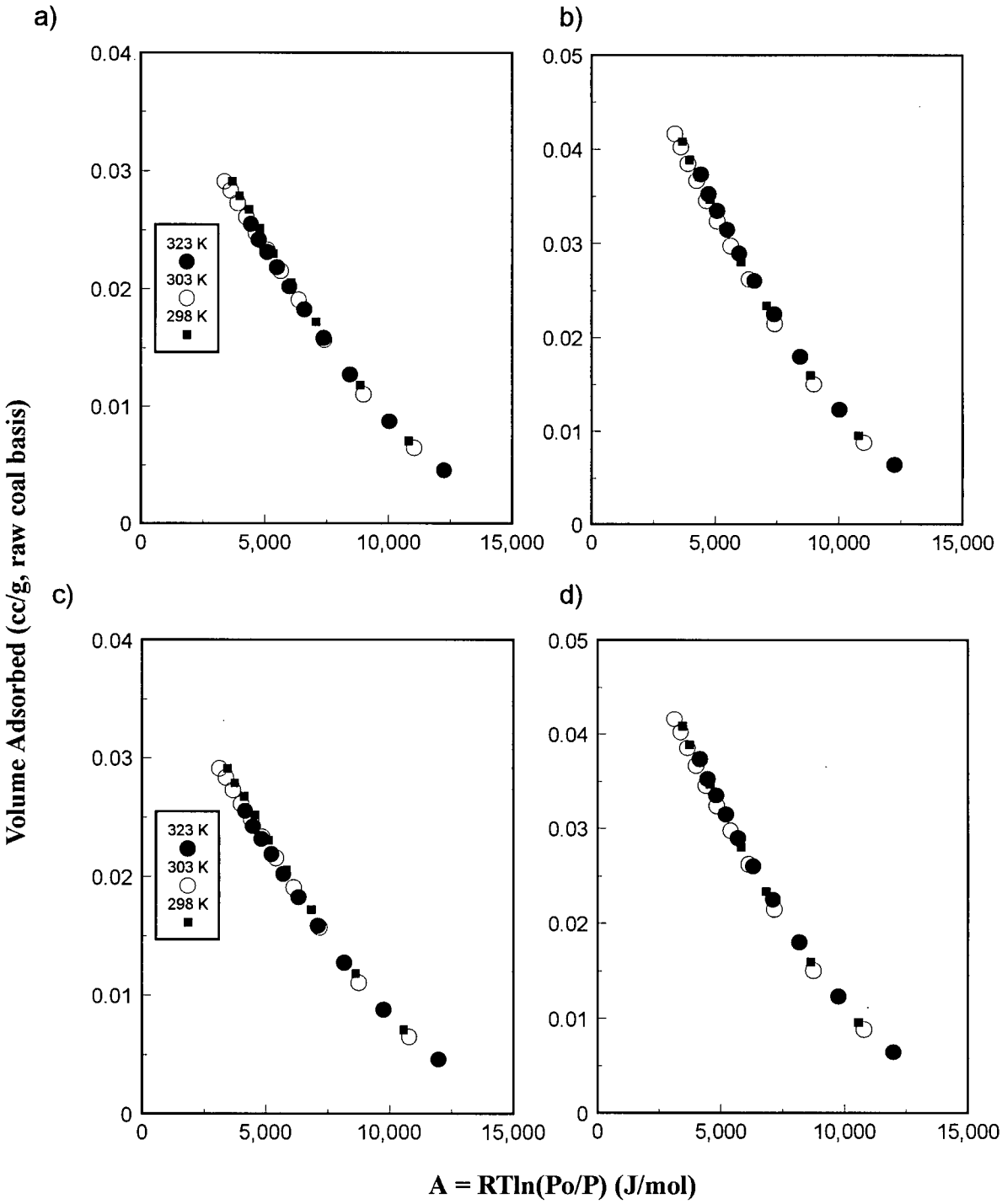

Figure 2-8. Methane characteristic curves for sample GHA1-09. Po was calculated using extrapolated vapour pressures (a,b) and the Kirchoff equation (c,d). Thermal expansion of the adsorbate is accounted for in (b) and (d).

Characteristic curves calculated using the reduced Kirchoff equation to determine pseudo (extrapolated) vapour pressures are shown in Figure 2-8 (c and d). The maximum deviation for these plots is also about $\pm$ 2%. The use of the Kirchoff extrapolation for pseudo-vapour pressures in the calculation of the characteristic curves therefore yields similar results to those calculated using the extrapolation described above.

Characteristic curves using the Dubinin technique for pseudo-vapour pressure extrapolation however display larger deviations than the other two vapour pressure extrapolation techniques (Figure 2-9). The maximum deviation is over 4%. Correction for the thermal expansion of the adsorbate does appear to decrease the deviation from temperature invariance of the characteristic curve, however.

Correcting for non-ideality of the adsorbate vapour does not have a significant effect upon the characteristic curve. A characteristic curve calculated using the extrapolated vapour pressure technique and the assumption of a constant liquid density is shown in Figure 2-10. Fugacities of the free-gas in equilibrium with the adsorbate are obtained by calculation of the fugacity coefficient using a virial series with Redlich-Kwong constants. This procedure is outlined in Noggle[36].

A plot of the experimental isotherms and the D-A fit calculated from the characteristic curve are shown in Figure 2-11. The curve fit was performed by plotting $\log W$ vs. A^n, where W is equal to the product of the number of moles of gas adsorbed and the liquid molar volume of methane at normal boiling point, A is the calculated differential molar work of adsorption, and n is the optimized Astakhov coefficient (1.9). The curve fit appears to be reasonable, with an average relative error of less than 2%.

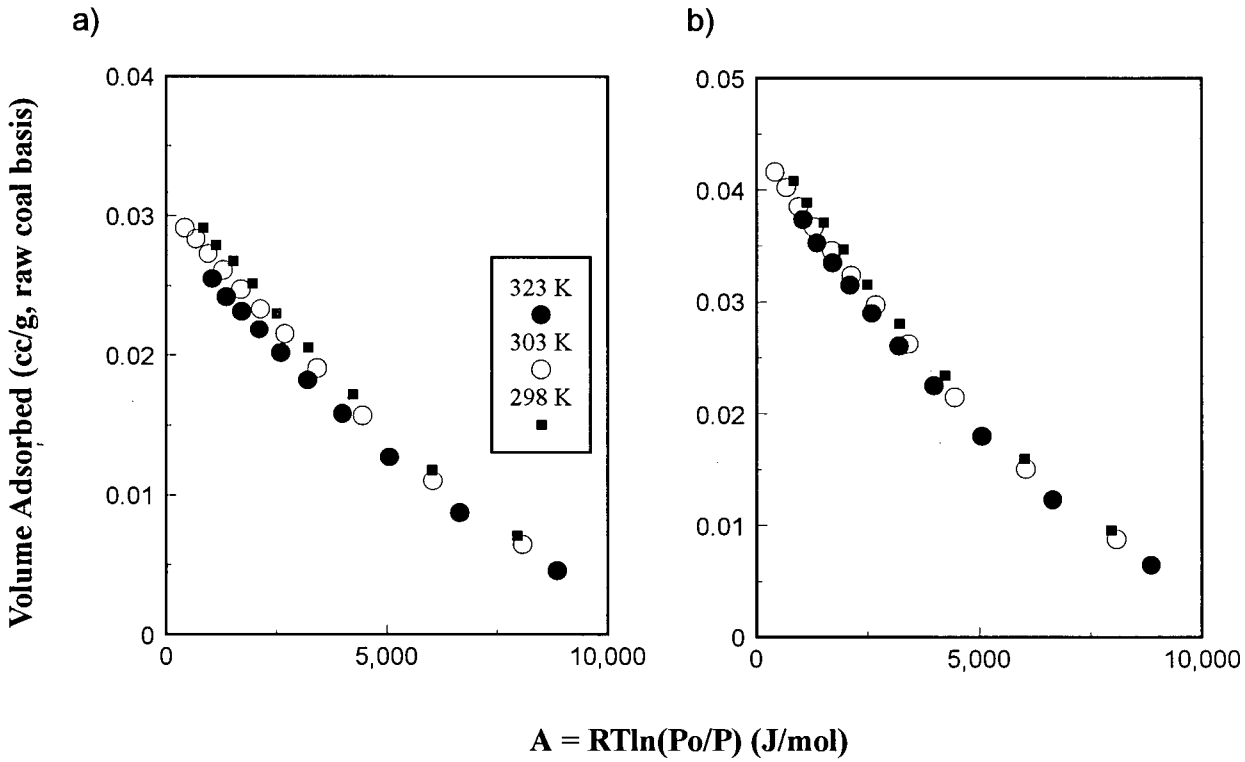

Figure 2-9. Methane characteristic curves for sample GHA1-09. Po was calculated using the Dubinin method. Thermal expansion of the adsorbate is accounted for in (b).

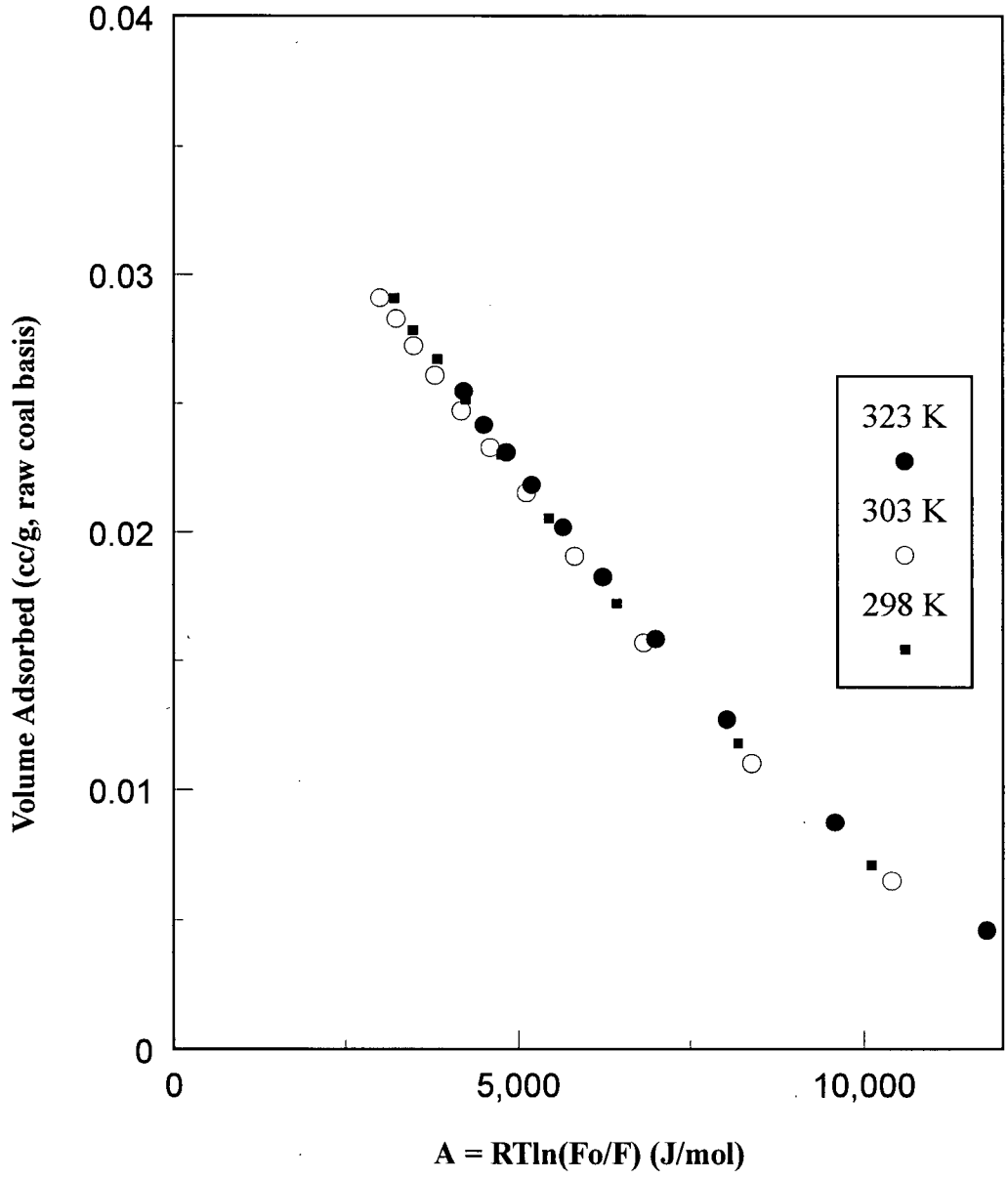

Figure 2-10. Methane characteristic curves for sample GHA1-09 using fugacities instead of pressures.

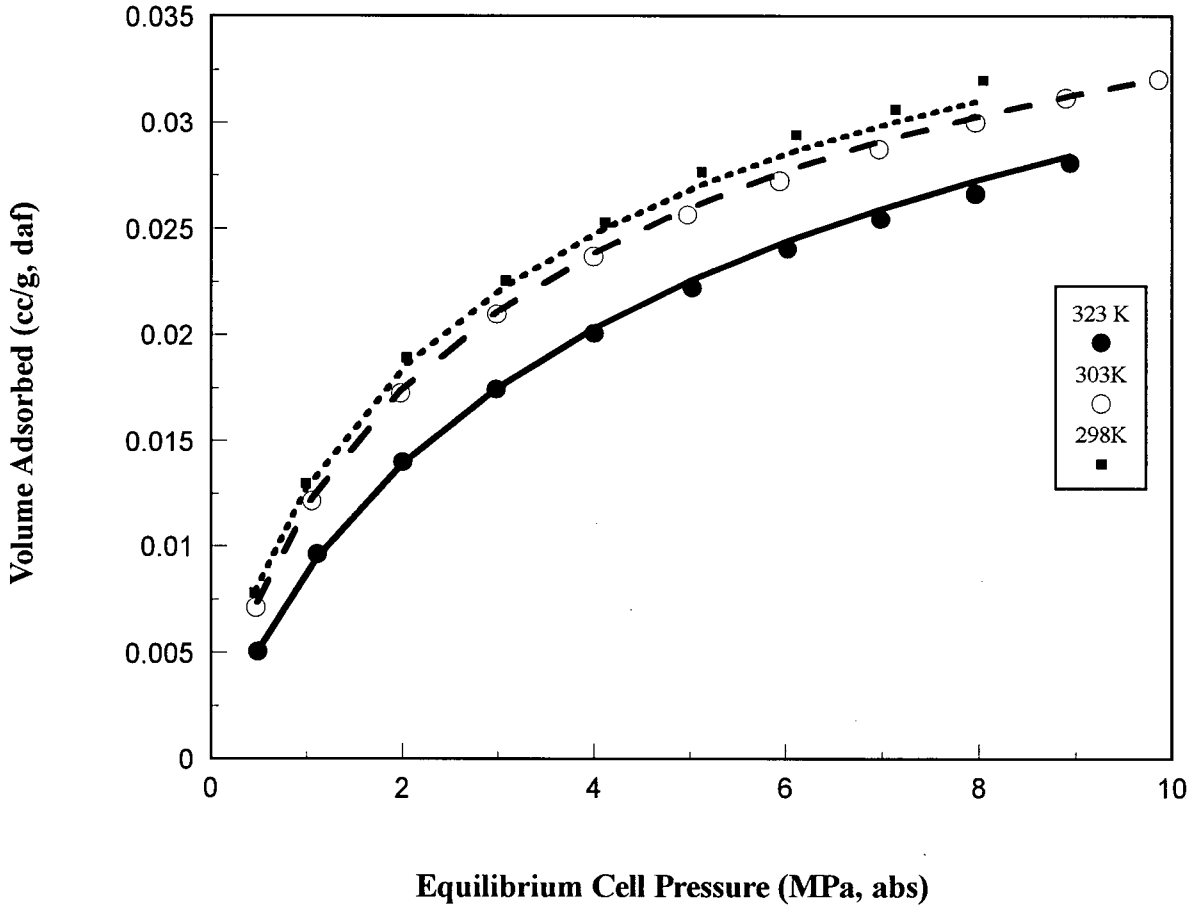

Figure 2-11. Recalculated D-A isotherms for GHA1-09.

The characteristic curve (Figure 2-12) for sample GHA1-09, plotted using the low pressure carbon dioxide data at 298 K and 273 K and no correction for adsorbate density variation with temperature shows a deviation of up to +/- 3%. These results are in agreement with Toda *et al.*[37] who found that carbon dioxide adsorption at a variety of temperatures could be expressed by a single Dubinin-Polanyi plot.

There is some evidence that adsorption of carbon dioxide on coal may not be strictly physical adsorption. A study by Greaves *et al.*[38] demonstrated that high pressure adsorption (up to about 7 MPa) of methane and carbon dioxide mixtures on dry coal exhibited hysteresis between the adsorption and desorption branches of the isotherm which became more pronounced with percentage of carbon dioxide used in the mix. The hysteresis was interpreted by the authors to be due to the retention of carbon dioxide preferentially over methane upon desorption. This experimental behaviour indicates that adsorption of carbon dioxide in coal is not strictly due to physical adsorption. This phenomenon is currently being investigated.

In summary, high-pressure methane and low-pressure carbon dioxide adsorption characteristic curves are temperature-independent in the range of temperatures studied. The assumption of liquid density of the adsorbate for methane is sound and temperature dependence of this parameter need not be accounted for to attain temperature-invariant characteristic curves in the range of temperatures utilized here. Of the several methods used to obtain pseudo-saturation pressures for methane, the extrapolation of the vapour pressure curve and the reduced Kirchoff equation are the best for calculating characteristic curves. The Dubinin technique for obtaining saturation pressures does not yield temperature-invariant characteristic curves regardless of the value used for

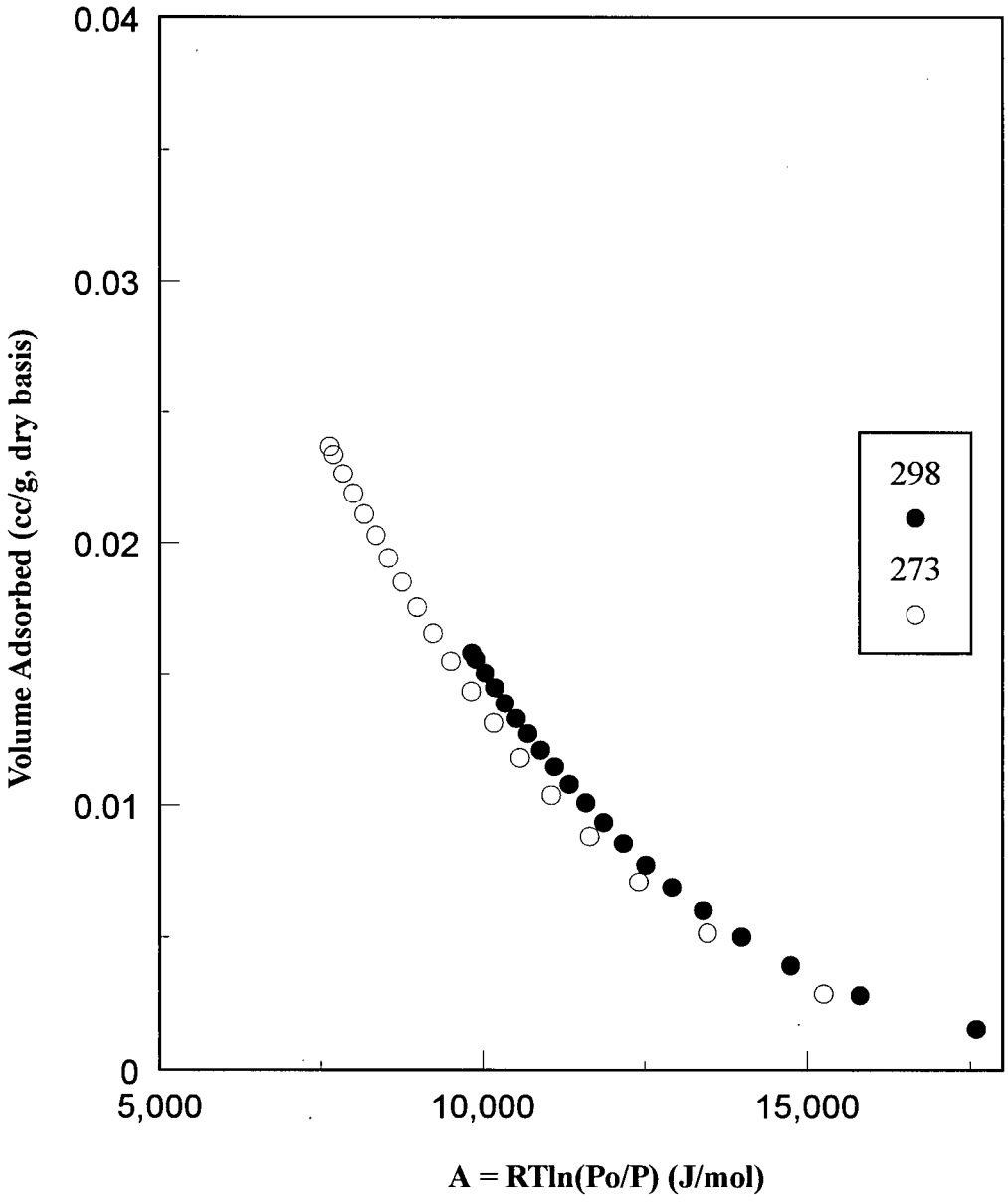

Figure 2-12. Carbon dioxide characteristic curves for sample GHA1-09.

adsorbate density. A recent study by Amankwah and Schwartz[12] has shown that a modified Dubinin equation for the attainment of pseudo-saturation fugacity yields better results than the original Dubinin equation for high-pressure methane and hydrogen adsorption. The equation, however, introduces yet another parameter into the D-A equation that needs to be optimized.

2.6 CONCLUSIONS

A number of classical isotherm equations have been applied to model the adsorption of supercritical methane on coals at high-pressures (up to 10 MPa) in an attempt to determine which yield the best curve-fit to the experimental data and which are the most physically realistic models. In addition carbon dioxide adsorption at low-pressures on these same coals was analyzed by these equations.

The three-parameter Dubinin-Astakhov equation yields the best curve-fit to the high-pressure (> .101 MPa) methane experimental data, but both the two-parameter Dubinin-Radushkevich and BET equations are better than the Langmuir equation. The same is true for the adsorption of carbon dioxide at low pressure (< .127 MPa).

The validity of the monolayer and adsorption potential theories was also tested. The temperature dependence of the Langmuir B parameter is exponential in accordance with theory, although only three estimates of the parameter were obtained. The calculated isotherms from this relationship were in reasonable agreement with the experimental data. The assumption of an energetically homogeneous surface of

adsorption is not strictly true, thus one of the postulates of Langmuir theory is violated for methane adsorption on coal.

In order to test the validity of potential theory, methane characteristic curves were plotted for a coal run at several temperatures. The curves are coincident if either the reduced Kirchoff equation or extrapolated vapour pressures are used to obtain the pseudo-saturation pressure of the adsorbate. The adsorbate is assumed to have the same density as the liquid adsorptive at the normal boiling point. Correction for thermal expansion of the adsorbate in the limited range of temperatures used here does not appear to be necessary, although the correction may be appropriate for a wider temperature range.

In the pressure and temperature range studied here, the adsorption potential theory for methane adsorption appears to be valid. For higher pressures, application of the BET isotherm equation may be more appropriate, but this requires further testing.

Low-pressure characteristic curves were also plotted for carbon dioxide at two different temperatures for the same coal. The characteristic curve for this adsorbate appears to be temperature-invariant.

Future studies will involve testing the validity of potential theory for high-pressure methane and carbon dioxide adsorption on a variety of coals at a wider range of temperatures than those applied here. In addition mixed gas analyses will be performed in order to test the validity of potential theory for these gases.

2.7 REFERENCES

1. Gregg, and Sing, K.S.W. 'Adsorption, Surface Area and Porosity', 2nd edition, Academic Press, New York, 1982

2. T.C. Ruppel, Grein, C.T., and Beinstock, D. *Fuel* 1974, **53**, 152

3. Kim, A.G. U.S. Bureau of Mines Report of Investigations 8245, 1977

4. Smith, D.M., and Williams, F.L. *Society of Petroleum Engineers Journal* 1984, **24**, 529

5. Hall, F.E., Zhou, C., Gasem, K.A.M., Robinson, R.L., Jr., and Yee, D. SPE Paper 29194, presented at the Eastern Regional Conference and Exhibition, Charleston, WV, November 8-10, 1994, pp. 329-343

6. Polanyi, M. *Science* 1963, **141,** 1010

7. Lewis, W.K., Gilliland, E.R., Chertow, B.and Cadogen, W.P. *Ind. Eng. Chem.* 1950, **42**, 1319

8. Maslan, F.D., Altman, M. and Alberth, E.R. *J. Phy. Chem.* 1953, **57**, 106

9. Grant, R.J., Manes, M. and Smith, S.B. *AIChEJ.* 1964, **8,** 403

10. Cook, W.H. and D. Basmadjian, *Can. J. Chem. Eng.* 1964**, 42**, 146

11. Agarwal, R.K. and Schwartz, J.A. *Carbon* 1988, **26**, 873

12. Amankwah, K.A.G., and Schwartz, J.A., *Carbon* 1995, **33**, 1313

13. Yang, R.T. 'Gas Separation by Adsorption Processes', Butterworths, Boston, Mass., 1987

14. Yang, R.T. and Saunders, J.T. *Fuel* 1985, **64**, 616

15. Mavor, M.J., Owen, L.B., and Pratt, T.J. Paper SPE 20728, presented at the 65th Annual Technical Conference of the Society of Petroleum Engineers, New Orleans, Louisiana, Sept. 23-26, 1990, pp.1-14

16. Harpalani, S. and Pariti, U.M. In Proceedings of the 1993 International Coalbed Methane Symposium, Tuscaloosa, May 17-21, 1993, pp. 151

17. Langmuir, I. *J. Am. Chem. Soc.* 1918, **40**, 1361

18. G.J. Bell, and K.C. Rakop, *SPE* 15454, paper presented at the SPE 61st Annual Technical Conference and Exhibition, New Orleans, Louisiana, October 5-8, 1986

19. Brunauer, S., Emmett, P.H., and Teller, E. *J. Am. Chem. Soc.* 1938, **60**, 309

20. Lowell, S. and Shield, J.E. 'Powder Surface Area and Porosity', 2nd edition, Chapman and Hall, London, 1984

20. Dubinin, M.M. In 'Chemistry and Physics of Carbon', Vol. 2, (Ed P.L. Walker, Jr), Edward Arnold, Ltd., New York, 1966

21. Dubinin, M.M. In 'Progress in Surface and Membrane Science', Vol. 9 (Eds D.A.Cadenhead, J.F. Danielli and M.D. Rosenberg),Ch. 1., Academic Press, New York, 1975

22. Kapoor, A., Ritter, J.A., and Yang, R.T. *Langmuir* 1989, **5**, 1118

23. Bering, B.P., Dubinin, M.M., and Serpinsky, V.V. *J. Colloid Interface Sci.* 1966, **21**, 378

24. Wakasugi, Y., Ozawa, S., and Ogino, Y. *J. Colloid Interface Sci.* 1976, **79**, 399

25. Ozawa, S., Kusumi, S., and Ogino, Y. *J. Colloid Interface. Sci.* 1981, **56**, 83

26. Bustin, R.M., Clarkson, C., and Levy, J. In Proceedings of the 29th Newcastle Symposium, "Advances in the Study of the Sydney Basin", University of Newcastle, 1995, pp. 22-28

28. Bustin, R.M., Cameron, A.R., Grieve, D.A., and Kalkreuth, W.D. 'Coal Petrology: Its Principals, Methods and Applications, 2nd edition, Geological Association of Canada Short Course Notes, 3', 1985

29. Levy, J.H., Killingley, J.S., and Day, S.J. In Proceedings of the Symposium on Coalbed Methane Research and Development in Australia, v. 4, 1992, pp. 1-8

30. Handbook of Chemistry and Physics (David R. Lide, editor-in-chief) , 71st Edition, section **6**-82, 1990-1991

31. Yee, D., Seidle, J.P. and Hanson, W.B. In 'Hydrocarbons from Coal', AAPG Studies Geology #38 (Eds B.E. Law and D.D. Rice), 1993, pp. 203-218

32. Marsh, H. and Siemieniewska, T. *Fuel* 1965, **44**, 355

33. Brunauer, S. 'The Adsorption of Gases and Vapors', Vol 1., Princeton University Press, Princeton 1943

34. Koresh, J. *J. Colloid. Interface. Sci.*, 1982, **88**, 398

35. Dubinin, M.M. and Astakhov, V.A. In *Adv. Chem. Ser.* 1971, **102**, 69

36. Noggle, J.H. 'Physical Chemistry', 2nd edition, Harper Collins Publishers, 1989

37. Toda, Y., Hatami, M., Toyoda S., Yoshida, Y, and Honda, H. *Fuel* 1971, **50**, 187

38. Greaves, K.H., Owen, L.B., and McLennan, J.D. In Proceedings of the 1993 International Coalbed Methane Symposium, Tuscaloosa, May 17-21, 1993, pp. 151-160

CHAPTER 3

THE EFFECT OF PORE STRUCTURE AND GAS PRESSURE UPON THE TRANSPORT PROPERTIES OF COAL: A LABORATORY AND MODELING STUDY 1. ISOTHERMS AND PORE VOLUME DISTRIBUTIONS

3.1 ABSTRACT

The effect of coal composition upon pore structure and adsorption characteristics of four bituminous coals of the Cretaceous Gates Formation coal is investigated. All coals have multi-modal pore volume distributions as determined from low-pressure (< 127 kPa) nitrogen adsorption at 77 K, carbon dioxide adsorption at 273 K, and high-pressure (up to 200 MPa) mercury porosimetry. The individual lithotypes, however, differ in their pore volume distributions and adsorption characteristics. The dull coals (high inertinite, high ash content) have a greater percentage of mesoporosity and less microporosity than bright or banded bright coals (high vitrinite, low ash content) of the same rank. In addition, one banded bright coal has a greater amount of macroporosity than the other coals.

High-pressure (up to ~ 8 MPa) methane isotherms determined on dried and moisture-equilibrated coals, and carbon dioxide isotherms (up to ~ 5 MPa) determined on dried coal at 303 K, show that bright coals tend to sorb more gas than dull coals. The Dubinin-Astakhov equation provides a better fit to coal gas isotherm data, particularly for carbon dioxide, than the conventionally used Langmuir equation. There is a linear correlation between high-pressure methane and carbon dioxide Langmuir volumes and

Dubinin-Radushkevich micropore volumes, indicating that micropore volume is a primary control upon high-pressure gas adsorption.

3.2 INTRODUCTION

Knowledge of coal adsorption characteristics and pore structure is useful for a variety of different applications including the prediction of coal gas outbursts in coal mines, the economic recovery of natural gas from coal seams, and characterization of coals as a pre-cursor for activated carbons. Recent studies[1-4] have shown that pore structure has an important effect upon methane gas transport through the coal matrix.

Coal is a complex polymeric material with a complicated porous structure that is difficult to classify. Previous studies[5-8] have used traditional gas adsorption methods and helium and mercury porosimetry in an attempt to determine the pore volume distribution and total porosity of coal. Gan *et al.*[5] demonstrated that pore volume distribution is dependent upon the rank of coal. In the Gan *et al.* study, total pore volumes were divided into: micropores (0.4 – 1.2 nm), transitional pores (1.2 – 30 nm), and macropores (30 – 2960 nm). The current study utilizes the IUPAC classification[9]. Lower-rank coals (carbon content < 75%) contain mainly macropores, coals in the 76 – 85% fixed carbon content range contain mainly micro- and transitional pores, and high rank coals (carbon content > 84%) contain mainly micropores.

Some studies have focussed upon determining the microporosity and micropore distributions of coal using carbon dioxide gas adsorption[10-13]. The proportion of microporosity in coal samples is believed to be an important controlling factor upon the

adsorption of methane. Carbon dioxide isotherms, usually measured at 273 and 298 K, are useful in determining coal micropore volumes and surface areas, because carbon dioxide gas is able to access the finest porosity at these temperatures. Nitrogen gas at 77 K is generally not considered to have access to the finest microporosity of coal owing to the activated diffusion effect and/or pore shrinkage[14] at low temperatures. Possible complications arising from the use of carbon dioxide include specific interaction between coal and carbon dioxide due to the large quadrupole moment of carbon dioxide, and coal swelling during adsorption.

Confusion still exists about the effect of coal type upon gas adsorption capacity of coal. Lamberson and Bustin[15], who studied methane adsorption upon moisture-equilibrated coals of varying petrographic composition, have shown that methane gas adsorption, on a mineral matter-free basis, generally increases with an increase in vitrinite content. Levine *et al.*[16], have shown that the methane adsorption capacity of dry coal, determined using the gravimetric method, is greater for vitrinite concentrates than for intertinite concentrates. Bright coals of the Bowen Basin, Australia, were shown to have a greater methane adsorption capacity than dull coals of the same rank[16] and methane capacity was positively correlated with vitrinite content for moisture-equilibrated coals of the Sydney Basin[17]. Ettinger *et al.*[18], however, reported that gas yields increase with fusain content. Faiz *et al.*[8] noted that dry, ash-free Langmuir volumes show a slight negative correlation with inertinite content, but stated that the correlation may be masked by rank variations between samples. It is generally accepted that gas adsorption decreases with an increase in ash content in coal samples.

The purpose of the current study is to determine the (equilibrium) adsorption/desorption properties and pore volume distributions of four lithotypes from the Cretaceous Gates Formation of Northeast B.C. in order to assess the effect of these properties upon adsorption rate behaviour (the subject of Part 2). The current study utilizes an integrated approach to the characterization of pore volume distribution for coals of varying (organic and mineral) composition, similar to the approach used by Gan *et al.*[5] and Unsworth and Fowler[7], to determine the effect of pore volume distribution upon high-pressure adsorption methane and carbon dioxide isotherms. Ambiguities regarding the effect of coal type and pore volume distribution upon high-pressure methane and carbon dioxide will be addressed. The results of this study will be incorporated into a new numerical matrix gas transport model, developed in Part 2. Additionally, these results will lead to a better understanding of the factors controlling the release of methane or coalbed gas from the coal matrix, and hence will be applicable to the prediction of gas transport and outbursting phenomena.

3.3 METHODS

3.3.1 Sample Location and Preparation

Four medium-volatile bituminous coal lithotype samples from the Lower Cretaceous Gates Formation of northeastern British Columbia were chosen for this study. The samples were crushed by hand (stage crushed) to pass through a 4 mesh (4.75 mm) sieve and four sub-samples were obtained. A -4 mesh fraction was retained and the other sub-samples were crushed to pass through an 8 (2.38 mm), 20 (0.841 mm), and 60 (0.250

mm) mesh sieve. Only the -4 and -60 mesh fractions were used for isotherm analysis. The -60 mesh fraction was also utilized for proximate (ash and moisture) and petrographic analysis. Petrographic analysis was performed using manual point counts on polished pellets[19].

A seive analysis was performed on the –4 mesh coals in order to determine the mean particle size to be used in adsorption rate analysis (Part 2). For all coals, greater than 90 wt % was collected between seive size diameters 2.38 mm and 4.75 mm (Figure 3-1). Two estimates of mean particle size were used: the harmonic mean[20], and the arithmetic average of the upper and lower limits of the most frequent fraction. Using the latter estimate, the mean particle radius for all coals is 1.84 mm.

3.3.2 Low-pressure Isotherm Analysis

Low-pressure (< 0.127 MPa) isotherm analyses were performed on a Micromeritics ASAP 2010 ® volumetric gas adsorption apparatus. Carbon dioxide equilibrium isotherms were collected at 273 K (ice/water bath) for –4 and -60 mesh fractions of the lithotype samples. Samples were evacuated at 100°C for at least 12 hours on the apparatus until a pressure of < 0.25 Pa was reached. Other details of isotherm analysis are given elsewhere[13]. The Dubinin-Radushkevich (D-R) equation[21] was used to obtain micropore volumes. Coefficients of variation for D-R micropore volumes are less than 5% based upon repeat analysis of –60 and –4 mesh splits of the coals.

Nitrogen (77 K) adsorption/desorption isotherms were collected on the – 60 mesh splits. Difficulty in achieving equilibrium was encountered with the – 4 mesh splits, likely due to the extremely slow diffusion rates of nitrogen gas at 77 K, therefore the

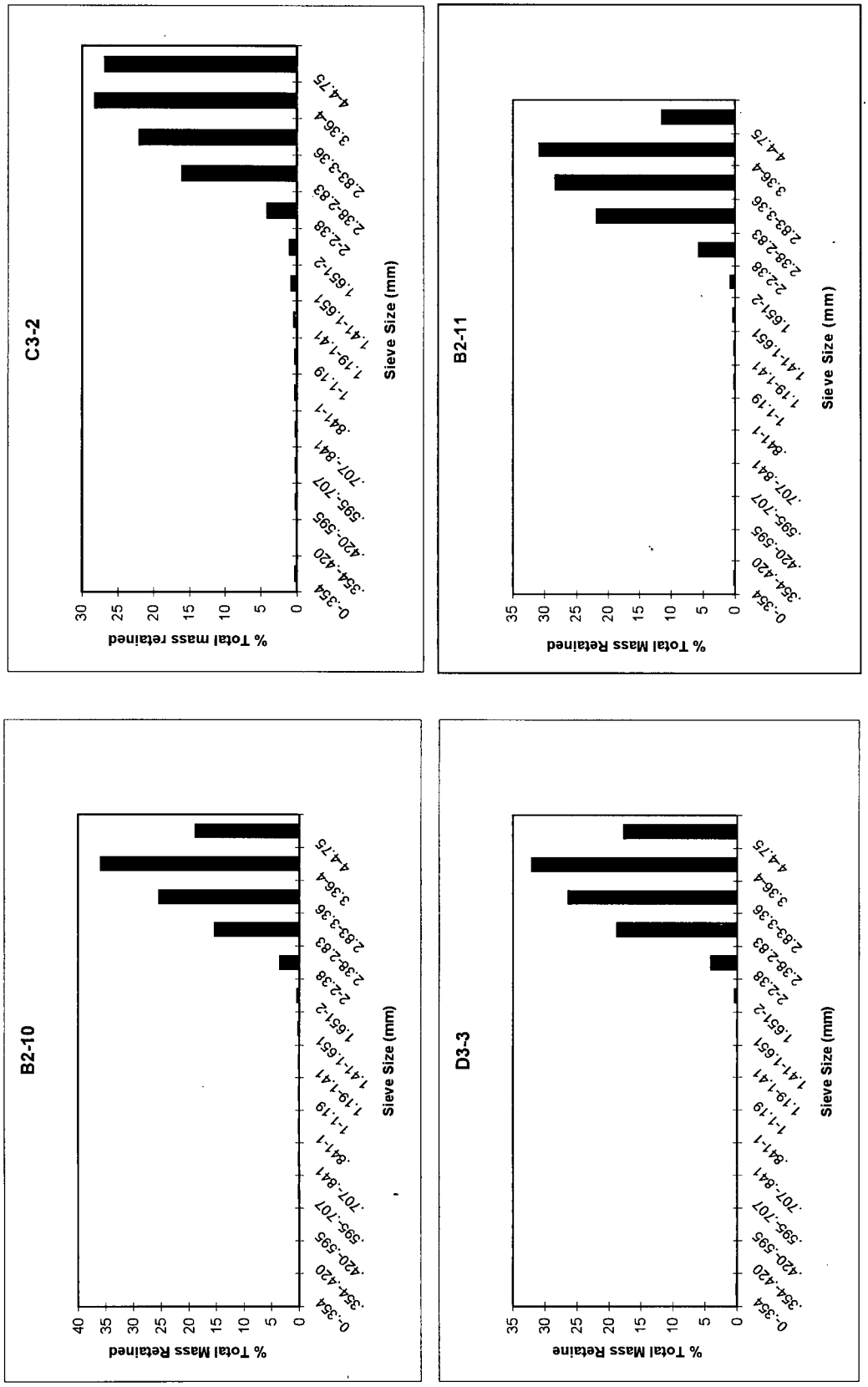

Figure 3-1. Particle size analysis for Gates coals.

coarser particles were not used for nitrogen adsorption work. The BET equation[22] was used to obtain surface areas from the nitrogen isotherm data. BET surface areas were calculated from data in the 0.06-0.2 relative pressure range. Barrett, Joyner, Halenda (BJH) theory [23] was used to obtain mesopore (pore diameter 2-50 nm) distributions from the desorption branch of the nitrogen isotherm. BJH cumulative and differential pore volume distributions were determined for the desorption branch of the isotherm. Coefficients of variation for mesopore volumes, determined from repeat runs of several samples, were less than 9%.

3.3.3 High-Pressure Isotherm Analysis

High-pressure methane (up to ~ 8 MPa) and carbon dioxide (up to ~ 5 MPa) 303 K isotherms were obtained using a static volumetric adsorption apparatus similar to that described by Mavor *et al.*[24].

Samples were dried in an oven at 110°C overnight and then evacuated at isotherm temperature for 24 hours. In addition, methane isotherms were determined on moisture-equilibrated coals. Equilibrium moisture (at 96-97% relative humidity) was achieved using a procedure similar to that described by Levy *et al.*[25].

Equilibrium at each isotherm point is assumed to have been reached if the pressure reading was stable (ΔP=0.000 MPa) for about 7 hours (400 minutes) for the – 4 mesh coals. Much less time was required for equilibrium for – 60 mesh coals. For the adsorption isotherm, a program, as described in Levy *et al.*[26], was used to automate data collection. Volume adsorbed calculations are performed according to the procedure described by Levy *et al.*[26].

The isotherm equation used to model equilibrium high-pressure gas adsorption data are that proposed by Langmuir[27]. The equation may be expressed for plotting purposes as:

$$\frac{P}{V} = \frac{P}{V_L} + \frac{P_L}{V_L} \qquad (1)$$

A linear regression is performed for *P/V vs. P* plots to obtain the Langmuir constants. The Langmuir equation was used to model equilibrium isotherm data for adsorption rate modeling (Part 2). The coefficient of variation of the Langmuir volume (V_L) and Langmuir pressure (P_L), determined from repeat measurements of methane isotherms on dried – 4 and – 60 mesh coals, were less than 6% and 17%, respectively.

Alternatively, the Dubinin-Astakhov equation may be used to model high-pressure adsorption data[28]. The D-A equation, written for plotting purposes, is:

$$\log W = \log W_o - D\left(\log P_o / P\right)^n$$

where W is the amount of gas adsorbed, W_0 is the micropore volume, P_0 is the saturation vapour pressure, and n is the Astakhov exponent. Procedures for determining pseudo-saturation vapour pressure above critical temperature are described elsewhere[28]. The three parameters W_0, D, and n were optimized using a least squares routine coupled with a multiparameter optimization algorithm in MATLAB ®.

3.3.4 He and Hg porosimetry

Helium densities were determined using helium expansion at 30°C on the high - pressure volumetric adsorption apparatus. A split of about 2 g was taken from the isotherm samples (-4 mesh) and used for mercury porosimetry analysis, on a Micromeritics Poresizer 9320 ®. Samples were evacuated at 110°C for at least 3 hours prior to analysis and then evacuated on the instrument for 15 hours until a stable pressure was reached.

As mentioned by Gan *et al.*[5], there is some uncertainty about what is the minimum pressure required to fill interparticle voids when powders are used in mercury density determination. For a – 20 mesh particle size, a pressure of about 0.41 MPa was required to fill the interparticle void volume[29]. The pressure required to fill the interparticle void space may be approximated by obtaining mercury intrusion volumes with pressure for nonporous materials of the same particle size (such as glass beads)[5]. In the current study, the –4 mesh coal particle density was determined using the following procedure: a known mass of mercury was injected at near ambient pressures into a penetrometer of known volume containing the coal of known mass; the volume of mercury injected was determined from its mass and the density of mercury at the analysis temperature; the difference between the injected mercury volume and the calibrated penetrometer volume was taken as the total particle volume of the coals; the coal (particle) density was determined from the coal mass and total particle volume. In this analysis, the volume of voids between particles is assumed to be filled at near ambient pressures. Negligible amounts of mercury were intruded below 0.207 MPa (~30 psia) for all samples therefore indicating that the interparticle void space had probably been filled

at pressures < 0.207 MPa. The coefficient of variation for Hg density measurements is less than 2% based upon repeated analysis of different (-4 mesh) sample splits.

Mercury intrusion data was collected up to a maximum pressure of about 200 MPa (30,000 psia). A contact angle of 130°[5] and surface tension of 485 dyn/cm was used in the Washburn equation to determine pore size distributions[21].

3.4 RESULTS AND DISCUSSION

3.4.1 Coal Petrographic Data

The selected Gates coals vary markedly in their maceral and ash contents, and therefore represent a wide range in composition (Table 3-1). The four coals represent three different lithotypes: bright (C3-2); banded bright (B2-11) and dull (B2-10 and D3-3). Two coals (C3-2 and B2-11) have high vitrinite (> 50 volume %, mineral matter-free) and low ash (< 20 weight %) contents, whereas samples B2-10 and D3-3 have low vitrinite (< 50 %) and high ash (> 20 %) contents.

3.4.2 Low Pressure Carbon Dioxide Adsorption Isotherm Data

Low-pressure carbon dioxide isotherms (273 K) (Figure 3-2) demonstrate that the high vitrinite, low ash coals (C3-2 and B2-11) have higher adsorbed carbon dioxide volumes than the low vitrinite, high ash coals (D3-3 and B2-10) on a dry, mineral matter containing (mmcb) basis. Carbon dioxide micropore volumes obtained for the – 60 mesh coals, using the D-R equation, are given in Table 3-2. D-R micropore volumes obtained from –4 mesh splits of the coals are also given in Table 3-2. Close agreement between

Table 3-1. Maceral composition (volume %, mmf), moisture (weight %, air-dry), and ash yields (weight %, dry-basis).

Sample	*Structured Vitrinite	Desmocollinite	Semifusinite	Fusinite	**Other Inertinite	Liptinite	Moisture (%)	Ash (%)
C3-2	75	23	1	1	-	-	0.5	12.7
B2-11	29	30	33	5	3	-	0.5	3.3
D3-3	20	30	23	-	27	-	1.2	46.7
B2-10	13	28	49	3	6	1	0.3	29.7

* *Includes telocollinite and telinite.*

** *Includes macrinite and inertodetrinite.*

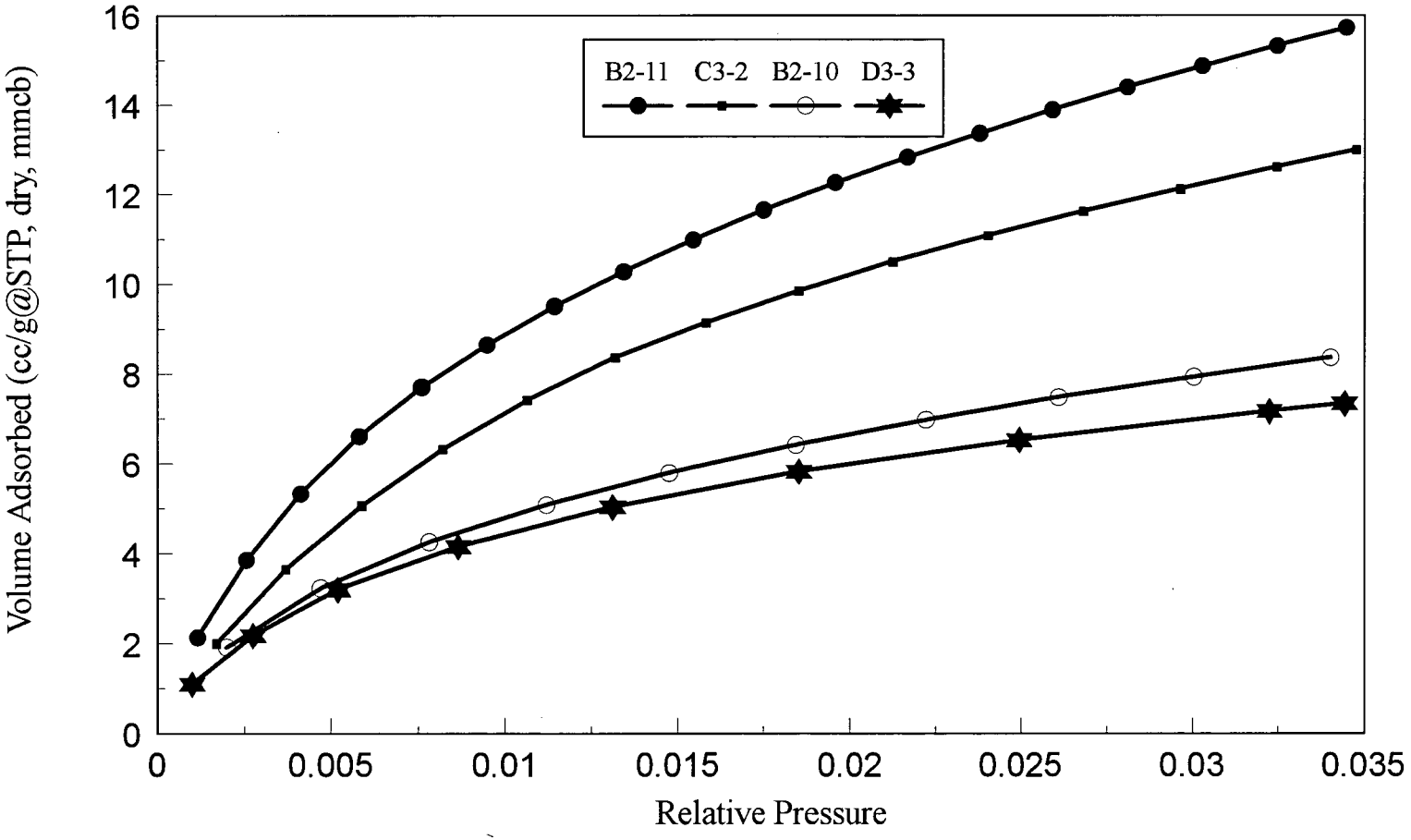

Figure 3-2. 273 K low-pressure carbon dioxide isotherms obtained from - 60 mesh splits.

Table 3-2. Surface areas and micro/mesopore volumes of coals.

Sample	BET s.a. (m^2/g, dry, mmcb)	BET s.a. (m^2/g,daf)	*D-R mic.v. (cm^3/g, dry, mmcb)	*D-R mic.v. (cm^3/g,daf)	**D-R mic.v. (cm^3/g, dry, mmcb)	BJH mes. v. (cm^3/g, dry, mmcb)	BJH mes. v. (cm^3/g,daf)
C3-2	0.7 (1)	0.8	.049	.057	N/A	0.0012 (1)	0.0014
B2-11	0.7 (3)	0.7	.055	.057	.054	0.0015 (3)	0.0015
D3-3	2.7 (3)	5.0	.025	.046	.027	0.0041 (3)	0.0078
B2-10	2.2 (1)	3.1	.028	.040	.027	0.0058 (1)	0.0082

* *Determined for – 60 mesh coal*
** *Determined for – 4 mesh coal*

Table 3-3. Densities and total pore volumes of (-4 mesh) coals. Numbers in parenthesis indicate number analyses performed.

Sample	Hg Density (g/cm^3, dry, mmcb)	Hg Density **(g/cm^3, daf)	He Density (g/cm^3 ,dry, mmcb)	He Density (g/cm^3, daf)	*Total Pore Volume (cm^3/g, dry, mmcb)	*Total Pore Volume (cm^3/g, daf)
C3-2	1.36 (1)	1.27	1.40 (3)	1.30	.021	.024
B2-11	1.28 (2)	1.26	1.35 (3)	1.33	.043	.045
D3-3	1.75 (2)	1.34	1.80 (3)	1.40	.016	.030
B2-10	1.74 (3)	1.51	1.81 (3)	1.59	.023	.032

$$*V_T = \left(\frac{1}{\rho_{Hg}} - \frac{1}{\rho_{He}}\right)$$

** assume ash density = 2.7g/cc

the values obtained for –60 and –4 mesh coals indicate that the splits are relatively homogeneous and that particle size has a negligible effect upon micropore volumes. The banded bright and bright coals B2-11 and C3-2 have a greater micropore volume (.057 cc/g, daf) than the dull coals D3-3 and B2-10 (.046 and .040 cc/g, respectively), which is consistent with previous studies[15,13]. Such results are attributed to a greater amount of microporosity in vitrinite-rich samples.

3.4.3 Low Pressure Nitrogen Adsorption Isotherm Data

Low-pressure nitrogen (77 K) isotherms (Figure 3-3) are Type IV according to the Brunauer, Deming, Deming and Teller classification[30]. The high ash, high inertinite coals display a greater amount of hysteresis than do the high vitrinite, low ash coals. Results are given here on a mineral-matter-containing basis (mmcb) as the contribution of entrained mineral matter to nitrogen adsorption is unknown. The hysteresis loop that terminates (desorption) at a relative pressure of ~ 0.45 is a Type H3, indicating slit-shaped pores[31]. The lack of closure of the hysteresis loop below a relative pressure of 0.45 may be due to swelling of the coal during adsorption[21].

Nitrogen BET surface areas (Table 3-2) are larger for the dull coals (> 2 m^2/g) than for the bright and banded bright coals (< 1 m^2/g). Gan *et al.*[5] similarly obtained nitrogen surface areas that were less than 1 m^2/g for some coals. Those authors[5] stated that nitrogen is probably not accessible to particulate minerals in the organic matrix of coal at the low temperatures.

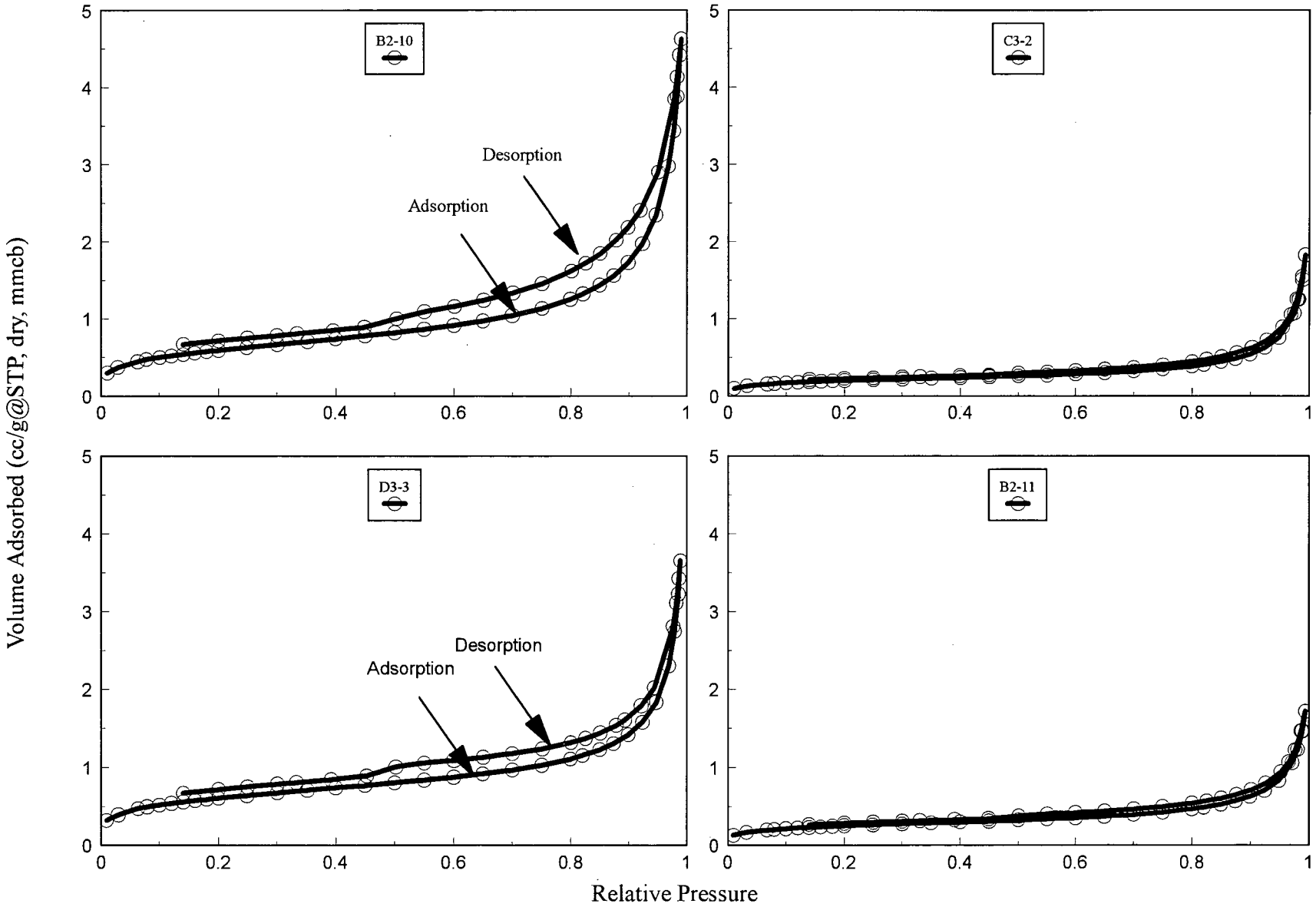

Figure 3-3. 77 K low-pressure nitrogen isotherms obtained for - 60 splits.

The dull coals have a greater amount of mesoporosity than the bright and banded bright coals, as evidenced by the cumulative pore volume plots (Figure 3-4a) and BJH mesopore volumes (Table 3-2). All samples have a pore volume distribution peak at around 4 nm (Figure 3-4b). A peak in this size range may only indicate that finer pores are present and hence may be an artifact[21,7]. Sample B2-10 has an additional (minor) peak at about 13 nm.

3.4.4 He and Hg Porosimetry

Mercury and helium densities, and total pore volumes for all coals are given in Table 3-3. The total pore volumes of all coals are actually less than the D-R micropore volumes. This finding is not unusual; the data of Walker *et al.*[29] demonstrates that CO_2 micropore volumes (V_{CO2}) are greater than the total pore volume for some coals Unsworth *et al.*[7] found that V_{CO2} for inertinite-rich (> 50%) coals are larger than the volume in pores < 30 nm. Unsworth *et al.*[7] suggested that the discrepancy is due to preferential adsorption of CO_2 (perhaps on oxygen functionalities) causing some swelling to occur.

Due to the highly compressible nature of coal, and the possibility of opening otherwise closed porosity at high pressure, pore volume distributions obtained from mercury porosimetry must be viewed with caution[32]. This is especially true for pressures greater than 68 MPa (10,000 psi). Qualitative information may be obtained about the pore structure, however.

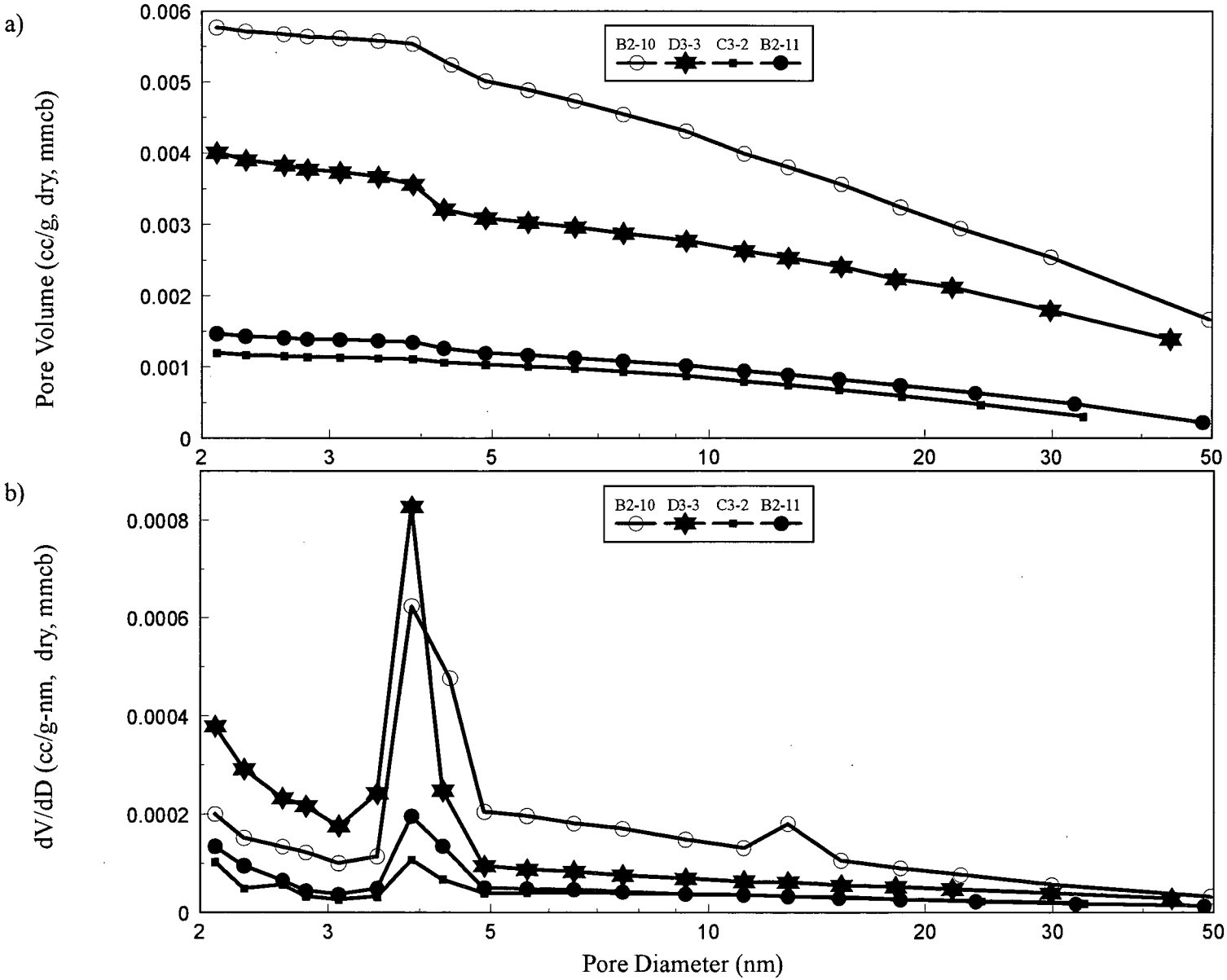

Figure 3-4. Cumulative desorption pore volume plots a) and pore size distributions b) obtained from nitrogen isotherms.

All Gates samples are multimodal with respect to pore volume distribution (Figure 3-5). Samples B2-11 and C3-2 have large peaks at around 1000 nm. Sample B2-11 appears to contain the greatest amount of macroporosity, possibly due to the large amounts of semifusinite in the sample.

The suite of coals chosen for the current study represents a broad range in pore structural characteristics. In particular, the high vitrinite, low ash coals have a greater percentage of microporosity than the low vitrinite, high ash coals. Conversely, the low vitrinite, high ash coals have a greater percentage of mesoporosity.

3.4.5 High Pressure Adsorption Isotherm Data

High-pressure methane isotherms collected for dried (Figure 3-6) and moisture equilibrated (Figure 3-7) – 4 mesh coals are essentially identical with the – 60 mesh coal isotherms, indicating equilibrium had been reached in the allotted time. The moisture-equilibrated –4 mesh C3-2 coal did not reach equilibrium in the alotted time and therefore this data is not used.

Considerably more carbon dioxide than methane is adsorbed on to the dry coals (Figure 3-6), which is consistent with previous studies[33-36]. Carbon dioxide isotherms have a slight inflection at high pressure, possibly a result of multilayer adsorption[36]. Significant enhancement of carbon dioxide adsorption at high pressures would have important implications for the injection of carbon dioxide into coal gas reservoirs at high pressures[36].

Although the Langmuir equation (1) was fit to the data in Figure 3-6, a better fit to the data was obtained by using the D-A equation (2) (Figure 3-8). This is particularly

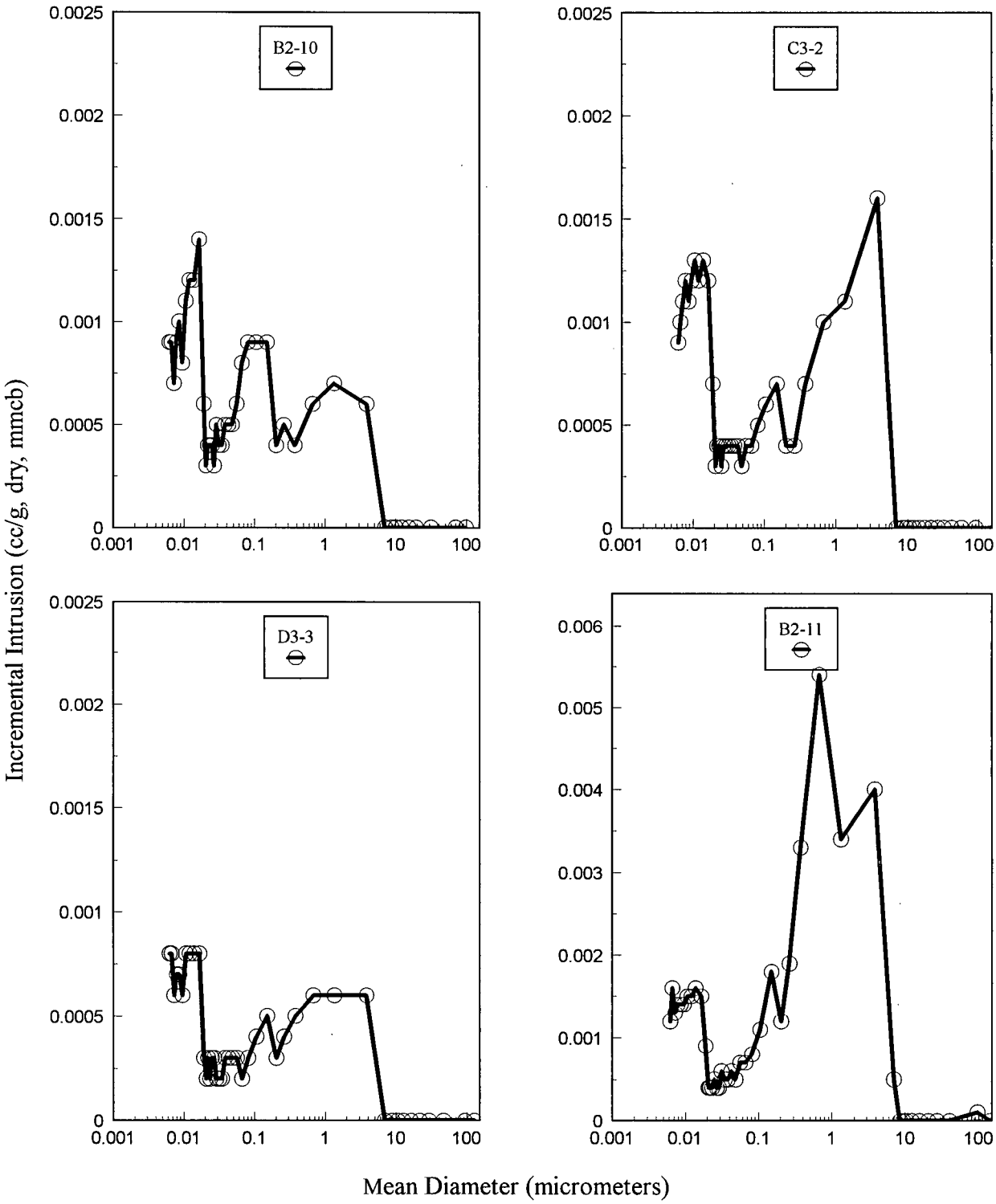

Figure 3-5. Incremental intrusion vs. diameter curves for -4 mesh splits. Note the scale change for sample B2-11.

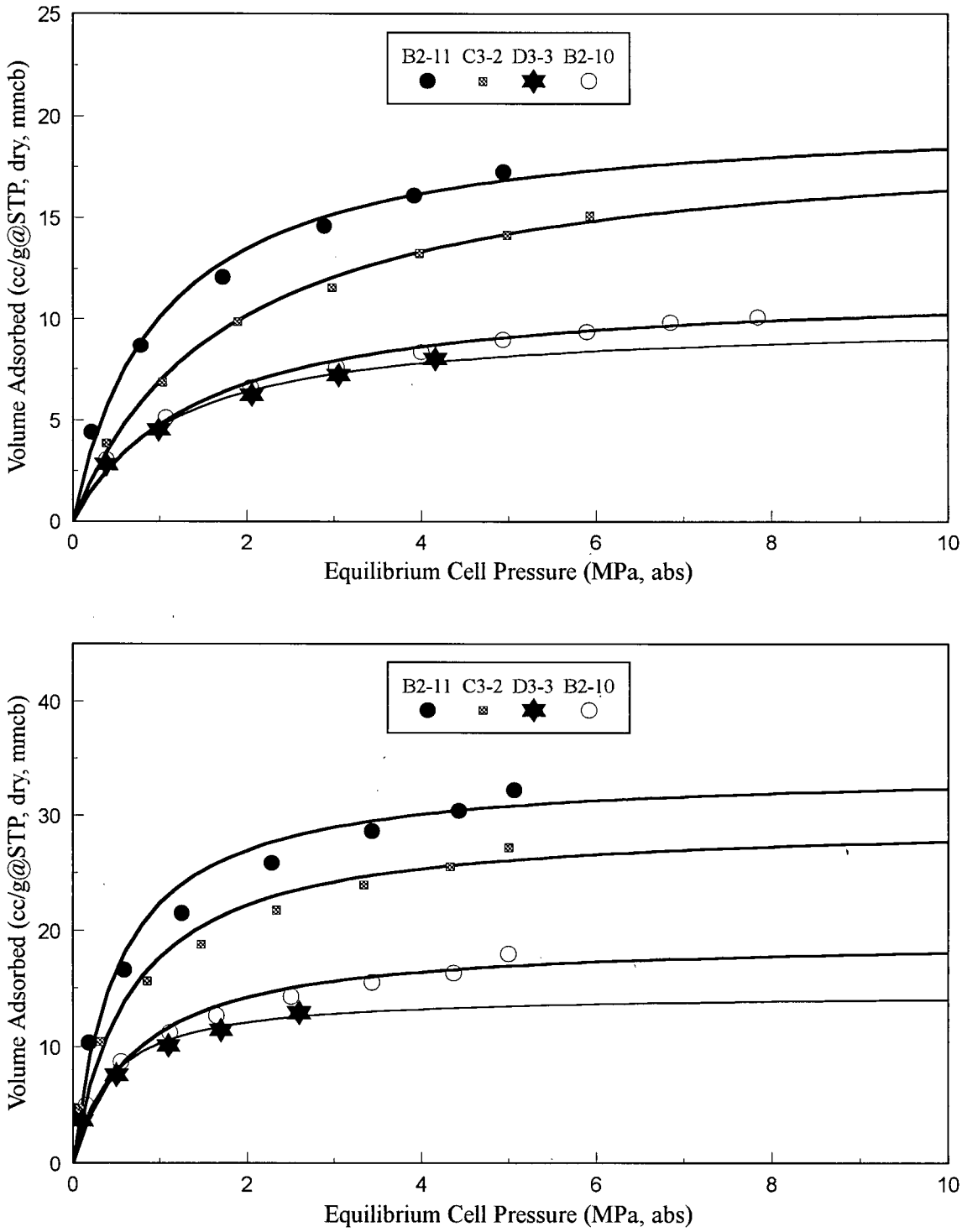

Figure 3-6. High pressure 303 K a) methane and b) carbon dioxide isotherms for dry -4 mesh splits. Lines are Langmuir fit to data.

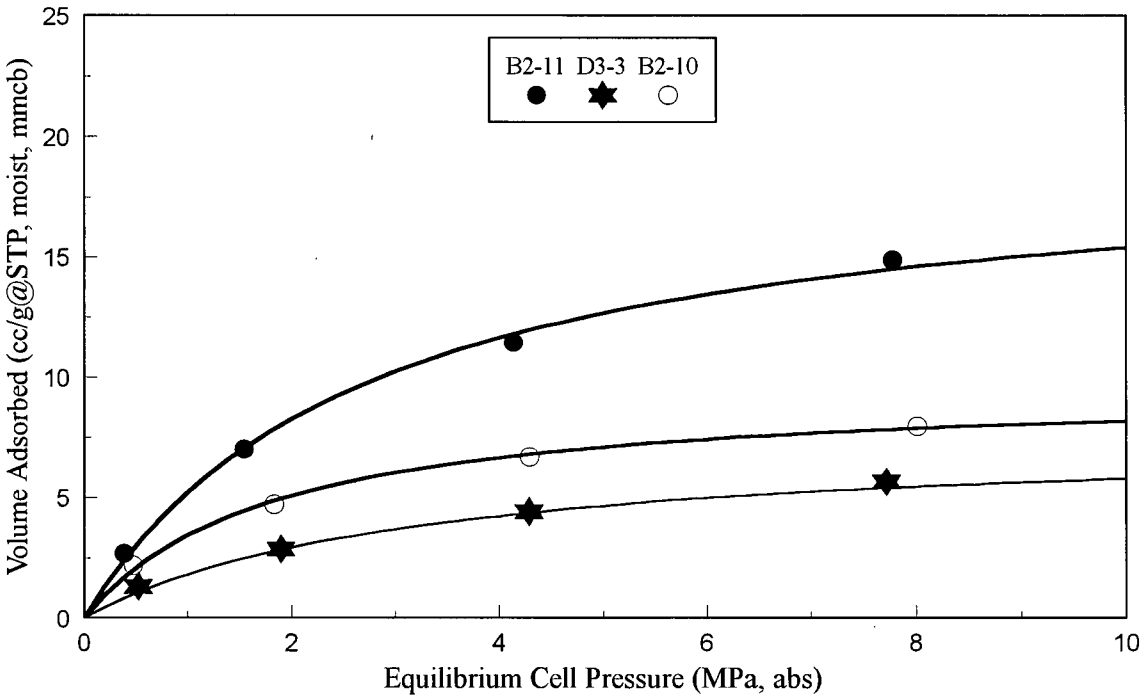

Figure 3-7. High pressure 303 K methane isotherms for moisture-equilibrated -4 mesh splits. Lines are Langmuir fit to data.

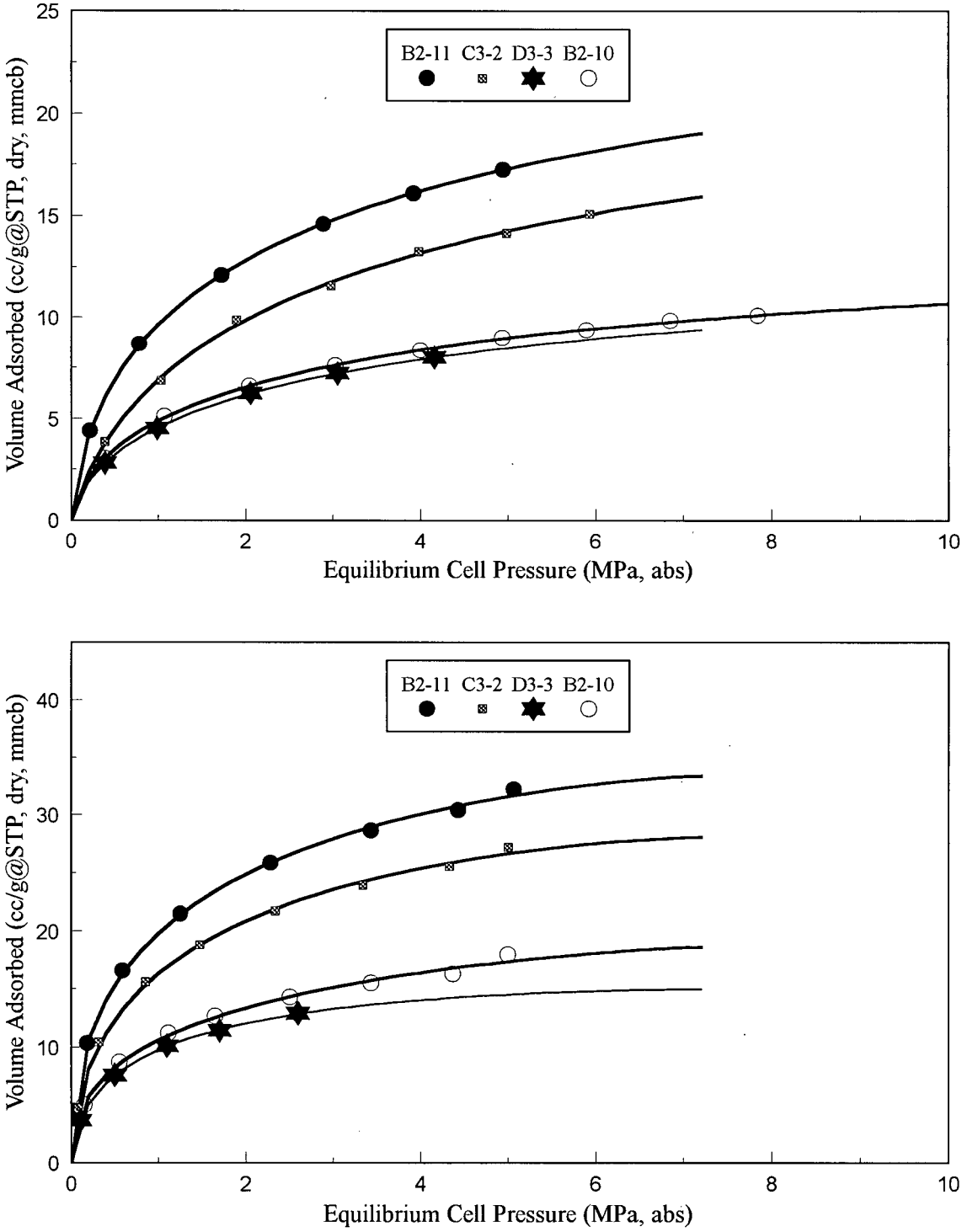

Figure 3-8. High pressure 303 K a) methane and b) carbon dioxide isotherms for dry -4 mesh splits. Lines are D-A fit to data.

true for the carbon dioxide data, where the average relative error[28] may be as large as 13 % for the Langmuir equation but is generally less than 2% for the D-A equation.

The high vitrinite/low ash coals have a higher adsorption capacity than the low vitrinite/high ash coals for both methane and carbon dioxide (Table 3-4, Figure 3-6). If the results are plotted on a dry, ash-free basis (Figure 3-9), the high vitrinite coals still sorb more methane and carbon dioxide, but there is less separation than for isotherms plotted without correcting for ash content. Previous studies[15] have shown that, although gas adsorption tends to increase with an increase in vitrinite content, the highest sorbing coals do not have the highest vitrinite content but have a mixture of vitrinite and inertinite. This appears to be the case for the current suite of samples; sample B2-11 has the highest adsorption capacity, but does not have the highest vitrinite content. As suggested by Lamberson and Bustin[15], semifusinite may also contribute substantially to the adsorption capacity of some coals.

3.4.6 Towards a Pore Structural Model for Adsorption Rate Analysis

Some general observations may be made regarding the pore structure of different lithotypes despite the difficulties of obtaining a quantitative evaluation of the pore volume distribution of coals from gas adsorption/mercury porosimetry. All the studied coals are multimodal with respect to pore volume distribution, but have varying proportions of micro-, meso-, and macroporosity. In particular, bright and banded bright coals have a greater micropore volume than dull coals of equivalent rank, whereas dull coals have a greater proportion of mesopores, as evidenced by nitrogen isotherm

Table 3-4. Langmuir parameters for high-pressure methane and carbon dioxide isotherm data. Langmuir volumes reported on a moist, mineral matter-containing basis.

Sample	*CH_4 on Dry Coal		**CH_4 on Wet Coal		**CO_2 on Dry Coal	
	V_L (cm^3/g, STP)	P_L (MPa)	V_L (cm^3/g, STP)	P_L (MPa)	V_L (cm^3/g, STP)	P_L (MPa)
C3-2	18.04 (3)	1.444 (3)	-	-	29.59 (1)	0.672 (1)
B2-11	20.51 (3)	1.043 (3)	19.74 (1)	2.719 (1)	34.05 (1)	0.525 (1)
D3-3	9.09 (2)	0.986 (2)	7.63 (1)	2.877 (1)	14.62 (1)	0.418 (1)
B2-10	11.10 (3)	1.191 (3)	9.67 (1)	1.806 (1)	19.38 (1)	0.727 (1)

* *First six points on isotherm (up to 5 MPa) were used in Langmuir regression for comparison*
** *All points on isotherm used in Langmuir regression*

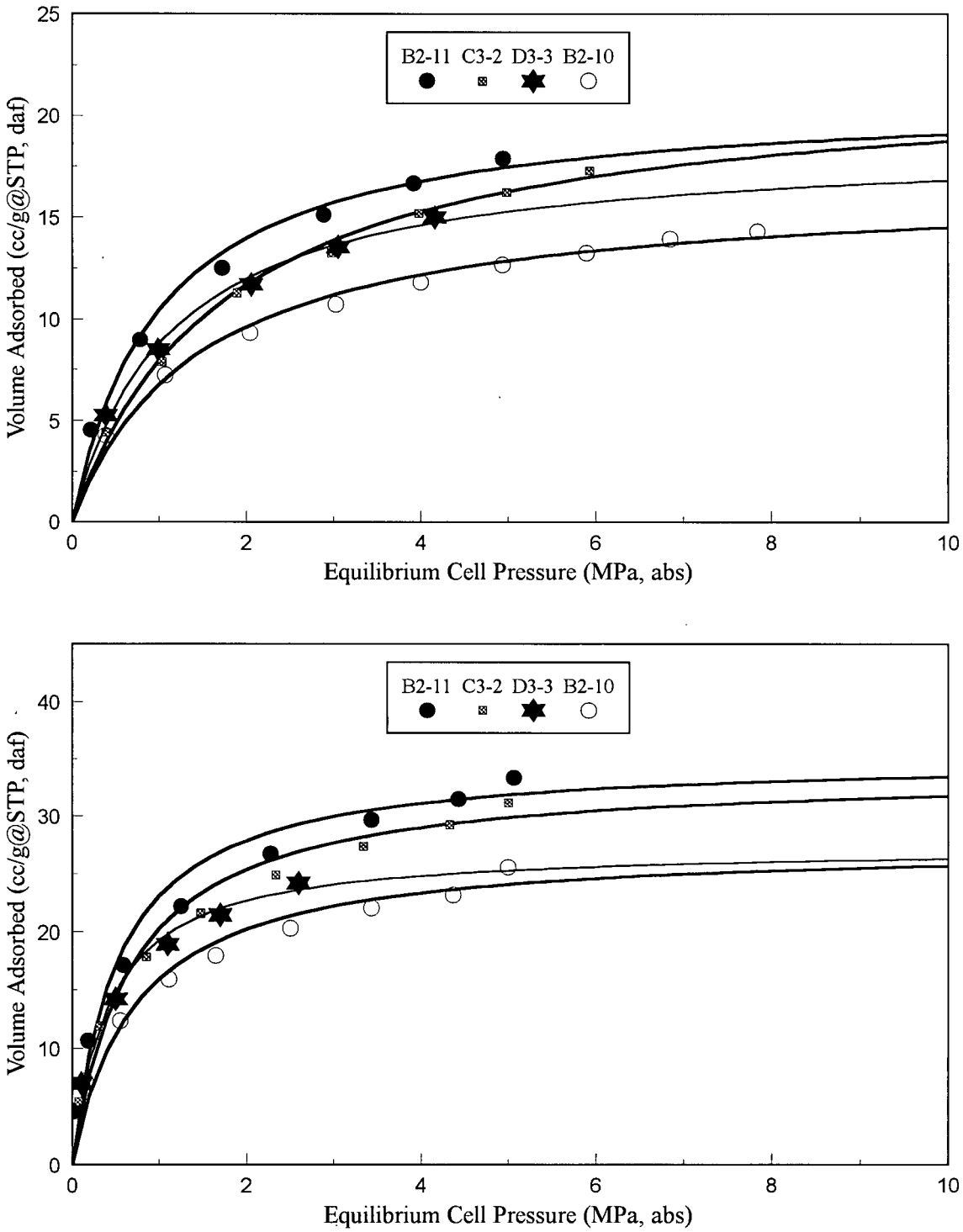

Figure 3-9. High pressure 303 K a) methane and b) carbon dioxide isotherms for dry -4 mesh splits. Lines are D-A fit to data.

hysteresis loops, and an estimation of mesopore volume from BJH theory. Mercury porosimetry indicates that although all coals have large pore volume distribution peaks in the macropore range, one coal, B2-11, has a much greater amount of macroporosity.

Although the findings of the current study are, in part, consistent with the Unsworth *et al.*[7] study for low rank bituminous coals who found that inertinite-rich coals generally have a higher mesoporosity than vitrinite-rich coals, it is probably not sufficient to state that vitrinite-rich coals have less macroporosity than inertinite-rich coal. Sample B2-11, which has > 50 % vitrinite (mmf), contradicts this trend. A number of factors including maceral and mineral composition and abundance affect pore volume distribution and the pore structure has been shown to be a function of rank[5].

The pore volume distributions may be used to predict the gas adsorption capacity of coal. Langmuir volumes for high-pressure methane adsorption on dry and moisture-equilibrated coal as well as carbon dioxide on dry coal are plotted against micropore volume (mmcb) in Figure 3-10. For each system, a linear increase in Langmuir volume, which is an estimate of total gas capacity, with micropore volume is observed, suggesting that micropore volume is the main control upon gas adsorption. Previous studies[38,25] have shown a similar trend for methane-coal systems, but it is obvious that micropore volume is also a control upon high-pressure carbon dioxide adsorption. Mesoporosity does not appear to have an important effect upon methane total gas capacity, although dull coals have a greater proportion of mesoporosity than bright and banded bright coals in this coal suite. The occurrence of an inflection in the high-pressure carbon dioxide isotherms, which could be attributed to the formation of multilayers in larger (meso) pores, may indicate that adsorption in mesoporosity is significant for carbon dioxide.

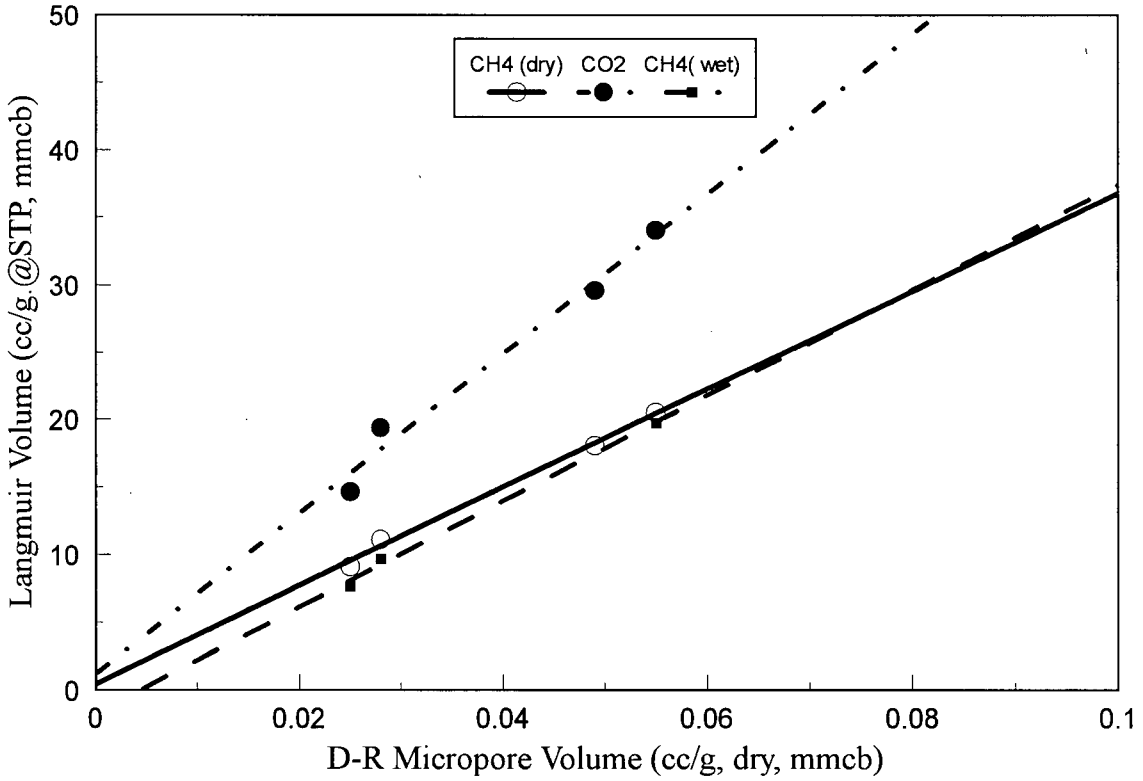

Figure 3-10. Langmuir volume versus D-R micropore volume (mmcb).

A comprehensive coal matrix gas transport model must account for many of the observations described above. Coal pore volume distribution, which varies with composition and rank, is typically multimodal, and therefore matrix transport models must describe transport in several pore systems. Equilibrium gas adsorption isotherms are non-linear, and must be accounted for in modeling gas adsorption rates. Micropore volume is the primary control upon high-pressure gas adsorption, and so most of the gas in coal may be assumed to be stored in the adsorbed form in microporosity. Meso- and macropores likely serve only as gas transport pathways, and little gas is stored in these pores in the adsorbed state, at least for methane. A new numerical model for describing matrix gas transport, which accounts for the above observations and is an extension of previous models, is developed in Part 2.

3.5 CONCLUSIONS

A variety of conventional adsorption/porosimetry analyses have been applied to four bituminous coal samples in order to determine the coal pore volume distribution and gas adsorption capacities. Pore volume distributions and gas adsorption capacities may reasonably be assumed to have an important effect upon gas transport properties of coal. Each analytical technique has some limitation in terms of either the accessibility of the adsorbate to the internal coal structure, complex interaction of the adsorbate with the coal, range of application, or physical distortion of the coal structure during analysis. In addition, problems with data interpretation exist[36]. The combination of gas adsorption/porosimetry, however, is useful in characterizing the properties of coal which

affect the gas adsorption and adsorption rate properties of coal, and hence the ultimate gas capacity and transport properties. The usefulness of combined analyses in terms of explaining the adsorption rate behaviour of coals of varying lithotype composition and hence pore structure, will become clear in the paper that follows.

The following conclusions have been made regarding the pore volume distributions and adsorption properties of the four coal lithotypes utilized in this study:

1) Bright and banded bright (high-vitrinite, low ash) coals have a greater micropore volume than dull (low vitrinite-high ash) bituminous coals of equivalent rank, as determined from low-pressure carbon dioxide adsorption. This finding is consistent with previous laboratory investigations.

2) Dull coals have a greater amount of mesoporosity than bright coals as assessed from nitrogen adsorption/desorption analysis. Nitrogen adsorption/desorption isotherms indicate a slit-shaped mesopore shape.

3) Mercury porosimetry shows that the coals have a multimodal pore volume distribution. The banded bright coal (B2-11) has a relatively large peak in the macropore range, possibly due to high amounts of semifusinite in the sample.

4) High-pressure methane and carbon dioxide isotherms illustrate that bright and banded bright coals adsorb more gas than dull coals. Correction of the isotherms to a dry-ash free basis yields the same general relationship, indicating that maceral type is a

control upon gas adsorption, but there is less of a discrepancy between coals. The Dubinin-Astakhov equation provides a better fit to the isotherm data than the conventionally used Langmuir equation.

5) High-pressure methane and carbon dioxide Langmuir volumes, used as an estimate of total gas capacity, are linearly correlated with Dubinin-Radushkevich micropore volumes, obtained from low-pressure carbon dioxide adsorption. This finding illustrates that micropore volume is the primary control upon gas adsorption in the Gates coals.

3.6 REFERENCES

1. Smith, D.M., and Williams, F.L. *Society of Petroleum Engineers Journal* 1984, **24**, 529
2. Smith, D.M. and Williams, F.L. In 'Coal Science and Chemistry', Elsevier Science Publishers B.V., Amsterdam, 1987, pp 381-403
3. Olague, N.E., and Smith, D.M. *Fuel* 1989, **51**, 1381
4. Beamish, B.B., and Crosdale, P.J. In Proceedings of the International Symposium cum Workshop on Management and Control of High Gas Emission and Outbursts, Wollongong, 20-24 March, 1995, pp. 353-361
5. Gan, H., Nandi, S.P., and Walker, P.L., Jr. *Fuel* 1972, **51**, 272
6. Parkash, S., and Chakrabartty, S.K. *Int. J. of Coal Geol.* 1986, **6**, 55
7. Unsworth, J.F., Fowler, C.S., Jones, L.F. *Fuel* 1989, **68**, 18
8. Faiz, M.M., Aziz, N.I., Hutton, A.C., and Jones, B.G. In Proceedings, Symposium on Coalbed Methane Research and Development in Australia, Townsville, Queensland, 1992, pp. 9-20
9. International Union of Pure and Applied Chemistry. *Pure Appl. Chem.* 1994, **66**,1739

10. Toda, Y., Hatami, M., Toyoda, S., Yoshida, Y., Honda, H. *Fuel* 1971, **50**, 187

11. Debelak, K.A., and Schrodt, J.T. *Fuel* 1979, **58**, 732

12. Amarasekera, G., Scarlett, M.J., Mainwaring, D.E. *Fuel* 1995, **74**, 115

13. Clarkson, C.R. and Bustin, R.M. *Fuel* 1996, **75**, 1483

14. Anderson, R.B., Bayer, J., and Hofer, L.J.E *Fuel* 1965, **44**, 443

15. Lamberson, M.N., and Bustin, R.M. *AAPG Bull.* 1993, **77**, 2062

16. Levine, J.R., Johnson, P., and Beamish, B.B. In Proceedings of the 1993 International Coalbed Methane Symposium, Tuscaloosa, May 17-21, 1993, pp. 187-195

17. Bustin, R.M., Clarkson, C., and Levy, J. In Proceedings of the 29th Newcastle Symposium, "Advances in the Study of the Sydney Basin", University of Newcastle, 1995, pp. 22-28

18. Ettinger, I., Eremin, I., Zimakov, B., and Yanovshaya, M. *Fuel* 1966, **45**, 267

19. Bustin, R.M., Cameron, A.R., Grieve, D.A., and Kalkreuth, W.D. 'Coal Petrology: Its Principals, Methods and Applications, 2nd edition, Geological Association of Canada Short Course Notes, 3', 1985

20. Perch, M. In 'Chemistry of Coal Utilization, Second Supplementary Volume' (Ed. M.A. Elliot), John Wiley and Sons Inc., New York, p. 943, 1981

21. Gregg, S.J., and K.S.W. Sing, K.S.W. 'Adsorption Surface Area and Porosity', 2nd edition, Academic Press, New York, 1982

22. Brunauer, S., Emmett, P.H., and Teller, E. *J. Am. Chem. Soc.* 1938, **62**, 1723

23. Barrett, E.P., Joyner, L.G., and Halenda, P.P. *J. Am. Chem. Soc.* 1951, **73**, p. 373

24. Mavor, M.J., Owen, L.B., and Pratt, T.J. Paper SPE 20728, presented at the 65th Annual Technical Conference of the Society of Petroleum Engineers, New Orleans, Louisiana, Sept. 23-26, 1990, pp.1-14

25. Levy, J.H., Day, S.J., and Killingley, J.S. *Fuel* 1997, **74**, 1

26. Levy, J.H., Killingley, J.S., and Day, S.J. In Proceedings of the Symposium on Coalbed Methane Research and Development in Australia, v. 4, 1992, pp. 1-8

27. Langmuir, I *J. Am. Chem. Soc.* 1918, **40**, p.1361

28. Clarkson, C.R., Bustin, R.M., and Levy, J.H. *Carbon* 1997, **35**, 1689

29. Walker, P.L., Jr., Verma, S.K., Rivera-Utrilla, J., and Davis, A. *Fuel* 1988, **67**, 1615

30. Brunauer, S., Deming, L.S., Deming, W.S., and Teller, E. *J. Am. Chem. Soc.* 1940, **62**, 1723

31. Sing, K.S.W., Everett, D.H., Haul, R.A.W, Moscou, L., Pierotti, R.A., Rouquerol, J., and Siemieniewska , T. *Pure and Appl. Chem.* 1985, **57**, 603

32. Mahajan, O.P., and Walker, P.L., Jr. In 'Analytical Methods for Coal and Coal Products' (Ed. C. Karr, Jr.), Academic Press, New York, 1978, p. 150

33. Stevenson, M.D., Pinczewski, W.V., Somers, M.L., and Bagio, S.E. SPE Paper 23026, presented at the SPE Asia-Pacific Conference, Perth, Western Australia, November 4-7, 1991, pp.741-755

34. Greaves, K.H., Owen, L.B., and McLennan, J.D. In Proceedings of the 1993 International Coalbed Methane Symposium, Tuscaloosa, May 17-21, 1993, pp. 151-160

35. Harpalani, S. and Pariti, U.M. In Proceedings of the 1993 International Coalbed Methane Symposium, Tuscaloosa, May 17-21, 1993, pp. 151-160

36. Hall, F.E., Zhou, C., Gasem, K.A.M., Robinson, R.L., Jr., and Yee, D. SPE Paper 29194, presented at the Eastern Regional Conference and Exhibition, Charleston, WV, November 8-10, 1994, pp. 329-343

37. Glaves, C.L., Davis, P.J., Gallegos, D.P., and Smith, D.M. *Energy and Fuels* 1988, **2**, 662

38. Smith, D.M., and Williams, F.L. In 'Coal Science and Chemistry', Elsevier Science Publishers, Amsterdam, 1987, p. 381

CHAPTER 4

THE EFFECT OF PORE STRUCTURE AND GAS PRESSURE UPON THE TRANSPORT PROPERTIES OF COAL: A LABORATORY AND MODELING STUDY 2. ADSORPTION RATE MODELING

4.1 ABSTRACT

The effect of coal composition, pore structure, and gas pressure upon methane and carbon dioxide gas transport in Cretaceous Gates Formation coal is investigated. Coal matrix gas transport models, which assume a homogeneous unimodal pore structure and linear adsorption isotherms, are not appropriate for modeling methane or carbon dioxide adsorption rates in all coal lithotypes.

A new numerical model for matrix gas diffusion/adsorption is developed and applied to methane and carbon dioxide volumetric adsorption rate data. The model accounts for non-linear adsorption in microporosity, a bimodal pore volume distribution, and time-varying gas pressure external to coal particles. Methane and carbon dioxide adsorption rate behaviour of bituminous coals with a multimodal pore volume distribution, such as dull or banded coals, are accurately captured with the current numerical model and an analytical solution which assumes a bimodal pore structure. Single parameter (diffusivity) models may be adequate for some bright coals. Careful consideration of coal pore structure is therefore required for accurate modeling of gas transport through the coal matrix.

Carbon dioxide numerical and analytical model diffusivities are larger than methane diffusivities obtained for dry coal. In addition, methane diffusivities obtained using the models for wet coal are smaller than model diffusivites obtained from dry coal.

The numerical model diffusivities, which are corrected for the effects of nonlinear adsorption, are larger than diffusivities obtained for analytical models for pore diffusion.

Methane and carbon dioxide gas analytical and numerical model effective diffusivities are sensitive to the starting pressure in a adsorption step. The pressure-dependence of the analytical solution diffusivities is likely due to the non-linearity of the adsorption isotherm. The effect of gas pressure upon diffusivities, obtained from the numerical model, indicate that the mechanism of gaseous diffusion is bulk diffusion.

Results of the current study have important implications for coalbed methane reservoir characterization, the determination of gas contents for gas resource calculations, gas production simulations, and the prediction of outbursting in coal seams.

4.2 INTRODUCTION

Knowledge of the transport properties of coal is important for the accurate prediction of gas and water production rates from coal seams. The mechanisms of storage and transport of gas and water in coal seams differ significantly from conventional gas reservoirs. It is commonly assumed that gas transport in coal may be analyzed at two scales: laminar flow through the macroscopic cleat, the natural fracture system of coal, and diffusion through the coal matrix bounded by cleat[1,2]. The flow through cleat is pressure-driven and may be modeled using Darcy's Law, whereas flow through the matrix is assumed to be concentration-driven and is modeled using Fick's Law. Significant gas storage, through the mechanism of physical adsorption, occurs mainly in the coal matrix, which acts as a source for gas production.

Recent modeling studies[3,4] have shown that adsorption time, which is dependent upon the coal matrix diffusion constant, has little effect upon long term gas production from coal seams, but has a marked effect upon short term production[4]. Gas transport through the coal seam fracture system, which is dependent upon relative permeability, is therefore considered to be a greater control upon long-term production. Production of gas from coal mine gob zones, on the other hand, may be more strongly controlled by the diffusional characteristics of the coal matrix[5].

Gas content determinations from conventional coal core often rely upon coal matrix gas transport modeling in order to obtain estimates of gas lost during core recovery[6]. For example, the Direct Method involves the solution of a partial differential equation describing isothermal diffusion following a step change in boundary concentration[6]. One of the main sources of error in determining diffusion coefficients and lost gas volumes is performing desorption at non-reservoir temperatures[7]. Further, the more gas that is lost during core recovery, the more difficult it is to accurately determine lost gas volumes and diffusivity.

The current study presents an experimental method and new numerical models for determining diffusivities from high-pressure methane and carbon dioxide adsorption/desorption volumetric isotherm data. The proposed method offers the advantage of simultaneous determination of the adsorption isotherm, from which the coal gas capacity can be determined, as well as adsorption rate data. These data may be obtained relatively rapidly as the experiments are performed on crushed coal particles. The isotherm data were used as input to new numerical models, which are developed and tested for coals of varying pore volume distribution and adsorption characteristics. Coals

of varying lithotype composition were chosen for this study as it is known that coal composition has an important control upon pore volume distributions[8,9] and gas adsorption characteristics[10-12]. Although Mavor *et al.*[13] obtained diffusion coefficients from adsorption isotherm data, the model proposed was not adequate for use at all pressure steps of the isotherm, or for coals with heterogenous pore structure.

Few studies[14,15] have reported experimentally-determined carbon dioxide diffusion parameters in coal even though carbon dioxide may be a significant component in coalbed gas[16]. In the current study, carbon dioxide adsorption rate data are reported and modeled under a variety of temperature and pressure conditions for Gates Formation coals in order to assess the factors controlling carbon dioxide coal matrix transport. This information will be important for the accurate evaluation of carbon dioxide injection strategies for the enhanced recovery of coalbed methane[17].

The method proposed here provides an alternative to gas canister desorption data for the determination of matrix transport parameters if these data are not available.

4.3 BACKGROUND

The conventional approach to modeling matrix gas transport is the application of the unipore diffusion model to transient volumetric[18-20] or gravimetric[21] adsorption or desorption data. The unipore model is based upon the solution to Fick's second law for spherically symmetric flow:

$$\frac{D}{r^2}\frac{\partial}{\partial r}\left(r^2\frac{\partial C}{\partial r}\right)=\frac{\partial C}{\partial t} \tag{1}$$

where r is radius, C is the adsorbate concentration , D is the diffusion coefficient and t is time. This form of the equation assumes that the diffusion coefficient is independent of concentration and location. Additional assumptions are:

1) isothermal conditions

2) homogenous pore structure

The solution to (1) for a constant surface concentration of the diffusing species may be expressed as follows[22]:

$$\frac{M_t}{M_\infty}=1-\frac{6}{\pi^2}\sum_{n=1}^{\infty}\frac{1}{n^2}\exp\left(-\frac{Dn^2\pi^2 t}{r_p^2}\right) \tag{2}$$

Where M_t is the total mass of the diffusing species, at time t, that has left the particle (i.e. desorption), and M_∞ is the total desorbed mass, and r_p is the diffusion path length. This relationship may be written for the case of gas desorbing from coal particles after a step change in surface concentration as:

$$\frac{V_t}{V_\infty}=1-\frac{6}{\pi^2}\sum_{n=1}^{\infty}\frac{1}{n^2}\exp\left(-\frac{Dn^2\pi^2 t}{r_p^2}\right) \tag{3}$$

Where V_t is the total volume of gas desorbed at time t, and V_∞ is the total adsorbed or desorbed volume. Equation (3) is commonly referred to as the "unipore" model solution.

A typical approach for obtaining the diffusion parameter D or D/r_p^2, referred to as the effective diffusivity[23], is to pressure up a leak-proof chamber containing dry or wet (crushed) coal sample with methane gas, allow the system to come to equilibrium, and then open the sample cell to atmospheric pressure. Both volumetric and gravimetric adsorption methods have been used to monitor the fraction of gas desorbed with time. Mavor *et al.*[13], using a volumetric method, obtained adsorption rate data between pressure steps of an adsorption isotherm.

The experimentally determined fraction of gas desorbed or adsorbed is usually plotted versus the square root of time and equation (3) may be curve-fit to the experimental data to obtain an estimate of D/r_p^2.

For $V_t / V_\infty < 0.5$, equation (3) may be approximated as:

$$\frac{V_t}{V_\infty} = 6\left(\frac{D_e t}{\pi}\right)^{1/2} \qquad (4)$$

where D_e is D/r_p^2. Smith and Williams[20] and Mavor *et al.*[13] have used equation (4) to obtain estimates of the effective diffusivity and the diffusion coefficient respectively. Mavor *et al.*[13] estimated the diffusion coefficient from the assumption of an average particle radius.

4.3.1 Problems with the Unipore Model

The concentration dependence of D/r_p^2 was investigated by Nandi and Walker[24] for three American coals. The diffusion parameter was shown to increase with average concentration of methane at high methane concentrations for two coals. Nandi and Walker[24] suggest that the concentration dependence of the diffusion coefficients is due to the non-linearity of the isotherm. Bielicki *et al.*[25] also were able to demonstrate a pressure-dependence of methane diffusivities measured using a volumetric apparatus. The conservation statement (equation 1) as written may be invalid for coal as it is assumed that the diffusion parameter is independent of concentration.

A more general form of the conservation equation that accounts for a concentration-dependent diffusivity is[22]:

$$\frac{1}{r^2}\frac{\partial}{\partial r}\left(r^2 D\frac{\partial C}{\partial r}\right) = \frac{\partial C}{\partial t} \tag{5}$$

where D is a function of concentration.

The effect of nonlinear adsorption upon the determination of diffusion/adsorption parameters has been investigated using a single parameter (effective diffusivity) diffusion /adsorption model[26] for single porous particles of various geometric shapes. Smith and Keller[26] noted that for spherical and slab geometries, the magnitude of the calculated kinetic parameters is different for the cases of nonlinear and linear adsorption, even though the adsorption rate curve shape may be similar. Further, the effects of nonlinear adsorption may become particularly pronounced when large step changes in gas

concentration are used during analysis, as is often the case in gravimetric adsorption rate experiments.

An additional problem with the unipore model is that it is not clear whether r_p, the diffusion path length, should be set equal to the equivalent (spherical) particle radius[19], although it is often assumed to be in the determination of micropore diffusion coefficients[13].

The unipore model has also been shown to be inadequate for coals with a heterogeneous pore structure[20].

4.3.2 Bidisperse Diffusion Model

Because some coals have a bimodal pore size distribution[27], Smith and Williams[20] adapted the bidisperse diffusion model developed by Ruckenstein *et al.*[28]. The model was formulated by considering the adsorbent to be a spherical particle (macrosphere) containing an assemblage of microspheres of uniform size. The model equations and analytical solution are provided elsewhere[28]. Linear isotherms and a step change in concentration of the adsorptive external to the particle are assumed in the Ruckenstein model. Solutions for a dual intraparticle resistance model with time varying boundary concentration are presented in Ma and Lee[29] and Lee[30].

Smith and Williams[20] found that the bidisperse diffusion model better described the entire desorption rate curve than the unipore model for some coals. The bidisperse model has also been successfully applied to Australian coal gravimetric transient adsorption data[31]. In particular, dull coal adsorption rate data are better fit with the bidisperse model than with the unipore model.

In a study by Bhatia[32], several transport models based on different interpretations of coal pore structure were compared. One such model compared was that of Ruckenstein *et al.*[28], neglecting concentration gradients in the macropores. The model was found to fit well the adsorption data of Nandi and Walker[19], however Bhatia[32] noted that some deviation of the model from the experimental data may be due to the assumption of linear isotherms.

4.3.3 Problems with the Bidisperse Model

The Ruckenstein model may be inadequate for application to high-pressure volumetric adsorption/desorption experiments. Firstly, the model assumes a step change in external (to sorbent particles) concentration of the diffusing species at time zero, and that this concentration remains unchanged with time. This assumption is not true for constant volume, variable pressure adsorption rate experiments as described by Mavor *et al.*[13], or as utilized here. Secondly, methane and carbon dioxide adsorption isotherms for bituminous coal are known to be nonlinear, and the application of linear adsorption models, is inadequate for most coals.

4.4 METHODS

4.4.1 Adsorption Rate Analysis

Adsorption rate data were collected during high-pressure methane and carbon dioxide adsorption isotherm analysis. During an adsorption step, gas is dosed into the reference cell, and three minutes are allowed for thermal equilibration. The gas is then

dosed into the sample cell for a few seconds and then dosing is stopped. The pressure in the sample cell is monitored until equilibrium is reached. For computer-controlled adsorption analysis, pressure data in the sample cell were collected at one second intervals for the first 300 seconds and then at increasing intervals (10, 60, and finally 3000 seconds) until equilibrium was achieved. Pressures were then converted to real gas densities using the Real Gas Law. Desorption analyses were performed manually following the same procedure as adsorption analysis. Pressure data were collected every 100 seconds.

One of the main problems with the variable pressure, constant volume adsorption technique is that time is required to attain thermal equilibrium in the cell after the gas has been adiabatically compressed into the cell. Thus, the first few seconds of adsorption data are unusable. To determine the length of time required to cool back to water bath temperature, an empty sample cell was filled with steel balls having a similar total solid volume as the coals used. An isotherm analysis at the same pressure steps as the coal samples was then performed to determine the length of time required for the pressure to drop due to re-equilibration with bath temperature. For the low-pressure steps, this time was less than 10 seconds, but became longer as the pressure was increased. This translates into an initial short time period where negative values of volume adsorbed are calculated. The "clock" was therefore started where the volume adsorbed passed through a value of zero.

Volume adsorbed and time data were also collected using an ASAP 2010 ® volumetric gas apparatus during low-pressure (273 K) carbon dioxide isotherm

collection. In this case, data were collected in 5 second increments for a total of 5000 seconds.

4.4.2 Isotherm and Adsorption Rate Model

The Langmuir isotherm equation[33] was used to model equilibrium high-pressure gas adsorption data for the dry and wet coals. The equation may be expressed for plotting purposes as:

$$\frac{P}{V} = \frac{P}{V_L} + \frac{P_L}{V_L} \tag{6}$$

A linear regression is performed for *P/V vs P* plots to obtain the Langmuir constants.

The adsorption rate model used in the current study assumes a bidisperse pore structure for coal (Figure 4-1), similar to the Ruckenstein[28] model. The Ruckenstein model assumes that the pore structure is bimodal and that the sorbent particle contains uniform radius (non-overlapping) microporous microspheres with the space between microspheres making up the macroporosity. The Ruckenstein model[28] also assumes linear isotherms in both macroporosity and microporosity and a step change in boundary concentration at the start of an adsorption/desorption step. Unlike the Ruckenstein model, the current numerical model assumes that no adsorption is occurring in the macroporosity (Part 1), nonlinear adsorption in microporosity, and a time-varying boundary pressure.

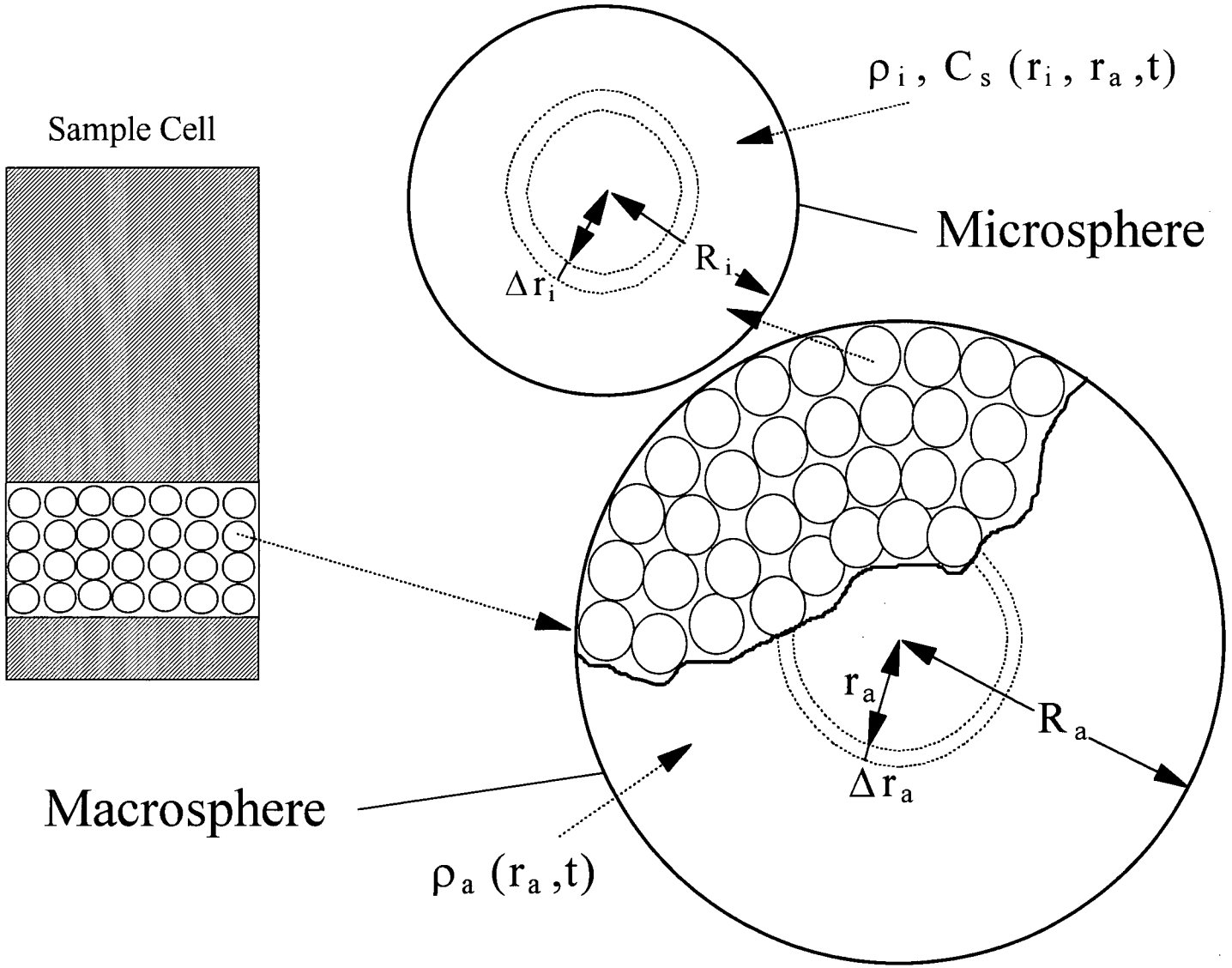

Figure 4-1. Conceptual model for bidisperse pore structure. The time and space dependent variables in the macro- and microspheres are indicated.

The assumptions for the current model may be summarized as follows:

1) Isothermal system.
2) Applicable transport equation is Fick's first law: $F=-D\nabla(\phi\rho)$, where F=mass flux (kg/m·s), D=diffusion coefficient (m^2/s), ϕ is porosity, and ρ is the gas phase density.
3) Gas phase densities can be expressed using the Real Gas Law: $\rho=MP/zRT$, where M is the molecular weight of the gas (kg/mole), P is gas pressure (Pascals), z is the compressibility factor, R is the universal gas constant (J/mole·K)
4) Transport mechanism is diffusion in both macro- and micropores.
5) Significant adsorption occurs only in the microporosity and adsorption isotherm can be described by the Langmuir equation.
6) Pores are incompressible.
7) Void volume is constant with time. No correction is made for void volume shrinkage during adsorption of gas.
8) The gas phase is mobile whereas the sorbed phase is immobile.
9) Coal particles are spherical in shape and uniform in size.

The macropore (7) and micropore (8) transport equations used in the current study are thus:

$$\frac{D_a}{r_a^2}\frac{\partial}{\partial r_a}\left(r_a^2\frac{\partial}{\partial r_a}(\phi_a\rho_a)\right)=\frac{\partial}{\partial t}(\phi_a\rho_a)+\frac{3(1-\phi_a)\phi_i}{R_i\phi_a}D_i\left(\frac{\partial\rho_i}{\partial r_i}\Big|r_i=R_i\right) \qquad (7)$$

$$\frac{D_i}{r_i^2}\frac{\partial}{\partial r_i}\left(r_i^2\frac{\partial}{\partial r_i}(\phi_i\rho_i)\right)=\frac{\partial}{\partial t}\left(\phi_i\rho_i+C_s\right) \qquad (8)$$

with initial conditions:

$$\rho_a(0, r_a) = \rho_o = \rho_i(0, r_i) \tag{9}$$

$$C_s(0, r_i) = C_{so} \tag{10}$$

and boundary conditions:

$$\frac{\partial}{\partial r_a}(\phi_a \rho_a) = 0 \text{ at } (t, 0) \tag{11}$$

$$\frac{\partial}{\partial r_i}(\phi_i \rho_i) = 0 \text{ at } (t, 0) \tag{12}$$

$$V v \frac{\partial \rho_a}{\partial t} = -N 4\pi R_a^2 D_a \phi_a \left.\frac{\partial \rho_a}{\partial r_a}\right|_{r_a = R_a} \qquad \text{at } (t, R_a) \tag{13}$$

$$\rho_i(t, R_i) = \rho_a(t, r_a) \tag{14}$$

At t=0, the gas density is assumed to be equal in the macro- and microspheres (equation 9) and the adsorbed phase concentration in microporosity is uniform for all microspheres (equation 10). A no (free gas) -flow internal boundary condition is used for the macrospheres and microspheres (equations 11 and 12). Equation (13) is a mass balance statement which expresses that the change in mass of gas stored in the interparticle void space is equal to the mass flux of gas across all (assumed spherical) particle (equal radius) boundaries for t>0. Equation (14) states that the gas density at the microsphere boundary is equal to the gas density in the macroporosity at r_a.

Introducing the dimensionless variables and parameters:

$$\rho_D = \frac{\rho}{\rho_o}, \qquad \gamma = \frac{r_i}{R_i}, \qquad \eta = \frac{r_a}{R_a}, \qquad \tau = \frac{D_a t}{R_a^2}$$

$$\alpha = \frac{R_a^2 D_i}{D_a R_i^2}, \qquad \beta = \frac{3(1-\phi_a)\phi_i}{\phi_a}\frac{R_a^2 D_i}{D_a R_i^2} = \frac{3(1-\phi_a)\phi_i}{\phi_a}\alpha$$

Equations (7) and (8) become:

$$\frac{1}{\eta^2}\frac{\partial}{\partial \eta}\left(\eta^2 \frac{\partial \rho_{Da}}{\partial \eta}\right) = \frac{\partial \rho_{Da}}{\partial \tau} + \beta \frac{\partial \rho_{Di}}{\partial \gamma}\bigg|_{\gamma=1} \tag{15}$$

$$\frac{\alpha}{\gamma^2}\frac{\partial}{\partial \gamma}\left(\gamma^2 \frac{\partial \rho_{Di}}{\partial \gamma}\right) = \frac{\partial}{\partial \tau}\left(\rho_{Di} + \frac{C_s}{\rho_o \phi_i}\right) \tag{16}$$

with initial conditions:

$$\rho_{Di}(0,\ \eta) = \rho_{Do} = \rho_{Di}(0,\ \gamma) \tag{17}$$

$$C_s(0,\ \gamma) = C_{so} \tag{18}$$

and boundary conditions:

$$\frac{\partial \rho_{Da}}{\partial \eta} = 0 \text{ at } (\tau, 0) \tag{19}$$

$$\frac{\partial \rho_{Di}}{\partial \gamma} = 0 \text{ at } (\tau, 0) \tag{20}$$

$$Vv\frac{\partial \rho_{Da}}{\partial \tau} = -N4\pi R_a^3 \phi_a \left.\frac{\partial \rho_{Da}}{\partial \eta}\right|_{\eta=1} \qquad \text{at } (\tau,\ \eta = 1) \tag{21}$$

$$\rho_{Di}(\tau,1) = \rho_{Da}(\tau,1) \tag{22}$$

The equations were discretized using the Integrated Finite Difference method[34] following a procedure similar to Kolesar *et al.*[35]. Numerical details are provided in Appendix VII.

For the bidisperse numerical model, a micropore volume must be provided as input. Micropore volumes were determined from the difference between the total pore volume, as determined from helium and mercury densities, and the macro/mesopore volume, as determined from nitrogen isotherms (see Part 1).

A simplified version of the bidiperse model, which assumes a unimodal pore volume distribution, was also applied to the adsorption rate data. The model equation and boundary conditions are expressed as follows:

$$\frac{1}{\gamma^2}\frac{\partial}{\partial \gamma}\left(\gamma^2 \frac{\partial \rho_{Di}}{\partial \gamma}\right) = \frac{\partial}{\partial \tau}\left(\rho_{Di} + \frac{C_s}{\rho_o \phi}\right) \tag{23}$$

with initial conditions:

$$\rho_{Do} = \rho_{Di}(0,\ \gamma) \tag{24}$$

$$C_s(0,\ \gamma) = C_{so} \tag{25}$$

and boundary conditions:

$$\frac{\partial \rho_{Di}}{\partial \gamma} = 0 \text{ at } (\tau, 0) \tag{26}$$

$$V v \frac{\partial \rho_{Di}}{\partial \tau} = -N 4\pi R_a^3 \phi \frac{\partial \rho_{Di}}{\partial \gamma}\bigg|_{\gamma=1} \text{ at } (\tau, 1) \tag{27}$$

where $\tau = \frac{D_i t}{R_a^2}$ and $\gamma = \frac{r_i}{R_a}$.

For the numerical models, the Langmuir equation is cast in the following dimensionless form:

$$\frac{\rho_D}{C_S} = \frac{\rho_{DL}}{C_S} + \frac{\rho_D}{C_{SL}}$$

where ρ_D is the dimensionless external gas density, ρ_{DL} is the Langmuir dimensionless gas density, analogous to the Langmuir pressure, and C_{SL} is the mass sorbed at infinite pressure. As with the Langmuir equation (6), a linear regression is performed for plots of ρ_D/C_S vs. ρ_D.

The unipore numerical solution, programmed in FORTRAN, was verified against analytical solutions for spherical diffusion presented in Crank[22]. The bidisperse numerical solution, also programmed in FORTRAN, was verified against the analytical solution (equation 11) presented in Ruckenstein *et al.*[28].

A least squares criterion was used to fit the model to the experimental gas density data. For the unipore model, the effective diffusivity (D_i/R_a^2) was adjusted to minimize the least squares function, using the Golden Section Search algorithm[36]. The bidisperse

numerical model parameters (D_a/R_a^2 , α, β) were optimized using the Downhill Simplex Method algorithm[36]. The least squares function utilized is:

$$L = \sum_{i=1}^{NP} \left(\rho_{\exp,i} - \rho_{calc,i} \right)^2$$

Where ρ_{exp}, and ρ_{calc} are the experimentally-determined and calculated gas densitities, respectively, external to the coal particles. Typically 3,000-10,000 timesteps were taken with the numerical model, and the model densities at each experimental real time step were determined from interpolation.

4.5 RESULTS AND DISCUSSION

4.5.1 High-Pressure Methane and Carbon Dioxide Adsorption Rate Data: Application of Unipore Models

High-pressure methane and carbon dioxide adsorption rate data (adsorption isotherm pressure step 2) on dry and moisture-equilibrated coal has been modeled using the unipore analytical model (equation 3) (Figures 4-2:4-4) and the current numerical model (equations 23-27) (Figures 4-5:4-7).

The best-fit effective diffusivities (D') (Table 4-1) for the analytical solution are apparent diffusivities that do not include nonlinear isotherm effects. The apparent diffusivity for the unipore pore diffusion analytical solution, which assume linear adsorption on the pore walls, may be expressed as:

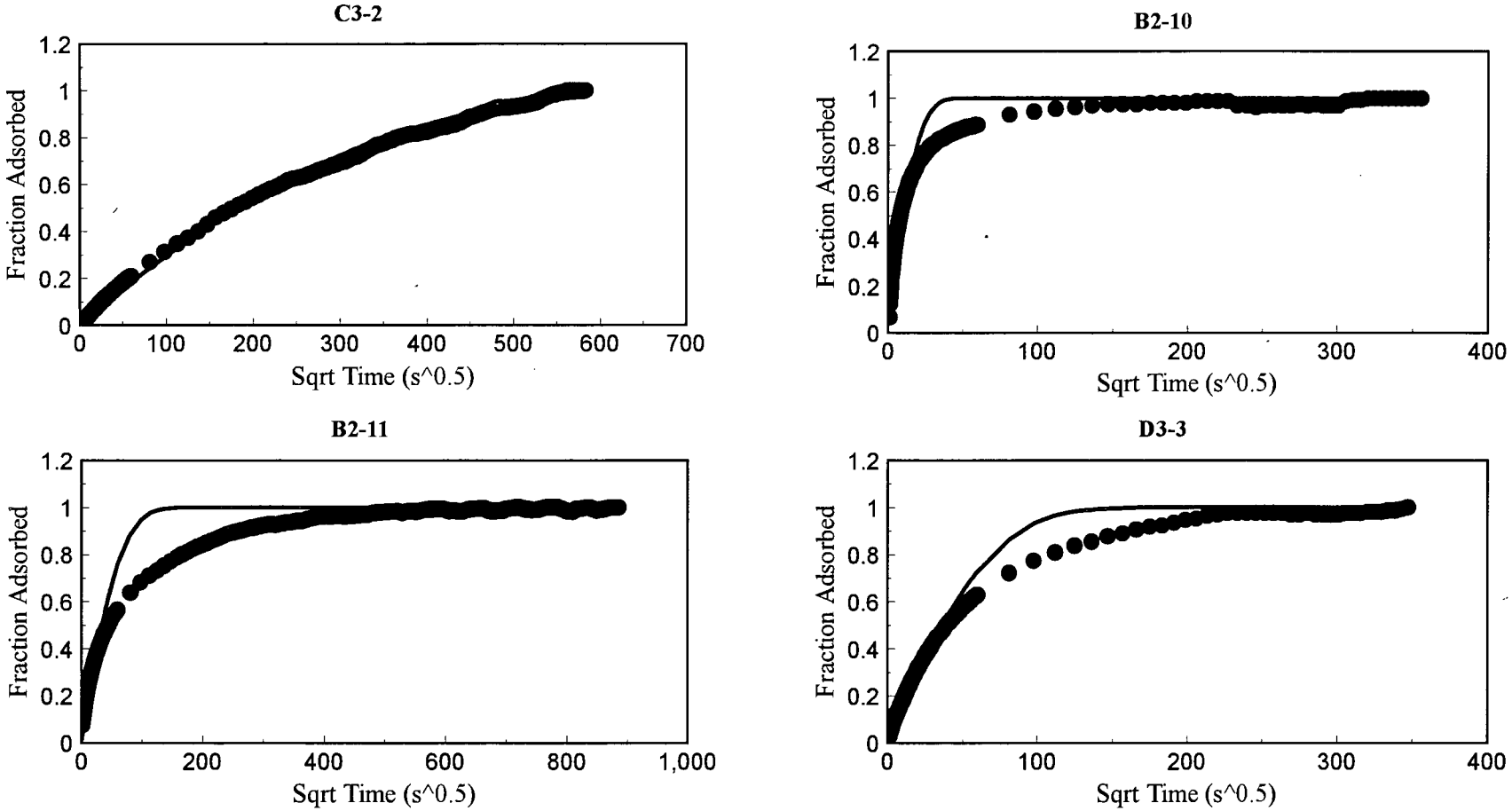

Figure 4-2. Unipore analytical model fit to-4 mesh (dry) coal methane sorption rate data.

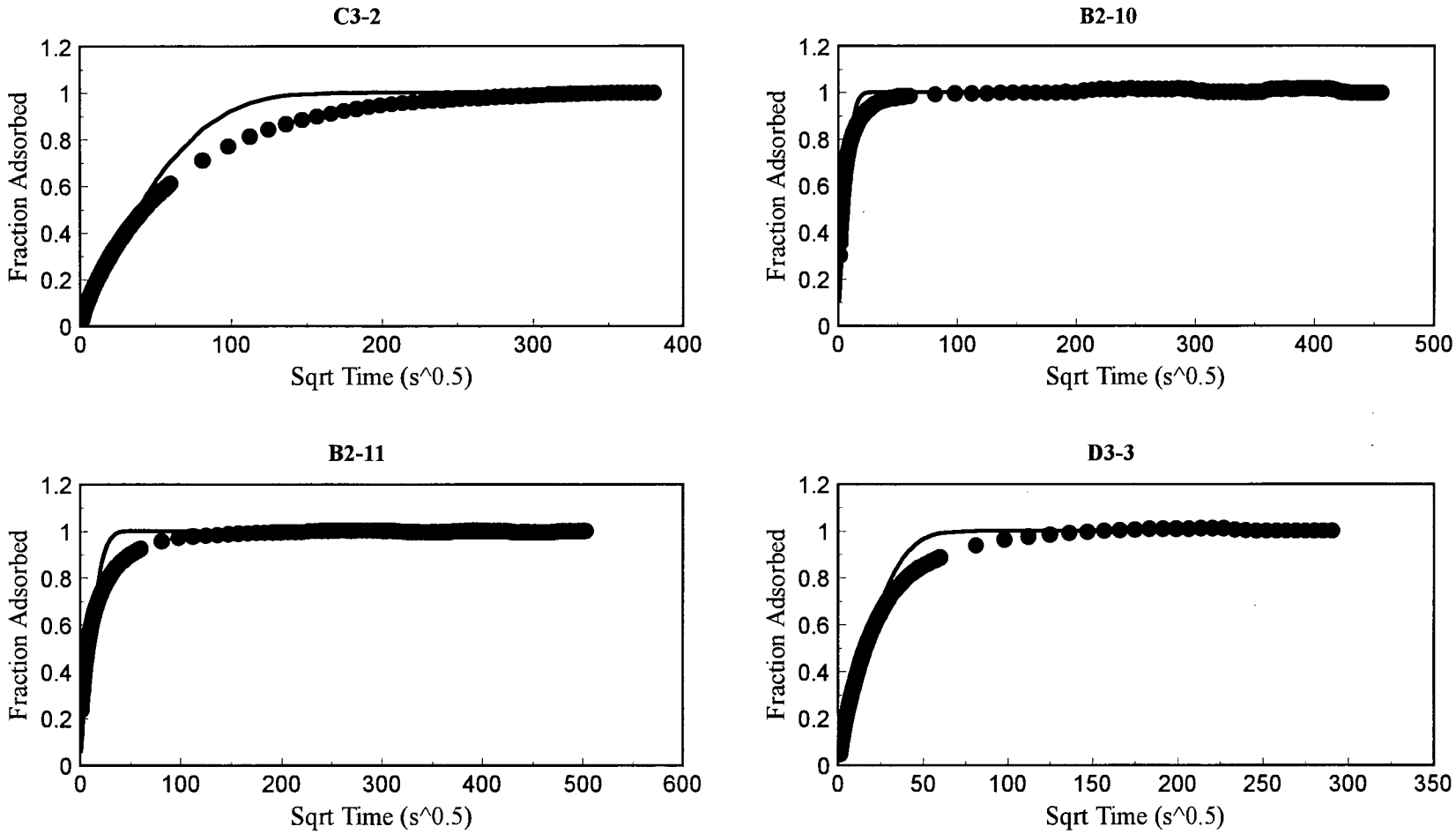

Figure 4-3. Unipore analytical model fit to-4 mesh (dry) coal carbon dioxide sorption rate data.

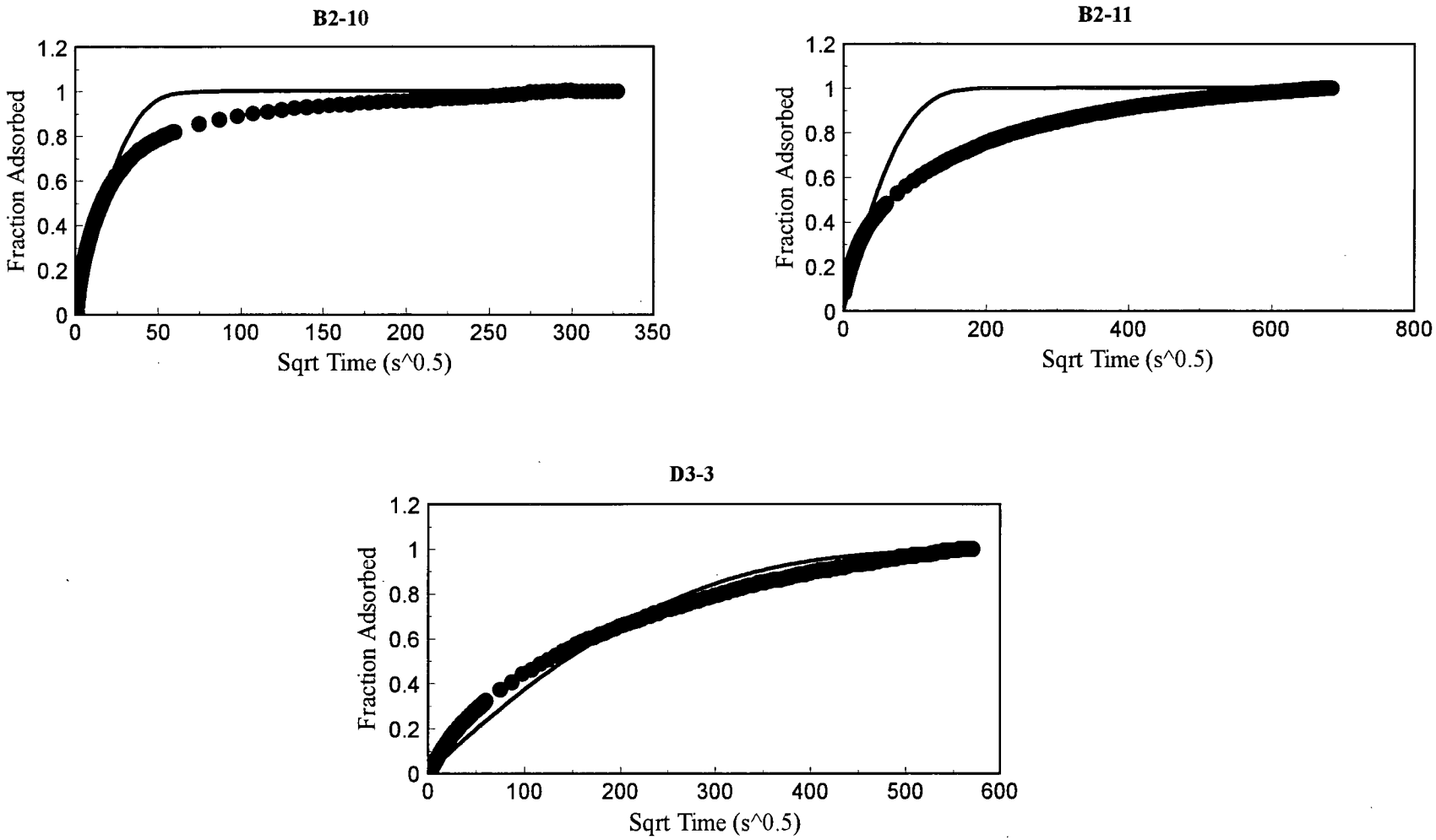

Figure 4-4. Unipore analytical model fit to-4 mesh (moisture-equilibrated) coal methane sorption rate data.

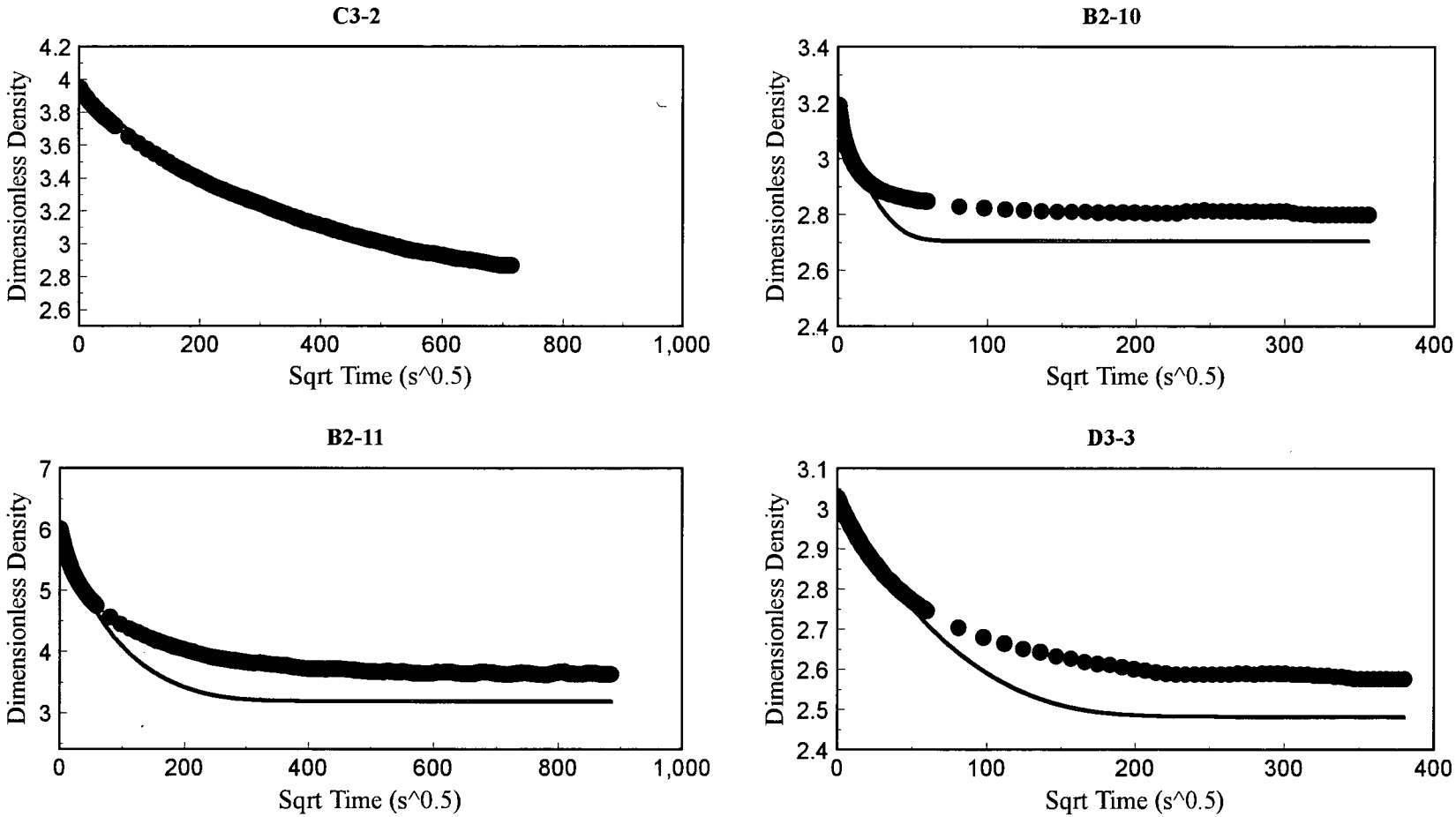

Figure 4-5. Unipore numerical model fit to-4 mesh (dry) coal methane sorption rate data.

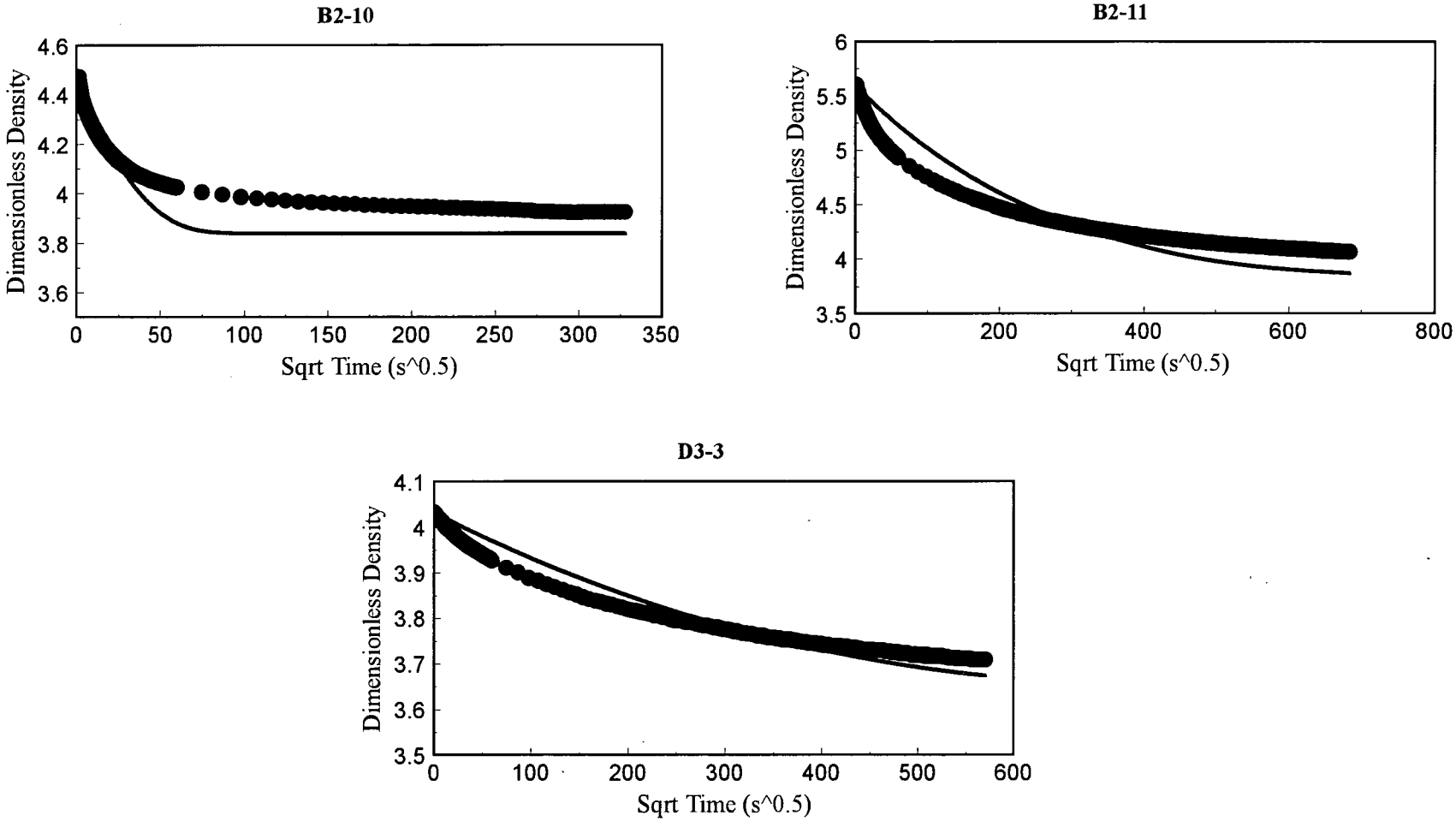

Figure 4-6. Unipore numerical model fit to-4 mesh (moisture-equilibrated) coal methane sorption rate data.

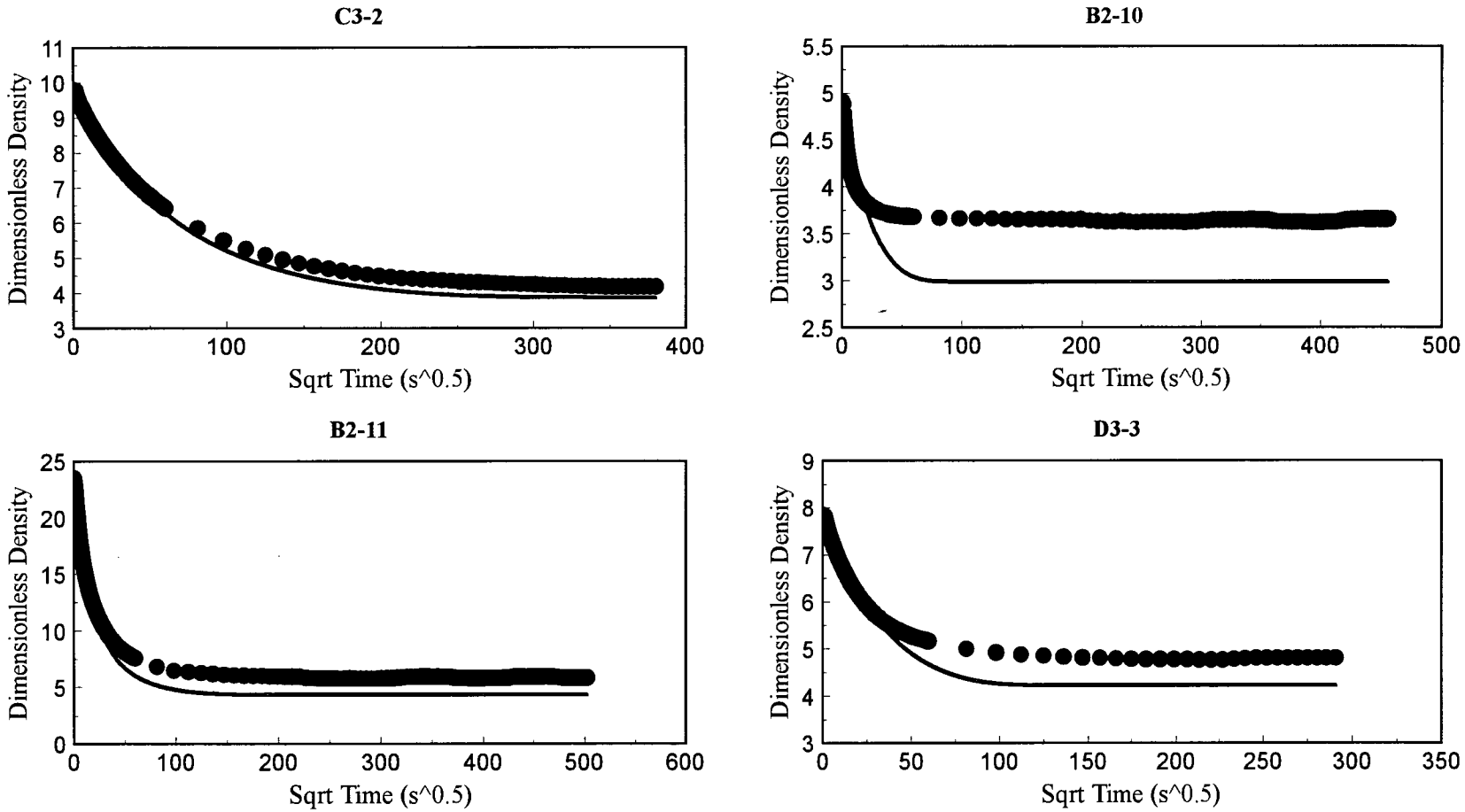

Figure 4-7. Unipore numerical model fit to-4 mesh (dry) coal carbon dioxide sorption rate data.

Table 4-1. Unipore analytical model parameters for sorption rate data-isotherm pressure step 2.

Sample	CH4 on dry coal		CH4 on moisture-equilibrated coal		CO2 on dry coal	
	P (MPa)	*D′ (s^-1)	P (MPa)	D′ (s^-1)	P (MPa)	D′ (s^-1)
C3-2	0.907	$7x10^{-7}$	-	-	0.320	$2x10^{-5}$
B2-11	0.784	$3x10^{-5}$	1.545	$2x10^{-5}$	0.187	$3x10^{-4}$
D3-3	0.987	$2x10^{-5}$	1.897	$2x10^{-6}$	0.503	$1x10^{-4}$
B2-10	1.074	$3x10^{-4}$	1.833	$1x10^{-4}$	0.556	$1x10^{-3}$

$$* D' = \frac{D}{r_p^2}\left(\frac{\phi}{\phi + S H}\right)$$

Table 4-2. Unipore numerical model parameters for sorption rate data-isotherm pressure step 2.

Sample	CH4 on dry coal		CH4 on moisture-equilibrated coal		CO2 on dry coal	
	P (MPa)	De(s^-1)	P (MPa)	De (s^-1)	P (MPa)	De (s^-1)
C3-2	0.907	$1x10^{-5}$	-	-	0.320	$4x10^{-4}$
B2-11	0.784	$6x10^{-5}$	1.545	$6x10^{-6}$	0.187	$1x10^{-3}$
D3-3	0.987	$2x10^{-4}$	1.897	$7x10^{-6}$	0.503	$2x10^{-3}$
B2-10	1.074	$1x10^{-3}$	1.833	$5x10^{-4}$	0.556	$3x10^{-3}$

$$D' = D\left(\frac{\phi}{\phi + SH}\right)$$

Sample C3-2 (high vitrinite/low ash) has a smaller effective diffusivity value than all other coals. In addition, the unipore model provides a reasonable fit to methane adsorption rate data over the entire time range only C3-2, whereas for all the other coals the unipore model significantly underestimates the time required to reach equilibrium. The unipore model also fails to adequately model the carbon dioxide adsorption rate data for sample C3-2.

Carbon dioxide diffusivities for dry coals obtained in this study are significantly larger than for the methane diffusivities (up to ~ 28 times), although direct comparison is difficult, due to the difference in final equilibrium pressure for methane and carbon dioxide isotherms. In a study by Marecka[15], a similar ratio of carbon dioxide to methane effective diffusivities was found using the unipore analytical model for constant pressure adsorption (~ 2.5 kPa, 303 K).

Analytical model diffusivities for the wet coal data (Table 4-1) are smaller than for the dry coals. As with the dry coal data, the unipore analytical model does not provide an adequate fit to adsorption rate data over the entire time scale (Figure 4-4). The possible exception, however, is sample D3-3. It is possible that water is occupying some of the larger pores of this sample, denying methane access to these pores, and hence the coal would be effectively unimodal with respect to pore volume distribution.

Results of the numerical model fit to the adsorption rate data are shown in Figures- 4-5:4-7, best-fit diffusivities are provided in Table 4-2 and numerical model input parameters are provided in Table 4-3. The numerical model diffusivities (D_i / R_a^2)

Table 4-3. Input parameters for numerical models-isotherm pressure step 2.

	Sample	C_{so} (kg/m^3)	ρ_o (kg/m^3)	$^*\rho_I$ (kg/m^3)	$^{**}S_L$	$^{**}I_L$	N	$^{***}\varphi$	$^{***}\varphi_i$	V_V (m^{3}x10^4)
CH_4 (dry coal)	C3-2	3.361	2.481	8.214	0.0554	0.242	2181	0.028	-	1.107
	B2-11	3.296	1.393	8.342	0.0546	0.249	2783	0.056	0.053	0.819
	B2-10	3.053	2.484	7.932	0.0698	0.258	1623	0.044	0.032	1.112
	D3-3	3.197	2.476	7.497	0.0812	0.232	1985	0.030	0.020	1.012
CO_2 (dry coal)	C3-2	7.826	1.359	13.305	0.0130	0.115	2181	0.029	-	1.107
	B2-11	4.678	0.564	13.252	0.0119	0.202	2746	0.055	0.051	0.828
	B2-10	11.136	0.273	13.403	0.0155	0.0743	1622	0.036	0.024	1.112
	D3-3	11.163	1.875	14.712	0.0219	0.0677	1799	0.029	0.019	1.061
CH_4 (wet coal)	B2-11	2.237	2.478	13.856	0.0574	0.390	2929	0.051	0.046	0.780
	B2-10	2.499	3.061	13.668	0.0853	0.315	1977	0.035	0.021	1.014
	D3-3	1.462	3.355	13.529	0.108	0.576	2044	0.019	0.0098	1.011

* *Gas density in cell immediately after dosing into cell (beginning of sorption step).*

** *Langmuir slope (S_L) and intercept (I_L), see text.*

*** *Total porosity (φ) and microporosity (φ_i) used in unipore and bidisperse numerical models, respectively.*

are relatively insensitive to the value used for the estimate of the mean particle radius (Part I). The unipore numerical model provides a reasonable fit only for sample C3-2. The poor fit for other samples may be due to the assumption of a unimodal pore volume distribution, error in the Langmuir equation fit to the adsorption isotherm data (as mentioned in Part 1) or errors in the porosity estimates. In addition, some curve fitting error results from the fact that time intervals for data collection were not evenly spaced, resulting in more pressure points taken at early time (see methods) than for later time. The greater number of data points at early time biases the curve fits toward the early time data.

The discrepancy in the magnitude of best-fit diffusivities between the analytical and numerical models (Tables 4-1, 4-2) is likely due to two factors. Firstly, the (external) boundary conditions for the models are different in that the analytical model was developed for a step change in boundary concentration at t=0, whereas a variable flux boundary condition was employed for the numerical model (equation 27). Secondly, the numerical model accounts for nonlinear adsorption during gas transport.

The adsorption rate behaviour of the Gates coals may be explained in terms of the relative proportions of micro, meso, and macroporosity determined in Part 1. The slowly sorbing sample C3-2 has a relatively large micropore volume (.049 cm^3/g) compared to D3-3 (.025 cm^3/g) and B2-10 (.025 cm^3/g). In addition, C3-2 has very little meso/macroporosity. The sample is homogenous with respect to pore volume distribution and therefore adsorption rate models based upon a unimodal pore structure are adequate. The dull (B2-10 and D3-3) samples contain an appreciable proportion of meso/macropores, and therefore dual resistance diffusion models are more appropriate

for describing adsorption rate behaviour. Sample B2-11 has a large micropore volume, small mesopore volume, and a large macropore volume, as indicated by mercury porosimetry data, and therefore dual resistance diffusion models are more appropriate for describing this sample's adsorption rate behaviour. The discrepancy in methane adsorption rate behaviour between bright and dull (dry) coals has been previously documented for Australian coals[37]. In the Gamson and Beamish study[37], the difference in dull and bright coal behaviour was explained with the aid of SEM imaging of the coal microstructure.

4.5.2 High-Pressure Methane and Carbon Dioxide Adsorption Rate Data: Application of Bidisperse Models

The bidisperse Ruckenstein[28] model equation (19) as well as the new bidisperse numerical model developed here were also applied to the high-pressure data (Figures 4-8: 4-13). Input to the numerical model is provided in Table 4-3. Macropore and micropore diffusivities are given in Tables 4-4, 4-5.

Both the analytical and numerical bidisperse models adequately describe the adsorption rate behaviour of the multimodal pore volume coals (B2-10, D3-3, and B2-11) (Figures 4-8:4-13). A transition occurs from macropore-dominated transport at early time, to micropore-dominated transport at later time. This finding is consistent with the findings of Gamson *et al.*[37] for Australian Bowen Basin coals. The Ruckenstein model[28] methane (macro- and micropore) diffusivities (Table 4-4) determined from methane adsorption on dry coal are comparable in magnitude (D_a': 3×10^{-4} to 2×10^{-3} s^{-1}, D_i': 2×10^{-6} to 4×10^{-5}) to those found by Beamish[31] but the macropore diffusivities are somewhat larger than those obtained by Smith and Williams[38]. Ruckenstein macro- and micropore

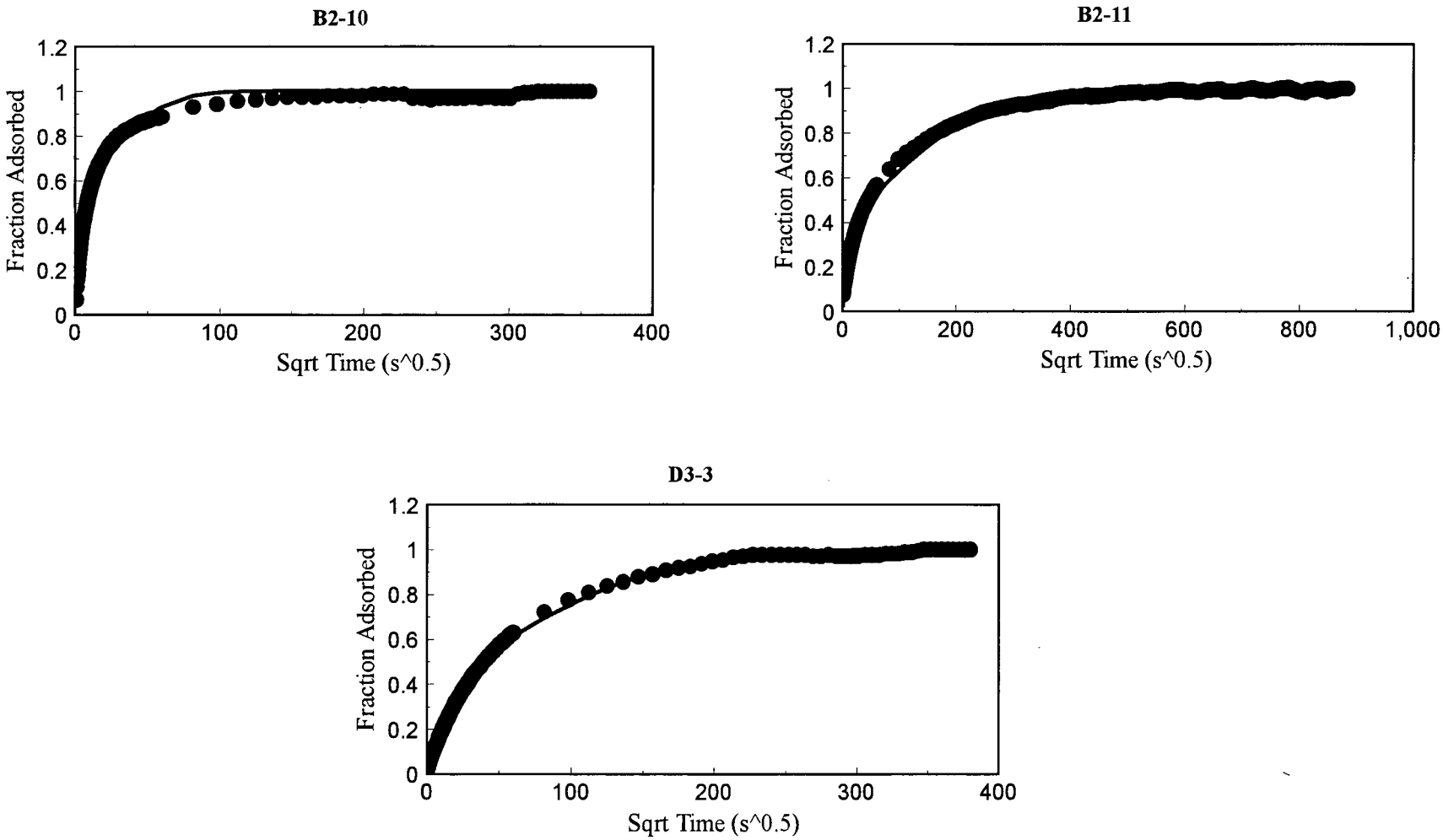

Figure 4-8. Bidisperse analytical model fit to-4 mesh (dry) coal methane sorption rate data.

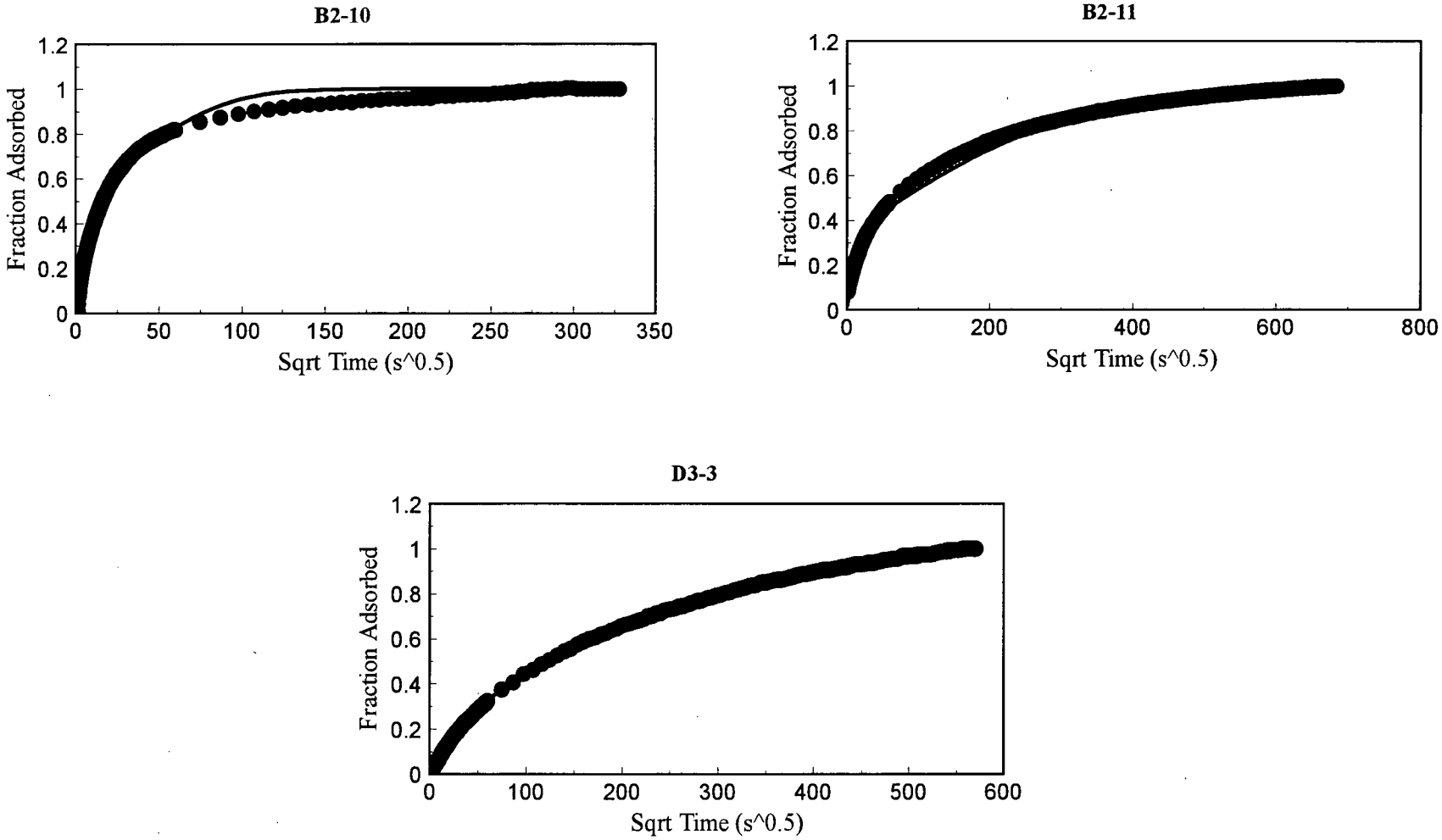

Figure 4-9. Bidisperse analytical model fit to-4 mesh (moisture-equilibrated) coal methane sorption rate data.

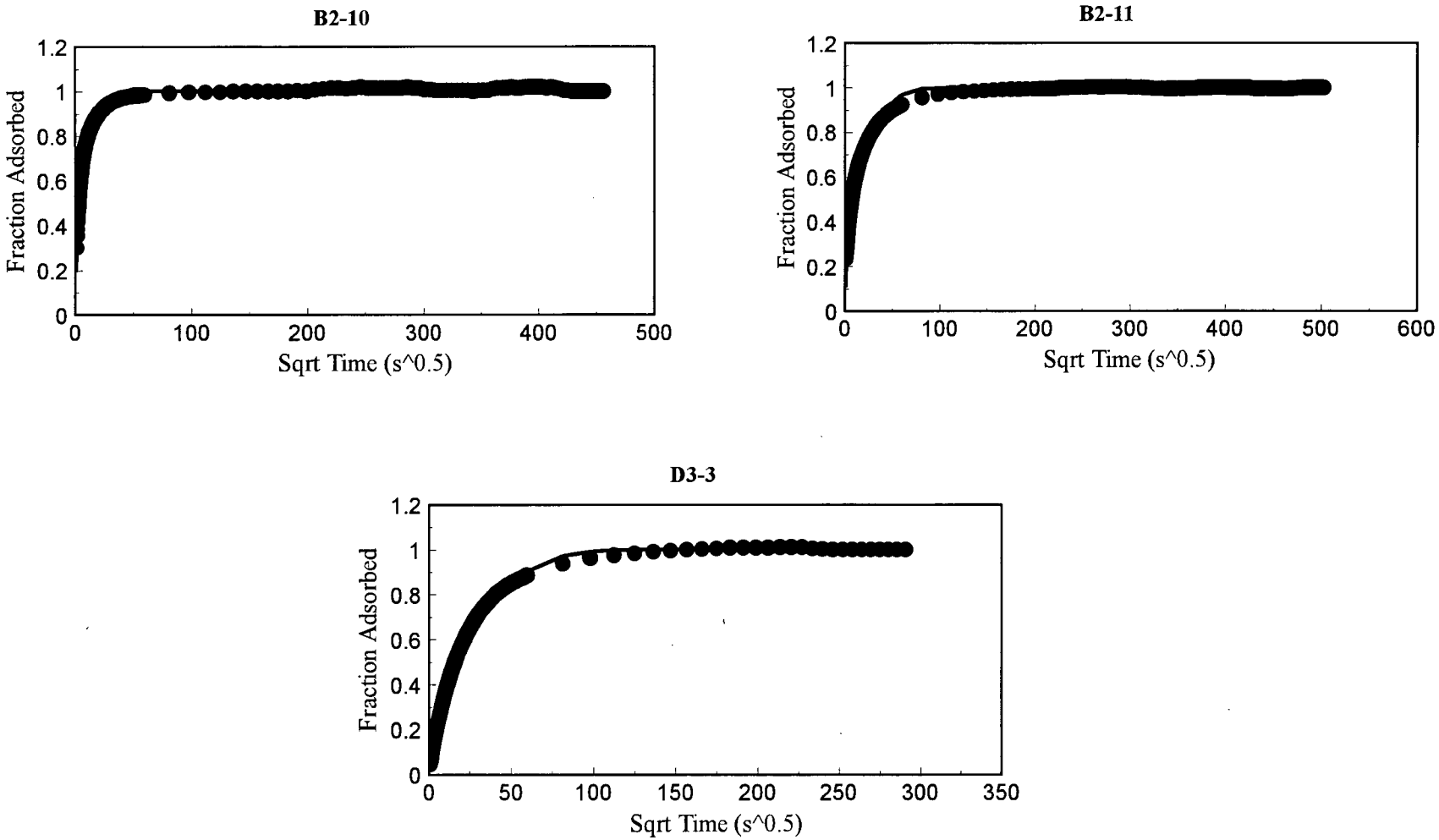

Figure 4-10. Bidisperse analytical model fit to-4 mesh (dry) coal carbon dioxide sorption rate data.

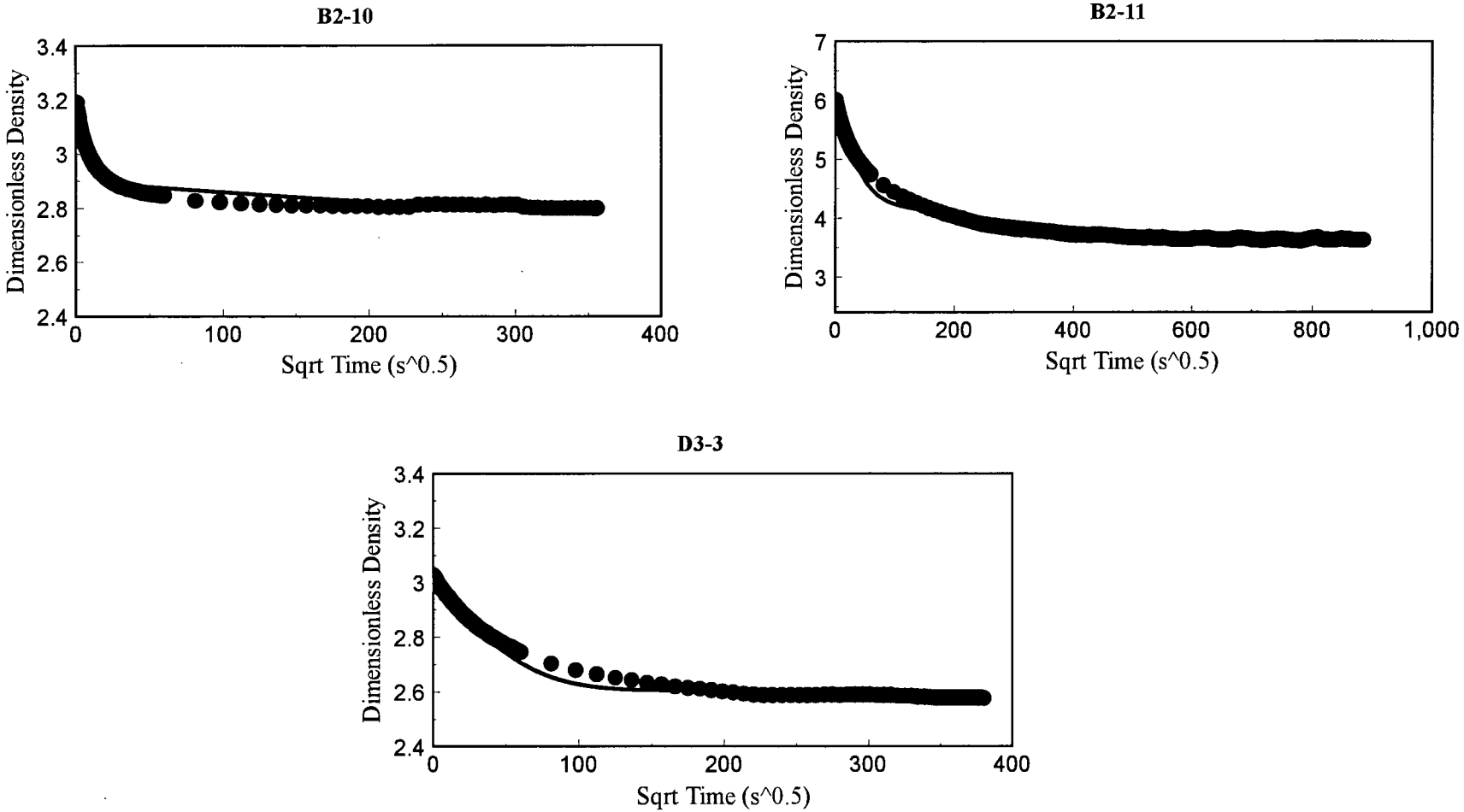

Figure 4-11. Bidisperse numerical model fit to-4 mesh (dry) coal methane sorption rate data.

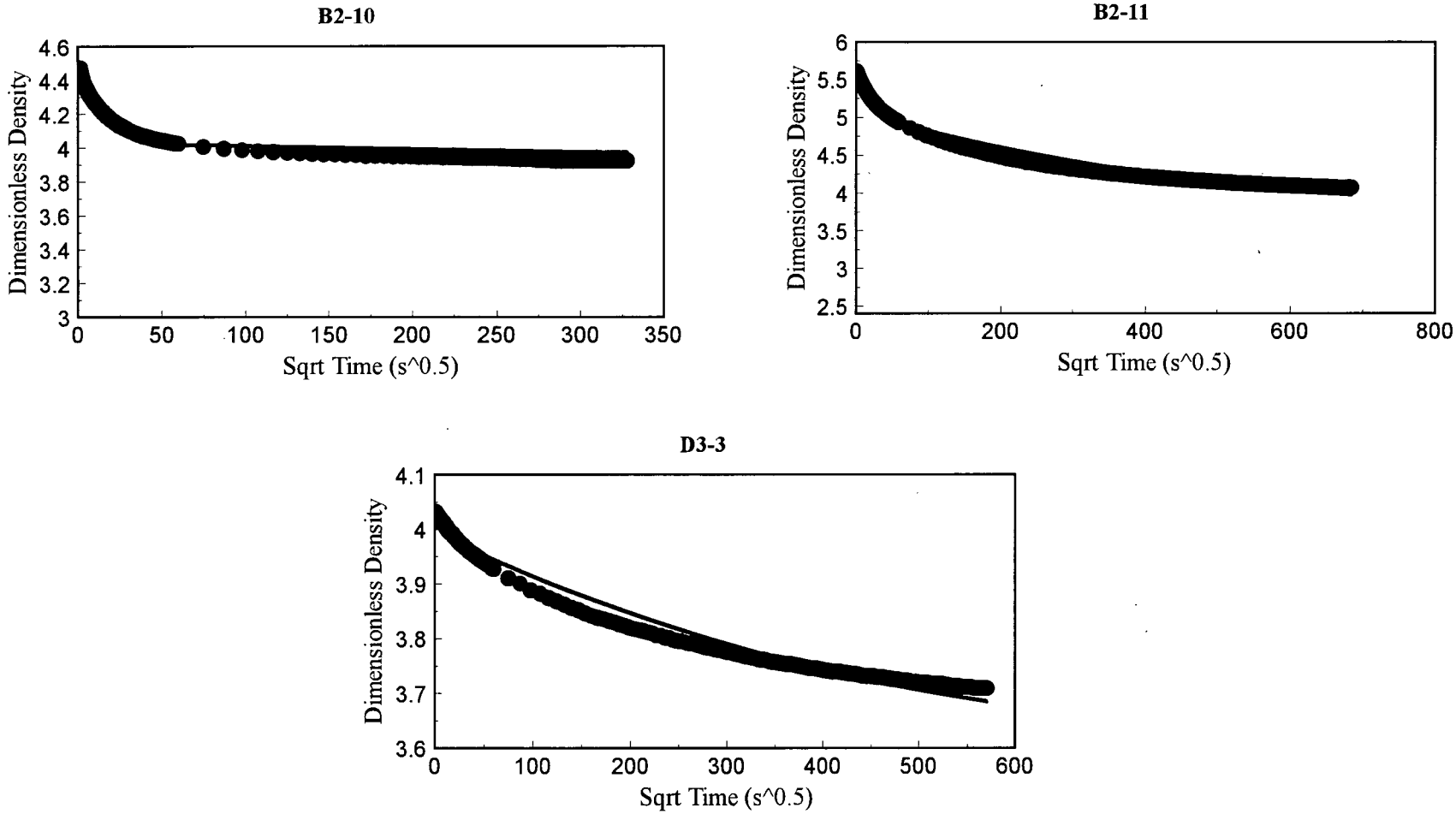

Figure 4-12. Bidisperse numerical model fit to-4 mesh (moisture-equilibrated) coal methane sorption rate data.

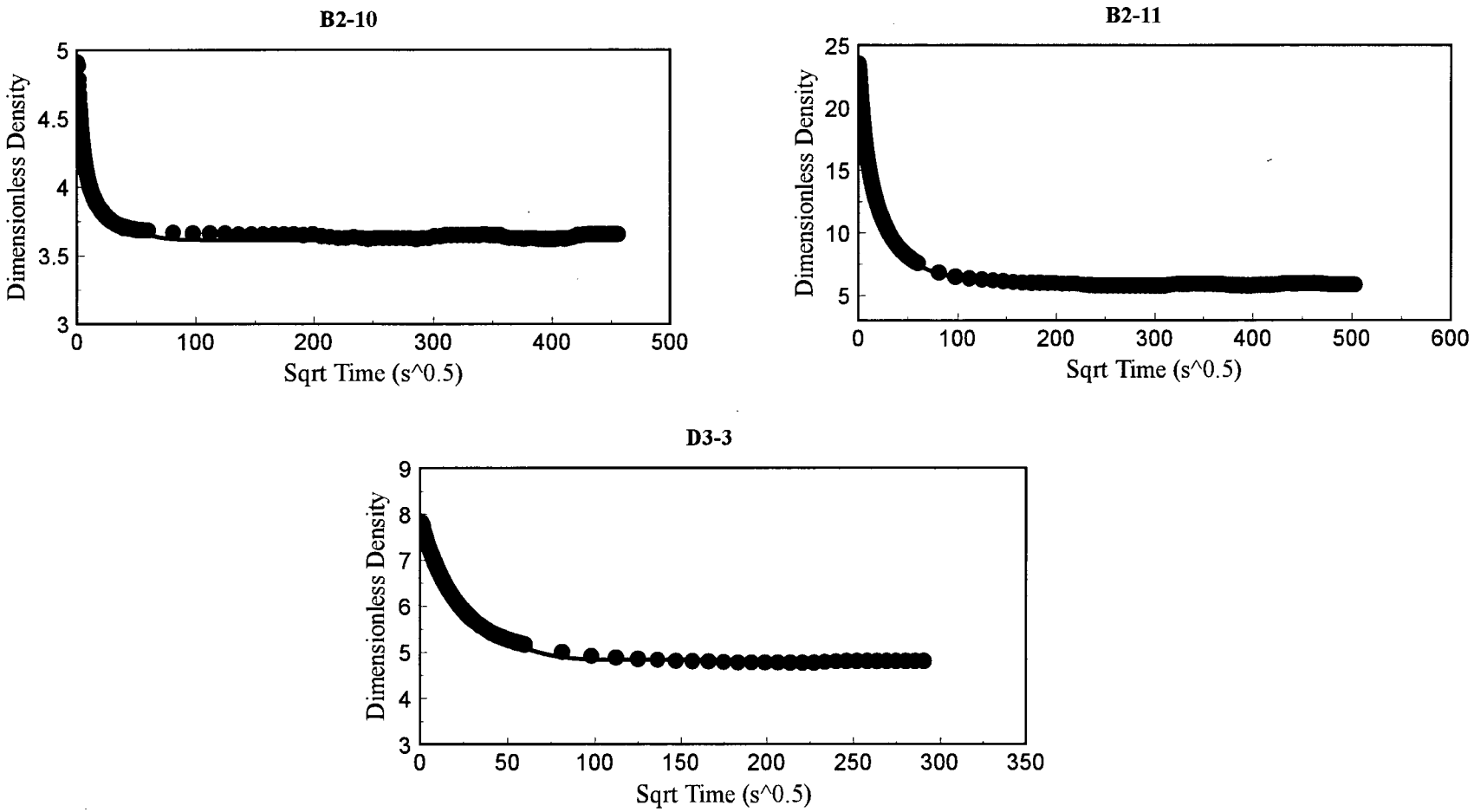

Figure 4-13. Bidisperse numerical model fit to-4 mesh (dry) coal carbon dioxide sorption rate data.

Table 4-4. Bidisperse analytical (Ruckenstein) model parameters for sorption rate data -isotherm pressure step 2

Sample	CH4 on dry coal		CH4 on moisture-equilibrated coal		CO2 on dry coal	
	$*D_a'(s^{-1})$	$**D_i'(s^{-1})$	$D_a'(s^{-1})$	$D_i'(s^{-1})$	$D_a'(s^{-1})$	$D_i'(s^{-1})$
C3-2	-	-	-	-	-	-
B2-11	$3x10^{-4}$	$2x10^{-6}$	$3x10^{-4}$	$1x10^{-6}$	$5x10^{-3}$	$6x10^{-5}$
D3-3	$2x10^{-4}$	$6x10^{-6}$	$5x10^{-5}$	$1x10^{-6}$	$6x10^{-4}$	$4x10^{-5}$
B2-10	$2x10^{-3}$	$4x10^{-5}$	$7x10^{-4}$	$2x10^{-5}$	$9x10^{-3}$	$2x10^{-4}$

$$* \quad D_a' = \frac{D_a}{R_a^2}\left(\frac{\phi_a}{\phi_a + S_a H_a}\right)$$

$$** \quad D_i' = \frac{D_i}{R_i^2}\left(\frac{\phi_i}{\phi_i + S_i H_i}\right)$$

Table 4-5. Bidisperse numerical model parameters for sorption rate data-isotherm pressure step 2

Sample	CH4 on dry coal		CH4 on moisture-equilibrated coal		CO2 on dry coal	
	$*D_a(s^{-1})$	$**D_i(s^{-1})$	$D_a(s^{-1})$	$D_i(s^{-1})$	$D_a(s^{-1})$	$D_i(s^{-1})$
C3-2	-	-	-	-	-	-
B2-11	$3x10^{-5}$	$5x10^{-6}$	$1x10^{-4}$	$3x10^{-6}$	$6x10^{-3}$	$2x10^{-3}$
D3-3	$2x10^{-5}$	$5x10^{-8}$	$5x10^{-4}$	$1x10^{-5}$	$1x10^{-3}$	$3x10^{-3}$
B2-10	$7x10^{-4}$	$5x10^{-6}$	$2x10^{-4}$	$3x10^{-7}$	$3x10^{-2}$	$4x10^{-3}$

effective diffusivities for methane adsorption on wet coal are generally only slightly smaller than for the dry coals, probably reflecting the small equilibrium moisture content of the Gates coals. The diffusivities for carbon dioxide on dry coal (Table 4-4) are larger than for methane, which is consistent with the unipore model diffusivities.

The numerical model, like the bidsiperse analytical solution, generally captures the adsorption rate behaviour of the multimodel pore volume distribution coals (Figures 4-11:4-13) better than the unipore models. Carbon dioxide diffusivities are much larger than the methane diffusivities. The micropore diffusivities (Table 4-5) are generally much smaller than the macropore diffusivities, with the exception of the diffusivities obtained for sample D3-3 carbon dioxide data. The anomalous values for sample D3-3 may be the result of a poor fit of the model to the data.

A problem with the bidisperse analytical model is that it is difficult to calculate some physical parameters of the coal from the model parameters. For example, the parameter β is defined in the same way as for the numerical model described above, but the ratio of the diffusivities, α, is unobtainable because the diffusivities obtained in the analytical model solution are not corrected for the effects of (assumed linear) adsorption. As a result, the values of micro- or macroporosity, or their ratios, are unobtainable. However, macroporosity may be obtained from the optimized value of β, α, and the input value of microporosity for the numerical model. For some samples, the estimated macroporosity is much greater (> 1 order of magnitude) than the experimentally-determined value obtained from nitrogen isotherms and He/Hg pycnometry. This discrepancy may be due to a number of factors including: 1) misfit of the experimental data by the Langmuir model; 2) the assumption of adsorption occurring only in the

microporosity of the coal; 3) inaccurate determination of pore volume distributions or porosities; 4) or the assumption of a single average particle size. Bhatia[32], using a random pore model, also found that unrealistically high macroporosities were required to obtain a reasonable fit to the adsorption rate data of Nandi and Walker[19]. Bhatia [opt. cit.] interpreted the unrealistic calculated macroporosities to be (possibly) due to a non-random distribution of macropores throughout the solid.

4.5.3 Low-Pressure Carbon Dioxide Adsorption Rate Data: Application of Bidisperse Models

Carbon dioxide adsorption rate data collected for the –4 mesh coals at low pressure (< 127 kPa) (Figure 4-14) showed similar trends to the high-pressure methane and carbon dioxide data described above. The unipore model was inadequate for modeling adsorption rate data for the banded bright or dull coals.

The carbon dioxide macropore and micropore effective diffusivities (Table 4-6) are smaller than for the high-pressure data, which is anticipated because the high-pressure analyses were performed at a higher temperature (303 K) than the low-pressure analyses (273 K).

4.5.4 Methane and Carbon Dioxide Adsorption Rate Data: Effect of Gas Pressure

To determine the effect of pressure upon calculated diffusivities, model (numerical and analytical) diffusivities were determined from several pressure steps of the adsorption isotherm. Methane diffusivities determined from the unipore analytical and numerical model are plotted against equilibrium adsorption pressure in Figure 4-15. One set of diffusivity values, obtained from desorption, is also plotted and is consistent

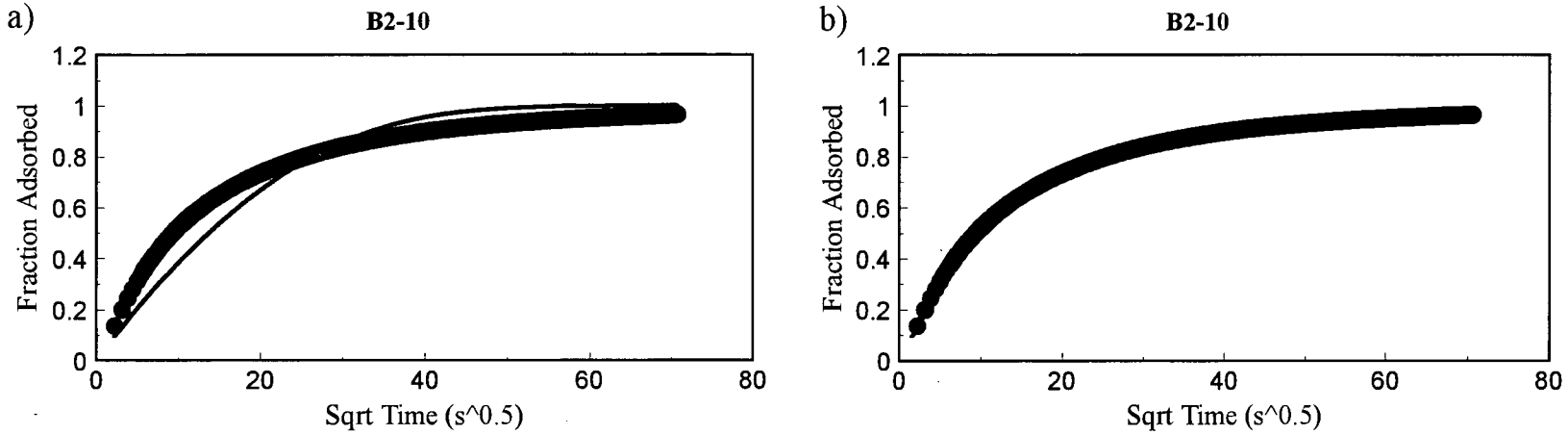

Figure 4-14. Analytical model fit to-4 mesh low pressure (roa) sorption rate data: a) unipore model, b) bidisperse model.

Table 4-6. Bidisperse analytical (Ruckenstein) model parameters for sample B2-10 sorption rate data.

Pressure (mmHg)	*D_a (s^{-1})	**D_i(s^{-1})
17.428	$5x10^{-4}$	$4x10^{-5}$
40.9583	$6x10^{-4}$	$4x10^{-5}$
264.264	$7x10^{-4}$	$4x10^{-5}$
310.911	$7x10^{-4}$	$4x10^{-5}$
359.419	$7x10^{-4}$	$5x10^{-5}$
728.509	$1x10^{-3}$	$6x10^{-5}$
786.327	$1x10^{-3}$	$8x10^{-5}$
845.385	$1x10^{-3}$	$1x10^{-4}$
888.567	$1x10^{-3}$	$1x10^{-4}$

* $$D_a' = \frac{D_a}{R_a^2}\left(\frac{\phi_a}{\phi_a + S_a H_a}\right)$$

** $$D_i' = \frac{D_i}{R_i^2}\left(\frac{\phi_i}{\phi_i + S_i H_i}\right)$$

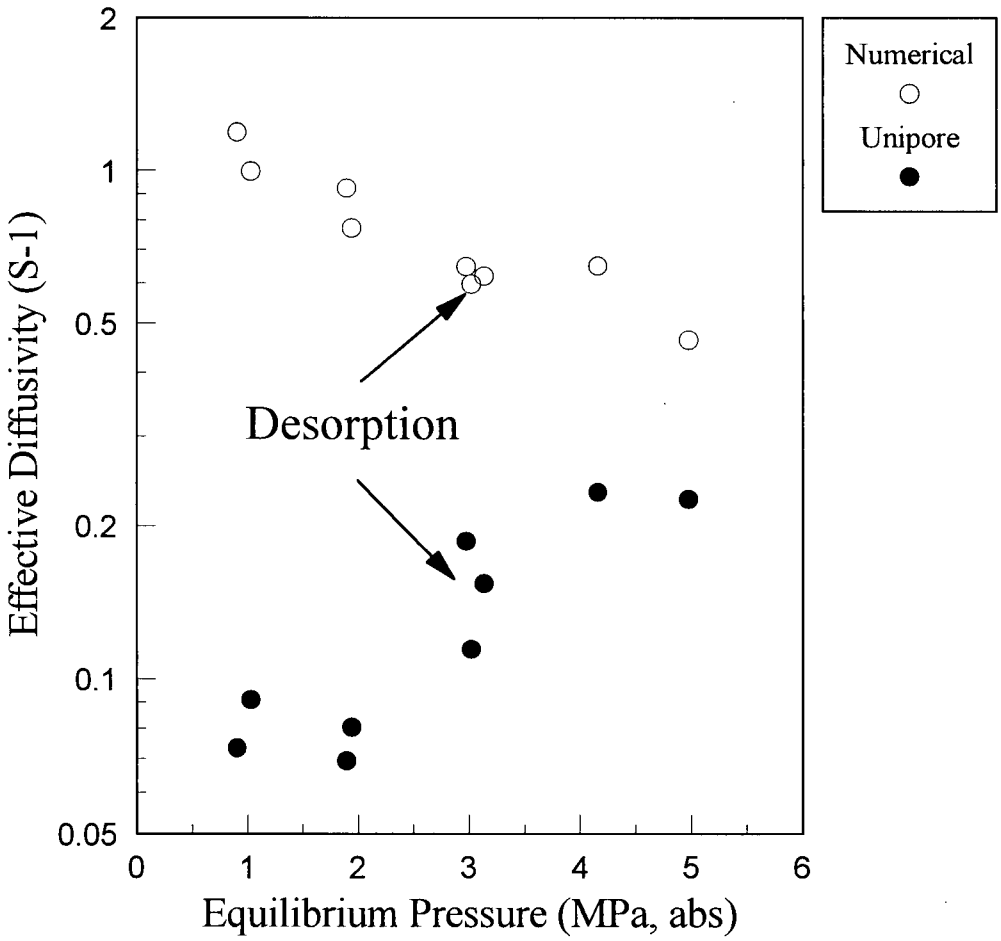

Figure 4-15. Methane effective diffusivities vs. pressure for sample C3-2.

with the trend of adsorption step diffusivities with pressure. The unipore diffusivities exhibit a strong dependence upon adsorption pressure. Although some scatter in the data exists, the numerical model diffusivities decrease with pressure, whereas the analytical model diffusivities increase with pressure. The increase in analytical model diffusivities with pressure may be due to the non-linearity of the isotherm as suggested by previous authors[24], but the decrease in numerical diffusivities, which have been corrected for the effects of non-linear adsorption, with pressure may be due the mechanism of gaseous diffusion.

The mechanism of methane gas diffusion in the Gates coals appears to be bulk diffusion. In an earlier study, Smith and Williams[20] have shown that the mechanisms of gaseous methane diffusion in bituminous coal vary with pressure. In particular, they (opt. cit.) note that the mechanism of diffusion changes from Knudsen type diffusion below a pressure of about 0.2 MPa to bulk diffusion at higher pressures, which they interpret to be due to the decrease in mean free path of the methane molecule with gas pressure. The decrease in the numerical model diffusivities, which are corrected for the effects of adsorption, with gas pressure is therefore consistent with a mechanism of bulk diffusion in the Gates coals.

The Ruckenstein (analytical) model diffusivities for low-pressure 273 K carbon dioxide adsorption obtained for sample B2-10 are plotted versus pressure in Figure 4-16. For this sample, both the macropore and the micropore diffusivities increase with pressure, although the micropore diffusivities are more strongly dependent upon pressure. The increase in diffusivity may (again) be due to the non-linearity of the isotherm. If so, the results suggest that some adsorption is occurring in both the meso/macroporosity and

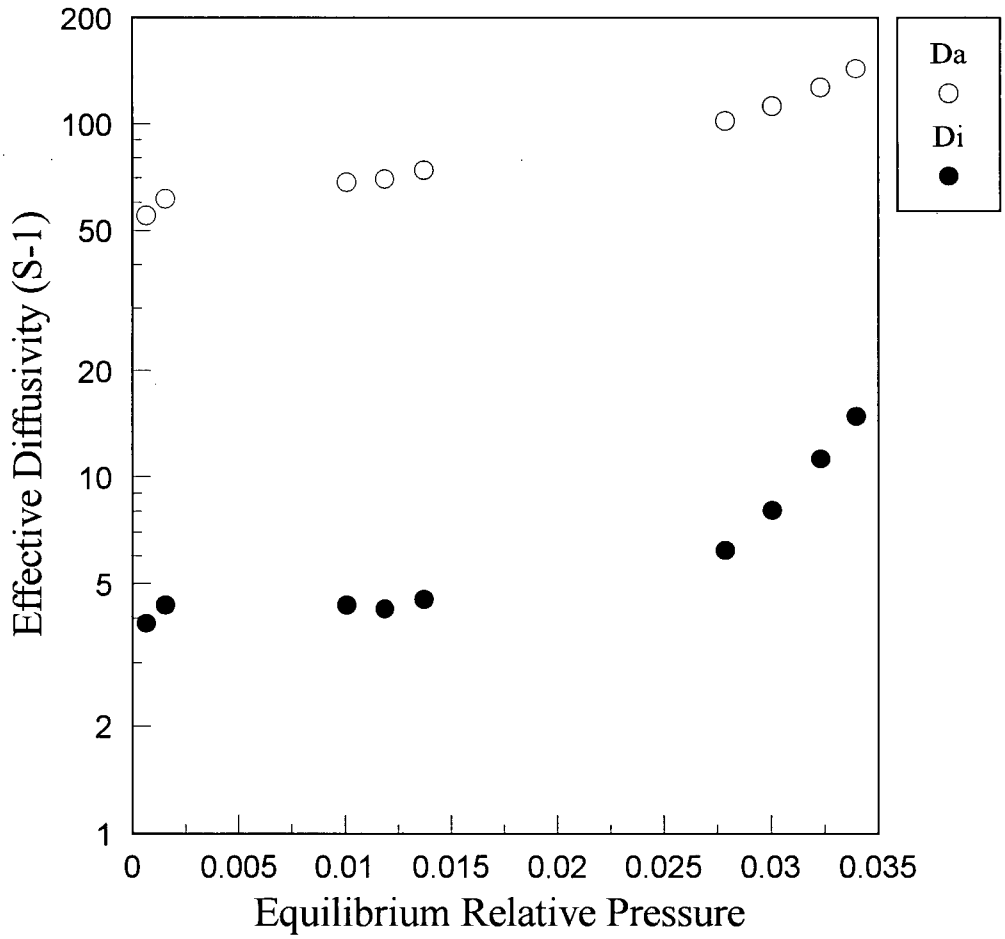

Figure 4-16. Low pressure carbon dioxide macropore (Da) and micropore (Di) effective diffusivities vs. pressure for sample B2-10.

the microporosity, which contradicts the assumptions used in the bidisperse numerical model. Further work is required to resolve this issue.

4.5.5 Implications for Reservoir Characterization and Modeling

The above results have demonstrated that two factors have a strong effect upon the transport of methane and carbon dioxide gas through the matrix of coals: pore volume distribution and gas pressure. Some current techniques for determining lost gas for canister desorption tests[6] assume that a single diffusion coefficient, independent of gas concentration or pressure, is adequate for the description of coal matrix gas transport. The current study shows that, because the coal pore volume distribution is a function of coal composition, a single parameter (diffusion coefficient or diffusivity) matrix gas diffusion model may be inadequate for describing adsorption rate behaviour for all coal sampled from a reservoir. Reservoirs are not entirely homogeneous with respect to organic and mineral composition, or organic and mineral content. Thus, a single parameter diffusivity model may lead to error (underestimate) in lost gas determination, and hence total in-situ gas content for a coal reservoir. This study shows that the diffusivity errors may be up to an order of magnitude if a single parameter model is used instead of dual resistance models. In a study by Mavor and Pratt[40], the Ruckenstein bidisperse model and the Direct Method[6], which uses an estimate of a single diffusivity value, were applied to gas canister desorption data. For most samples (4 out of 5) the two models gave similar estimates of lost gas, and hence total gas content, but the differences between the two estimates became greater as the lost gas content increased[40]. It is anticipated, based on the adsorption rate data given above, that dull coals, or coals with a

significant fraction of meso- and macroporosity, would have a greater percentage of lost gas than coals with less macro/mesoporosity. Lost gas determinations obtained using single diffusivity models may therefore have a greater error for coals of particular composition, which would create error in total gas content estimates for heterogeneous reservoirs. Additionally, because the pore volume distribution of coals is known to be a function of rank[27], or thermal maturity of the coal, models utilizing single diffusivity values may be adequate in the determination of lost gas only for certain rank ranges.

The pressure-dependence exhibited by the numerical and analytical model diffusivities has important implications for the determination of diffusion parameters during adsorption isotherm collection (as shown above), but also for the use of diffusivities in reservoir production modeling. The pressure-dependence of diffusivities is particularly important if adsorption rate data are obtained over a large pressure step which is often the case in desorption measurements. The assumption of a linear isotherm, as with the Ruckenstein model[28], may lead to erroneous values of diffusivity for coal. We suggest that the pressure-dependence of diffusivities should be ascertained prior to the application of diffusion models for the determination of lost gas calculations[6], as well as for reservoir simulators, where coal cleat and matrix fluid pressure varies with time during production. The diffusivity would be expected to vary during production and production models based upon constant diffusivity values may be in error. The impact of pressure and concentration upon diffusivities upon production forecasting requires study.

4.5 CONCLUSIONS

1) Carbon dioxide diffusivities are generally larger than methane diffusivities obtained for dry coal. Wet coal methane diffusivities are generally smaller than methane diffusivities determined for dry coals.

2) Bright coals have a uniform micropore structure and their adsorption rate data are adequately modeled using the classic unipore analytical solution or the proposed numerical model. Dull or banded coals have a more complicated pore structure, and are adequately modeled with diffusion models that incorporate a bisdisperse pore volume distribution. Close examination of numerical model optimized parameters suggest that some of the assumptions of the bidisperse model may be invalid.

3) Methane effective diffusivities obtained using the unipore analytical and numerical solutions are dependent upon adsorption pressure. The pressure dependence of the numerical model diffusivities is consistent with a bulk gaseous diffusion mechanism. Carbon dioxide diffusivities obtained using low-pressure (< 127 kPa) 273 K isotherm and the Ruckenstein model also exhibit a pressure dependence. These findings may have important implications for gas content determination and reservoir simulations, although further study is required.

Nomenclature

C = *sorbate concentration* $[kg/m^3]$
D = *diffusion coefficient* $[m^2/s]$

$D' = D\left(\frac{\phi}{\phi + SH}\right)$, *apparent diffusivity* $[s^{-1}]$

g = *micropore/macropore mass transfer term* $[kg/m^3]$
H = *Henry's Law constant* $[m^3/m^2]$
M = *mass content* $[kg/m^3]$
N = *number of coal particles (macrospheres) in system*
r = *radius [m]*
r_p = *diffusion path length [m]*
S = *pore surface area per unit bulk volume of coal* $[m^2/m^3]$
t = *time[s]*
V = *volume* $[m^3]$, *or volume adsorbed* $[cm^3/g@STP]$

Subscripts

a = *macropore*
D=*dimensionless*
i = *micropore*
L= *Langmuir*
s = *sorbate*
v = *voids*

Greek Symbols

$\alpha = \frac{R_a^2 D_i}{D_a R_i^2}$, *dimensionless parameter*

$\beta = \frac{3(1-\phi_a)\phi_i}{\phi_a}\frac{R_a^2 D_i}{D_a R_i^2} = \frac{3(1-\phi_a)\phi_i}{\phi_a}\alpha$, *dimensionless parameter*

$\gamma = \frac{r_i}{R_i}$, *dimensionless microsphere radial position*

$\eta = \frac{r_a}{R_a}$, *dimensionless macrosphere radial position*

ϕ = *porosity*
ρ = *gas density* $[kg/m^3]$

$\tau = \frac{D_a t}{R_a^2}$, *dimensionless time*

4.6 REFERENCES

1. King, G.R., Ertekin, T., and Schwerer, F.C. *SPE Formation Evaluation* 1986, 165

2. Kolesar, J.E., and Ertekin, T. In Proceedings of the Society of Petroleum Engineers Unconventional Gas Technology Symposium, Louisville, Kentucky, May 18-21, 1986, Houston, Texas, pp. 289-314

3. Sawyer, W.K., Zuber, M.D., Kuuskra, V.A., Horner, D.M. In Proceedings of the 1987 Coalbed Methane Symposium, Tuscaloosa, Nov. 16-19, 1987, pp.295-307

4. Reid, G.W., Towler, B.F., and Harris, H.G. Paper SPE 24360 presented at the SPE Rocky Mountain Regional Meeting, Casper, Wyoming, May18-21, 1992, pp. 425-432

5. Harpalani, S., 1996: Personal communication.

6. McLennan, J.D., Schafer, P.S., and Pratt, T.J. 'A Guide to Determining Coalbed Gas Content', Gas Research Institute Report No. GRI-94/0396, Chicago, Illinois, 1995

7. Mavor, M.J., Pratt, T.J., and Nelson, C.R. In Proceedings of the 1995 Intergas Symposium, Tuscaloosa, May14-20, 1995, pp. 379-388

8. Unsworth, J.F., Fowler, C.S., and Jones, L.F. *Fuel* 1989, **68**, 18

9. Clarkson, C.R., and Bustin, R.M. *Fuel* 1996, **75**, 1483

10. Lamberson, M.N., and Bustin, R.M. *AAPG Bull.* 1993, **77**, 2062

11. Beamish, B.B., and Crosdale, P.J. In Proceedings of the International Symposium cum Workshop on Management and Control of High Gas Emission and Outbursts, Wollongong, 20-24 March, 1995, pp. 353-361

12. Bustin, R.M., Clarkson, C., and Levy, J. In Proceedings of the 29th Newcastle Symposium, "Advances in the Study of the Sydney Basin", University of Newcastle, 1995, pp. 22-28

13. Mavor, M.J., Owen, L.B., and Pratt, T.J. Paper SPE 20728, presented at the 65th Annual Technical Conference of the Society of Petroleum Engineers, New Orleans, Louisiana, Sept. 23-26, 1990, pp. 1-14

14. Ciembroniewicz, A., and Marecka, A. *Fuel* 1993, **72**, 405

15. Marecka, A. *Coal Science* 1995, 23

16. Greaves, K.H., Owen, L.B., McLennan, J.D. In Proceedings of the 1993 International Coalbed Methane Symposium, Tuscaloosa, May 17-21, 1993, pp. 151-160

17. Gunter, W.D., Gentzis, T., Rottenfusser, B.A. and Richardson, R.J.H. *Preprint paper* presented at the Third International conference on carbon dioxide removal, Massachusetts Institute of Technology, September 9-11, 1996

18. Sevenster, P.G. *Fuel* 1959, **38**, 403

19. Nandi, S.P., and Walker, P.L., Jr. *Fuel* 1970, **34**, 309-323

20. Smith, D.M., and Williams, F.L. *Soc. of Pet. Eng. J.* 1984, **24**, 529

21. Crosdale, P.J., and Beamish, B. B. In Proceedings of the International Symposium cum Workshop on Management and Control of High Gas Emissions and Outbursts, Wollongong, March 20-24, 1995, pp. 363-367

22. Crank, J. 'Mathematics of Diffusion', Oxford Press, London, 1975

23. Smith, D.M., and Williams, F.L. *Fuel* 1984, **63**, 251

24. Nandi, S.L., and Walker, P.L., Jr. *Fuel* 1975, **54**, 81

25. Bielicki, R.J., Perkins, J.H., and Kissell, F.N. U.S. Bureau of Mines RI 7697, 1972, 12 p.

26. Smith, D.M., and Keller, J.F. *Ind. Eng. Chem. Fundam.* 1985, **24**, 497

27. Gan, H., Nandi, S.P., and Walker, P.L., Jr. *Fuel* 1972, **51**, 271

28. Ruckenstein, E., Vaidyanathan, A.S., and Youngquist, G.R. *Chem. Eng. Sci.* 1971, **26**, 1305

29. Ma , Y.H., and Lee, T.Y. *AIChE J.* 1976, **22**, 147

30. Lee, L. K. *AIChE J.* 1978, **24**, 531

31. Beamish, B. Basil, 1995: Personal communication

32. Bhatia, S.K. *AIChE J.* 1987, **33**, 1707

33. Langmuir, I. *J. Am. Chem. Soc.* 1918, **40**, 1361

34. Narasimhan, T.N., and Witherspoon, P.A. *Water Resour. Res.* 1976, **12**, 57

35. Kolesar, J.E., Ertekin, T., and Obut, S.T. *SPE Formation Evaluation* 1990, 81

36. Press, W.H., Teukolsky, S.A., Vettering, W.T., and Flannery, B.P. 'Numerical Recipes in FORTRAN: The Art of Scientific Computing', second edition, Cambridge University Press, Cambridge, 1994

37. Gamson, P.D., Beamish, B., Johnson, D. In 'Coalbed Methane and Coal Geology' (Eds. R. Gayer and I. Harris), Geological Society of America Special Publication no. 109, 1996, pp.165-179

38. Smith, D.M., and Williams, F.L. *Fuel* 1984, **63**, 256

39. Nandi, S.P., and Walker, P.L., Jr. *Fuel* 1970, **49**, 309

40. Mavor, M.J., and Pratt, T.J. 'Improved Methodology for Determining Total Gas Content Volume II. Comparative Evaluation of the Accuracy of Gas-In-Place Estimates and Review of Lost Gas Models', Gas Research Institute Report No. GRI-94/0429, Chicago, Illinois, 1996

CHAPTER 5

BINARY GAS ADSORPTION/DESORPTION ISOTHERMS: EFFECT OF MOISTURE AND COAL COMPOSITION UPON COMPONENT SELECTIVITY

5.1 ABSTRACT

The effect of coal moisture content and composition upon methane/carbon dioxide mixed gas adsorption characteristics is investigated. Experimental data indicate that carbon dioxide separation factors vary slightly between coal lithotypes, but the effect of variable coal composition and moisture upon selective adsorption are difficult to isolate. Model predictions based upon single component isotherms show that coal composition has an insignificant effect upon carbon dioxide separation factors. Model predictions also indicate that coal moisture decreases carbon dioxide selectivity. IAS theory and the extended Langmuir model differ substantially in their ability to predict binary gas adsorption behaviour, particularly for dry coals. Comparison of model predictions to experimental data demonstrate that IAS theory, in conjunction with the Dubinin-Astakhov single component isotherm equations are more accurate for the prediction of mixed gas desorption isotherms collected in this study than the extended Langmuir. IAS predictions, however, are strongly dependent upon the choice of pure gas isotherm equation.

5.2 INTRODUCTION

Coalbed gas generally consists of mixtures of methane, carbon dioxide, nitrogen and heavier hydrocarbons ($>C_2$), although methane is often the primary component. Because gas adsorption is the primary mechanism of gas storage in most economic coalbed gas reservoirs, accurate modeling of adsorption behaviour is necessary for economic forecasting of coalbed gas production. Further, the effect of coal properties, such as composition and moisture content, upon adsorbent selectivity for component gases is important for the economic evaluation of heterogeneous coal reservoirs. Of considerable theoretical and practical interest is the study of mixed gas adsorption/desorption in coal.

The composition of coalbed gas, and hence the commercial value of the gas, changes during production. For example, coalbed gas from the San Juan Basin has increased in carbon dioxide concentration[1] during gas well production. Accurate economic forecasts must account for evolving gas compositions through time during the production life of a coalbed gas reservoir.

Coalbed gas adsorption isotherms, measured in the laboratory, are commonly used to predict desorbed gas volumes as reservoir pressure decreases during production[2]. Adsorption isotherms are usually determined using pure methane as an analysis gas and are inaccurate for predicting multicomponent gas desorption volumes. The composition of adsorbate gas significantly affects the total and single component adsorbed gas volumes in coal systems[3-7]. Multicomponent desorption isotherms, determined using realistic initial reservoir gas compositions, are required for accurate predictions of adsorbed gas content during production.

N_2 or CO_2 gas injection may be used to increase methane gas recovery during production, either by lowering the methane partial pressure in the free-gas, or by competitive adsorption[8]. Reznik *et al.*[9] demonstrated that carbon dioxide injection increases the recovery of in-situ methane in coalbeds. Puri and Yee[10] showed that nitrogen flooding also increases methane recovery. Enhanced recovery principles may also be used to reduce greenhouse gas emissions through the disposal of anthropogenic carbon dioxide into coalseams[11]. Knowledge of multicomponent adsorption characteristics of coal is therefore necessary for the accurate assessment of enhanced recovery operations.

Most studies of multicomponent adsorption on coal have focused on the accurate modeling of equilibrium gas adsorption with little consideration of coal compositional effects. To the authors' knowledge, no systematic study has been performed to assess the effect of coal properties such as moisture content and composition (organic and mineral) upon the selective adsorption of carbon dioxide in carbon dioxide-methane-water-coal adsorption systems. Because pure gas adsorption has been shown to be a function of water content[12-14] and coal composition[15], it is reasonable to anticipate that binary gas adsorption is also a function of these properties. The current study examines the effect of coal moisture and composition upon binary gas adsorption using experimental data as well as model predictions from pure component isotherm data. The commonly applied extended Langmuir equation[16,17], as well as IAS theory[18], are used to predict binary gas adsorption. First, to examine differences in the performance of the models, predictions of binary gas equilibrium, over a broad range of pressures and gas compositions, are made. A variety of commonly used pure gas isotherm models are used in conjunction with IAS

theory in order to assess the effect of isotherm curve-fit error upon IAS theory predictions. The effect of gas pressure and composition upon predicted carbon dioxide selectivities over methane is examined. Model predictions using dry and moisture-equilibrated coal pure gas isotherm data are also used to determine the effect of moisture and coal composition upon binary gas adsorption. Binary gas experimental data are examined to determine the effect of gas composition, and pressure and coal lithotype upon the desorption characteristics of moisture-equilibrated coals. Finally, the results of model predictions are used to interpret binary gas experimental data, and the model fits are assessed using the current experimental data, as well as that of Hall *et al.*[7]

5.2.1 Previous Studies

Few experimental studies have examined the adsorption/desorption behaviour of mixed gases in coal under reservoir conditions. Stevenson *et al.*[3] measured and examined adsorption of binary and ternary mixtures of CH_4, CO_2, and N_2 on dry Australian Westcliff Bulli seam coals at 30°C and pressures up to 5.2 MPa. Greaves *et al.*[5] studied mixed gas (CH_4, CO_2) adsorption/desorption isotherms on dry Sewickley seam coal at 23°C. The Greaves *et al.*[5] study demonstrates the importance of adsorption/desorption isotherm hysteresis in predicting adsorbed phase compositions.

The presence of moisture in the coal matrix significantly changes the adsorption equilibrium characteristics of mixed gases. Arri *et al.*[4] collected binary (methane-nitrogen and methane-carbon dioxide) gas isotherm (46°C) data at various pressures for a moisture-equilibrated coal system. Arri *et al.* showed that each component gas does not sorb independently, but competes for adsorption space. The extended Langmuir

isotherm[16,17] provided a reasonable fit to the Arri *et al.* data. Harpalani and Pariti[6] obtained ternary gas (methane-carbon dioxide-nitrogen) adsorption/desorption data for a moisture-equilibrated coal system at 44°C. The methane concentration in the free-gas (non-sorbed) phase was shown to decrease with pressure during desorption. A reasonable fit to the Harpalani and Pariti[6] data was also obtained using the extended Langmuir isotherm.

There have been several attempts to apply thermodynamically rigorous mixed gas adsorption models to moisture-equilibrated and dry coal/mixed gas adsorption systems[3,19,7] Hall *et al.*[7] applied a variety of models to pure and mixed gas Fruitland coal isotherm data and quantitatively assessed model predictions using an extensive data set. Hall *et al.*[7] found that although all models used for pure gas adsorption performed comparably, the ideal adsorbed solution (IAS) theory of Myers and Prausnitz[18] and 2-D equation-of-state (EOS) models were more accurate than the extended Langmuir model for mixed gas adsorption. In the Stevenson *et al.*[3] study, IAS theory was found to be adequate for predicting binary and ternary mixed gas adsorption on dry coal.

5.2.2 Theory

The extended Langmuir model [16,17] and IAS theory[18] are most commonly used for the prediction of mixed gas adsorption on coal. Both the extended Langmuir model and IAS theory require pure component isotherm data for multicomponent predictions. The simplest model used for prediction of multicomponent adsorption isotherms is the extended Langmuir equation:

$$V_i = \frac{(V_L)_i b_i P_i}{1 + \sum_j b_j P_j} \quad (1)$$

where $(V_L)_i$ and b_i are the pure gas isotherm Langmuir constants. Partial pressures of the component gases in the free gas phase are determined using the following equation:

$$P_i = P y_i \quad (2)$$

Langmuir parameters for pure component isotherms are used to predict component adsorbed volumes for gas mixtures at any total gas pressure and free-gas composition.

A convenient method for expressing the relative adsorption of components in an adsorption system is through the calculation of a separation factor. The separation factor, or selectivity ratio, for a multicomponent gas adsorption system may be defined as[16]:

$$\alpha_{ij} = \frac{(x/y)_i}{(x/y)_j} \quad (3)$$

For the extended Langmuir isotherm, the separation factor is simply the ratio of the adsorption equilibrium constants for the pure component isotherms[16] and is independent of concentration and total pressure. The assumption of a constant separation factor is not, however, necessarily accurate for all systems[16]. An increasing selectivity for the most strongly adsorbed component with decreasing concentration of that component is generally observed[20].

The ideal adsorbed solution (IAS) theory[18] is based upon the assumption that the adsorbed mixture behaves like an ideal, adsorbed solution, and hence is analogous to Raoult's law for bulk solutions. Activity coefficients of the adsorbed solution are therefore assumed to be unity and the equilibrium between the gas phase mole fraction of a component and the adsorbed phase mole fraction is given by:

$$P y_i = P_i^{\circ}(\pi) x_i \tag{4}$$

where P_i° is the gas (vapour) pressure of the pure component adsorbed at the same temperature and spreading pressure as the solution. Fugacities may be substituted for pressures in equation (4) to account for gas phase non-idealities. The spreading pressure for the pure components are determined through integration of the Gibbs adsorption isotherm to the vapour pressure of the pure component, P_i°:

$$\pi_i^* = \frac{\pi_i A}{RT} = \int_0^{P_i^{\circ}} \frac{n(P)}{P} dP \tag{5}$$

where π_i^*, π_i, A, and $n(P)$ are the component reduced spreading pressure, spreading pressure, adsorbent surface area, and pure component adsorption isotherm, respectively. The spreading pressure may be defined as the reduction in surface tension of a surface due to the spreading of the adsorbate over the surface[16]. Any pure component isotherm equation may be used to evaluate equation (5).

Mole fraction constraints include:

$$\sum_{i=1}^{nc} x_i = 1; \quad \sum_{i=1}^{nc} y_i = 1 \tag{6}$$

where *nc* is the number of components. The total amount of adsorbed gas in the mixture (for an ideal solution) is given by:

$$\frac{1}{n_t} = \sum_{i=1}^{nc} \frac{x_i}{n_i^o} \tag{7}$$

where n_t is the total amount adsorbed, and n_i^o is the amount of pure component adsorbed from pure gas at the same temperature and spreading pressure as the adsorbed mixture. The actual amount of each component adsorbed in the mixture is given by:

$$n_i = n_t x_i \tag{8}$$

Equation (5) may be evaluated for each component using an isotherm equation, such as the Langmuir single component isotherm equation, or may be determined graphically. Richter *et al.*[21] demonstrated the effect of fitting pure component isotherm data with different isotherm equations upon the prediction of multicomponent adsorption equilibria using the IAS method. The calculations of mixed gas equilibria were shown to be very sensitive to curve-fit error of the pure gas isotherm equation.

Although the Dubinin-Radushkevich (D-R) and Dubinin-Astakhov (D-A) equations have been shown to be more accurate for the modeling of coal/pure gas

isotherms[22], the incorrect low-pressure limit of these isotherm equations may affect spreading pressure calculations for IAS theory. The correct low-pressure limit of any adsorption isotherm equation should be[21]:

$$\lim_{p \longrightarrow 0} {}^{n}/_{p} = H \qquad (9)$$

where H is the Henry's Law coefficient. Although the Langmuir equation has the correct low-pressure limit, the D-R/D-A equation low-pressure limit is zero[23]. The effect of the incorrect low-pressure limits of the D-R and D-A equations upon spreading pressure calculations are examined in a later section.

5.3 METHODS

5.3.1 Sample Preparation

Four medium-volatile bituminous coal lithotype samples from the Lower Cretaceous Gates Formation of northeastern British Columbia were used in this study. The coals were chosen for their variable organic contents and compositions. The samples were crushed by hand (stage crushed) to pass through a 4 mesh (4.75 mm) sieve and four sub-samples were obtained. A -4 mesh fraction was retained and the other sub-samples were crushed to pass through an 8 (2.38 mm), 20 (0.841 mm), and 60 (0.250 mm) mesh sieve. Only the -4 and -60 mesh fractions were used for isotherm analysis. Proximate (ash and moisture) was performed for each of the subsamples used for isotherm analysis. Petrographic analysis was performed on – 60 mesh splits using manual point counts on polished pellets[24]. Coals were stored in vacuum dessicators or refrigerated sealed

containers between isotherm runs to prevent oxidation. Periodic free-swelling index tests[25] of bright coals demonstrated that the coals were not oxidized.

Minus 4 mesh coal samples were dried in an oven at 110°C overnight and then evacuated at isotherm temperature for 24 hours prior to "dry" isotherm analysis. The –60 mesh coals were equilibrated with moisture (at 96-96% relative humidity) at 30°C prior to desorption isotherm analysis. Equilibrium moisture was achieved using a procedure similar to that described by Levy *et al.*[14].

5.3.2 Experimental Procedure

High-pressure (up to ~ 8 MPa) 303.15 K isotherms were obtained using a volumetric adsorption apparatus similar to that described by Mavor *et al.*[2] and Levy *et al.*[26]. Sample void volume calibrations were performed using helium expansion as described elsewhere[2]. Pure gas adsorption isotherm data collection for the –4 mesh coals is also described elsewhere[27].

Methane and carbon dioxide desorption isotherms were collected for the – 60 mesh, moisture-equilibrated coal using the following procedure. The reference cell was charged with gas to a pressure greater than the anticipated sample cell starting pressure and allowed to thermally equilibrate with the thermostated water bath. Gas was then dosed from the reference cell to the sample cell for a few seconds and then the valve between the two cells closed. Pressure in the sample cell dropped as gas was adsorbed to the equilibrium value. Equilibrium was considered reached when the pressure in the sample cell remain constant ($\Delta P = 0.000$ MPa) over a period of 2 hours. Twelve hours total was generally sufficient. Desorption isotherm steps were then collected by

reversing the adsorption step procedure: gas was dosed from the (evacuated) reference cell and the sample cell was isolated from the reference cell until equilibrium was achieved. The following mass balance calculation was used in conjunction with the real-gas law to calculate pure gas adsorbed volumes isotherms at STP (T = 273.15 K, P = 0.101325 MPa) at each isotherm step:

$$V_{ads} = \left[\frac{T_{STD}}{T P_{STD} m_c}\right] \times \left[V_{ref}\left(\frac{P_{ref}^{I-1}}{z} - \frac{P_{ref}^{I}}{z}\right) - (V_{void} - V_s)\left(\frac{P_{sc}^{I}}{z} - \frac{P_{sc}^{I-1}}{z}\right)\right] \qquad (10)$$

The sample void volume (V_{void}), which is the volume in the sample cell not occupied by solid coal, may be corrected for the volume occupied by the adsorbate (V_s) if a molar density of the adsorbate is assumed. In the current study, the adsorbate density was taken as that at normal boiling for methane (0.423 g/cm^3) and at the triple point for carbon dioxide (1.18 g/cm^3). If the adsorbate volume is neglected, the Gibbs isotherm is obtained.

For mixed gas studies, a similar procedure to the pure gas isotherms was used, except that small gas samples were taken during a desorption step for gas chromatographic (GC) analysis. Sample cells were used to extract small (~ 3 ml) gas samples with a syringe following pressure stabilization in the sample cell during a adsorption step. The pressure drop after extraction was usually small (<< .01 MPa), and the pressure was again allowed to stabilize for several hours prior to the next desorption step. As with the Greaves *et al.*[5] study, the pressure drop accompanying extraction was assumed to have a negligible effect on adsorbed gas composition. The reference cell was

then dosed with a small amount of mixed gas from the sample cell to initiate the next desorption step. A gas sample was extracted from the reference cell for GC analysis to determine the composition of the gas in the reference cell.

Compositional (mole fraction) equilibrium as well as mechanical (pressure) is required for an equilibrium multicomponent isotherm. Compositional equilibrium was tested for periodically during desorption steps by gas compositional analyses. Equilibrium times for mixed gas adsorption were generally much longer than for pure gas adsorption. For example, for the 75%CH_4/25%CO_2 binary gas desorption isotherm, 5 – 7 days were allowed for equilibration at each step.

For binary gas isotherms, mass balance was performed for each component using the following equation:

$$V_{ads}^{j} = \left[\frac{T_{STD}}{T P_{STD} m_c}\right] \times \left[V_{ref}\left(\frac{(y_{ref}^{j} P_{ref})^{I-1}}{z} - \frac{(y_{ref}^{j} P_{ref})^{I}}{z}\right) - (V_{void} - V_s)\left(\frac{(y_{sc}^{j} P_{sc})^{I}}{z} - \frac{(y_{sc}^{j} P_{sc})^{I-1}}{z}\right)\right] \quad (11)$$

where V_{ads}^{j} is the volume of component j adsorbed from the mixture at each adsorption step, and y^{j} is the free gas (unadsorbed) mole fraction of component j. The volume of the sorbed phase, assuming the sorbed gas behaves like an ideal solution, was calculated using the following equation:

$$V_s = \sum_{i=1}^{nc} x_i V_{mi} \quad (12)$$

where V_{mi} is the molar volume of the liquid adsorbate. Equations (10) and (11) must be solved iteratively at each adsorption step, with the Gibbs adsorption volumes used as the initial guess for equation (10). Gas compressibility factors for pure and mixed gases were determined using the Peng-Robinson equation-of-state[28].

Replicate runs performed for methane adsorption isotherms on the dried – 4 mesh coals and methane desorption isotherms for moisture-equilibrated – 60 mesh coals were within 6% and 10% relative, respectively. The estimated uncertainties determined from replicate analysis vary with coal type. For example, for the dry, -4 mesh coals the methane adsorption isotherm the relative errors are around 2% for the two bright coals (B2-11 and C3-2), but around 4 and 6% for the two dull coals (B2-10 and D3-3, respectively). Similarly, for the moist –60 mesh coals, the desorption isotherm errors are around 5% for the bright coals, but about 10% for the dull coals. The dull coals have a higher ash content, and sorb much less gas and thus have greater measurement errors than the bright coals. The moist coal desorption isotherms have a greater uncertainty than the dry adsorption isotherms possibly due to slight variations in moisture content between replicate analyses. The estimated uncertainty in methane adsorption isotherms on moist coals, however, is generally less than 3%, for a variety of coals analyzed by the authors.

Gas mixture compositions are known within 0.002 mole fraction based upon replicate analysis of calibration standards and analysis gas.

5.3.3 Isotherm Regression Analysis

The Langmuir, D-R and D-A isotherm equations were fit to single component isotherm data. The relevant equations, written in linearized form, are:

Langmuir[29]: $$\frac{P}{V} = \frac{P}{V_L} + \frac{1}{bV_L} \quad (13)$$

Dubinin-Radushkevich (D-R)[17]: $$\log V = \log V_o - D\left(\log P_o / P\right)^2 \quad (14)$$

Dubinin-Astakhov (D-A)[30]: $$\log V = \log V_o - D\left(\log P_o / P\right)^n \quad (15)$$

Application of the Langmuir, D-R, and D-A equations to adsorption isotherm data has been discussed previously[20]. The parameters b and V_L in the Langmuir equation, and V_o, D, and n were optimized using a least squares routine coupled with a multiparameter optimization algorithm in MATLAB®.

Application of IAS theory for multicomponent adsorption isotherm predictions requires integration of the pure component isotherms in the spreading pressure equation (equation 5). For the Langmuir isotherm, the spreading pressure equation was calculated using an analytical equation, whereas for the D-A and D-R equations, the spreading pressure was calculated by numerical integration. A diagram summarizing the analytical protocol is given in Figure 5-1.

5.4 RESULTS AND DISCUSSION

5.4.1 Coal Petrographic Data

The selected Gates coals represent a wide range in maceral and ash contents (Table 5-1). Two coals (C3-2 and B2-11) have high vitrinite (> 50 volume %, mineral matter-free) and low ash (< 20 weight %) contents, whereas B2-10 and D3-3 have low vitrinite (< 50 volume %) and high ash (> 20 weight %) contents.

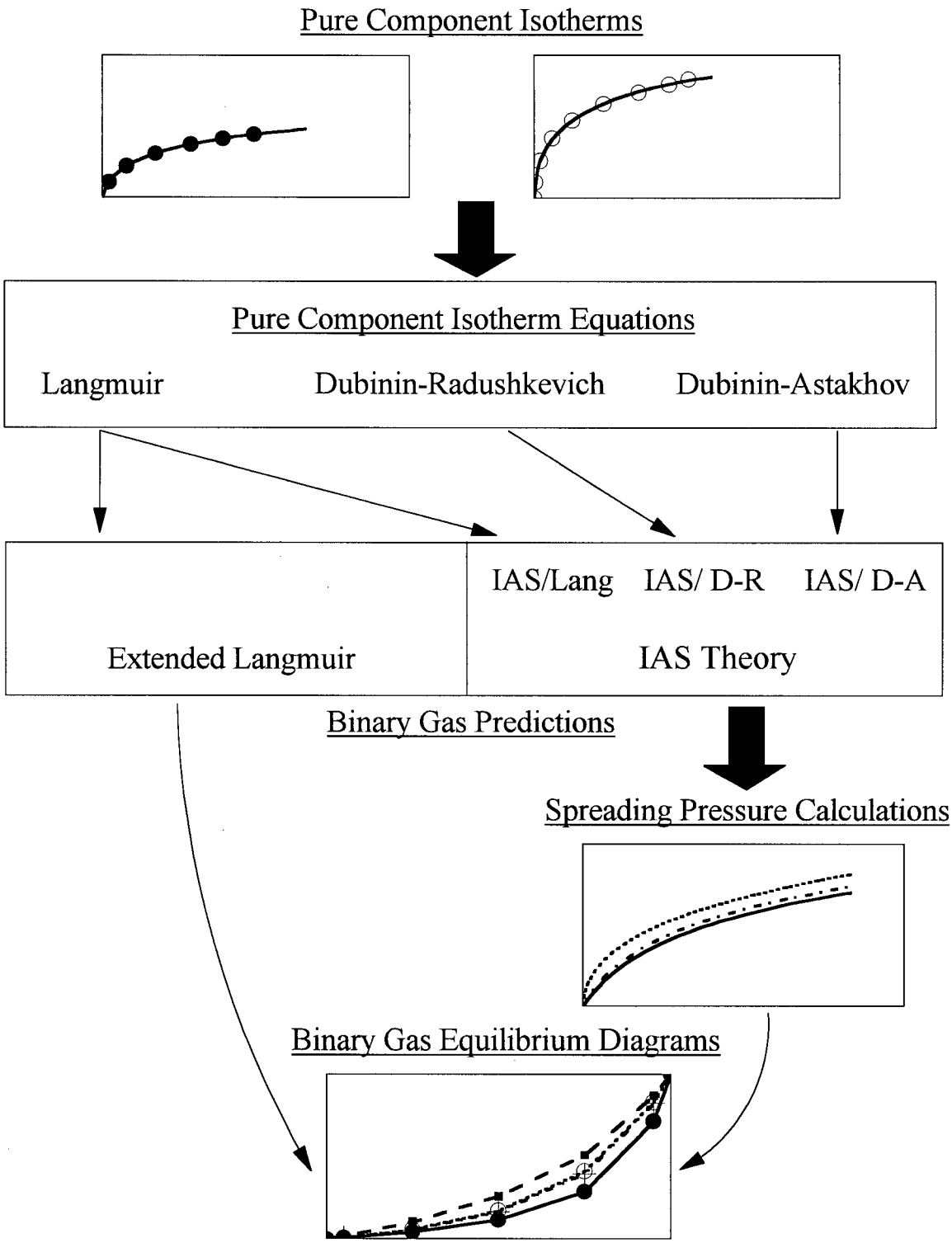

Figure 5-1. Diagram illustrating protocol for binary gas adsorption predictions.

Table 5-1. Maceral composition (volume %, mineral matter-free), equilibrium moisture (weight %, 30°C), and ash yields (weight %, dry-basis).

Sample	*Structured Vitrinite	Desmocollinite	Semifusinite	Fusinite	**Other Inertinite	Liptinite	Eq. M. (%)	Ash (%)
C3-2	75	23	1	1	-	-	2.4	13.0
B2-11	29	30	33	5	3	-	2.7	3.7
D3-3	20	30	23	-	27	-	1.4	46.1
B2-10	13	28	49	3	6	1	1.6	30.3

* *Includes telocollinite and telinite.*

** *Includes macrinite and inertodetrinite.*

5.4.2 Pure Gas Isotherms

High-pressure methane and carbon dioxide isotherms (303 K;Figure 5-2) exhibit the expected trend of increasing gas adsorption with a decrease in ash content. If the results are plotted on an ash-free basis (Figure 5-3), which assumes that mineral matter adsorbs negligible amounts of gas, there is still a significant difference in the amount adsorbed between the coals. Maceral composition thus exhibits some control upon gas adsorption. The trend of increasing gas adsorption with total vitrinite content, as demonstrated in previous studies[15], is not strictly obeyed here, however. The highest sorbing coal (B2-11) does not have the highest vitrinite content. Lamberson and Bustin[15] also found that although methane gas adsorption generally increased with vitrinite content, the highest sorbing coals did not have the highest vitrinite content, but had a mixture of vitrinite and inertinite.

As observed in previous studies[12-14], moisture has the effect of decreasing the amount adsorbed for all coals studied (Figure 5-4). For example, at 3 MPa, the ratio of the volume adsorbed on the dry coal (B2-11) to the volume adsorbed on the moisture-equilibrated coal (V_{dry}/V_{wet}) is ~ 1.28 for methane adsorption and ~ 1.25 for carbon dioxide adsorption for sample B2-11.

The D-R, D-A and Langmuir equations were applied to pure gas isotherm data and an estimate of curve-fit error is given in Table 5-2. The D-A equation fits the moisture-equilibrated and dry coal isotherm data within experimental error, whereas the Langmuir fits are poorer. The D-R equation, which is a 2-parameter equation like the Langmuir equation, provides a fit intermediate to the D-A and Langmuir equations. The curve-fits for all equations are generally better for methane isotherms than for carbon

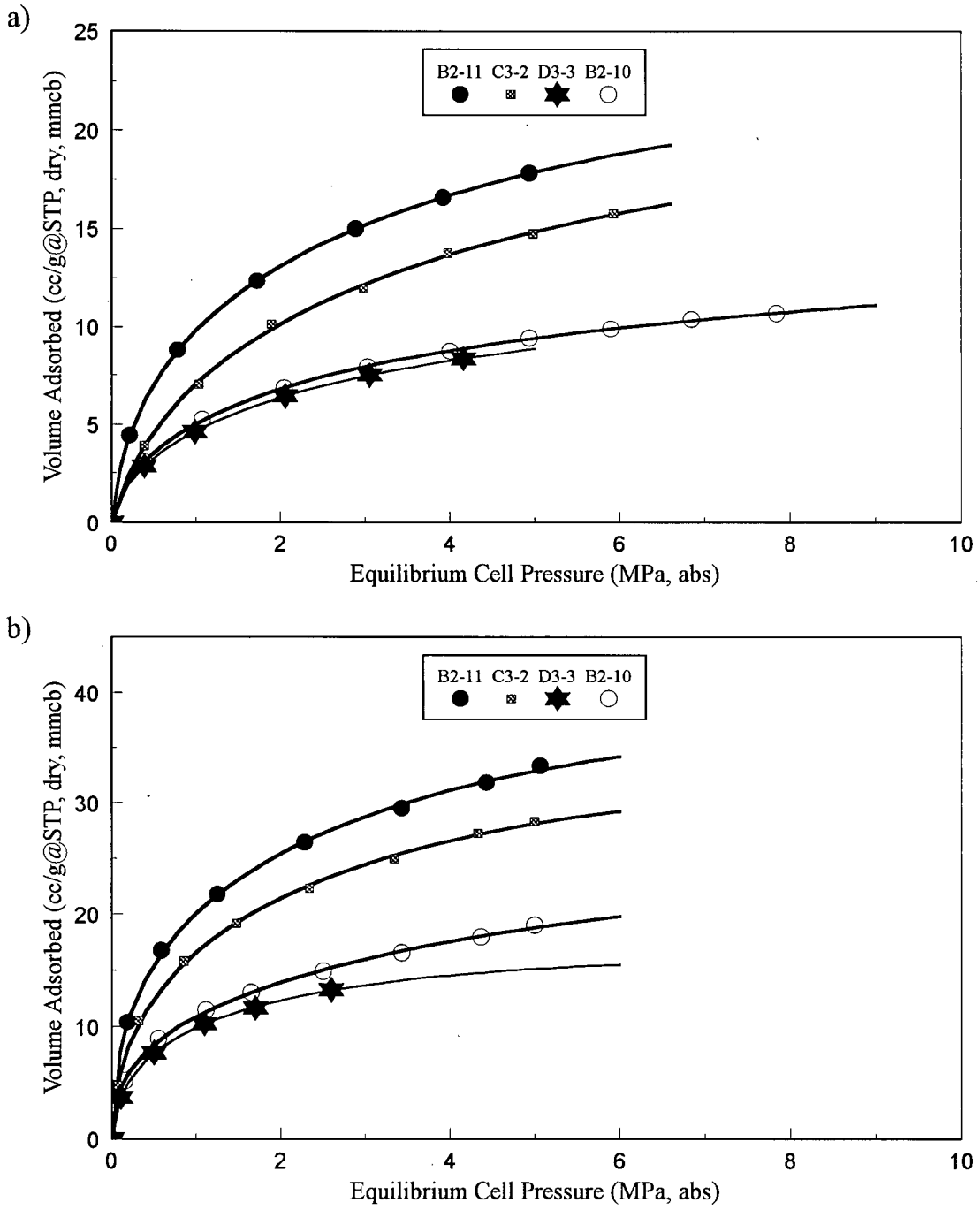

Figure 5-2. Methane (a) and carbon dioxide (b) adsorption isotherm data for dry -4 mesh coals. Results are presented on a dry, mineral matter-containing coal basis (mmcb). Lines are D-A fit to data

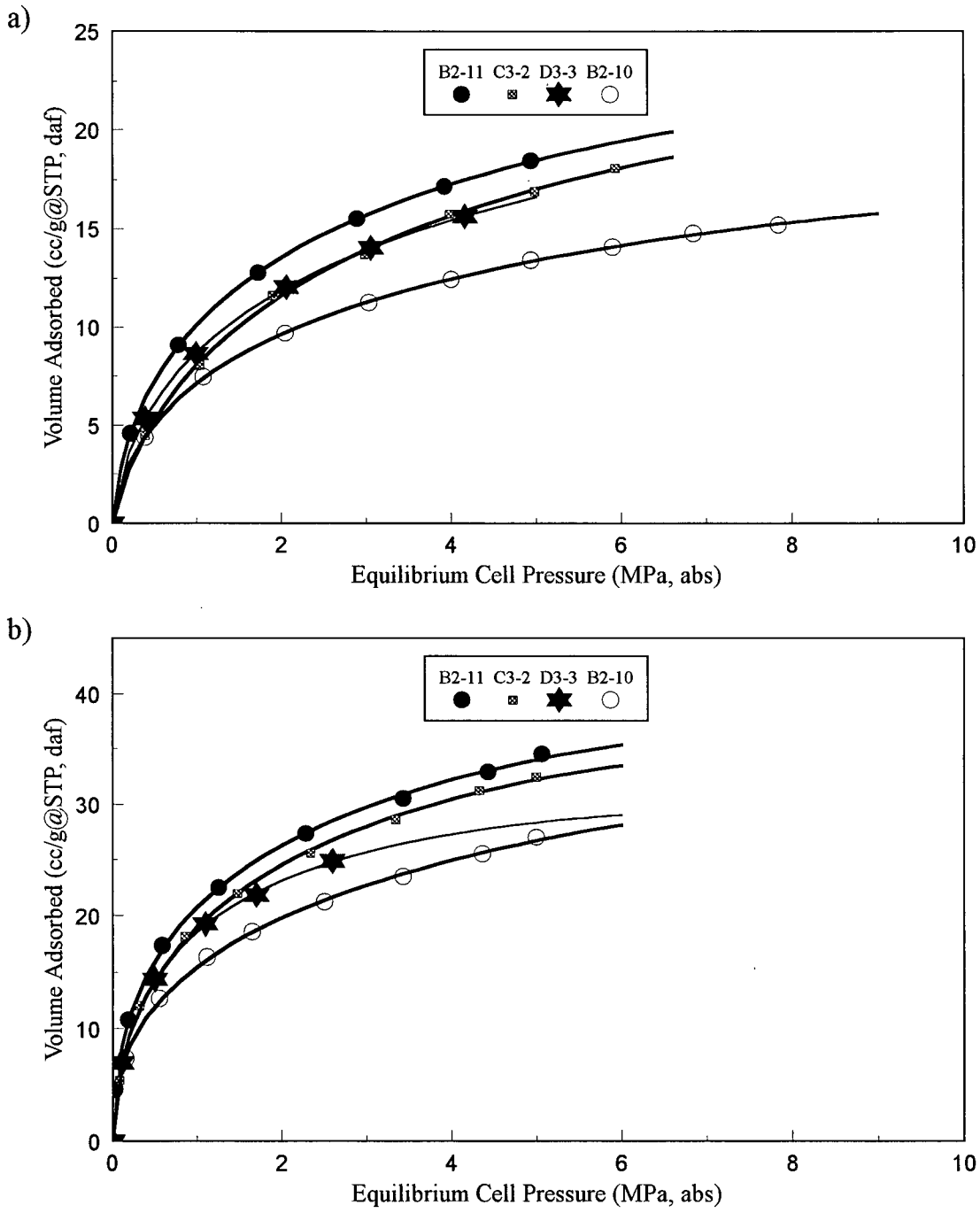

Figure 5-3. Methane (a) and carbon dioxide (b) desorption isotherm data for dry -4 mesh coals. Results presented on a dry, ash-free (daf) coal basis. Lines are D-A fit to data.

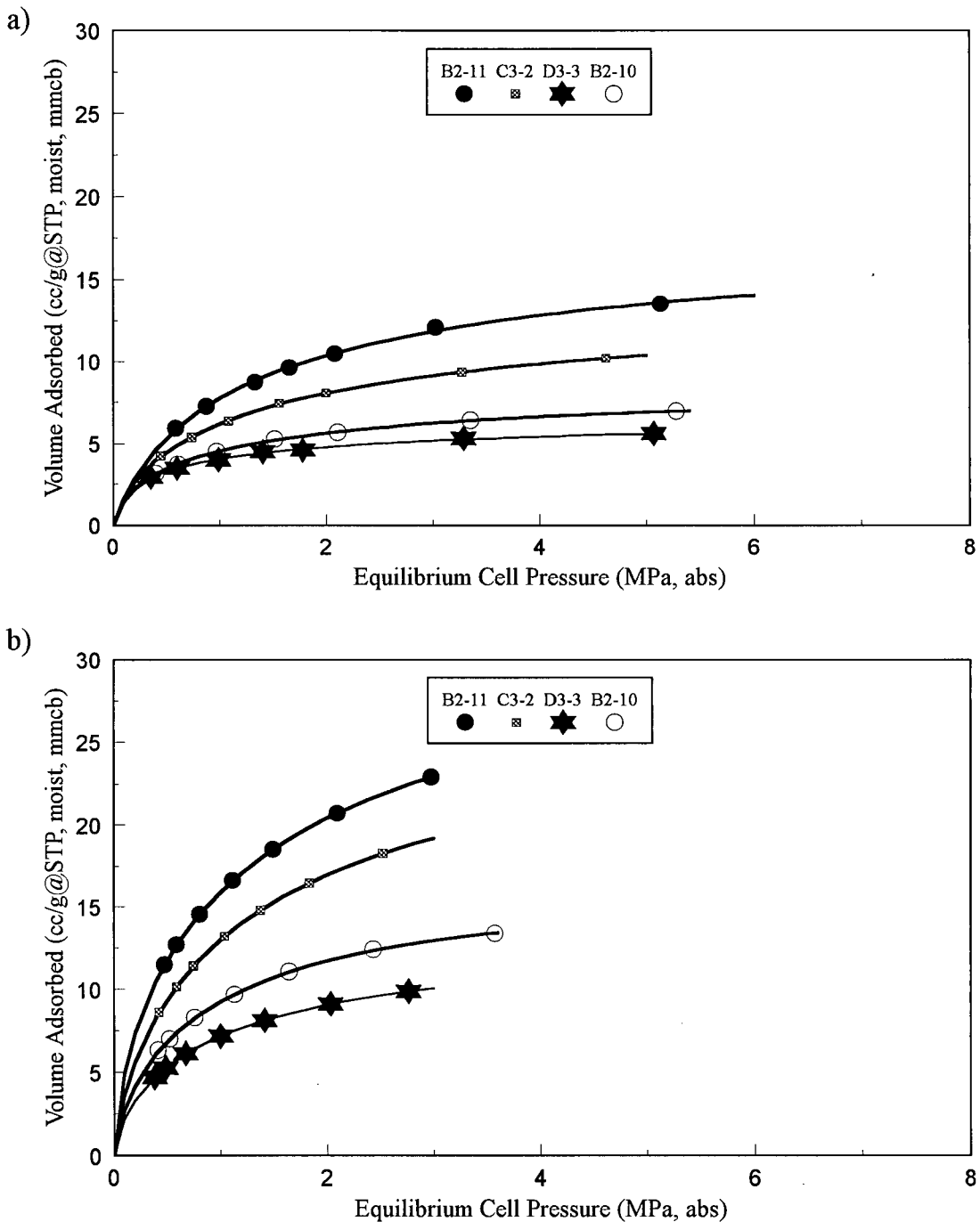

Figure 5-4. Methane (a) and carbon dioxide (b) desorption isotherm data for moisture-equilibrated -60 mesh. Results presented on a moisture-equilibrated, mineral matter-containing (mmcb) coal basis. Lines are D-A fit to data.

Table 5-2. Relative error* calculations for isotherm fits.

	DRY COAL						MOISTURE-EQUILIBRATED COAL					
	CH_4 Isotherm			CO_2 Isotherm			CH_4 Isotherm			CO_2 Isotherm		
Sample	Lang	D-R	D-A	Lang	D-R	D-A	Lang	D-R	D-A	Lang	D-R	D-A
B2-11	5.16 %	1.29 %	0.18 %	13.6 %	12.0 %	1.25 %	1.79 %	0.98 %	0.83 %	1.71 %	1.47 %	0.05 %
C3-2	2.91 %	1.76 %	1.29 %	9.76 %	9.10 %	2.05 %	2.19 %	0.44 %	0.37 %	1.48 %	1.26 %	0.00 %
D3-3	3.78 %	1.16 %	0.19 %	6.97 %	4.00 %	0.56 %	2.89 %	0.89 %	0.81 %	1.67 %	1.13 %	0.11 %
B2-10	4.74 %	1.63 %	0.53 %	8.41 %	7.73 %	1.23 %	2.43 %	0.72 %	0.54 %	1.63 %	1.21 %	0.39 %

* $Average\ Relative\ Error = (100/N)\sum_{j=1}^{N} abs\left(V_{calc} - V_{\exp}\right)_j / V_{\exp}$, *where* N = *number of data points.*

dioxide. The Langmuir curve-fits are much better for the moisture-equilibrated coal data than for the dry coal. This is possibly due to water occupying some of the higher energy adsorption sites, thereby making the remaining coal surface energetically homogeneous, which is consistant with the assumptions of the Langmuir model. The effect of curve-fit error upon IAS predictions will be examined in the following section.

The D-R, D-A and Langmuir equations were also applied to the pure gas adsorption isotherm data of Hall *et al.*[7], to facilitate comparison with their 2-D equation-of-state (EOS) models. The pressure ranges and objective functions for least squares fitting specified by Hall *et al.*[7] were used for comparison. The D-A isotherm equation provided as good a fit to the data as the 2-D EOS models used by Hall *et al.*[7]. The average relative error or, average percent deviation, for the D-A equation is about 0.7 for methane and 1.8 for carbon dioxide compared to about 0.7 and 1.7 for the EOS models, respectively. Both the D-A and 2-D EOS equations have 3 adjustable parameters. The D-R equation generally provides better fits than the Langmuir equation for pure component isotherm correlation, despite having the same number of adjustable parameters.

5.4.3 Binary Gas Isotherm Predictions: Effect of Pure Gas Isotherm Equation

The extended Langmuir (equation 1) and IAS theory (equations 4-7), using the Langmuir, D-R, and D-A equations for spreading pressure calculation, were applied to the pure gas isotherm data for prediction of binary gas adsorption behaviour. Prior to assessing the results of the model predictions, however, the issue of the incorrect zero-pressure limit of n/P for the D-R and D-A isotherms, and hence the suitability of these equations for spreading pressure calculation, is addressed.

The function n/P, calculated using the Langmuir, D-R, and D-A equations, is plotted versus pressure for dry sample B2-11 in Figure 5-5. The zero-pressure assymptote for the D-A/D-R equations does not show up in the pressure range of the experimental data, whereas the low pressure-limit is clearly approached for the Langmuir model. All models provide excellent fits to the data for pressures greater than > 0.5 MPa for methane and carbon dioxide, but the Langmuir model deviates substantially from the D-A/D-R at P < 0.5 MPa. Because significant deviation occurs only at very low pressures, the incorrect limit of the D-A/D-R isotherm is unlikely to substantially affect spreading pressure calculations in the range of pressures used in the current study. A similar conclusion was reached by Richter *et al.*[21], who used the D-R equation for spreading pressure calculations for methane and ethane adsorption on activated carbon. Reduced spreading pressure plots (Figure 5-5) show that all models predict similar spreading pressures for methane, but are substantially different for carbon dioxide. The difference in spreading pressure plots likely reflects the difference in the curve fits for the isotherm equations.

Calculated equilibrium adsorption data plots (Figures 5-6, 5-7) for the methane/carbon dioxide binary system illustrate the differences in predictions of the extended Langmuir model and IAS theory (with different pure gas adsorption isotherm fits). At a constant pressure of 2.5 MPa and a given gas concentration, the extended Langmuir model consistently predicts a greater adsorbed methane mole fraction than the IAS predictions using the Langmuir (IAS/Lang), D-R (IAS/D-R) and D-A equations (IAS/D-A). The IAS/D-R and IAS/Lang yield comparable predictions, whereas the

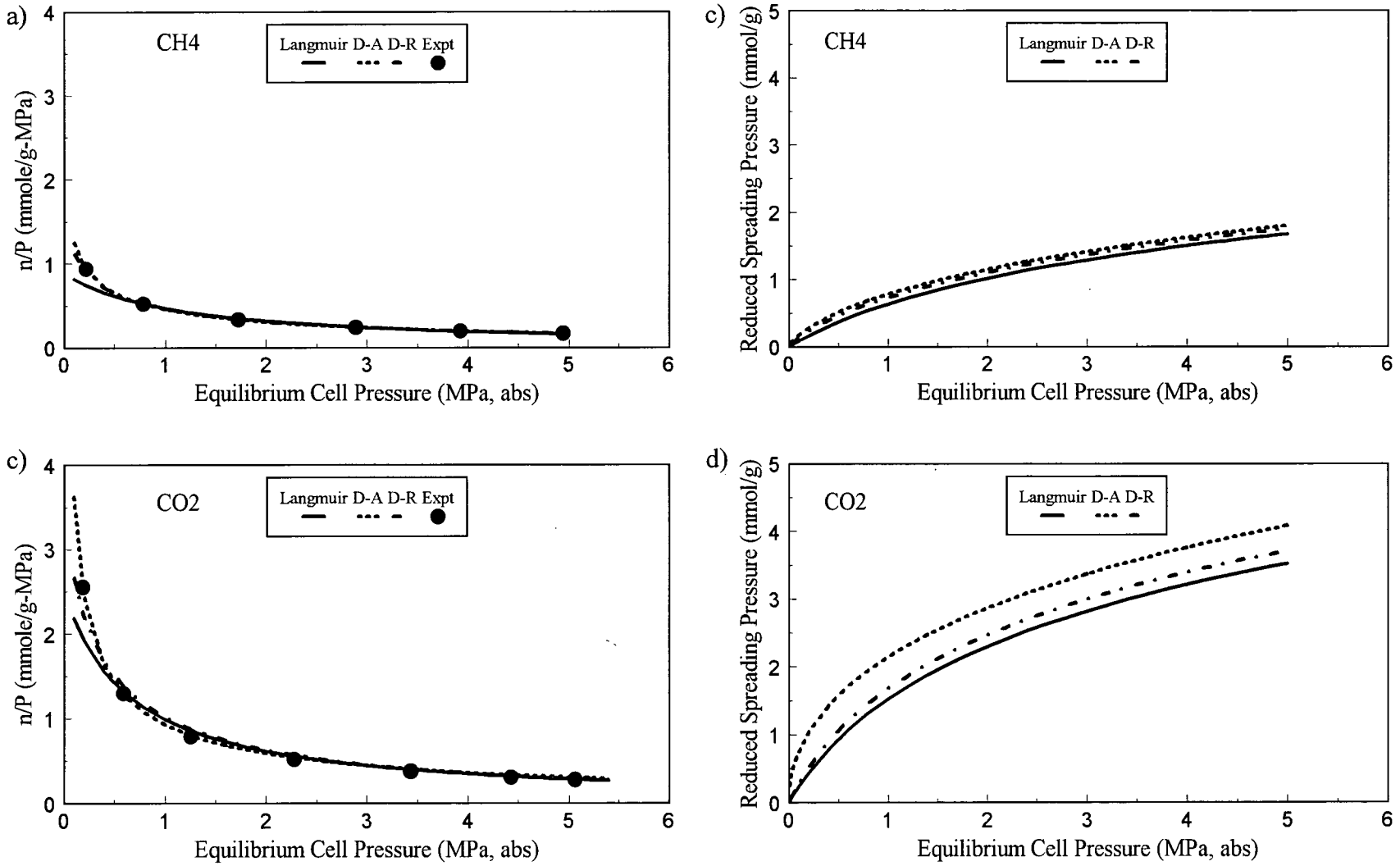

Figure 5-5. n/p (a and c) and reduced spreading pressure plots (b and d) for methane and carbon dioxide B2-11 (dry) isotherm data.

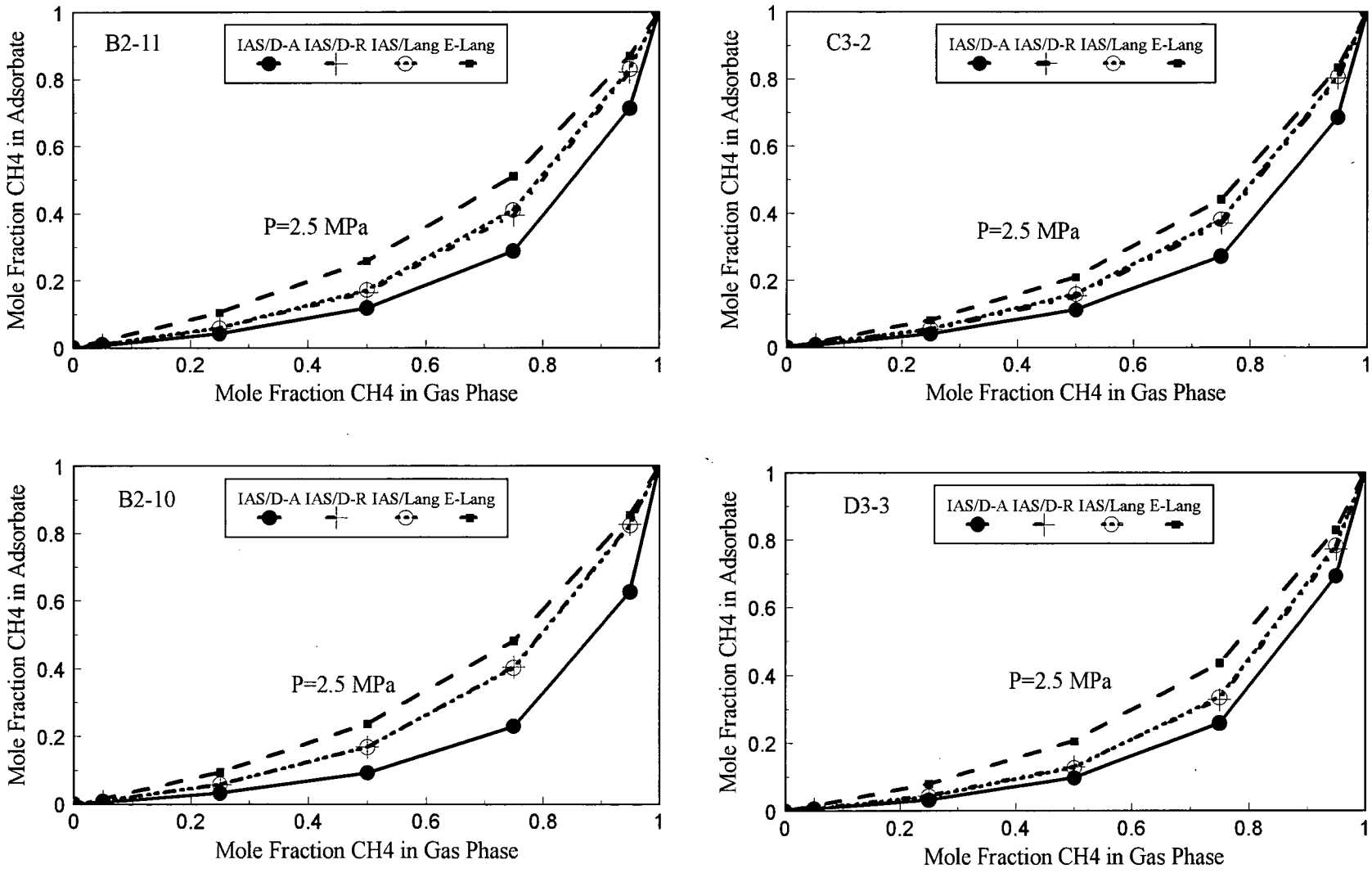

Figure 5-6. Predicted equilibrium compositions for dry -4 mesh coal binary gas adsorption isotherm data.

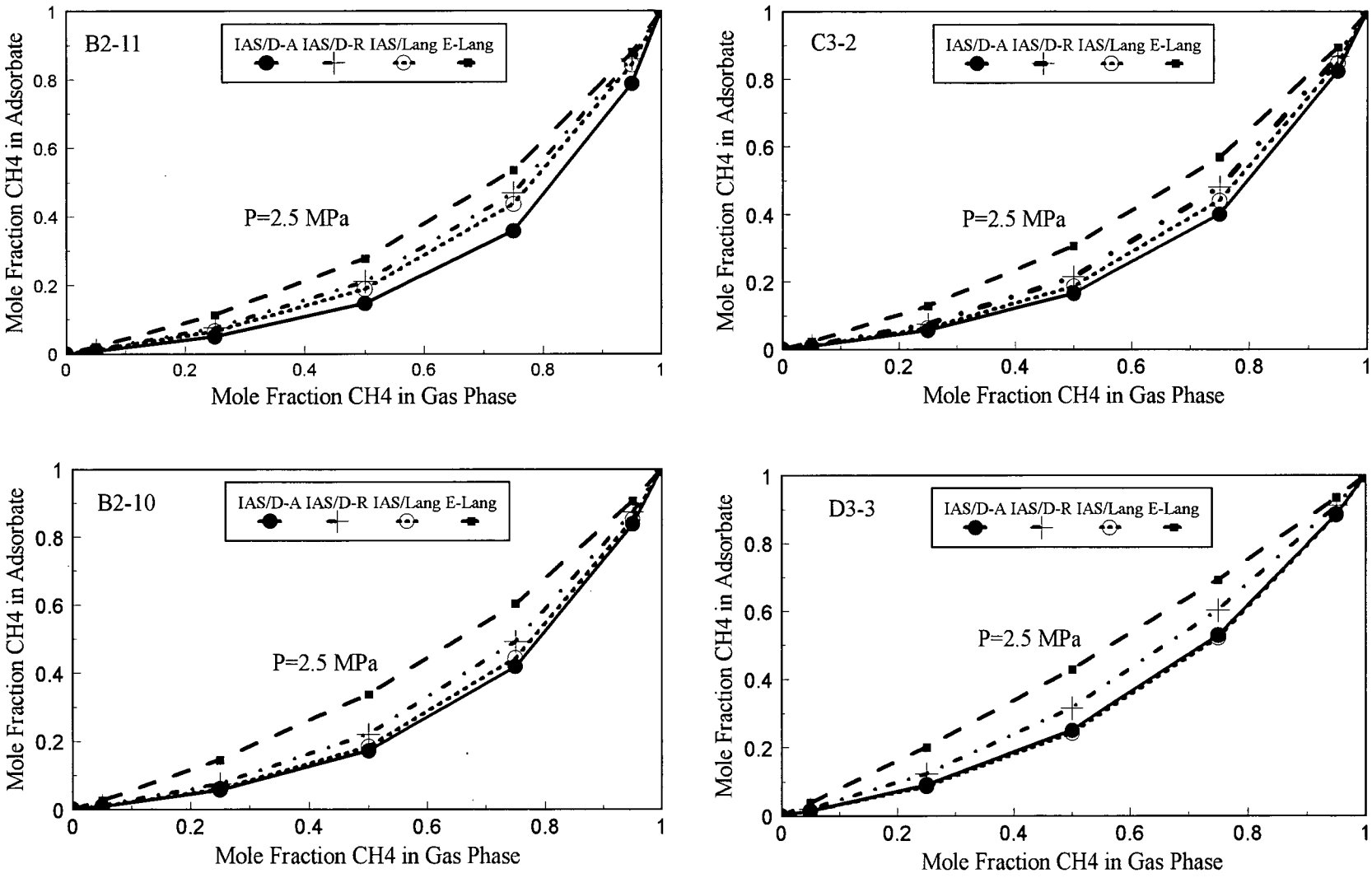

Figure 5-7. Predicted equilibrium compositions for moisture-equilibrated -60 mesh coal binary gas desorption isotherm data.

IAS/D-A predicts lower adsorbed methane mole fractions. Model predictions are in better agreement for the moisture-equilibrated coal desorption data than for the dry adsorption data, which is likely due to smaller difference between isotherm curve fits for the moisture-equilibrated coal isotherm data than for the dry coal data.

The effect of total gas pressure, moisture content, and coal composition upon binary gas adsorption, as predicted from single component isotherms, can be illustrated using separation factor (equation 3) plots (Figures 5-8, 5-9). For purposes of clarity, only three model predictions are shown: the extended Langmuir, IAS/Lang and IAS/D-A. For dry coal, the carbon dioxide separation factor, as determined from IAS theory, is a function of pressure (Figure 5-8). The IAS/D-A theory predicts a decrease in carbon dioxide separation factor with an increase in pressure and with carbon dioxide concentration, with the exception of sample D3-3. The trend of decreasing selectivity with an increase in concentration of the more strongly sorbed component is consistent with previous findings[20]. The IAS/Langmuir theory predicts the opposite: carbon dioxide selectivity increases with pressure and gas phase concentration. The extended Langmuir equation gives a constant separation factor, which is independent of total gas pressure and concentration. For moisture-equilibrated coal data, IAS/D-A and IAS/Langmuir predictions are similar and separation factors increase with an increase in total pressure, and with an increase in carbon dioxide gas concentration. The carbon dioxide separation factors for moisture-equilibrated coal data are generally smaller than for dry coal data.

Model predictions indicate that the presence of moisture in coal decreases the selectivity for carbon dioxide. Water competes with both gases for adsorption sites on

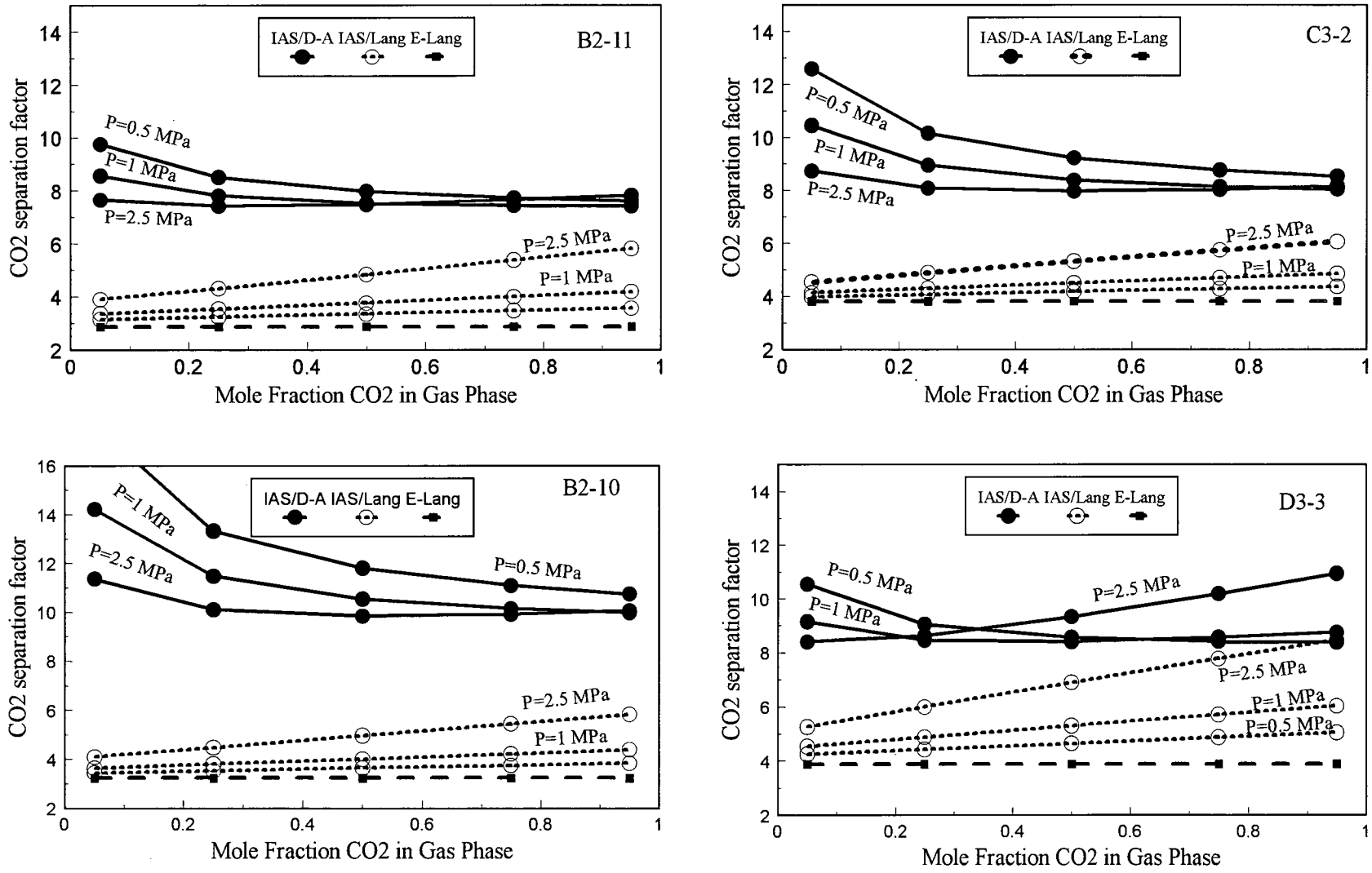

Figure 5-8. Predicted carbon dioxide separation factors for dry -4 mesh coal binary gas adsorption isotherm data.

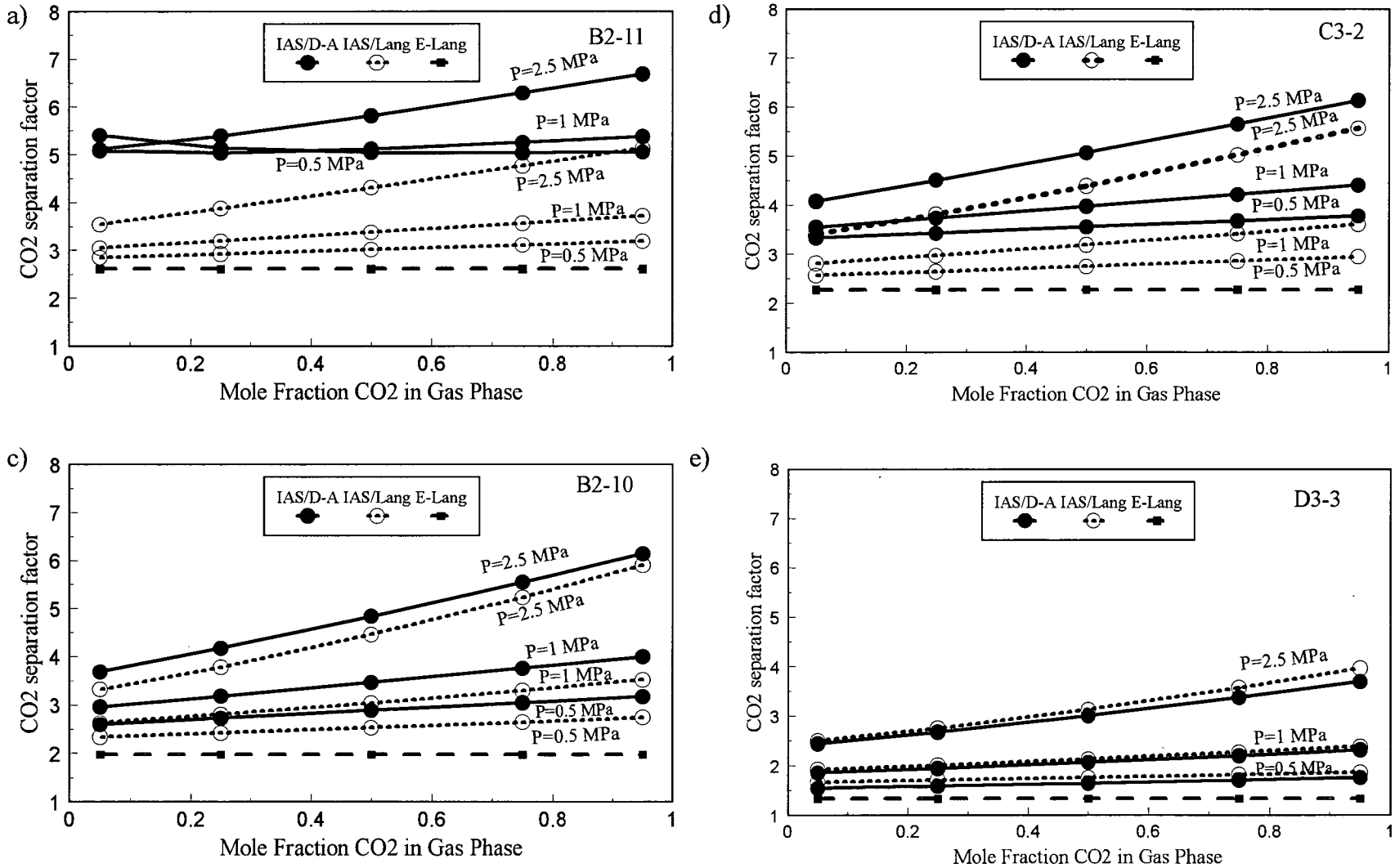

Figure 5-9. Predicted carbon dioxide separation factors for moisture-equilibrated -60 mesh coal binary gas desorption isotherm data. Note scale change from Figure 5-8.

the coal surface, and apparently occupies the higher energy sites that would otherwise be occupied by carbon dioxide if the coal were dry.

The effect of coal composition upon carbon dioxide selectivity, as determined from model predictions, is not obvious. Although some variablity between coals exists, there is no obvious relationship between coal composition and carbon dioxide selectivity, particularly for dry coal (Figure 5-8). For the wet coals, the bright (C3-2) and banded bright (B2-11) coals have higher carbon dioxide selectivities than the dull coals (B2-10 and D3-3), despite having a higher moisture content (Table 5-1). The difference in selectivities is minor, however.

5.4.4 Experimental Binary Gas Isotherms

Binary gas desorption (303 K) isotherms for two feed gas compositions (90% CH_4/10% CO_2 and 75% CH_4/25% CO_2) illustrate similar trends with coal composition as found with pure gas isotherms (Figure 5-10). The total adsorbed gas volumes are greater for the banded bright and bright coals than for the two dull coals. If the results are plotted on a dry, ash- free (daf) basis (Figure 5-11), there is less of a discrepancy between isotherms (as was observed for pure component isotherm data). Although a relationship between coal maceral composition and gas adsorption appears to exist, this relationship is not simply one of increasing gas adsorption with increasing total vitrinite content. Inertinite macerals such as semifusinite may also contribute greatly to the adsorption capacity of coals[15]; the highest sorbing coal in this study contains a mixture of vitrinite and semifusinite macerals.

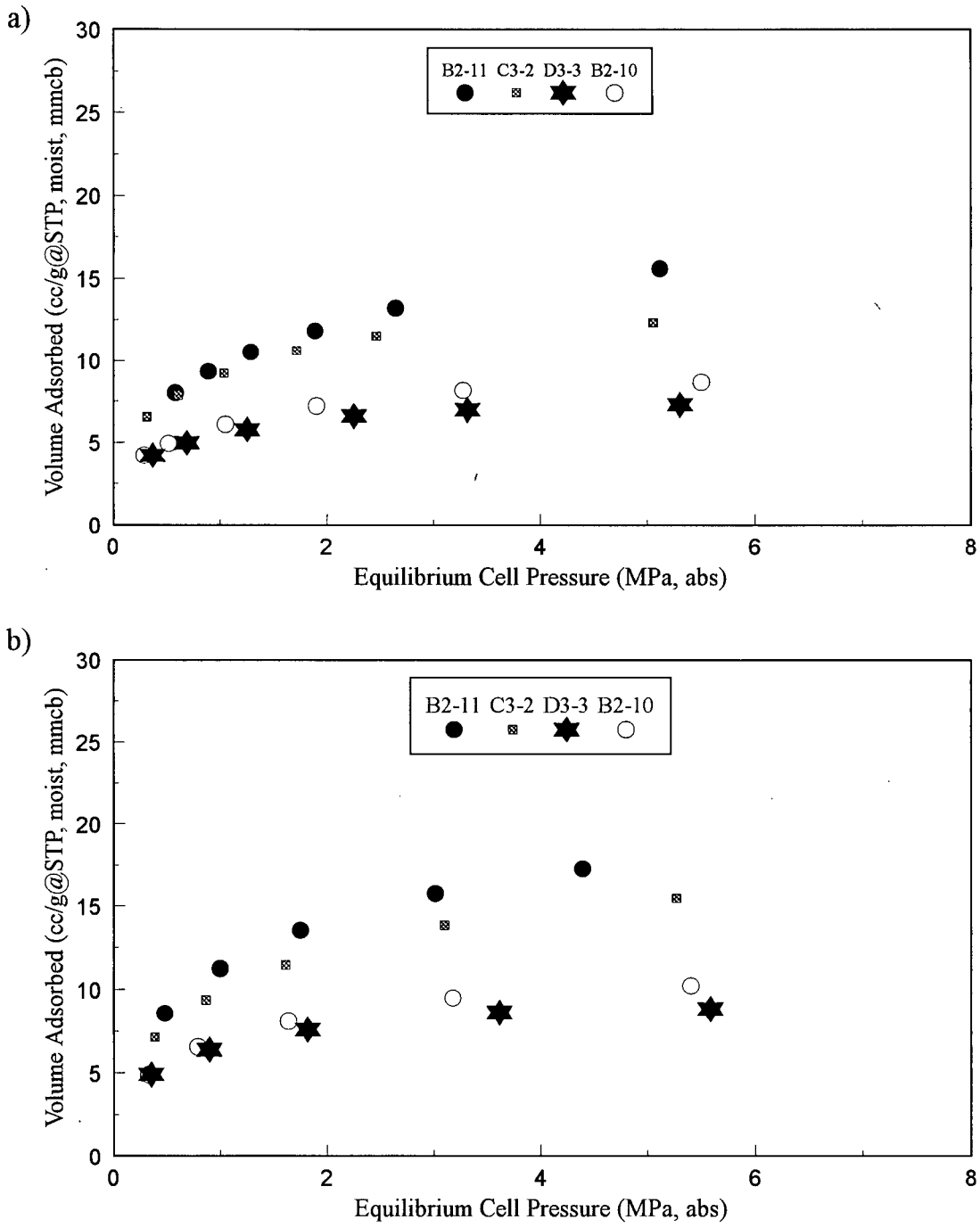

Figure 5-10. (a) 90% methane/10% carbon dioxide and (b) 75% methane /25% carbon dioxide total desorption isotherm data for moisture -equilibrated -60 mesh coals. Results presented on a moisture -equilibrated, mineral matter-containing (mmcb) coal basis.

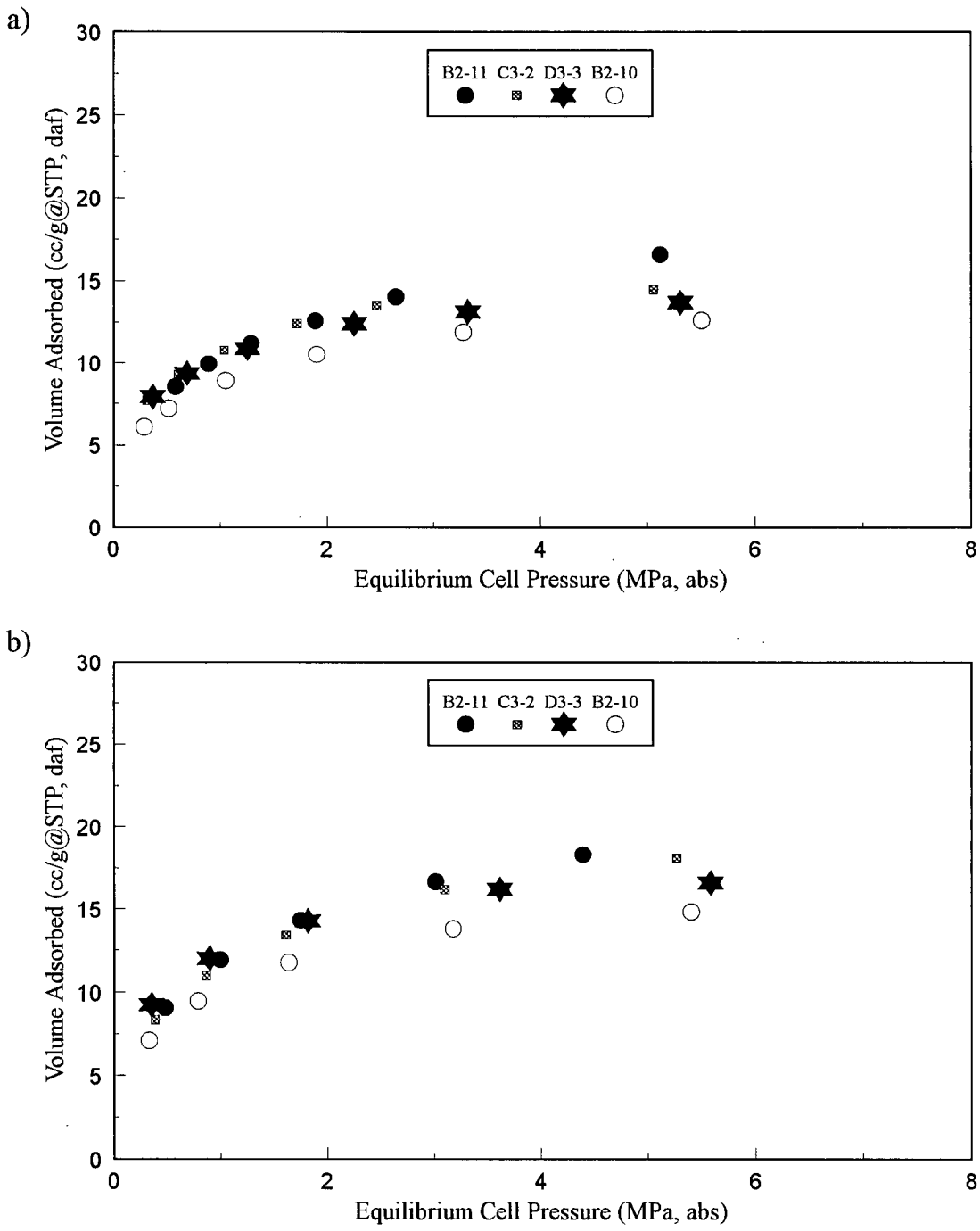

Figure 5-11. (a) 90% methane/10% carbon dioxide and (b) 75% methane / 25% carbon dioxide total desorption isotherm data for moisture -equilibrated -60 mesh coals. Results presented on a dry, ash-free (daf) coal basis.

Component adsorption isotherms (Figure 5-12) demonstrate that the methane is preferentially released at higher pressures during desorption; thus, the methane adsorbed phase mole fraction decreases with a decrease in total gas pressure. For the 90% CH_4/10% CO_2 (feedgas) isotherm, significant carbon dioxide desorption occurs only at relatively low pressure. Greaves *et al.*[5], who studied binary gas adsorption/desorption on dry coal, observed a similar retention of carbon dioxide until low pressures. As suggested by those authors, economic assessments must take into consideration the relative adsorption of component gases for the accurate prediction of economic gas (methane) reserves.

CO_2 separation factors for the 75% CH_4/25% CO_2 (feedgas) desorption isotherm are plotted against gas composition in Figure 5-13. The separation factors decrease with the CO_2 gas phase mole fraction. Separation factors determined from 90% CH_4/10% CO_2 (feedgas) desorption isotherm also generally decrease with CO_2 gas phase mole fraction (not shown). Although there is some variability between coals, the difference in carbon dioxide selectivities is probably not significant based upon a 10% experimental error in each component. Model predictions from pure component data suggest that coal moisture content is a control upon carbon dioxide selectivity. Because the coals studied vary in moisture content as well as organic composition and mineral content, the control of these factors upon gas selectivity is difficult to isolate with the current binary gas data set. It appears, however, that although coal bulk composition and organic matter composition are important controls upon the adsorbed volume of each component, the selectivity of carbon dioxide over methane is not significantly affected.

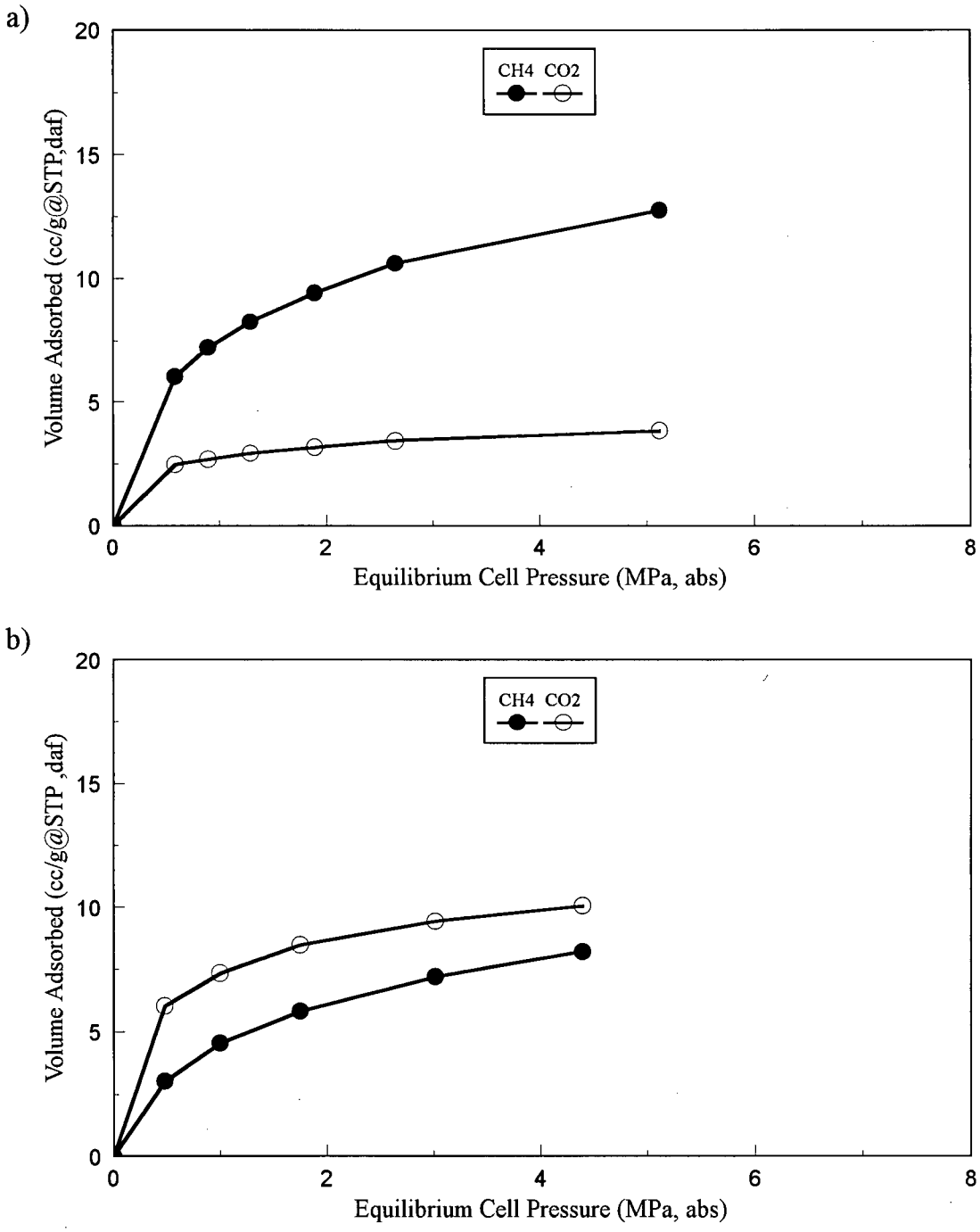

Figure 5-12. Sample B2-11 component desorption isotherm for (a) 90% methane /10% carbon dioxide and (b) 75% methane/25% carbon dioxide gas mixtures. Results presented on a dry, ash-free (daf) basis.

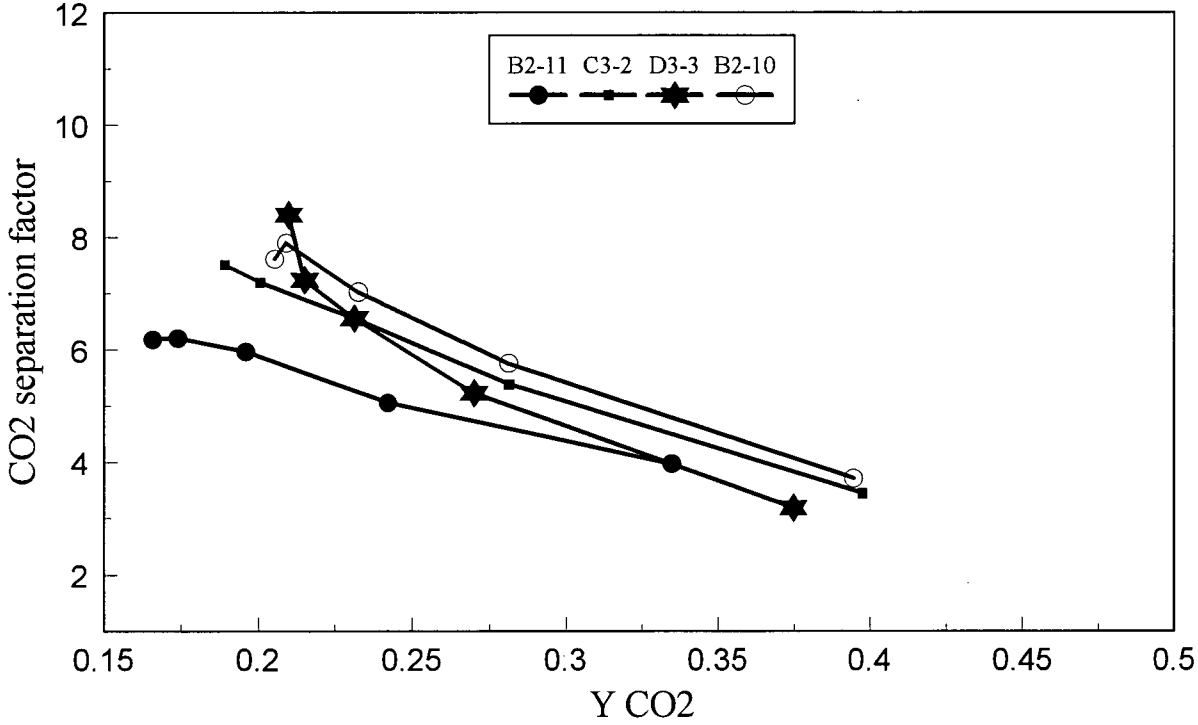

Figure 5-13. Experimental carbon dioxide separation factors for moisture-equilibrated -60 mesh coal 75% methane/25% carbon dioxide desorption isotherm data. Note system is not at constant pressure.

5.4.5 Binary Gas Model Fits to Experimental Data

The extended Langmuir model and IAS theory were used to predict the binary gas adsorption data of sample B2-11, the purest (lowest ash) coal in the current data set. In addition, the data of Hall *et al.*[7] were used for model comparison, as the Hall *et al.*[7] data spans a much greater range of gas compositions than the current data set. Only Hall *et al.*[7] binary gas data at total pressures less than ~ 5.5 MPa were used to facilitate comparison with the current data set.

Table 5-3 contains the relative error estimates of each model for sample B2-11 total gas, methane and carbon dioxide adsorption. For total gas adsorption, the IAS models are slightly more accurate than the extended Langmuir equation. The IAS models are also generally superior for component adsorption, particularly for the 75% CH_4 isotherm. Of the IAS models, the IAS/D-A provides a better fit than all other models for the 75% isotherm.

Relative error estimates for the binary gas data of Hall *et al.*[7] (Table 5-4) are quite variable, and depend upon the feed gas composition. Relative errors for total gas adsorption are comparable for the extended Langmuir and IAS models, but are variable for the single component adsorption. Surprisingly, the extended Langmuir and the IAS/Lang models provide, on average, a better fit to component data than the IAS/D-R and IAS/D-A models. This is despite the fact that the D-A and D-R equations fit the pure component isotherms better than the Langmuir equation. A possible cause of the poorer curve fits of the IAS/D-A and IAS/D-R for component adsorption is the error introduced in the spreading pressure calculation do to the incorrect limit expressed by equation (9). This potential source of error could be tested by applying modified Dubinin equations, as

Table 5-3. Relative error* calculations for binary gas isotherm fits.

	90 % CH_4/10 % CO_2 (feedgas) Isotherm (6 data points)											
	Extended Langmuir			IAS/Lang			IAS/D-R			IAS/D-A		
Sample	Vtotal	VCH_4	VCO_2	Vtotal	VCH_4	VCO_2	Vtotal	VCH_4	VCO_2	Vtotal	VCH_4	VCO_2
B2-11	9 %	5 %	30 %	8 %	6 %	13 %	8 %	2 %	24 %	7 %	16 %	19 %
	75 % CH_4/25 % CO_2 (feedgas) Isotherm (5 data points)											
	Vtotal	VCH_4	VCO_2	Vtotal	VCH_4	VCO_2	Vtotal	VCH_4	VCO_2	Vtotal	VCH_4	VCO_2
B2-11	11 %	28 %	38 %	9 %	14 %	25 %	9 %	25 %	32 %	7 %	7 %	8 %

* *Average Relative Error* $= (100/N)\sum_{j=1}^{N} abs\left(V_{calc} - V_{\exp}\right)_j / V_{\exp}$, *where N = number of data points.*

Table 5-4. Relative error* (absolute average percent deviation) calculations for Hall *et al.*[7] binary gas isotherm fits. The terminology of Hall *et al.*[7] is retained.

20 % CH_4 (1)/80 % CO_2 (2) (feedgas) Isotherm (5 data points)											
Langmuir			IAS/Lang			IAS/D-R			IAS/D-A		
ω	ω1	ω2	ω	ω1	ω2	ω	ω1	ω2	ω	ω1	ω2
4 %	20 %	3 %	4 %	13 %	5 %	4 %	17 %	5 %	3 %	21 %	5 %
40 % CH_4 (1) /60 % CO_2 (2) (feedgas) Isotherm (5 data points)											
ω	ω1	ω2	ω	ω1	ω2	ω	ω1	ω2	ω	ω1	ω2
7 %	17 %	6 %	8 %	13 %	10 %	8 %	16 %	10 %	7 %	18 %	14 %
60 % CH_4(1) /40 % CO_2 (2) (feedgas) Isotherm (5 data points)											
ω	ω1	ω2	ω	ω1	ω2	ω	ω1	ω2	ω	ω1	ω2
4 %	13 %	6 %	5 %	7 %	9 %	5 %	11 %	10 %	4 %	14 %	15 %
80 % CH_4(1) /20 % CO_2 (2) (feedgas) Isotherm (5 data points)											
ω	ω1	ω2	ω	ω1	ω2	ω	ω1	ω2	ω	ω1	ω2
3 %	6 %	11 %	4 %	6 %	16 %	3 %	7 %	17 %	3 %	10 %	27 %

* *Average Relative Error* $= (100/N)\sum_{j=1}^{N} abs\left(\omega_{calc} - \omega_{\exp}\right)_j / \omega_{\exp}$, *where N = number of data points.*

proposed by Kapoor *et al.*[31], which have the correct Henry's law limit. The modification suggested by Kapoor *et al.*[31], however, involves the addition of two extra parameters for each Dubinin equation, giving a total of 4 and 5 adjustable parameters for the D-R and D-A equations, respectively.

Model predictions for the variation of carbon dioxide selectivity with gas concentration also differ (Figure 5-14). The experimental results of Hall *et al.*[7] show that the carbon dioxide selectivity for each isotherm slightly decreases with an increase in carbon dioxide gas phase mole fraction or partial pressure. The IAS/D-A model is the only model to at least qualitatively predict the experimental trend in carbon dioxide selectivity, despite predicting a higher selectivity than the other models. The extended Langmuir model predicts a constant carbon dioxide separation factor, which is not consistent with the experimental data. The IAS/D-R and IAS/Langmuir models both predict an increase in CO_2 selectivity with an increase in partial pressure, which is also in disagreement with the experimental data. The variablility of carbon dioxide selectivity with gas composition and pressure for the Hall *et al.*[7] data set is quite small, but in systems where the selectivity varies greatly, the incorrect selectivity predictions by the IAS and extended Langmuir models could lead to serious errors in predictions of binary gas adsorption/desorption.

5.4.6 Implications for Carbon Dioxide Sequestering and Reservoir Characterization

Mixed gas desorption isotherms collected using realistic initial feedgas compositions and pressures are an important tool for the accurate prediction of gas storage capacities, which are in turn used for economic assessment of gas reservoirs.

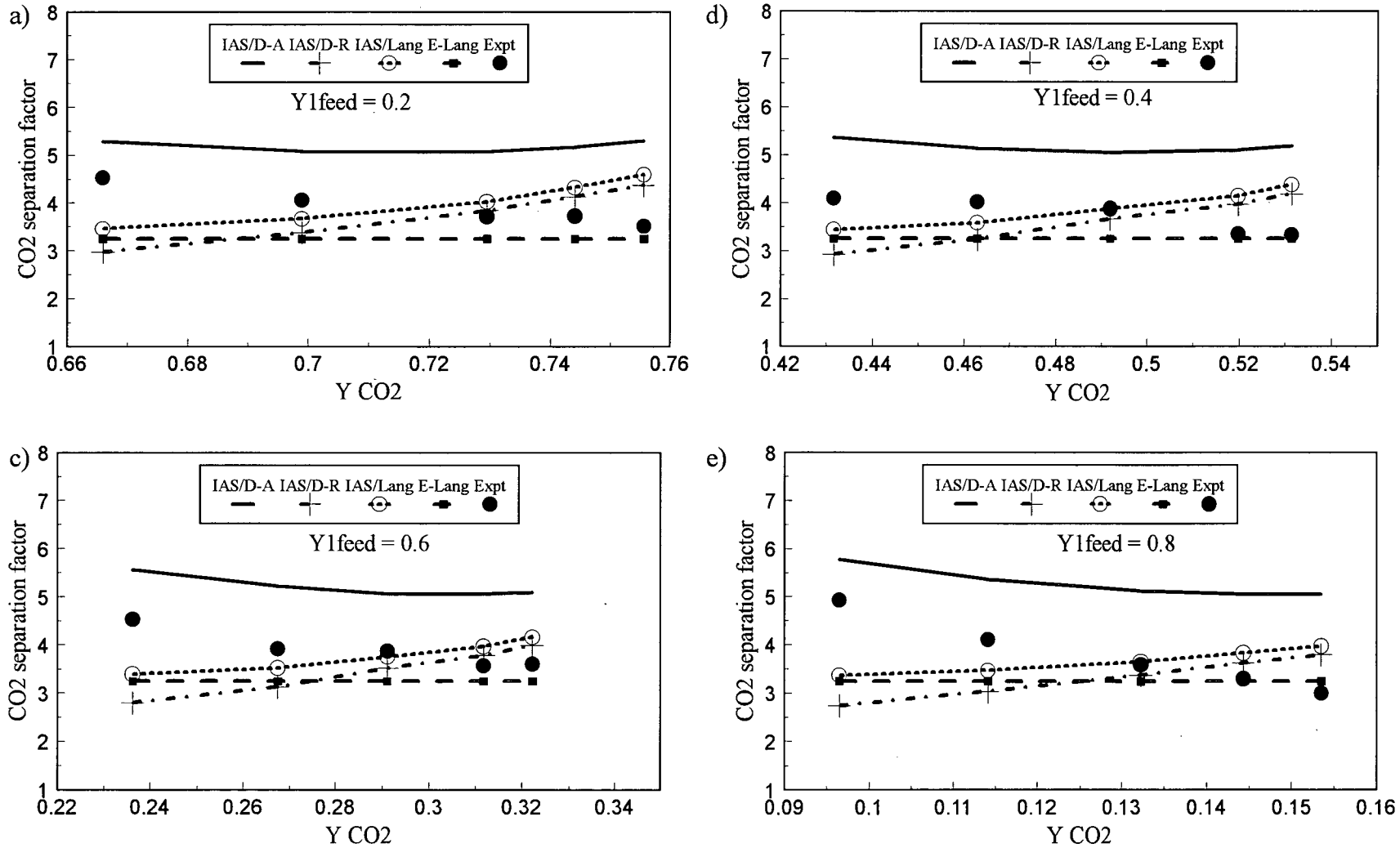

Figure 5-14. Experimental carbon dioxide separation factors for moisture-equilibrated coal desorption isotherm data. Note system is not at constant pressure.

Experimental results for moisture-equilibrated coal in the current study have demonstrated that the adsorbed phase methane mole fraction generally decreases with total gas pressure, which is consistent with previous studies of dry coal/binary gas systems[5].

Carbon dioxide selective adsorption over methane is an important coal characteristic that will have important implications for the success of any enhanced recovery project involving carbon dioxide injection. The relative insensitivity of CO_2 selectivity to coal composition should simplify recovery predictions in regions where coal seams are highly heterogeneous with respect to organic and mineral content. Complicating predictions, however, is the fact that selectivity, particularly in the case of dry coals, is a function of carbon dioxide concentration and total gas pressure. In addition, selectivity is a function of coal moisture content, and therefore an accurate estimate of in-situ coal matrix water content is required for the accurate prediction of binary gas adsorption.

Models used for binary gas adsorption differ in their ability to predict carbon dioxide selectivity trends with reservoir pressure. For moisture-equilibrated coals used in this study, the experimentally determined carbon dioxide selectivities vary only slightly with pressure, and hence the extended Langmuir model, which predicts a constant selectivity, is relatively accurate for binary gas predictions. If the selectivity varies strongly with pressure for a particular coal compositon or rank, the extended Langmuir model may not be adequate for binary gas adsorption predictions. The poor fit of the Langmuir isotherm to pure gas adsorption isotherms for some coal/gas systems, such as

for dry coals used in the current study, could lead to inaccurate extended Langmuir predictions for binary gas adsorption.

5.5 CONCLUSIONS

The effect of coal composition and moisture content upon binary gas adsorption, as well as the effect of various single component isotherm equations upon binary gas predictions was investigated. The following conclusions are drawn:

1) The Dubinin-Astakhov and Dubinin-Radushkevich equations are clearly superior to the Langmuir equation for fitting methane and carbon dioxide pure component isotherm data on dry and moisture-equilibrated coals. This conclusion is based on curve-fitting of dry and moisture-equilibrated Gates Formation coal isotherm data, as well as for moisture-equilibrated coal data of Hall *et al.*[7]. The Langmuir curve-fit errors are much larger for dry coal than for moisture-equilibrated coal data. This is possibly due to water occupying some of the higher energy adsorption sites, thereby making the remaining coal surface energetically homogeneous, which is consistant with the assumptions of the Langmuir model.

2) IAS and extended Langmuir predictions using pure component isotherm data show no significant difference between carbon dioxide selectivities of different coal types.

3) IAS and extended Langmuir predictions using pure component dry coal adsorption isotherm data and moisture-equilibrated coal desorption isotherm data suggest that carbon dioxide selectivity is greater for dry coals than for moisture-equilibrated coals.

4) Predicted equilibrium compositional diagrams illustrate a large discrepancy between the IAS models and the extended Langmuir model. The IAS models typically predict lower methane sorbed phase concentrations at a given pressure than the extended Langmuir model, particularly for dry coals. Only the IAS/D-A predicts a decrease in carbon dioxide selectivity with increasing carbon dioxide concentration for dry coal data, which is in agreement with experimental findings. The IAS/D-R and IAS/Langmuir models both predict an increase in carbon dioxide selectivity with carbon dioxide concentration. The discrepancy between IAS models, particularly for dry coal data, is likely a result of pure component isotherm curve-fit errors. The extended Langmuir model predicts a constant selectivity. All models are in better agreement for moisture-equilibrated coal data, but the IAS models all predict a slight increase in carbon dioxide selectivity with concentration.

5) Experimental binary gas adsorption data demonstrates that total gas adsorption is affected by coal composition, but the selectivity of carbon dioxide over methane is not. A slight variation in selectivity exists between coal types, but the variation is not large and is difficult to separate from the effect of varying coal moisture content.

6) Methane adsorbed phase concentration decreases with pressure for the moisture-

equilibrated coal/binary gas desorption isotherms in agreement with previous studies of dry coal.

7) IAS models are generally more accurate for both total gas adsorption and component adsorption than the extended-Langmuir model for the current experimental binary gas adsorption data set. IAS predictions for the Hall *et al.*[7] binary gas adsorption data, however, are generally not superior to the extended Langmuir model.

8) Carbon dioxide selectivities, obtained from the data of Hall *et al.*[7] , decrease with an increase in carbon dioxide concentration. All model predictions, with the exception of the IAS/D-A model, fail to qualitatively predict this behaviour.

Nomenclature

A = *adsorbent surface area*
b = *Langmuir model constant*
D = *constant of D-A or D-R equation*
m = *mass of coal*
n = *amount adsorbed [mol/g or mmol/g] or D-A equation exponent*
n_i° = *is the amount of pure component adsorbed from pure gas at the same temperature and spreading pressure as the adsorbed mixture*
P = *total pressure*
P_i = *Partial pressure of component i*
P_i° = *gas (vapour) pressure of the pure component adsorbed at the same temperature and spreading pressure as the solution*
P_o = *adsorbate saturation vapour pressure*
R = *gas constant. 8.3145 [J/mol K]*
T = *temperature*
V = *volume or volume adsorbed @STP*
V_L = *Langmuir isotherm adsorption constant*
V_o = *D-A or D-R micropore capacity*
x_i = *adsorbed phase mole fraction of component i*
y_i = *gas phase mole fraction of component i*

Subscripts

ads = adsorbed
i = component i
j = component j
L= Langmuir
m = molar quantity
ref = reference cell
s = sorbate
sc = sample cell
STD = standard conditions
v = voids
z = gas compressibility factor

Superscripts

I = current pressure step
I-1 = previous pressure step

Greek Symbols

α = *separation factor or selectivity ratio, Eqn. (3)*
π = *spreading pressure*
π^* = *reduced spreading pressure, Eqn. (5)*

5.6 REFERENCES

1. Deo, M.D., Whitney, E.M., and Bodily, D.M. In Proceedings of the 1993 International Coalbed Methane Symposium Tuscaloosa, May 17-21, 1993, pp. 223-232.

2. Mavor, M.J., Owen, L.B., and Pratt, T.J. Paper SPE 20728, presented at the 65th Annual Technical Conference of the Society of Petroleum Engineers, New Orleans, Louisiana, Sept. 23-26, 1990, pp.1-14

3. Stevenson, M.D., Pinczewski, W.V., Somers, M.L., and Bagio, S.E. SPE Paper 23026, presented at the SPE Asia-Pacific Conference, Perth, Western Australia, November 4-7, 1991, pp.741-755

4. Arri, L.E., Yee, D., Morgan, W.D., and Jeansonne, M.W. SPE Paper 24363, presented at the SPE Rocky Mountain Regional Meeting, Casper, Wyoming, May 18-21, 1992, pp. 459-472

5. Greaves, K.H., Owen, L.B., and McLennan, J.D. In Proceedings of the 1993 International Coalbed Methane Symposium, Tuscaloosa, May 17-21, 1993, pp. 151-160

6. Harpalani, S. and Pariti, U.M. In Proceedings of the 1993 International Coalbed Methane Symposium, Tuscaloosa, May 17-21, 1993, pp. 151-160

7. Hall, F.E., Zhou, C., Gasem, K.A.M., Robinson, R.L., Jr., and Yee, D. Paper SPE 29194, presented at the 1994 Eastern Regional Conference and Exhibition, Charleston, WV, Nov. 8-10, 1994, pp. 329-344.

8. Zuber, M.D., Saulsberry, J.L., and Sparks, D.P. In 'A Guide to Coalbed Methane Reservoir Engineering', Gas Research Institute Report No. GRI-94/0397, Chicago, Illinois, 1996

9. Reznik, A.A., Singh, P.K., and Foley, W.L. *SPE J.* 1984, **24**, 521.

10. Puri, R., and Yee, D. Paper SPE 20732, presented at the 65th Annual Technical Conference and Exhibition of the SPE, New Orleans Louisiana, Sept. 23-26, 1990, pp.193-202.

11. Gunter, W.D., Gentzis, T., Rottenfusser, B.A., and Richardson, R.J.H. Paper Presented at the Third International Conference on Carbon Dioxide Removal, Massachusetts Institute of Technology, Sept. 9-11, 1996.

12. Joubert, J.I., Grein, C.T., and Bienstock, D. *Fuel* 1973, **52**, 181

13. Joubert, J.I., Grein, C.T., and Bienstock, D. *Fuel* 1974, **53**, 186

14. Levy, J.H., Day, S.J., and Killingley, J.S. *Fuel* 1997, **74**, 1

15. Lamberson, M.N., and Bustin, R.M. *AAPG Bull.* 1993, **77**, 2062

16. Ruthven, D.M. 'Principles of Adsorption and Adsorption Processes', John Wiley and Sons, Inc., New York, 1984

17. Yang, R.T. 'Gas Separation by Adsorption Processes', Butterworths, Boston, Mass., 1987

18. Myers, A.L., and Prausnitz, J.M. *A.I.Ch.E. J.* 1965, **11**, 121

19. DeGance, A.E. *Fluid Phase Equilibria* 1992, **78**, 99

20. Myers, A.L. *Ind. Eng. Chem.* 1968, **60**, 45

21. Richter, E., Schutz, W., and Myers, A.L. *Chem. Eng. Sci.*, **44**, 1609

22. Clarkson, C.R., Bustin, R.M., and Levy, J.H. *Carbon*, **35**, 1689

23. Talu, O., and Myers, A.L. *A.I.Ch.E. J.*, **34**, 1988

24. Bustin, R.M., Cameron, A.R., Grieve, D.A., and Kalkreuth, W.D. 'Coal Petrology: Its Principals, Methods and Applications, 2nd edition, Geological Association of Canada Short Course Notes, 3', 1985

25. American Society for Testing and Materials. '1980 Annual Book of ASTM Standards', Part 26, D-720.

26. Levy, J.H., Killingley, J.S., and Day, S.J. In Proceedings of the Symposium on Coalbed Methane Research and Development in Australia, v. 4, 1992, pp. 1-8

27. Clarkson, C.R., and Bustin, R.M. *submitted to Fuel*

28. Peng, D-Y., and Robinson, D.B. *Ind. Eng. Chem. Fundam.* 1976, **15**, 59

29. Langmuir, I *J. Am. Chem. Soc.* 1918, **40**, p.1361

30. Dubinin, M.M., and Astakhov, V.A. In 'Advances in Chemistry Series', No. 102, American Chemical Society Publications, Washington, D.C., 1971

31. Kapoor, A., Ritter, J.A., and Yang, R.T. *Langmuir*, **5**, 1118

CHAPTER 6

CONCLUSIONS

6.1 INTRODUCTION

Accurate gas content determination is critical for the economic assessment of coal gas reservoirs and gas production forecasts. Gas content estimates are typically obtained from sub-samples of the reservoir, and therefore it is necessary to understand how variability in coal properties affects such estimates. The use of accurate equilibrium and non-equilibrium adsorption models is also required to obtain reasonable gas-in-place values.

Coal is a compositionally complex material containing both organic and inorganic components. The compositional heterogeneity of coal is expressed at all scales, from the molecular to the seam scale[1]. Of particular interest to coalbed methane exploration and development programs is the heterogeneity at the seam scale. Compositional heterogeneity imparts heterogeneity in other coal physical properties, such as gas adsorption and pore structure, which significantly affect gas contents and transport. Failure to properly characterize this heterogeneity could lead to inaccurate economic assessments of gas reserves. An understanding of how coal property variations affect gas transport at the seam scale could aid in short and long term gas production forecasting. This thesis has addressed the effects of compositional heterogeneity, moisture content, and pore structure upon multicomponent equilibrium adsorption and matrix transport at the laboratory scale. The goal of this research has been to understand and quantify these effects for coals at the laboratory scale in order to aid in the characterization of a coal gas

resource at the seam scale. The "scaling up" of laboratory results to the seam or multiple seam level is a difficult task, but laboratory investigations of this nature will eventually lead to a greater understanding of the factors affecting coalbed methane exploitation. Coals of the Gates Formation of Northeastern B.C. Canada, and coals from Australia were used for the current investigation.

Models commonly used for correlating and predicting equilibrium and non-equilibrium adsorption were tested against experimental data in this thesis. Some success has been met with the application of simplistic single and multicomponent equilibrium and non-equilibrium adsorption models, but these models are not necessarily accurate for all coal types. The systematic evaluation of commonly used equilibrium and non-equilibrium models has been undertaken, and in the case of non-equilibrium adsorption models, new models have been developed and tested.

6.2 EFFECT OF COAL COMPOSITION UPON PORE STRUCTURE AND GAS STORAGE

Coal lithotype composition, which is a function of organic content and composition, has a marked effect upon coal pore volume distributions of Gates Formation coals. Low-pressure volumetric adsorption analyses indicate that bright and banded bright coals (low ash, high vitrinite content) have greater micropore volumes than dull coals (high ash, low vitrinite content) of the same rank whereas dull coals have greater mesoporosities. Mercury porosimetry results show that all coals have multimodal pore volume distributions; one banded-bright coal has a large peak in the macropore range, which may be due high amounts of semifusinite in the sample.

Composition of the Gates Formation coals affect pure gas adsorption capacity. High-pressure methane and carbon dioxide adsorption isotherms illustrate that bright and banded bright coals, which have a large micropore volume, adsorb more gas than dull coals. Although maceral composition has some effect upon gas adsorption, there is no clear relationship between adsorption and the quantity of any particular maceral group. There is, however, a clear (linear) relationship between micropore volume and gas adsorption for the Gates coals.

Coal composition also affects total gas adsorption for binary gas/moisture-equilibrated coal systems, but does not appear to significantly alter component selectivity. Experimental data indicate that carbon dioxide selectivity varies slightly between coal lithotypes, but the effect of variable coal composition and moisture upon selective adsorption are difficult to isolate. Model predictions based upon pure component, moisture-equilibrated isotherm data show that coal composition has an insignificant effect upon carbon dioxide selectivity. Carbon dioxide selectivities are dependent upon coal moisture content, however. A comparison of predicted carbon dioxide selectivity from dry and moisture-equilibrated coal pure gas isotherm data reveals that carbon dioxide selectivity decreases with moisture content.

6.3 APPLICATION OF PURE AND MULTICOMPONENT ADSORPTION MODELS

The traditionally used Langmuir isotherm equation, which assumes monolayer adsorption, is not as accurate as the Dubinin-Radushkevich (D-R) and Dubinin-Astakhov (D-A) equations, which are based upon pore volume filling/potential theory, for fitting

coal adsorption isotherm data. These models were applied to high-pressure (up to 10 MPa) methane adsorption isotherms (303 K) and low-pressure (< 0.127 MPa) carbon dioxide isotherms obtained for 13 Australian coals. In all cases, the Dubinin equations, particularly the D-A equation, provide a better fit to adsorption data. This result was also demonstrated for high-pressure methane and carbon dioxide isotherm data collected using dried and moisture-equilibrated coals of the Gates Formation. The Langmuir isotherm fits are particularly poor for dried coal data.

The validity of the Langmuir and Dubinin models was checked by testing model assumptions. The assumption of an energetically homogeneous surface, as proposed by Langmuir theory, is not true for coal. Application of potential theory to the methane-coal system resulted in temperature-invariant methane characteristic curves, which is an assumption of the Dubinin models. The application of isotherms based on pore volume filling/potential theory therefore have general validity in their application to high-pressure supercritical methane-coal systems as well as providing a better fit to isotherm data.

Discrepancies exist between extended Langmuir model and IAS theory predictions for binary (CH_4/CO_2) gas adsorption. IAS theory, used in conjunction with the Langmuir, D-R, and D-A equations, consistently predicts lower methane sorbed phase concentrations, at a given gas phase composition and pressure, than the extended Langmuir model. Only the IAS/D-A predicts a decrease in carbon dioxide selectivity with increasing carbon dioxide concentration. The discrepancy between IAS predictions, particularly for dry coal data, is likely due to pure component isotherm curve-fit errors. IAS model fits to experimental data are generally better than the extended Langmuir

model for binary gas data collected in this thesis, but this is not true for the data collected by Hall *et al.*[2]

6.4 EFFECT OF PORE STRUCTURE AND GAS ADSORPTION UPON MATRIX TRANSPORT

Pore volume distributions have a significant effect upon adsorption rate or matrix gas transport behaviour of coal. Bright coals, which have a unimodal, microporous structure tend to sorb methane and carbon dioxide gas more slowly than dull or banded coals, which have a multimodal pore structure. Diffusion models which assume a unimodal pore volume distribution are adequate only for bright coals; banded and dull coals require models that must account for a multimodal pore structure.

Methane effective diffusivities, obtained using the commonly applied unipore diffusion analytical solution, increase with an increase in methane gas pressure. This pressure dependence is likely due to the failure of the unipore analytical model to account for nonlinear adsorption.

To account for the bimodal pore volume distribution and non-linear adsorption characteristics of some coals, new numerical models were developed for application to adsorption rate data. The new bidisperse numerical model performs adequately for dull and banded coals, but close examination of optimized parameters suggest that some of the assumptions of the model may be invalid. The optimized numerical model methane diffusivities decrease with an increase in gas pressure, which is consistent with a bulk gaseous diffusion mechanism.

6.4 POSSIBILITIES FOR FUTURE RESEARCH

The research presented in this thesis could be expanded upon by the systematic investigation of coals of different ranks and compositions from localities within and outside of the Western Canadian Sedimentary Basin. A recent study by Bustin and Clarkson[3] has demonstrated that "provincialism" may exist with respect to coal adsorption characteristics of different coal basins. For example, a relationship between coal composition and adsorption capacity may be readily demonstrated for a particular iso-rank coal deposit, but this relationship may not stand up for different coal deposits of similar rank. This suggests that the relationship between coal properties and gas content is still incompletely understood, and further investigation is required to obtain a "global" relationship.

Much more work is required to understand multicomponent gas adsorption characteristics of coals of all ranks and compositions. A systematic investigation of many more coal lithotypes is required to test the conclusions arrived at in this thesis; to date, no other studies of this kind have been undertaken. Currently, only a handful of mixed gas studies exist for coal, and most of these have focused upon the accurate prediction of equilbrium adsorption. Improved models are still needed to predict mixed gas adsorption within experimental accuracy.

To date, the effect of improved adsorption rate/matrix transport models upon lost gas calculations has not been fully investigated. Mavor *et al.*[4] investigated the effect of improved diffusion models upon core desorption for a limited number of coals and found that more sophisticated models do not necessarily result in more accurate estimates of

lost and total gas contents. Investigations of this kind, however, are required for a greater variety of coals than those used in the Mavor *et al.*[4] study.

6.6 REFERENCES

1. Lamberson, M.L. Unpublished Ph.D. thesis, 1993

2. Hall, F.E., Zhou, C., Gasem, K.A.M., Robinson, R.L., Jr., and Yee, D. Paper SPE 29194, presented at the 1994 Eastern Regional Conference and Exhibition, Charleston, WV, Nov. 8-10, 1994, pp. 329-344

3. R. M. Bustin, R.M. and Clarkson, C.R., accepted with revision, *Int. J. Coal Geol.*

4. Mavor, M.J., and Pratt, T.J. 'Improved Methodology for Determining Total Gas Content Volume II. Comparative Evaluation of the Accuracy of Gas-In-Place Estimates and Review of Lost Gas Models', Gas Research Institute Report No. GRI-94/0429, Chicago, Illinois, 1996

APPENDICES

APPENDIX I - Description of high-pressure volumetric gas adsorption apparatus and adsorption isotherm collection procedures

Equipment

The volumetric apparatus used for experimental determination of equilibrium gas adsorption/desorption isotherms and adsorption rate analysis is based upon the design described by Levy *et al.*[1] which is in turn based upon the design described by Mavor *et al.*[2] . A schematic diagram of the apparatus is provided in Figure 1. The apparatus is capable of collecting adsorption isotherm data for four samples simultaneously. Continuous unmanned operation (system calibration, helium and sample gas dosing and venting, and data acquisition) are achieved via computer control. A program, written in Turbo Pascal, V 6.0 by CSIRO, Lucas Heights, Australia, was purchased for system operation.

A brief description of instrument components is provided below:

Pressure Transducers – high precision variable capacitance SETRA ® C280E (0-3000 PSI) pressure transducers with 2-wire, 4-20 mA output. Quoted full-scale accuracy is 0.11%.

Sample Cells – 150 cc internal volume WHITEY ® 316L stainless steel rated at 5000 PSI (34.4 MPa). 1/4″ female NPT ends

Reference Cell – 300 cc internal volume WHITEY ® 316L stainless steel rated at 5000 PSI (34.4 MPa). 1/4″ female NPT ends.

Ball Valves – air-actuated, 2-position, 2-way WHITEY ® 316 stainless steel ball valves, pressure- rated to 3000 PSIG (20.6 MPa). 1/4″ SWAGELOK ® connections.

Air Actuators - WHITEY ® spring return pneumatic actuator.

Metering Valves – 21 series WHITEY ® 316 stainless steel Micro-metering valves, pressure-rated to 3000 PSI (20.6 MPa). 1/4″ SWAGELOK ® connections.

Tubing– 1/4″ outer diameter, thick walled seamless stainless steel.

Water Bath – ~100 litre insulated water bath thermostatted at 30.0 ± 0.1°C.

The transducer 4-20 mA current output is to controllers which display pressure and transmit data to a serial converter. All five transducer outputs are accessed from a single computer serial port. Pneumatic valve switching is achieved via solenoid valves, which direct air pressure to the pneumatic actuators. The solenoid valves are tripped via

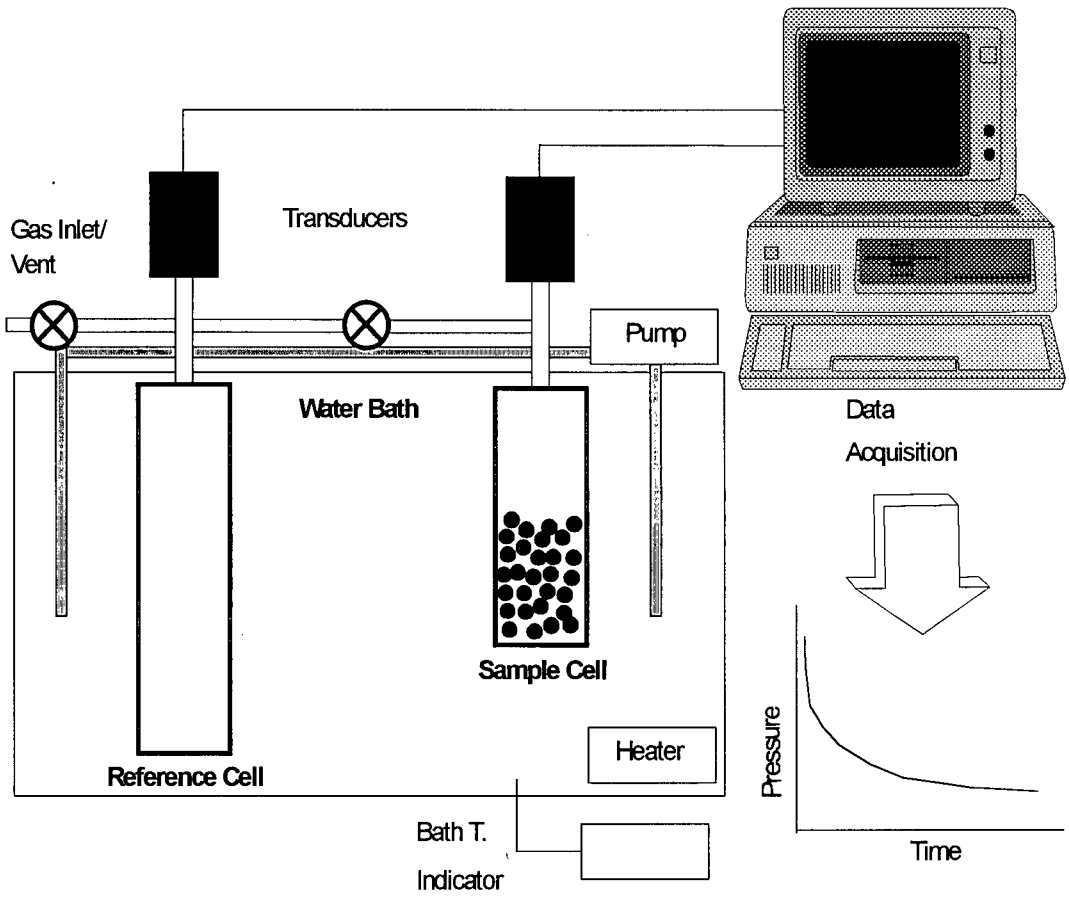

Figure 1. Diagram illustrating high-pressure volumetric apparatus.

solid state relays, which are interfaced with the computer through a commercial interface card. Solenoid valves are equipped with a manual override. The pneumatic valves are in the "normally closed" position in the event of a power failure.

The apparatus is equipped with a safety relief valve, which will vent the system above a setpoint pressure of about 17 MPa.

Pressure Transducer Cross-Correlation

The high-pressure volumetric adsorption apparatus is equipped with four separate sample cells and one reference cell for the simultaneous (automatic) determination of four adsorption isotherms. Each cell has a corresponding pressure transducer. In order that each pressure transducer effectively reads the same gas pressure, the transducer readings are corrected for pressure offset. This procedure is performed using the following steps:

1) All cells are first evacuated simultaneously and then charged with helium gas to the same pressure. Cells are allowed to thermally equilibrate for several minutes, and pressure readings are obtained from each transducer. The cells are then charged to a higher gas pressure, and pressure readings re-taken. Typically, about 16 pressure steps are taken at pressure increments of 0.2 – 1 MPa.

2) The zero-offset pressure is subtracted from each transducer pressure reading, and the pressure reading for each transducer is averaged for each pressure step.

3) The offsets from the average pressures were calculated and graphed.

4) A second order polynomial ($ax+bx^2+c$) was fitted to the offset data regression as in some cases the offset curves were slightly parabolic. Good fits were obtained in all cases. The zero offset was added back on to the c parameter in the polynomial.

5) The second order polynomial coefficients were then tabulated in spreadsheets used for isotherm determination, and raw pressure readings on transducers were corrected for offset.

Sample and Reference Cell Calibration

A series of helium expansions from the reference cell to each sample cell are performed with the sample cell empty and filled with a known reference volume to determine the volumes of the reference and sample cells. The expansions are carried out in 12 steps from an initial pressure of about 1 MPa to about 6 MPa.

Empty Sample Cell

The equation relating the volume of the sample cell (V_S) to the volume of the reference cell (V_R) is:

$$V_S = \frac{\overline{(P_2 - P_3)}}{(P_3 - P_1)} \times V_R$$

Where P_1 is the pressure in the reference and sample cells prior to expansion, P_2 is the pressure in the reference cell after charging with helium, and P_3 is the pressure in the sample and reference cell after expansion. The bar symbol above the pressure ratio term indicates that this ratio is averaged over all twelve pressure steps. Helium gas pressures are corrected for non-ideality.

Sample Cell filled with Reference Volume

The sample cell is filled with a known volume of steel balls, and the above procedure is repeated. The equation relating the volume of the sample cell and to the volume of the reference cell is:

$$V_S = V_{SB} + \frac{\overline{(P_2 - P_3)}}{(P_3 - P_1)} \times V_R$$

where V_{SB} is the total volume of the standard steel balls.

In order to determine the sample and reference cell volumes, equations 1) and 2) are equated. The reference cell volume is actually calculated four times during this procedure, and the average value of the reference cell volume is used in the calculation of the sample cell volume. The coefficient of variation for the reference cell volume is less than 0.15 % based upon repeated calibrations.

Pure Gas Isotherm Collection

The pre-weighed, moisture-equilibrated (Appendix II) or dried coal samples are placed in a sample cell, equipped with an inlet metal frit filters to prevent coal loss from the sample cell during venting or evacuation. Sample masses used are usually between 70 – 100 g. The following procedures are then followed for an isotherm run:

1) Leak Testing

Prior to analysis, the system manifold and cells are leak tested with helium. The system is tested for isolated cell leaks and through-valve leaks. Typically, the system is briefly evacuated and pressured up to > 7 MPa. Several minutes are allowed for thermal equilibration, and pressure readings are taken at approximately 20 minute intervals for 1-2 hours. In addition, the high-pressure fittings are periodically leak tested with SNOOP ®.

2) Void Volume Determination

A series of helium expansions from the calibrated volume of the reference cell to the sample cell are performed in order to determine the sample cell void volume (volume not occupied by solid coal). This procedure is similar to the volume calibration procedure described above.

3) Isotherm Collection

After the leak tests and sample void volume calibrations have been performed, the system is depressurized and briefly evacuated. The following procedure is then used for (adsorption) isotherm collection:

1) The sample cells are isolated (sample valve shut) and the initial pressure in the sample cell is recorded.

2) The reference cell is charged with a pressure 1-1.5 MPa greater than the pressure of the sample cell with pure gas (methane or carbon dioxide) and isolated. About 3 minutes is allowed for thermal equilibration of the reference cell.

3) The sample cell is dosed with pure gas from the reference cell for approximately 3 seconds and then the sample valve is closed.

4) Pressure in the sample cell is allowed to stabilize. A typical equilibrium requirement for – 60 mesh (250 μm) powdered coal is that the pressure in the sample cell remain constant (ΔP = 0.000 MPa) for a 2 hour period. A much more stringent requirement is used for coarser particle sizes.

5) Steps 2) – 4) are repeated over a cycle of 8 –10 pressure points.

Calculation of the volume of gas adsorbed STP (T = 273.15 K, P = 0.101325 MPa) at each pressure step is determined using real gas densities and mass balance:

$$V_{ads} = \left[\frac{T_{STD}}{T P_{STD} m_c}\right] \times \left[V_{ref}\left(\frac{P_{ref}^{I-1}}{z} - \frac{P_{ref}^{I}}{z}\right) - (V_{void} - V_s)\left(\frac{P_{sc}^{I}}{z} - \frac{P_{sc}^{I-1}}{z}\right)\right] \quad (1)$$

The sample void volume (V_{void}), which is the volume in the sample cell not occupied by solid coal, may be corrected for the volume occupied by the adsorbate (V_s) if a molar density of the adsorbate is assumed. Gas compressibilities, unless otherwise specified, are determined from values tabulated in the Gas Encyclopedia[3].

Desorption isotherms are collected (manually) using the reverse of the procedure outlined above.

Isotherm reproducibility for moisture-equilibrated coals, determined from replicate analyses in different cells, is typically < 2-3%. To determine the inter-laboratory reproducibility of isotherms, a methane adsorption isotherm was collected, for a moisture-equilibrated coal sample, by the CSIRO Division of Coal and Energy in NSW, Australia, using a similar volumetric apparatus. The same coal sample, re-equilibrated with moisture, was also run using the above-described apparatus. The resulting isotherms were within 5%.

Binary Gas Desorption Isotherm Collection

Binary gas (methane and carbon dioxide) desorption isotherms were collected in a similar manner to the pure gas isotherms, except that small gas samples were taken at two stages during a desorption step for GC analysis. Sample cells were used to extract small (~ 3 ml) gas with a syringe after the pressure had stabilized in the sample cell during a adsorption step. The pressure drop after extraction was usually small (<< .01 MPa) (check), and the pressure was again allowed to stabilize for several hours prior to the next desorption step. As with the Greaves *et al.*[4] study, the pressure drop accompanying extraction was found to have a negligible effect on adsorbed gases. The reference cell was then dosed with a small amount of mixed gas from the sample cell to initiate the next desorption step. A gas sample was extracted from the vent for GC analysis (Appendix III) to determine the composition of the gas in the reference cell.

For binary gas isotherms, a mass balance was performed for each component using the following equation (2):

$$V_{ads}^{j} = \left[\frac{T_{STD}}{T P_{STD} m_c}\right] \times \left[V_{ref}\left(\frac{(y_{ref}^{j} P_{ref})^{I-1}}{z} - \frac{(y_{ref}^{j} P_{ref})^{I}}{z}\right) - (V_{void} - V_s)\left(\frac{(y_{sc}^{j} P_{sc})^{I}}{z} - \frac{(y_{sc}^{j} P_{sc})^{I-1}}{z}\right)\right]$$

where V_{ads}^{j} is the volume of component j adsorbed from the mixture at each adsorption step, and y^{j} is the free gas (unadsorbed) mole fraction of component j. The volume of the sorbed phase was calculated using the following equation, which assumes the sorbed gas behaves like an ideal solution:

$$V_s = \sum_{i=1}^{nc} x_i V_{mi} \quad (3)$$

where V_{mi} is the molar volume of the liquid adsorbate. Equations (2) and (3) must be solved iteratively at each adsorption step, with the Gibbs adsorption volumes as the initial guess for equation (2). Gas compressibility factors for pure and mixed gases were determined using the Peng-Robinson equation-of-state[5].

Nomenclature

m = mass of coal [g]
P = total pressure [MPa]

T = temperature [K]
V = volume [cm^3] or volume adsorbed [cm^3/g@STP]
x_i = adsorbed phase mole fraction of component i
y_i = gas phase mole fraction of component i

Subscripts

ads = adsorbed
i = component i
m = molar quantity
ref = reference cell
s = sorbate
sc = sample cell
STD = standard conditions
v = voids
z = gas compressibility factor

Superscripts

I = current pressure step
I-1 = previous pressure step

References

1. Levy, J.H., Killingley, J.S., and Day, S.J. In Proceedings of the Symposium on Coalbed Methane Research and Development in Australia, v. 4, 1992, pp. 1-8

2. Mavor, M.J., Owen, L.B., and Pratt, T.J. Paper SPE 20728, presented at the 65th Annual Technical Conference of the Society of Petroleum Engineers, New Orleans, Louisiana, Sept. 23-26, 1990, pp.1-14

3. Encyclopedie des Gaz, L'Air Liquide, Elsevier, Amsterdam, 1976

4. Greaves, K.H., Owen, L.B., and McLennan, J.D. In Proceedings of the 1993 International Coalbed Methane Symposium, Tuscaloosa, May 17-21, 1993, pp. 151-160

4. Peng, D-Y., and Robinson, D.B. *Ind. Eng. Chem. Fundam.* 1976, **15**, 59

APPENDIX II - Determination of equilibrium moisture

The procedure used to determine equilibrium moisture of coal samples for isotherm analysis is similar to that described in Mavor *et al.*[1] and follows exactly the procedure described by Levy *et al.*[2]. This procedure is summarized below:

1) Samples to be used for isotherm analysis are crushed to pass through a 60 mesh sieve (< 250 μm particle diameter). Approximately 100 grams of sample are required for isotherm analysis.
2) The weighed isotherm samples are placed in a vacuum-type desiccator containing water vapour in equilibrium with a saturated solution of K_2SO_4 at 30°C. The desiccator is evacuated with a water venturi pump.
3) The sample is periodically reweighed (every 24 hours) until the sample weight is constant (to within 0.02 g). Equilibrium is usually achieved within 60 hours.
4) The moisture of a 1g representative split of the isotherm sample is determined using ASTM procedure D 3173 – 73 (Reapproved 1979)[3].

References

1. Mavor, M.J., Owen, L.B., and Pratt, T.J. Paper SPE 20728, presented at the 65th Annual Technical Conference of the Society of Petroleum Engineers, New Orleans, Louisiana, Sept. 23-26, 1990, pp.1-14

2. Levy, J.H., Day, S.J., and Killingley, J.S. *Fuel* 1997, **74**, 1

3. American Society for Testing and Materials. '1980 Annual Book of ASTM Standards', Part 26, D-3173.

APPENDIX III - Gas Chromatography

Gas samples for binary gas desorption isotherm experiments were analyzed using a Varian 3600 CX gas chromatograph equipped with a thermal conductivity detector (TCD) and a flame ionization detector (FID). A 1/8"x12' 60/80 mesh Hayesep R column was used. The TCD was used for quantitative analysis of carbon dioxide and methane mole fractions. Helium was used as a carrier gas, with a column flow rate of 30 ml/min in the column. Oven temperatures for either detector were programmed to vary from 70°C to 200°C at 10°C/min followed by a 5 minute hold. Each analysis was completed in 22 minutes. Quantitative analysis was achieved via calibration with primary standard grade (guaranteed 0.02 % absolute accuracy) methane/carbon dioxide mixtures with known mole fractions, obtained from Praxair Inc. Calibration standards were chosen to span the range of expected analyzed gas concentrations. TCD counts for each component in a standard mixture, determined from chromatogram peak integration, were ratioed and plotted against methane mole fraction to obtain calibration curves. Precision of analyzed mixtures were estimated to be within 0.002 mole fraction based upon replicate analysis of calibration standards and analysis gas.

APPENDIX IV - Isotherm Data used in Chapter 2

*** Gas compressibility factors determined from tabulated values in the Gas Encyclopedia[1]**

HIGH PRESSURE (> .101 MPa) METHANE ISOTHERMS-moisture –equilibrated coal

Sample Description: Bulli Seam Coal B1
Sample Number: B1
Reference Number: cbm222

Experiment Date:	20/5/94	**Reference Volume (cm^3):**	310.79	**Moisture(%):**	0.9
Sample Cell No:	5	**Void Volume (cm^3):**	71.85	**Ash(%):**	10.2
Temp (°C):	30.0	**Coal Volume (cm^3):**	86.64		
Mass of Coal (g):	119.47	**Coal Density (g/ cm^3):**	1.412		

Step Number	**Equilibrium Cell Pressure (MPa)**	**Volume CH_4 Adsorbed (cm3/g@STP, raw coal)**
1	0.249	2.28
2	0.707	5.04
3	1.656	8.33
4	2.756	10.50
5	3.871	12.00
6	4.951	12.98
7	6.090	13.99
8	7.002	14.72
9	7.995	15.21
10	8.961	15.76

Sample Description: Bulli Seam Coal B2
Sample Number: B2
Reference Number: cbm230

Experiment Date:	14/6/94	**Reference Volume (cm^3):**	310.79	**Moisture(%):**	0.8
Sample Cell No:	5	**Void Volume (cm^3):**	95.00	**Ash(%):**	9.6
Temp (°C):	30.0	**Coal Volume (cm^3):**	61.48		
Mass of Coal (g):	85.7	**Coal Density (g/ cm^3):**	1.394		

Step Number	**Equilibrium Cell Pressure (MPa)**	**Volume CH_4 Adsorbed (cm3/g@STP, raw coal)**
1	0.295	3.30
2	0.844	6.34
3	1.828	9.37
4	2.868	11.35
5	3.896	12.75
6	4.934	13.85
7	5.921	14.65
8	6.910	15.31
9	7.895	15.91
10	8.862	16.47

HIGH PRESSURE (> .101 MPa) METHANE ISOTHERMS (Cont'd)-moisture-equilibrated coal

Sample Description: Bulli Seam Coal B3
Sample Number: B3
Reference Number: cbm224

Experiment Date:	20/5/94	**Reference Volume (cm^3):**	310.79	**Moisture(%):**	0.7
Sample Cell No:	7	**Void Volume (cm^3):**	82.43	**Ash(%):**	8.6
Temp (°C):	30.0	**Coal Volume (cm^3):**	69.96		
Mass of Coal (g):	96.35	**Coal Density (g/ cm^3):**	1.377		

Step Number	**Equilibrium Cell Pressure (MPa)**	**Volume CH_4 Adsorbed (cm3/g@STP, raw coal)**
1	0.266	2.98
2	0.788	5.99
3	1.750	9.16
4	2.858	11.22
5	3.893	12.75
6	4.940	13.79
7	5.947	14.56
8	6.932	15.47
9	7.942	15.93
10	8.943	16.35
11	9.905	16.82

Sample Description: Bulli Seam Coal B4
Sample Number: B4
Reference Number: cbm225

Experiment Date:	20/5/94	**Reference Volume (cm^3):**	310.79	**Moisture(%):**	0.8
Sample Cell No:	8	**Void Volume (cm^3):**	75.14	**Ash(%):**	7.5
Temp (°C):	30.0	**Coal Volume (cm^3):**	80.19		
Mass of Coal (g):	108.46	**Coal Density (g/ cm^3):**	1.352		

Step Number	**Equilibrium Cell Pressure (MPa)**	**Volume CH_4 Adsorbed (cm3/g@STP, raw coal)**
1	0.267	2.55
2	0.704	5.64
3	1.669	9.18
4	2.813	11.52
5	3.913	13.14
6	4.974	14.21
7	5.969	15.09
8	6.998	15.77
9	7.987	16.28
10	8.972	16.80
11	9.961	17.23

HIGH PRESSURE (> .101 MPa) METHANE ISOTHERMS (Cont'd)-moisture-equilbrated coal

Sample Description: Bulli Seam Coal B5
Sample Number: B5
Reference Number: cbm232

Experiment Date:	14/6/94	**Reference Volume (cm^3):**	310.79	**Moisture(%):**	0.7
Sample Cell No:	7	**Void Volume (cm^3):**	84.30	**Ash(%):**	9.8
Temp (°C):	30.0	**Coal Volume (cm^3):**	68.09		
Mass of Coal (g):	92.24	**Coal Density (g/ cm^3):**	1.355		

Step Number	**Equilibrium Cell Pressure (MPa)**	**Volume CH_4 Adsorbed (cm3/g@STP, raw coal)**
1	0.278	3.12
2	0.795	6.20
3	1.809	9.45
4	2.886	11.55
5	3.946	13.11
6	4.979	14.09
7	6.020	14.89
8	6.951	15.75
9	7.941	16.36
10	8.908	16.83

Sample Description: Bulli Seam Coal B6
Sample Number: B6
Reference Number: cbm223

Experiment Date:	20/5/94	**Reference Volume (cm^3):**	310.79	**Moisture(%):**	0.6
Sample Cell No:	6	**Void Volume (cm^3):**	100.96	**Ash(%):**	3.4
Temp (°C):	30.0	**Coal Volume (cm^3):**	54.02		
Mass of Coal (g):	70.50	**Coal Density (g/ cm^3):**	1.305		

Step Number	**Equilibrium Cell Pressure (MPa)**	**Volume CH_4 Adsorbed (cm3/g@STP, raw coal)**
1	0.342	4.38
2	0.907	7.72
3	1.906	10.86
4	2.931	13.02
5	3.969	14.51
6	4.966	15.62
7	5.936	16.54
8	6.922	17.26
9	7.903	17.89
10	8.880	18.41
11	9.863	18.75

HIGH PRESSURE (> .101 MPa) METHANE ISOTHERMS (Cont'd)-moisture-equilibrated coal

Sample Description: Bulli Seam Coal B7
Sample Number: B7
Reference Number: cbm231

Experiment Date:	14/6/94	**Reference Volume (cm^3):**	310.79	**Moisture(%):**	0.7
Sample Cell No:	6	**Void Volume (cm^3):**	87.12	**Ash(%):**	9.8
Temp (°C):	30.0	**Coal Volume (cm^3):**	67.86		
Mass of Coal (g):	94.07	**Coal Density (g/ cm^3):**	1.386		

Step Number	**Equilibrium Cell Pressure (MPa)**	**Volume CH_4 Adsorbed (cm3/g@STP, raw coal)**
1	0.296	3.15
2	0.825	6.09
3	1.852	9.02
4	2.959	11.30
5	3.976	12.43
6	4.969	13.53
7	6.012	14.30
8	6.959	15.12
9	7.940	15.63
10	8.934	16.12

Sample Description: Wongawilli Seam Coal W1
Sample Number: W1
Reference Number: cbm227

Experiment Date:	14/6/94	**Reference Volume (cm^3):**	310.79	**Moisture(%):**	0.8
Sample Cell No:	6	**Void Volume (cm^3):**	77.29	**Ash(%):**	22.3
Temp (°C):	30.0	**Coal Volume (cm^3):**	77.69		
Mass of Coal (g):	116.02	**Coal Density (g/ cm^3):**	1.493		

Step Number	**Equilibrium Cell Pressure (MPa)**	**Volume CH_4 Adsorbed (cm3/g@STP, raw coal)**
1	0.277	2.64
2	0.811	5.17
3	1.829	7.81
4	2.928	9.65
5	3.966	10.96
6	4.968	12.02
7	5.999	12.88
8	6.993	13.57
9	7.968	14.23
10	8.973	14.77

HIGH PRESSURE (> .101 MPa) METHANE ISOTHERMS (Cont'd)-moisture-equilibrated coal

Sample Description: Wongawilli Seam Coal W2
Sample Number: W2
Reference Number: cbm229

Experiment Date:	14/6/94	**Reference Volume (cm^3):**	310.79	**Moisture(%):**	0.6
Sample Cell No:	8	**Void Volume (cm^3):**	78.28	**Ash(%):**	15.4
Temp (°C):	30.0	**Coal Volume (cm^3):**	77.05		
Mass of Coal (g):	108.56	**Coal Density (g/ cm^3):**	1.409		

Step Number	**Equilibrium Cell Pressure (MPa)**	**Volume CH_4 Adsorbed (cm3/g@STP, raw coal)**
1	0.273	2.74
2	0.789	5.58
3	1.757	8.58
4	2.841	10.83
5	3.893	12.50
6	4.929	13.72
7	5.948	14.79
8	6.971	15.67
9	7.973	16.32
10	8.954	17.00

Sample Description: Wongawilli Seam Coal W3
Sample Number: W3
Reference Number: cbm228

Experiment Date:	14/6/94	**Reference Volume (cm^3):**	310.79	**Moisture(%):**	0.8
Sample Cell No:	7	**Void Volume (cm^3):**	71.43	**Ash(%):**	32.4
Temp (°C):	30.0	**Coal Volume (cm^3):**	80.96		
Mass of Coal (g):	132.61	**Coal Density (g/ cm^3):**	1.683		

Step Number	**Equilibrium Cell Pressure (MPa)**	**Volume CH_4 Adsorbed (cm3/g@STP, raw coal)**
1	0.291	2.12
2	0.818	4.06
3	1.803	6.22
4	2.912	7.79
5	3.943	8.94
6	4.985	9.82
7	5.990	10.46
8	6.975	11.12
9	7.976	11.68
10	8.998	12.06

HIGH PRESSURE (> .101 MPa) METHANE ISOTHERMS (Cont'd)-moisture-equilibrated coal

Sample Description: Wongawilli Seam Coal W4
Sample Number: W4
Reference Number: cbm233

Experiment Date:	14/6/94	**Reference Volume (cm^3):**	310.79	**Moisture(%):**	1.0
Sample Cell No:	8	**Void Volume (cm^3):**	86.57	**Ash(%):**	19.3
Temp (°C):	30.0	**Coal Volume (cm^3):**	68.76		
Mass of Coal (g):	100.31	**Coal Density (g/ cm^3):**	1.459		

Step Number	**Equilibrium Cell Pressure (MPa)**	**Volume CH_4 Adsorbed (cm3/g@STP, raw coal)**
1	0.302	3.03
2	0.841	5.81
3	1.839	8.56
4	2.907	10.39
5	3.932	11.80
6	4.948	12.89
7	5.951	13.82
8	6.951	14.67
9	7.932	15.32
10	8.933	15.84

Sample Description: Wongawilli Seam Coal W5
Sample Number: W5
Reference Number: cbm226

Experiment Date:	14/6/94	**Reference Volume (cm^3):**	310.79	**Moisture(%):**	0.9
Sample Cell No:	5	**Void Volume (cm^3):**	81.07	**Ash(%):**	10.8
Temp (°C):	30.0	**Coal Volume (cm^3):**	75.41		
Mass of Coal (g):	103.26	**Coal Density (g/ cm^3):**	1.369		

Step Number	**Equilibrium Cell Pressure (MPa)**	**Volume CH_4 Adsorbed (cm3/g@STP, raw coal)**
1	0.268	2.90
2	0.761	5.80
3	1.758	9.11
4	2.841	11.56
5	3.875	13.26
6	4.927	14.59
7	5.953	15.61
8	6.942	16.43
9	7.918	17.23
10	8.923	17.93

HIGH PRESSURE (> .101 MPa) METHANE ISOTHERMS (Cont'd)-moisture-equilbrated coal

Sample Description: Bowen Basin Coal
Sample Number: GHA1-09
Reference Number: cbm052

Experiment Date:	29/10/95	**Reference Volume (cm^3):**	313.68	**Moisture(%):**	1.8
Sample Cell No:	1	**Void Volume (cm^3):**	92.96	**Ash(%):**	7.5
Temp (°C):	50.0	**Coal Volume (cm^3):**	61.95		
Mass of Coal (g):	82.64	**Coal Density (g/ cm^3):**	1.334		

Step Number	**Equilibrium Cell Pressure (MPa)**	**Volume CH_4 Adsorbed (cm3/g@STP, raw coal)**
1	0.489	2.71
2	1.111	5.16
3	2.007	7.50
4	2.982	9.35
5	4.007	10.76
6	5.028	11.91
7	6.019	12.89
8	6.985	13.64
9	7.966	14.28
10	8.946	15.05

Sample Description: Bowen Basin Coal
Sample Number: GHA1-09
Reference Number: cbm061

Experiment Date:	11/12/95	**Reference Volume (cm^3):**	313.68	**Moisture(%):**	1.8
Sample Cell No:	3	**Void Volume (cm^3):**	94.50	**Ash(%):**	7.5
Temp (°C):	30.0	**Coal Volume (cm^3):**	60.66		
Mass of Coal (g):	82.28	**Coal Density (g/ cm^3):**	1.356		

Step Number	**Equilibrium Cell Pressure (MPa)**	**Volume CH_4 Adsorbed (cm3/g@STP, raw coal)**
1	0.471	3.82
2	1.056	6.51
3	1.985	9.25
4	2.991	11.25
5	3.999	12.70
6	4.977	13.75
7	5.935	14.60
8	6.967	15.41
9	7.968	16.09
10	8.902	16.71
11	9.862	17.18

HIGH PRESSURE (> .101 MPa) METHANE ISOTHERMS (Cont'd)-moisture-equilbrated coal

Sample Description: Bowen Basin Coal
Sample Number: GHA1-09
Reference Number: cbm065

Experiment Date:	23/01/96	**Reference Volume (cm^3):**	313.68	**Moisture(%):**	1.7
Sample Cell No:	4	**Void Volume (cm^3):**	97.73	**Ash(%):**	7.5
Temp (°C):	25.0	**Coal Volume (cm^3):**	55.31		
Mass of Coal (g):	75.62	**Coal Density (g/ cm^3):**	1.367		

Step Number	**Equilibrium Cell Pressure (MPa)**	**Volume CH_4 Adsorbed (cm3/g@STP, raw coal)**
1	0.454	4.19
2	0.993	6.97
3	2.045	10.17
4	3.078	12.12
5	4.114	13.59
6	5.123	14.85
7	6.109	15.79
8	7.136	16.45
9	8.045	17.19

LOW PRESSURE (< .127 MPa) CARBON DIOXIDE ISOTHERMS

Sample Description: Bulli Seam Coal
Sample Number: B4
Reference Number: N/A

Experiment Date: N/A
Sample Cell No: N/A
Temp (°C): 0.0
Mass of Coal (g):

Moisture(%): 0.0
Ash(%): 7.5

Step Number	**Relative Pressure (P/Po)**	**Volume CO_2 Adsorbed (cm3/g@STP, raw coal)**
1	0.0016	1.69
2	0.0034	3.07
3	0.0053	4.18
4	0.0073	5.13
5	0.0094	6.08
6	0.0114	6.84
7	0.0136	7.59
8	0.0158	8.27
9	0.0179	8.83
10	0.0202	9.37
11	0.0225	9.90
12	0.0247	10.36
13	0.0268	10.81
14	0.0291	11.24
15	0.0314	11.71
16	0.0337	12.07
17	0.0346	12.28

LOW PRESSURE (< .127 MPa) CARBON DIOXIDE ISOTHERMS (Cont'd)

Sample Description: Wongawilli Seam Coal
Sample Number: W1
Reference Number: N/A

Experiment Date:
Sample Cell No: N/A
Temp (°C): 0.0
Mass of Coal (g):

Moisture(%): 0.0
Ash(%): 22.3

Step Number	Relative Pressure (P/Po)	Volume CO_2 Adsorbed (cm3/g@STP, raw coal)
1	0.0017	1.94
2	0.0039	3.38
3	0.0062	4.55
4	0.0087	5.57
5	0.0113	6.43
6	0.0140	7.22
7	0.0167	7.91
8	0.0196	8.57
9	0.0223	9.17
10	0.0251	9.74
11	0.0280	10.26
12	0.0310	10.75
13	0.0339	11.21
14	0.0348	11.38

LOW PRESSURE (< .127 MPa) CARBON DIOXIDE ISOTHERMS (Cont'd)

Sample Description: Bowen Basin Coal
Sample Number: GHA1-09
Reference Number: N/A

Experiment Date: 13/03/96
Sample Cell No: N/A
Temp (°C): 25.0
Mass of Coal (g): 0.4461

Moisture(%): 0.0
Ash(%): 7.5

Step Number	Relative Pressure (P/Po)	Volume CO_2 Adsorbed (cm3/g@STP, raw coal)
1	0.0008	0.92
2	0.0017	1.68
3	0.0026	2.36
4	0.0035	2.99
5	0.0045	3.58
6	0.0054	4.12
7	0.0064	4.63
8	0.0073	5.12
9	0.0083	5.59
10	0.0093	6.04
11	0.0103	6.46
12	0.0113	6.86
13	0.0123	7.24
14	0.0133	7.61
15	0.0143	7.96
16	0.0153	8.31
17	0.0164	8.67
18	0.0174	9.00
19	0.0185	9.32
20	0.0189	9.47

LOW PRESSURE (< .127 MPa) CARBON DIOXIDE ISOTHERMS (Cont'd)

Sample Description: Bowen Basin Coal
Sample Number: GHA1-09
Reference Number: N/A

Experiment Date: 13/03/96
Sample Cell No: N/A
Temp (°C): 0.0
Mass of Coal (g): 0.4920

Moisture(%): 0.0
Ash(%): 7.5

Step Number	Relative Pressure (P/Po)	Volume CO_2 Adsorbed (cm3/g@STP, raw coal)
1	0.0012	1.71
2	0.0027	3.08
3	0.0042	4.24
4	0.0059	5.28
5	0.0077	6.21
6	0.0095	7.07
7	0.0114	7.86
8	0.0132	8.59
9	0.0152	9.27
10	0.0171	9.91
11	0.0191	10.51
12	0.0212	11.08
13	0.0232	11.62
14	0.0253	12.14
15	0.0274	12.63
16	0.0295	13.10
17	0.0316	13.56
18	0.0337	14.00
19	0.0346	14.20

References

1. Encyclopedie des Gaz, L'Air Liquide, Elsevier, Amsterdam, 1976

APPENDIX V - Isotherm Data and Mercury Intrusion Data used in Chapter 3

*** Gas compressibility factors determined from tabulated values in the Gas Encyclopedia[1]**

HIGH PRESSURE (> .101 MPa) METHANE ISOTHERMS – dried coal

Analysis Gas: Methane
Sample Description: Gates Formation Coal, -4 mesh, dried
Sample Number: B2-11
Reference Number: cbm118

Experiment Date: 7/9/96 **Reference Volume (cm^3):** 312.89 **Moisture(%):** 0.0
Sample Cell No: 1 **Void Volume (cm^3):** 85.96 **Ash(%):** 3.7
Temp (°C): 30.0 **Coal Volume (cm^3):** 68.53
Mass of Coal (g): 92.89 **Coal Density (g/ cm^3):** 1.355

Step Number	Equilibrium Cell Pressure (MPa)	Volume CH_4 Adsorbed (cm3/g@STP, raw coal)
1	0.218	4.39
2	0.784	8.66
3	1.723	12.09
4	2.889	14.61
5	3.922	16.10
6	4.941	17.27

Analysis Gas: Methane
Sample Description: Gates Formation Coal, -4 mesh, dried
Sample Number: B2-10
Reference Number: cbm119

Experiment Date: 7/9/96 **Reference Volume (cm^3):** 312.89 **Moisture(%):** 0.0
Sample Cell No: 2 **Void Volume (cm^3):** 113.07 **Ash(%):** 30.3
Temp (°C): 30.0 **Coal Volume (cm^3):** 40.47
Mass of Coal (g): 73.53 **Coal Density (g/ cm^3):** 1.817

Step Number	Equilibrium Cell Pressure (MPa)	Volume CH_4 Adsorbed (cm3/g@STP, raw coal)
1	0.388	3.02
2	1.074	5.12
3	2.043	6.59
4	3.030	7.59
5	4.001	8.34
6	4.936	8.95
7	5.897	9.35
8	6.846	9.84
9	7.843	10.10

HIGH PRESSURE (> .101 MPa) METHANE ISOTHERMS (Cont'd)-dried coal

Analysis Gas: Methane
Sample Description: Gates Formation coal, -4 mesh, dried
Sample Number: C3-2
Reference Number: cbm120

Experiment Date:	7/9/96	**Reference Volume (cm^3):**	312.89	**Moisture(%):**	0.0
Sample Cell No:	3	**Void Volume (cm^3):**	112.33	**Ash(%):**	13.0
Temp (°C):	30.0	**Coal Volume (cm^3):**	55.31		
Mass of Coal (g):	77.24	**Coal Density (g/ cm^3):**	1.397		

Step Number	**Equilibrium Cell Pressure (MPa)**	**Volume CH_4 Adsorbed (cm3/g@STP, raw coal)**
1	0.388	3.85
2	1.033	6.86
3	1.895	9.86
4	2.978	11.56
5	3.979	13.26
6	4.981	14.16
7	5.928	15.10

Analysis Gas: Methane
Sample Description: Gates Formation coal, -4 mesh, dried
Sample Number: D3-3
Reference Number: cbm109

Experiment Date:	19/6/96	**Reference Volume (cm^3):**	312.89	**Moisture(%):**	0.0
Sample Cell No:	4	**Void Volume (cm^3):**	102.74	**Ash(%):**	46.1
Temp (°C):	30.0	**Coal Volume (cm^3):**	50.27		
Mass of Coal (g):	90.74	**Coal Density (g/ cm^3):**	1.805		

Step Number	**Equilibrium Cell Pressure (MPa)**	**Volume CH_4 Adsorbed (cm3/g@STP, raw coal)**
1	0.387	2.81
2	0.987	4.52
3	2.055	6.24
4	3.053	7.22
5	4.160	8.00

HIGH PRESSURE (> .101 MPa) CARBON DIOXIDE ISOTHERMS – dried coal

Analysis Gas: Carbon Dioxide
Sample Description: Gates Formation Coal, -4 mesh, dried
Sample Number: B2-11
Reference Number: cbm126

Experiment Date:	12/11/96	**Reference Volume (cm^3):**	312.89	**Moisture(%):**	0.0
Sample Cell No:	1	**Void Volume (cm^3):**	86.79	**Ash(%):**	3.7
Temp (°C):	30.0	**Coal Volume (cm^3):**	67.69		
Mass of Coal (g):	91.64	**Coal Density (g/ cm^3):**	1.354		

Step Number	**Equilibrium Cell Pressure (MPa)**	**Volume CO_2 Adsorbed (cm3/g@STP, raw coal)**
1	0.032	4.44
2	0.187	10.30
3	0.591	16.56
4	1.254	21.43
5	2.281	25.83
6	3.432	28.64
7	4.429	30.40
8	5.064	32.22

Analysis Gas: Carbon Dioxide
Sample Description: Gates Formation Coal, -4 mesh, dried
Sample Number: B2-10
Reference Number: cbm127

Experiment Date:	12/11/96	**Reference Volume (cm^3):**	312.89	**Moisture(%):**	0.0
Sample Cell No:	2	**Void Volume (cm^3):**	112.74	**Ash(%):**	30.3
Temp (°C):	30.0	**Coal Volume (cm^3):**	40.80		
Mass of Coal (g):	73.51	**Coal Density (g/ cm^3):**	1.802		

Step Number	**Equilibrium Cell Pressure (MPa)**	**Volume CO_2 Adsorbed (cm3/g@STP, raw coal)**
1	0.155	5.02
2	0.556	8.69
3	1.117	11.19
4	1.650	12.64
5	2.503	14.27
6	3.433	15.48
7	4.367	16.27
8	4.999	17.95

HIGH PRESSURE (> .101 MPa) CARBON DIOXIDE ISOTHERMS (Cont'd)-dried coal

Analysis Gas: Carbon Dioxide
Sample Description: Gates Formation Coal, -4 mesh, dried
Sample Number: C3-2
Reference Number: cbm128

Experiment Date:	12/11/96	**Reference Volume (cm^3):**	312.89	**Moisture(%):**	0.0
Sample Cell No:	3	**Void Volume (cm^3):**	112.38	**Ash(%):**	13.0
Temp (°C):	30.0	**Coal Volume (cm^3):**	55.26		
Mass of Coal (g):	77.23	**Coal Density (g/ cm^3):**	1.398		

Step Number	**Equilibrium Cell Pressure (MPa)**	**Volume CO_2 Adsorbed (cm3/g@STP, raw coal)**
1	0.078	4.71
2	0.320	10.42
3	0.854	15.59
4	1.474	18.83
5	2.339	21.69
6	3.342	23.91
7	4.328	25.52
8	4.998	27.21

Analysis Gas: Carbon Dioxide
Sample Description: Gates Formation Coal, -4 mesh, dried
Sample Number: D3-3
Reference Number: cbm129

Experiment Date:	12/9/96	**Reference Volume (cm^3):**	312.89	**Moisture(%):**	0.0
Sample Cell No:	4	**Void Volume (cm^3):**	107.41	**Ash(%):**	46.1
Temp (°C):	30.0	**Coal Volume (cm^3):**	45.60		
Mass of Coal (g):	82.26	**Coal Density (g/ cm^3):**	1.804		

Step Number	**Equilibrium Cell Pressure (MPa)**	**Volume CO_2 Adsorbed (cm3/g@STP, raw coal)**
1	0.107	3.70
2	0.503	7.59
3	1.097	10.10
4	1.700	11.43
5	2.597	12.90

HIGH PRESSURE (> .101 MPa) METHANE ISOTHERMS – moisture-equilibrated coal

Analysis Gas: Methane
Sample Description: Gates Formation Coal, -4 mesh, moisture-equilibrated
Sample Number: B2-11
Reference Number: cbm090

Experiment Date:	3/12/96	**Reference Volume (cm^3):**	312.89	**Moisture(%):**	N/A
Sample Cell No:	1	**Void Volume (cm^3):**	81.83	**Ash(%):**	3.7
Temp (°C):	30.0	**Coal Volume (cm^3):**	72.65		
Mass of Coal (g):	97.77	**Coal Density (g/ cm^3):**	1.346		

Step Number	**Equilibrium Cell Pressure (MPa)**	**Volume CH_4 Adsorbed (cm3/g@STP, raw coal)**
1	0.387	2.66
2	1.545	6.99
3	4.141	11.42
4	7.775	14.86

Analysis Gas: Methane
Sample Description: Gates Formation Coal, -4 mesh, moisture-equilibrated
Sample Number: B2-10
Reference Number: cbm093

Experiment Date:	3/12/96	**Reference Volume (cm^3):**	312.89	**Moisture(%):**	N/A
Sample Cell No:	4	**Void Volume (cm^3):**	103.14	**Ash(%):**	30.3
Temp (°C):	30.0	**Coal Volume (cm^3):**	49.86		
Mass of Coal (g):	89.59	**Coal Density (g/ cm^3):**	1.797		

Step Number	**Equilibrium Cell Pressure (MPa)**	**Volume CH_4 Adsorbed (cm3/g@STP, raw coal)**
1	0.478	2.17
2	1.833	4.71
3	4.293	6.68
4	8.008	7.96

HIGH PRESSURE (> .101 MPa) METHANE ISOTHERMS (Cont'd) – moisture-equilibrated coal

Analysis Gas: Methane
Sample Description: Gates Formation Coal, -4 mesh, moisture-equilibrated
Sample Number: D3-3
Reference Number: cbm093

Experiment Date:	4/24/96	**Reference Volume (cm^3):**	312.89	**Moisture(%):**	N/A
Sample Cell No:	1	**Void Volume (cm^3):**	102.19	**Ash(%):**	46.1
Temp (°C):	30.0	**Coal Volume (cm^3):**	52.30		
Mass of Coal (g):	93.42	**Coal Density (g/ cm^3):**	1.786		

Step Number	**Equilibrium Cell Pressure (MPa)**	**Volume CH_4 Adsorbed (cm3/g@STP, raw coal)**
1	0.523	1.30
2	1.897	2.86
3	4.288	4.42
4	7.716	5.65

LOW PRESSURE (< .127 MPa) CARBON DIOXIDE ISOTHERMS

Sample Description: Gates Formation Coal, -60 mesh
Sample Number: B2-11
Reference Number: N/A

Experiment Date: 08/02/96
Sample Cell No: N/A
Temp (°C): 0.0
Mass of Coal (g): 0.5662

Moisture(%): 0.0
Ash(%): 3.7

Step Number	**Relative Pressure (P/Po)**	**Volume CO_2 Adsorbed (cm3/g@STP, raw coal)**
1	0.0012	2.13
2	0.0026	3.85
3	0.0041	5.32
4	0.0058	6.60
5	0.0076	7.70
6	0.0095	8.64
7	0.0114	9.50
8	0.0134	10.27
9	0.0154	10.98
10	0.0175	11.65
11	0.0196	12.25
12	0.0217	12.82
13	0.0238	13.35
14	0.0259	13.88
15	0.0281	14.39
16	0.0303	14.86
17	0.0325	15.31
18	0.0345	15.71

LOW PRESSURE (< .127 MPa) CARBON DIOXIDE ISOTHERMS (Cont'd)

Sample Description: Gates Formation Coal, -60 mesh
Sample Number: B2-10
Reference Number: N/A

Experiment Date: 26/02/96
Sample Cell No: N/A
Temp (°C): 0.0
Mass of Coal (g): 0.9693

Moisture(%): 0.0
Ash(%): 30.3

Step Number	Relative Pressure (P/Po)	Volume CO_2 Adsorbed (cm3/g@STP, raw coal)
1	0.0020	1.91
2	0.0047	3.22
3	0.0078	4.25
4	0.0112	5.07
5	0.0148	5.78
6	0.0184	6.41
7	0.0222	6.96
8	0.0261	7.47
9	0.0300	7.92
10	0.0340	8.35

Sample Description: Gates Formation Coal, -60 mesh
Sample Number: C3-2
Reference Number: N/A

Experiment Date: 07/02/96
Sample Cell No: N/A
Temp (°C): 0.0
Mass of Coal (g): 0.7111

Moisture(%): 0.0
Ash(%): 13.0

Step Number	Relative Pressure (P/Po)	Volume CO_2 Adsorbed (cm3/g@STP, raw coal)
1	0.0017	1.99
2	0.0037	3.64
3	0.0059	5.06
4	0.0082	6.31
5	0.0106	7.41
6	0.0132	8.35
7	0.0158	9.13
8	0.0185	9.84
9	0.0213	10.49
10	0.0240	11.08
11	0.0268	11.61
12	0.0296	12.11
13	0.0325	12.60
14	0.0348	12.99

LOW PRESSURE (< .127 MPa) CARBON DIOXIDE ISOTHERMS (Cont'd)

Sample Description: Gates Formation Coal, -60 mesh
Sample Number: D3-3
Reference Number: N/A

Experiment Date: 26/02/97
Sample Cell No: N/A
Temp (°C): 0.0
Mass of Coal (g): 8.3541

Moisture(%): 0.0
Ash(%): 46.1

Step Number	**Relative Pressure (P/Po)**	**Volume CO_2 Adsorbed (cm3/g@STP, raw coal)**
1	0.0010	1.09
2	0.0028	2.17
3	0.0052	3.19
4	0.0087	4.14
5	0.0131	5.02
6	0.0185	5.81
7	0.0249	6.51
8	0.0323	7.15
9	0.0344	7.32

LOW PRESSURE (< .127 MPa) NITROGEN ISOTHERMS

Sample Description: Gates Formation Coal, -60 mesh
Sample Number: B2-11
Reference Number: N/A

Experiment Date: 18/07/96
Sample Cell No: N/A
Temp (°C): 0.0
Mass of Coal (g): 5.3487

Moisture(%): 0.0
Ash(%): 3.7

Step Number	Relative Pressure (P/Po)	Volume N_2 Adsorbed (cm3/g@STP, raw coal)
1	0.0097	0.13
2	0.0326	0.17
3	0.0676	0.20
4	0.0803	0.20
5	0.1006	0.21
6	0.1206	0.22
7	0.1407	0.23
8	0.1606	0.24
9	0.1807	0.24
10	0.2009	0.25
11	0.2504	0.26
12	0.3009	0.27
13	0.3509	0.29
14	0.4004	0.30
15	0.4505	0.31
16	0.5004	0.32
17	0.5505	0.34
18	0.6005	0.35
19	0.6502	0.37
20	0.7004	0.39
21	0.7502	0.42
22	0.8000	0.46
23	0.8207	0.49
24	0.8505	0.53
25	0.8752	0.57
26	0.9001	0.62
27	0.9247	0.70
28	0.9490	0.83
29	0.9722	1.06
30	0.9816	1.23
31	0.9897	1.46
32	0.9949	1.71
33	0.9879	1.46
34	0.9775	1.22
35	0.9667	1.07
36	0.9530	0.94

37	0.9269	0.79
38	0.9023	0.71
39	0.8771	0.65
40	0.8510	0.60
41	0.8259	0.57
42	0.8005	0.54
43	0.7502	0.49
44	0.7008	0.46
45	0.6508	0.44
46	0.6005	0.42
47	0.5507	0.40
48	0.5016	0.37
49	0.4500	0.34
50	0.3908	0.33
51	0.3317	0.31
52	0.3008	0.31
53	0.2506	0.30
54	0.2006	0.28
55	0.1405	0.27

Sample Description: Gates Formation Coal, -60 mesh
Sample Number: B2-10
Reference Number: N/A

Experiment Date: 14/07/96
Sample Cell No: N/A
Temp (°C): 0.0
Mass of Coal (g): 6.2189

Moisture(%): 0.0
Ash(%): 30.3

Step Number	**Relative Pressure (P/Po)**	**Volume N_2 Adsorbed (cm3/g@STP, raw coal)**
1	0.0110	0.30
2	0.0294	0.37
3	0.0638	0.44
4	0.0787	0.47
5	0.1014	0.50
6	0.1207	0.52
7	0.1406	0.54
8	0.1604	0.56
9	0.1807	0.58
10	0.2007	0.59
11	0.2497	0.63
12	0.3015	0.67
13	0.3522	0.70
14	0.4002	0.74
15	0.4502	0.78
16	0.5003	0.82
17	0.5502	0.86

18	0.6002	0.91
19	0.6502	0.97
20	0.7000	1.04
21	0.7498	1.13
22	0.7994	1.25
23	0.8211	1.32
24	0.8505	1.44
25	0.8747	1.56
26	0.8994	1.73
27	0.9239	1.97
28	0.9473	2.35
29	0.9688	2.98
30	0.9778	3.43
31	0.9839	3.88
32	0.9909	4.62
33	0.9879	4.41
34	0.9837	4.13
35	0.9788	3.85
36	0.9513	2.90
37	0.9203	2.40
38	0.8989	2.18
39	0.8788	2.02
40	0.8513	1.84
41	0.8259	1.72
42	0.8013	1.62
43	0.7504	1.45
44	0.7011	1.33
45	0.6513	1.24
46	0.6012	1.16
47	0.5509	1.09
48	0.5038	1.00
49	0.4486	0.89
50	0.3957	0.85
51	0.3343	0.81
52	0.3009	0.78
53	0.2505	0.75
54	0.2005	0.72
55	0.1410	0.67

Sample Description: Gates Formation Coal, -60 mesh
Sample Number: C3-2
Reference Number: N/A

Experiment Date: 21/07/96
Sample Cell No: N/A
Temp (°C): 0.0
Mass of Coal (g): 5.1456

Moisture(%): 0.0
Ash(%): 13.0

Step Number	**Relative Pressure (P/Po)**	**Volume N_2 Adsorbed (cm3/g@STP, raw coal)**
1	0.0106	0.10
2	0.0331	0.13
3	0.0681	0.15
4	0.0803	0.16
5	0.1006	0.17
6	0.1206	0.18
7	0.1406	0.18
8	0.1606	0.19
9	0.1807	0.19
10	0.2009	0.20
11	0.2505	0.21
12	0.3010	0.22
13	0.3509	0.23
14	0.4006	0.24
15	0.4505	0.25
16	0.5005	0.26
17	0.5504	0.27
18	0.6004	0.28
19	0.6504	0.30
20	0.7003	0.32
21	0.7503	0.35
22	0.8002	0.38
23	0.8209	0.40
24	0.8504	0.44
25	0.8752	0.48
26	0.9000	0.54
27	0.9248	0.63
28	0.9490	0.76
29	0.9756	1.07
30	0.9831	1.25
31	0.9897	1.51
32	0.9948	1.82
33	0.9892	1.55
34	0.9804	1.25
35	0.9695	1.05
36	0.9553	0.89
37	0.9286	0.72
38	0.9037	0.62
39	0.8775	0.56
40	0.8514	0.51
41	0.8255	0.47
42	0.8008	0.44
43	0.7505	0.40
44	0.7006	0.37
45	0.6508	0.34
46	0.6005	0.32
47	0.5507	0.31

48	0.5008	0.29
49	0.4504	0.27
50	0.3997	0.26
51	0.3317	0.25
52	0.3007	0.24
53	0.2505	0.23
54	0.2004	0.22
55	0.1408	0.21

Sample Description: Gates Formation Coal, -60 mesh
Sample Number: D3-3
Reference Number: N/A

Experiment Date: 25/07/96
Sample Cell No: N/A
Temp (°C): 0.0
Mass of Coal (g): 5.4596

Moisture(%): 0.0
Ash(%): 46.1

Step Number	**Relative Pressure (P/Po)**	**Volume N_2 Adsorbed (cm3/g@STP, raw coal)**
1	0.0097	0.32
2	0.0301	0.39
3	0.0641	0.47
4	0.0798	0.49
5	0.1005	0.52
6	0.1205	0.54
7	0.1405	0.56
8	0.1608	0.57
9	0.1806	0.59
10	0.2007	0.61
11	0.2499	0.64
12	0.3015	0.67
13	0.3518	0.71
14	0.4005	0.74
15	0.4503	0.77
16	0.5003	0.80
17	0.5504	0.84
18	0.6003	0.87
19	0.6502	0.92
20	0.7002	0.96
21	0.7501	1.03
22	0.7998	1.10
23	0.8207	1.15
24	0.8507	1.22
25	0.8747	1.30
26	0.8997	1.42
27	0.9242	1.57
28	0.9479	1.83

29	0.9696	2.30
30	0.9798	2.74
31	0.9862	3.22
32	0.9899	3.65
33	0.9870	3.42
34	0.9826	3.11
35	0.9768	2.81
36	0.9447	2.02
37	0.9222	1.79
38	0.8938	1.60
39	0.8794	1.54
40	0.8515	1.44
41	0.8260	1.37
42	0.8007	1.32
43	0.7508	1.24
44	0.7008	1.18
45	0.6510	1.13
46	0.6007	1.09
47	0.5506	1.05
48	0.5021	1.00
49	0.4533	0.89
50	0.3923	0.84
51	0.3334	0.80
52	0.3015	0.78
53	0.2505	0.75
54	0.2007	0.72
55	0.1407	0.67

MERCURY INCREMENTAL INTRUSION DATA

Sample Description: Gates Formation Coal, -4 mesh
Sample Number: B2-11
Reference Number: N/A

Experiment Date: 19/12/96
Sample Cell No: N/A
Temp (°C): 22.0
Mass of Coal (g): 1.268

Moisture(%): 0.0
Ash(%): 3.7

Step Number	Mean Pore Diameter (μm)	Incremental Hg Intrustion (cm3/g, raw coal)
1	144.267	0.0000
2	96.902	0.0001
3	40.277	0.0000
4	27.098	0.0000
5	20.507	0.0000
6	15.746	0.0000
7	12.313	0.0000
8	10.415	0.0000
9	9.371	0.0000
10	8.501	0.0000
11	7.024	0.0005
12	3.854	0.0040
13	1.342	0.0034
14	0.678	0.0054
15	0.378	0.0033
16	0.265	0.0019
17	0.204	0.0012
18	0.151	0.0018
19	0.106	0.0011
20	0.082	0.0008
21	0.067	0.0007
22	0.056	0.0007
23	0.049	0.0005
24	0.043	0.0006
25	0.038	0.0005
26	0.035	0.0005
27	0.032	0.0006
28	0.029	0.0004
29	0.027	0.0004
30	0.025	0.0005
31	0.024	0.0004
32	0.022	0.0004

33	0.021	0.0004
34	0.019	0.0009
35	0.017	0.0015
36	0.014	0.0016
37	0.012	0.0015
38	0.011	0.0015
39	0.010	0.0014
40	0.009	0.0014
41	0.008	0.0014
42	0.007	0.0013
43	0.007	0.0016
44	0.006	0.0012

Sample Description: Gates Formation Coal, -4 mesh
Sample Number: B2-10
Reference Number: N/A

Experiment Date: 09/01/97
Sample Cell No: N/A
Temp (°C): 22.0
Mass of Coal (g): 1.292

Moisture(%): 0.0
Ash(%): 30.3

Step Number	**Mean Pore Diameter (μm)**	**Incremental Hg Intrustion (cm3/g, raw coal)**
1	98.322	0.0000
2	69.575	0.0000
3	31.226	0.0000
4	19.521	0.0000
5	15.403	0.0000
6	12.028	0.0000
7	10.071	0.0000
8	8.758	0.0000
9	7.018	0.0000
10	3.890	0.0006
11	1.343	0.0007
12	0.674	0.0006
13	0.376	0.0004
14	0.264	0.0005
15	0.203	0.0004
16	0.151	0.0009
17	0.106	0.0009
18	0.082	0.0009
19	0.067	0.0008
20	0.056	0.0006
21	0.049	0.0005
22	0.043	0.0005
23	0.038	0.0005
24	0.035	0.0004

25	0.032	0.0004
26	0.029	0.0005
27	0.027	0.0003
28	0.025	0.0004
29	0.024	0.0004
30	0.022	0.0004
31	0.021	0.0003
32	0.019	0.0006
33	0.017	0.0014
34	0.014	0.0012
35	0.012	0.0012
36	0.011	0.0011
37	0.010	0.0008
38	0.009	0.0010
39	0.008	0.0009
40	0.007	0.0007
41	0.007	0.0009
42	0.006	0.0009

Sample Description: Gates Formation Coal, -4 mesh
Sample Number: C3-2
Reference Number: N/A

Experiment Date: 17/12/96
Sample Cell No: N/A
Temp (°C): 22.0
Mass of Coal (g): 1.436

Moisture(%): 0.0
Ash(%): 13.0

Step Number	**Mean Pore Diameter (μm)**	**Incremental Hg Intrustion (cm3/g, raw coal)**
1	267.154	0.0000
2	190.704	0.0000
3	90.205	0.0000
4	56.781	0.0000
5	41.740	0.0000
6	32.487	0.0000
7	26.294	0.0000
8	21.419	0.0000
9	17.563	0.0000
10	14.551	0.0000
11	12.179	0.0000
12	10.690	0.0000
13	9.748	0.0000
14	8.688	0.0000
15	6.992	0.0000
16	3.884	0.0016
17	1.359	0.0011
18	0.680	0.0010

19	0.376	0.0007
20	0.264	0.0004
21	0.204	0.0004
22	0.151	0.0007
23	0.106	0.0006
24	0.082	0.0005
25	0.067	0.0004
26	0.056	0.0004
27	0.049	0.0003
28	0.043	0.0004
29	0.038	0.0004
30	0.035	0.0004
31	0.032	0.0004
32	0.029	0.0004
33	0.027	0.0004
34	0.025	0.0003
35	0.024	0.0004
36	0.022	0.0004
37	0.021	0.0003
38	0.019	0.0007
39	0.017	0.0012
40	0.014	0.0013
41	0.012	0.0012
42	0.011	0.0013
43	0.010	0.0012
44	0.009	0.0011
45	0.008	0.0012
46	0.007	0.0011
47	0.007	0.0010
48	0.006	0.0009

Sample Description: Gates Formation Coal, -4 mesh
Sample Number: D3-3
Reference Number: N/A

Experiment Date: 2/01/96
Sample Cell No: N/A
Temp (°C): 22.0
Mass of Coal (g): 1.081

Moisture(%): 0.0
Ash(%): 46.1

Step Number	**Mean Pore Diameter (μm)**	**Incremental Hg Intrustion (cm3/g, raw coal)**
1	128.1808	0.0000
2	93.7839	0.0000
3	46.8451	0.0000
4	29.3602	0.0000
5	21.5598	0.0000
6	16.4627	0.0000

7	12.8234	0.0000
8	10.6518	0.0000
9	8.9413	0.0000
10	6.9488	0.0000
11	3.8442	0.0006
12	1.3490	0.0006
13	0.6793	0.0006
14	0.3779	0.0005
15	0.2639	0.0004
16	0.2037	0.0003
17	0.1509	0.0005
18	0.1057	0.0004
19	0.0816	0.0003
20	0.0665	0.0002
21	0.0561	0.0003
22	0.0485	0.0003
23	0.0428	0.0003
24	0.0382	0.0003
25	0.0346	0.0002
26	0.0317	0.0002
27	0.0291	0.0002
28	0.0269	0.0003
29	0.0250	0.0003
30	0.0235	0.0002
31	0.0220	0.0003
32	0.0208	0.0002
33	0.0192	0.0003
34	0.0166	0.0008
35	0.0140	0.0008
36	0.0121	0.0008
37	0.0107	0.0008
38	0.0096	0.0006
39	0.0087	0.0007
40	0.0079	0.0007
41	0.0073	0.0006
42	0.0067	0.0008
43	0.0063	0.0008

References

1. Encyclopedie des Gaz, L'Air Liquide, Elsevier, Amsterdam, 1976

APPENDIX VI - Isotherm Data used in Chapter 5

* Gas compressibility factors calculated using Peng-Robinson Equation of State[1]

HIGH PRESSURE (> 0.101 MPa) METHANE ISOTHERMS-dried coal

Analysis Gas: Methane
Sample Description: Gates Formation Coal, -4 mesh, dried
Sample Number: B2-11
Reference Number: cbm118

Experiment Date:	7/9/96	**Reference Volume (cm^3):**	312.89	**Moisture(%):**	0.0
Sample Cell No:	1	**Void Volume (cm^3):**	85.96	**Ash(%):**	3.7
Temp (°C):	30.0	**Coal Volume (cm^3):**	68.53		
Mass of Coal (g):	92.89	**Coal Density (g/ cm^3):**	1.355		

Step Number	**Equilibrium Cell Pressure (MPa)**	**Volume CH_4 Adsorbed (cm3/g@STP, raw coal)**
1	0.218	4.42
2	0.784	8.79
3	1.723	12.35
4	2.889	15.00
5	3.922	16.58
6	4.941	17.82

Analysis Gas: Methane
Sample Description: Gates Formation Coal, -4 mesh, dried
Sample Number: B2-10
Reference Number: cbm119

Experiment Date:	7/9/96	**Reference Volume (cm^3):**	312.89	**Moisture(%):**	0.0
Sample Cell No:	2	**Void Volume (cm^3):**	113.07	**Ash(%):**	30.3
Temp (°C):	30.0	**Coal Volume (cm^3):**	40.47		
Mass of Coal (g):	73.53	**Coal Density (g/ cm^3):**	1.817		

Step Number	**Equilibrium Cell Pressure (MPa)**	**Volume CH_4 Adsorbed (cm3/g@STP, raw coal)**
1	0.388	3.06
2	1.074	5.24
3	2.043	6.82
4	3.030	7.91
5	4.001	8.75
6	4.936	9.43
7	5.897	9.90
8	6.846	10.39
9	7.843	10.69

HIGH PRESSURE (> 0.101 MPa) METHANE ISOTHERMS (Cont'd)-dried coal

Analysis Gas: Methane
Sample Description: Gates Formation coal, -4 mesh, dried
Sample Number: C3-2
Reference Number: cbm120

Experiment Date: 7/9/96
Sample Cell No: 3
Temp (°C): 30.0
Mass of Coal (g): 77.24
Reference Volume (cm^3): 312.89
Void Volume (cm^3): 112.33
Coal Volume (cm^3): 55.31
Coal Density (g/ cm^3): 1.397
Moisture(%): 0.0
Ash(%): 13.0

Step Number	Equilibrium Cell Pressure (MPa)	Volume CH_4 Adsorbed (cm3/g@STP, raw coal)
1	0.388	3.89
2	1.033	7.01
3	1.895	10.13
4	2.978	11.96
5	3.979	13.77
6	4.981	14.76
7	5.928	15.77

Analysis Gas: Methane
Sample Description: Gates Formation coal, -4 mesh, dried
Sample Number: D3-3
Reference Number: cbm109

Experiment Date: 19/6/96
Sample Cell No: 4
Temp (°C): 30.0
Mass of Coal (g): 90.74
Reference Volume (cm^3): 312.89
Void Volume (cm^3): 102.74
Coal Volume (cm^3): 50.27
Coal Density (g/ cm^3): 1.805
Moisture(%): 0.0
Ash(%): 46.1

Step Number	Equilibrium Cell Pressure (MPa)	Volume CH_4 Adsorbed (cm3/g@STP, raw coal)
1	0.387	2.84
2	0.987	4.61
3	2.055	6.43
4	3.053	7.49
5	4.160	8.34

HIGH PRESSURE (> 0.101 MPa) CARBON DIOXIDE ISOTHERMS-dried coal

Analysis Gas: Carbon Dioxide
Sample Description: Gates Formation Coal, -4 mesh, dried
Sample Number: B2-11
Reference Number: cbm126

Experiment Date:	12/11/96	**Reference Volume (cm^3):**	312.89	**Moisture(%):**	0.0
Sample Cell No:	1	**Void Volume (cm^3):**	86.79	**Ash(%):**	3.7
Temp (°C):	30.0	**Coal Volume (cm^3):**	67.69		
Mass of Coal (g):	91.64	**Coal Density (g/ cm^3):**	1.354		

Step Number	**Equilibrium Cell Pressure (MPa)**	**Volume CO_2 Adsorbed (cm3/g@STP, raw coal)**
1	0.032	4.46
2	0.187	10.37
3	0.591	16.74
4	1.254	21.77
5	2.281	26.44
6	3.432	29.55
7	4.429	31.84
8	5.064	33.38

Analysis Gas: Carbon Dioxide
Sample Description: Gates Formation Coal, -4 mesh, dried
Sample Number: B2-10
Reference Number: cbm127

Experiment Date:	12/11/96	**Reference Volume (cm^3):**	312.89	**Moisture(%):**	0.0
Sample Cell No:	2	**Void Volume (cm^3):**	112.74	**Ash(%):**	30.3
Temp (°C):	30.0	**Coal Volume (cm^3):**	40.80		
Mass of Coal (g):	73.51	**Coal Density (g/ cm^3):**	1.802		

Step Number	**Equilibrium Cell Pressure (MPa)**	**Volume CO_2 Adsorbed (cm3/g@STP, raw coal)**
1	0.155	5.18
2	0.556	8.91
3	1.117	11.47
4	1.650	13.03
5	2.503	14.92
6	3.433	16.53
7	4.367	17.94
8	4.999	18.99

HIGH PRESSURE (> 0.101 MPa) CARBON DIOXIDE ISOTHERMS (Cont'd)-dried coal

Analysis Gas: Carbon Dioxide
Sample Description: Gates Formation Coal, -4 mesh, dried
Sample Number: C3-2
Reference Number: cbm128

Experiment Date: 12/11/96 **Reference Volume (cm^3):** 312.89 **Moisture(%):** 0.0
Sample Cell No: 3 **Void Volume (cm^3):** 112.38 **Ash(%):** 13.0
Temp (°C): 30.0 **Coal Volume (cm^3):** 55.26
Mass of Coal (g): 77.23 **Coal Density (g/ cm^3):** 1.398

Step Number	Equilibrium Cell Pressure (MPa)	Volume CO_2 Adsorbed (cm3/g@STP, raw coal)
1	0.078	4.74
2	0.320	10.51
3	0.854	15.80
4	1.474	19.18
5	2.339	22.32
6	3.342	25.00
7	4.328	27.26
8	4.998	28.35

Analysis Gas: Carbon Dioxide
Sample Description: Gates Formation Coal, -4 mesh, dried
Sample Number: D3-3
Reference Number: cbm129

Experiment Date: 12/9/96 **Reference Volume (cm^3):** 312.89 **Moisture(%):** 0.0
Sample Cell No: 4 **Void Volume (cm^3):** 107.41 **Ash(%):** 46.1
Temp (°C): 30.0 **Coal Volume (cm^3):** 45.60
Mass of Coal (g): 82.26 **Coal Density (g/ cm^3):** 1.804

Step Number	Equilibrium Cell Pressure (MPa)	Volume CO_2 Adsorbed (cm3/g@STP, raw coal)
1	0.107	3.72
2	0.503	7.67
3	1.097	10.26
4	1.700	11.65
5	2.597	13.28

HIGH PRESSURE (> 0.101 MPa) METHANE ISOTHERMS-moisture-equilibrated coal

Analysis Gas: Methane
Sample Description: Gates Formation Coal, -60 mesh, moisture-equilibrated
Sample Number: B2-11
Reference Number: N/A

Experiment Date:	12/9/97	**Reference Volume (cm^3):**	314.17	**Moisture(%):**	N/A
Sample Cell No:	1	**Void Volume (cm^3):**	105.33	**Ash(%):**	3.7
Temp (°C):	30.0	**Coal Volume (cm^3):**	59.46		
Mass of Coal (g):	79.35	**Coal Density (g/ cm^3):**	1.335		

Step Number	Equilibrium Cell Pressure (MPa)	Volume CH_4 Adsorbed (cm3/g@STP, raw coal)
1	5.129	13.53
2	3.026	12.11
3	2.085	10.48
4	1.656	9.63
5	1.334	8.73
6	0.878	7.25
7	0.590	5.94

Analysis Gas: Methane
Sample Description: Gates Formation Coal, -60 mesh, moisture-equilibrated
Sample Number: B2-10
Reference Number: N/A

Experiment Date:	12/9/97	**Reference Volume (cm^3):**	314.17	**Moisture(%):**	N/A
Sample Cell No:	2	**Void Volume (cm^3):**	120.74	**Ash(%):**	30.3
Temp (°C):	30.0	**Coal Volume (cm^3):**	41.98		
Mass of Coal (g):	75.29	**Coal Density (g/ cm^3):**	1.794		

Step Number	Equilibrium Cell Pressure (MPa)	Volume CH_4 Adsorbed (cm3/g@STP, raw coal)
1	5.277	6.97
2	3.353	6.43
3	2.110	5.70
4	1.515	5.27
5	0.975	4.51
6	0.610	3.75
7	0.402	3.17

HIGH PRESSURE (> 0.101 MPa) METHANE ISOTHERMS (Cont'd)-moisture-equilibrated coal

Analysis Gas: Methane
Sample Description: Gates Formation Coal, -60 mesh, moisture-equilibrated
Sample Number: C3-2
Reference Number: N/A

Experiment Date:	12/9/97	**Reference Volume (cm^3):**	314.17	**Moisture(%):**	N/A
Sample Cell No:	3	**Void Volume (cm^3):**	117.87	**Ash(%):**	13.0
Temp (°C):	30.0	**Coal Volume (cm^3):**	50.30		
Mass of Coal (g):	69.98	**Coal Density (g/ cm^3):**	1.391		

Step Number	**Equilibrium Cell Pressure (MPa)**	**Volume CH_4 Adsorbed (cm3/g@STP, raw coal)**
1	4.618	10.20
2	3.269	9.36
3	1.998	8.07
4	1.562	7.44
5	1.082	6.37
6	0.737	5.39
7	0.448	4.26

Analysis Gas: Methane
Sample Description: Gates Formation Coal, -60 mesh, moisture-equilibrated
Sample Number: D3-3
Reference Number: N/A

Experiment Date:	12/9/97	**Reference Volume (cm^3):**	314.17	**Moisture(%):**	N/A
Sample Cell No:	4	**Void Volume (cm^3):**	121.98	**Ash(%):**	46.1
Temp (°C):	30.0	**Coal Volume (cm^3):**	43.07		
Mass of Coal (g):	75.95	**Coal Density (g/ cm^3):**	1.763		

Step Number	**Equilibrium Cell Pressure (MPa)**	**Volume CH_4 Adsorbed (cm3/g@STP, raw coal)**
1	5.065	5.62
2	3.288	5.32
3	1.780	4.61
4	1.403	4.51
5	0.988	4.01
6	0.601	3.49
7	0.353	2.93

HIGH PRESSURE (> 0.101 MPa) CARBON DIOXIDE ISOTHERMS-moisture-equilibrated coal

Analysis Gas: Carbon Dioxide
Sample Description: Gates Formation Coal, -60 mesh, moisture-equilibrated
Sample Number: B2-11
Reference Number: N/A

Experiment Date:	16/10/97	**Reference Volume (cm^3):**	314.17	**Moisture(%):**	2.7
Sample Cell No:	1	**Void Volume (cm^3):**	107.77	**Ash(%):**	3.7
Temp (°C):	30.0	**Coal Volume (cm^3):**	57.02		
Mass of Coal (g):	76.71	**Coal Density (g/ cm^3):**	1.345		

Step Number	**Equilibrium Cell Pressure (MPa)**	**Volume CO_2 Adsorbed (cm3/g@STP, raw coal)**
1	2.981	22.92
2	2.099	20.70
3	1.494	18.49
4	1.120	16.59
5	0.807	14.55
6	0.590	12.66
7	0.476	11.46

Analysis Gas: Carbon Dioxide
Sample Description: Gates Formation Coal, -60 mesh, moisture-equilibrated
Sample Number: B2-10
Reference Number: N/A

Experiment Date:	16/10/97	**Reference Volume (cm^3):**	314.17	**Moisture(%):**	1.6
Sample Cell No:	2	**Void Volume (cm^3):**	121.82	**Ash(%):**	30.3
Temp (°C):	30.0	**Coal Volume (cm^3):**	40.90		
Mass of Coal (g):	72.88	**Coal Density (g/ cm^3):**	1.782		

Step Number	**Equilibrium Cell Pressure (MPa)**	**Volume CO_2 Adsorbed (cm3/g@STP, raw coal)**
1	3.574	13.36
2	2.437	12.40
3	1.648	11.04
4	1.135	9.69
5	0.762	8.28
6	0.527	7.00
7	0.416	6.31

HIGH PRESSURE (> 0.101 MPa) CARBON DIOXIDE ISOTHERMS (Cont'd)-moisture-equilibrated coal

Analysis Gas: Carbon Dioxide
Sample Description: Gates Formation Coal, -60 mesh, moisture-equilibrated
Sample Number: C3-2
Reference Number: N/A

Experiment Date: 16/10/97 **Reference Volume (cm^3):** 314.17 **Moisture(%):** 2.4
Sample Cell No: 3 **Void Volume (cm^3):** 120.07 **Ash(%):** 13.0
Temp (°C): 30.0 **Coal Volume (cm^3):** 48.10
Mass of Coal (g): 67.08 **Coal Density (g/ cm^3):** 1.395

Step Number	Equilibrium Cell Pressure (MPa)	Volume CO_2 Adsorbed (cm3/g@STP, raw coal)
1	2.525	18.25
2	1.835	16.44
3	1.376	14.77
4	1.038	13.18
5	0.749	11.41
6	0.590	10.14
7	0.424	8.60

Analysis Gas: Carbon Dioxide
Sample Description: Gates Formation Coal, -60 mesh, moisture-equilibrated
Sample Number: D3-3
Reference Number: N/A

Experiment Date: 16/10/97 **Reference Volume (cm^3):** 314.17 **Moisture(%):** 1.4
Sample Cell No: 4 **Void Volume (cm^3):** 122.69 **Ash(%):** 46.1
Temp (°C): 30.0 **Coal Volume (cm^3):** 42.36
Mass of Coal (g): 74.37 **Coal Density (g/ cm^3):** 1.756

Step Number	Equilibrium Cell Pressure (MPa)	Volume CO_2 Adsorbed (cm3/g@STP, raw coal)
1	2.766	9.88
2	2.035	9.12
3	1.416	8.12
4	1.003	7.18
5	0.675	6.11
6	0.487	5.26
7	0.383	4.70

HIGH PRESSURE (> 0.101 MPa) BINARY GAS ISOTHERMS -moisture-equilibrated coal

Analysis Gas: 90% CH_4/10% CO_2
Sample Description: Gates Formation Coal, -60 mesh, moisture-equilibrated
Sample Number: B2-11
Reference Number: N/A

Experiment Date: 3/11/97
Sample Cell No: 1
Temp (°C): 30.0
Mass of Coal (g): 74.56
Reference Volume (cm^3): 314.17
Void Volume (cm^3): 109.10
Coal Volume (cm^3): 55.68
Coal Density (g/ cm^3): 1.339
Moisture(%): 2.4
Ash(%): 3.7

Step Number	Equilibrium Cell Pressure (MPa)	Gas Phase Equilbrium Mole Fraction CH_4	Vol CH_4 Adsorbed (cm3/g@STP)	Vol CH_4 Adsorbed (cm3/g@STP
1	5.116	0.929	11.96	3.64
2	2.648	0.923	9.94	3.26
3	1.893	0.918	8.82	3.02
4	1.291	0.910	7.74	2.79
5	0.893	0.900	6.72	2.55
6	0.586	0.892	5.59	2.35

Analysis Gas: 90% CH_4/10% CO_2
Sample Description: Gates Formation Coal, -60 mesh, moisture-equilibrated
Sample Number: B2-10
Reference Number: N/A

Experiment Date: 3/11/97
Sample Cell No: 2
Temp (°C): 30.0
Mass of Coal (g): 70.21
Reference Volume (cm^3): 314.17
Void Volume (cm^3): 123.68
Coal Volume (cm^3): 39.04
Coal Density (g/ cm^3): 1.798
Moisture(%): 1.4
Ash(%): 30.3

Step Number	Equilibrium Cell Pressure (MPa)	Gas Phase Equilbrium Mole Fraction CH_4	Vol CH_4 Adsorbed (cm3/g@STP)	Vol CH_4 Adsorbed (cm3/g@STP
1	5.503	0.918	6.12	2.53
2	3.279	0.915	5.82	2.34
3	1.907	0.909	5.15	2.07
4	1.051	0.897	4.34	1.77
5	0.521	0.877	3.46	1.49
6	0.292	0.852	2.92	1.27

HIGH PRESSURE (> 0.101 MPa) BINARY GAS ISOTHERMS (Cont'd)-moisture-equilibrated coal

Analysis Gas: 90% CH_4/10% CO_2
Sample Description: Gates Formation Coal, -60 mesh, moisture-equilibrated
Sample Number: C3-2
Reference Number: N/A

Experiment Date: 3/11/97 **Reference Volume (cm^3):** 314.17 **Moisture(%):** 2.0
Sample Cell No: 3 **Void Volume (cm^3):** 122.04 **Ash(%):** 13.0
Temp (°C): 30.0 **Coal Volume (cm^3):** 46.13
Mass of Coal (g): 64.51 **Coal Density (g/ cm^3):** 1.399

Step Number	Equilibrium Cell Pressure (MPa)	Gas Phase Equilbrium Mole Fraction CH_4	Vol CH_4 Adsorbed (cm3/g@STP)	Vol CH_4 Adsorbed (cm3/g@STP
1	5.054	0.922	9.07	3.29
2	2.465	0.916	8.57	2.96
3	1.717	0.910	7.90	2.71
4	1.038	0.898	6.83	2.38
5	0.610	0.879	5.84	2.04
6	0.316	0.851	4.83	1.73

Analysis Gas: 90% CH_4/10% CO_2
Sample Description: Gates Formation Coal, -60 mesh, moisture-equilibrated
Sample Number: D3-3
Reference Number: N/A

Experiment Date: 3/11/97 **Reference Volume (cm^3):** 314.17 **Moisture(%):** 1.2
Sample Cell No: 4 **Void Volume (cm^3):** 124.26 **Ash(%):** 46.1
Temp (°C): 30.0 **Coal Volume (cm^3):** 40.78
Mass of Coal (g): 71.55 **Coal Density (g/ cm^3):** 1.754

Step Number	Equilibrium Cell Pressure (MPa)	Gas Phase Equilbrium Mole Fraction CH_4	Vol CH_4 Adsorbed (cm3/g@STP)	Vol CH_4 Adsorbed (cm3/g@STP
1	5.304	0.916	5.17	2.13
2	3.319	0.914	5.01	1.98
3	2.257	0.910	4.78	1.83
4	1.255	0.901	4.22	1.58
5	0.690	0.888	3.63	1.35
6	0.368	0.871	3.04	1.17

HIGH PRESSURE (> 0.101 MPa) BINARY GAS ISOTHERMS -moisture-equilibrated coal

Analysis Gas: 75% CH_4/25% CO_2
Sample Description: Gates Formation Coal, -60 mesh, moisture-equilibrated
Sample Number: B2-11
Reference Number: N/A

Experiment Date: 8/12/97 **Reference Volume (cm^3):** 314.17 **Moisture(%):** 1.9
Sample Cell No: 1 **Void Volume (cm^3):** 109.51 **Ash(%):** 3.7
Temp (°C): 30.0 **Coal Volume (cm^3):** 55.27
Mass of Coal (g): 73.87 **Coal Density (g/ cm^3):** 1.336

Step Number	Equilibrium Cell Pressure (MPa)	Gas Phase Equilbrium Mole Fraction CH_4	Vol CH_4 Adsorbed (cm3/g@STP)	Vol CH_4 Adsorbed (cm3/g@STP
1	4.395	0.834	7.704	9.565
2	3.018	0.826	6.804	8.975
3	1.754	0.804	5.491	8.066
4	0.998	0.758	4.286	7.007
5	0.480	0.665	2.836	5.766

Analysis Gas: 75% CH_4/25% CO_2
Sample Description: Gates Formation Coal, -60 mesh, moisture-equilibrated
Sample Number: B2-10
Reference Number: N/A

Experiment Date: 8/12/97 **Reference Volume (cm^3):** 314.17 **Moisture(%):** 1.1
Sample Cell No: 2 **Void Volume (cm^3):** 123.91 **Ash(%):** 30.3
Temp (°C): 30.0 **Coal Volume (cm^3):** 38.81
Mass of Coal (g): 70.00 **Coal Density (g/ cm^3):** 1.804

Step Number	Equilibrium Cell Pressure (MPa)	Gas Phase Equilbrium Mole Fraction CH_4	Vol CH_4 Adsorbed (cm3/g@STP)	Vol CH_4 Adsorbed (cm3/g@STP
1	5.402	0.795	3.44	6.76
2	3.180	0.791	3.07	6.41
3	1.642	0.768	2.58	5.49
4	0.790	0.719	2.01	4.52
5	0.334	0.605	1.43	3.46

HIGH PRESSURE (> 0.101 MPa) BINARY GAS ISOTHERMS (Cont'd)-moisture-equilibrated coal

Analysis Gas: 75% CH_4/25% CO_2
Sample Description: Gates Formation Coal, -60 mesh, moisture-equilibrated
Sample Number: C3-2
Reference Number: N/A

Experiment Date: 8/12/97 **Reference Volume (cm^3):** 314.17 **Moisture(%):** 1.8
Sample Cell No: 3 **Void Volume (cm^3):** 121.99 **Ash(%):** 13.0
Temp (°C): 30.0 **Coal Volume (cm^3):** 46.18
Mass of Coal (g): 64.10 **Coal Density (g/ cm^3):** 1.388

Step Number	Equilibrium Cell Pressure (MPa)	Gas Phase Equilbrium Mole Fraction CH_4	Vol CH_4 Adsorbed (cm3/g@STP)	Vol CH_4 Adsorbed (cm3/g@STP
1	5.266	0.811	5.61	9.84
2	3.100	0.799	4.92	8.89
3	1.611	0.770	3.86	7.59
4	0.863	0.719	3.01	6.35
5	0.388	0.602	2.18	4.95

Analysis Gas: 75% CH_4/25% CO_2
Sample Description: Gates Formation Coal, -60 mesh, moisture-equilibrated
Sample Number: D3-3
Reference Number: N/A

Experiment Date: 8/12/97 **Reference Volume (cm^3):** 314.17 **Moisture(%):** 1.3
Sample Cell No: 4 **Void Volume (cm^3):** 124.77 **Ash(%):** 46.1
Temp (°C): 30.0 **Coal Volume (cm^3):** 40.28
Mass of Coal (g): 71.31 **Coal Density (g/ cm^3):** 1.771

Step Number	Equilibrium Cell Pressure (MPa)	Gas Phase Equilbrium Mole Fraction CH_4	Vol CH_4 Adsorbed (cm3/g@STP)	Vol CH_4 Adsorbed (cm3/g@STP
1	5.583	0.790	2.73	6.09
2	3.615	0.785	2.88	5.72
3	1.820	0.769	2.55	5.03
4	0.898	0.730	2.17	4.20
5	0.353	0.625	1.69	3.23

References

1. Peng, D-Y., and Robinson, D.B. *Ind. Eng. Chem. Fundam.* 1976, **15**, 59

APPENDIX VII - Discretization of macropore and micropore transport equations and solution procedure

Discretization of Macropore Transport Equation

The (dimensionless) macropore transport equation is:

$$\frac{1}{\eta^2}\frac{\partial}{\partial\eta}\left(\eta^2\frac{\partial\rho_{Da}}{\partial\eta}\right)=\frac{\partial\rho_{Da}}{\partial\tau}+\beta\frac{\partial\rho_{Di}}{\partial\gamma}\Big|\gamma=1 \qquad (1)$$

Equation (1) may be written in the following generalized form:

$$\nabla\bullet q+-\frac{\partial\rho_{Da}}{\partial\tau}-g_i=0$$

where q is the (dimensionless) flux of gas in the macroporosity, and g_i is the macropore to microporous matrix mass flow rate. Following the integrated finite difference approach[1], this equation may be spatially integrated over a small subregion of the macrosphere domain:

$$\int_V(\nabla\bullet q)dV+-\frac{\partial}{\partial\tau}\int_V\rho_{Da}dV-\int_V g_i dV=0 \qquad (2)$$

In the current problem, the finite subvolume is a spherical shell within the macrosphere. In addition, we have assumed a spherically symmetrical system. The spherical volume element is:

$$dV=\eta^2 d\eta d\theta\sin\Phi d\Phi$$

where η is the radial coordinate, θ is the azimuth angle, and Φ is the angle of elevation. Substituting the divergence term (radial coordinates) from left hand side of equation (1) and the definition of the spherical volume element into (2):

$$\int_V\frac{1}{\eta^2}\frac{\partial}{\partial\eta}\left(\eta^2\frac{\partial\rho_{Da}}{\partial\gamma}\right)\eta^2 d\eta d\theta\sin\Phi d\Phi+-\frac{\partial}{\partial\tau}\int_V\rho_{Da}\eta^2 d\eta d\theta\sin\Phi d\Phi+-\int_V g_i d\eta d\theta\sin\Phi d\Phi=0$$

The discretization volume is an interior spherical subshell extending from $\eta_{I-1/2}$ to $\eta_{I+1/2}$ centered on node I. Equation (3) thus becomes:

$$\int_0^{\pi}\int_0^{2\pi}\int_{\eta_{I-1/2}}^{\eta_{I+1/2}} \frac{1}{\eta^2}\frac{\partial}{\partial\eta}\left(\eta^2\frac{\partial\rho_{Da}}{\partial\eta}\right)\eta^2 d\eta d\theta \sin\Phi d\Phi + -\frac{\partial}{\partial\tau}\int_0^{\pi}\int_0^{2\pi}\int_{\eta_{I-1/2}}^{\eta_{I+1/2}}\rho_{Da}\eta^2 d\eta d\theta\sin\Phi d\Phi +$$

$$-\int_0^{\pi}\int_0^{2\pi}\int_{\eta_{I-1/2}}^{\eta_{I+1/2}} g_i \eta^2 d\eta d\theta \sin\Phi d\Phi = 0$$

Carrying out the integrations:

$$4\pi\eta_{I+1/2}^2\left[\frac{\partial\rho_{Da}}{\partial\eta}\Big|_{Ii+1/2}\right] - 4\pi\eta_{I-1/2}^2\left[\frac{\partial\rho_{Da}}{\partial\eta}\Big|_{I-1/2}\right] - \frac{4}{3}\pi\left[\eta_{I+1/2}^3 - \eta_{I-1/2}^3\right]\frac{\partial\rho_{Da}}{\partial\tau}$$
$$-\frac{4}{3}\pi\left[\eta_{I+1/2}^3 - \eta_{I-1/2}^3\right]g_i = 0 \qquad (4)$$

The spatial derivatives may be approximated by 2nd order central differences, and the time derivative may be approximated by a backward difference. In addition we may define geometric term (G) at the $\eta_{I-1/2}$ and $\eta_{I+1/2}$ spherical interface and the discretized subshell volume as:

$$G(I-1/2) = 4\pi\eta_{I-1/2}^2 / (\eta_I - \eta_{I-1})$$
$$G(I+1/2) = 4\pi\eta_{I+1/2}^2 / (\eta_{I+1} - \eta_I)$$
$$Vol(I) = \frac{4}{3}\pi\left[\eta_{I+1/2}^3 - \eta_{I-1/2}^3\right]$$

Substituting these definitions into equation (4) yields the discretized form of equation (1) for the Ith interior spherical element:

$$G(I+1/2)(\rho_{DaI+1} - \rho_{DaI}) - G(I-1/2)(\rho_{DaI} - \rho_{DaI-1}) - Vol(I)\frac{\rho_{DaI} - \rho_{DaI}^{\vee}}{\Delta\tau}$$
$$-Vol(I)g_i = 0 \qquad (5)$$

$$-\Delta\tau\, G(I+1/2)(\rho_{DaI+1} - \rho_{DaI}) + \Delta\tau\, G(I-1/2)(\rho_{DaI} - \rho_{DaI-1}) + \Delta\tau\, Vol(I)gi$$
$$+Vol(I)\rho_{DaI} = Vol(I)\,\rho_{DaI}^{\vee}$$

where superscript $\vee$ refers to the previous timestep.

Equation (5) may be reduced to the following form:

$$A_{I-1}\rho_{DaI-1} + B_I\rho_{DaI} + C_{I+1}\rho_{DaI+1} = \rho_{DaI}^{\vee} - \Delta\tau g_i \qquad (6)$$

Discretization of Micropore Transport Equation

The (dimensionless) micropore transport equation is:

$$\frac{\alpha}{\gamma^2}\frac{\partial}{\partial\gamma}\left(\gamma^2\frac{\partial\rho_{Di}}{\partial\gamma}\right) = \frac{\partial}{\partial\tau}\left(\rho_{Di} + \frac{C_s}{\rho_o\phi_i}\right) \qquad (7)$$

or $$\frac{\alpha}{\gamma^2}\frac{\partial}{\partial\gamma}\left(\gamma^2\frac{\partial\rho_{Di}}{\partial\gamma}\right) = \frac{\partial\Theta}{\partial\tau}$$

where $\Theta = \rho_{Di} + \dfrac{C_S}{\rho_o\phi_i}$

Equation (7) may be written in the following generalized form:

$$\nabla \bullet q + -\frac{\partial\Theta}{\partial\tau} = 0$$

where q is the (dimensionless) flux of gas in the microporosity. Applying the integrated finite difference approach, this equation may be spatially integrated over a small subregion of the microsphere domain:

$$\int_V (\nabla \bullet q)dV + -\frac{\partial}{\partial\tau}\int_V \Theta dV = 0 \qquad (8)$$

In the current problem, the finite subvolume is a spherical shell within the microsphere. In addition, we have assumed a spherically symmetrical system. The spherical volume element is:

$$dV = \gamma^2 d\gamma\, d\theta \sin\Phi d\Phi$$

where γ is the radial coordinate, θ is the azimuth angle, and Φ is the angle of elevation. Substituting the divergence term (radial coordinates) from left hand side of equation (7) and the definition of the spherical volume element into (8):

$$\int_V \frac{\alpha}{\gamma^2}\frac{\partial}{\partial\gamma}\left(\gamma^2\frac{\partial\rho_{Di}}{\partial\gamma}\right)\gamma^2 d\gamma\, d\theta\sin\Phi d\Phi + -\frac{\partial}{\partial\tau}\int_V \Theta\gamma^2 d\gamma\, d\theta\sin\Phi d\Phi = 0 \qquad (9)$$

The discretization volume is an interior spherical subshell extending from $\gamma_{I-1/2}$ to $\gamma_{I+1/2}$ centered on node I. Equation (9) thus becomes:

$$\int_0^{\pi}\int_0^{2\pi}\int_{\gamma_{I-1/2}}^{\gamma_{I+1/2}} \frac{\alpha}{\gamma^2}\frac{\partial}{\partial\gamma}\left(\gamma^2\frac{\partial\rho_{Di}}{\partial\gamma}\right)\gamma^2 d\gamma\, d\theta\sin\Phi d\Phi + -\frac{\partial}{\partial\tau}\int_0^{\pi}\int_0^{2\pi}\int_{\gamma_{I-1/2}}^{\gamma_{I+1/2}} \Theta\gamma^2 d\gamma\, d\theta\sin\Phi d\Phi = 0$$

Carrying out the integrations and assuming a constant α:

$$\alpha 4\pi\gamma_{I+1/2}^2\left[\frac{\partial\rho_{Di}}{\partial\gamma}\Big|_{I+1/2}\right] - \alpha 4\pi\gamma_{I-1/2}^2\left[\frac{\partial\rho_{Di}}{\partial\gamma}\Big|_{I-1/2}\right] - \frac{4}{3}\pi\left[\gamma_{I+1/2}^3 - \gamma_{I-1/2}^3\right]\frac{\partial\Theta}{\partial\tau} = 0 \qquad (10)$$

The spatial derivatives may be approximated by 2nd order central differences, and the time derivative may be approximated by a backward difference. In addition we may define a geometric term (G) at the $\gamma_{I-1/2}$ and $\gamma_{I+1/2}$ spherical interface and the discretized subshell volume as:

$$\text{G(I-1/2)} = 4\pi\gamma_{I-1/2}^2\,\alpha/(\gamma_I - \gamma_{I-1})$$
$$\text{G(I+1/2)} = 4\pi\gamma_{I+1/2}^2\,\alpha/(\gamma_{I+1} - \gamma_I)$$
$$\text{Vol(I)} = \frac{4}{3}\pi\left[\gamma_{I+1/2}^3 - \gamma_{I-1/2}^3\right]$$

Substituting these definitions into equation (10) yields the discretized form of equation (7) for the ith interior spherical element:

$$\text{G(I+1/2)}(\rho_{DiI+1} - \rho_{DiI}) - \text{G(I-1/2)}(\rho_{DiI} - \rho_{DiI-1}) + \text{Vol(I)}\frac{\Theta_I - \Theta_I^{\vee}}{\Delta\tau} = 0 \qquad (11)$$

$$\Delta\tau\,\text{G(I+1/2)}(\rho_{DiI+1} - \rho_{DiI}) - \Delta\tau\,\text{G(I-1/2)}(\rho_{DiI} - \rho_{DiI-1}) + \text{Vol(I)}\Theta_I = \text{Vol(I)}\,\Theta_I^{\vee}$$

where superscript $\vee$ refers to the previous timestep.

Equation (11) may be reduced to the following form:

$$A_{I-1}\rho_{DiI-1} + B_I\rho_{DiI} + C_{I+1}\rho_{DiI+1} + \Theta_I = \Theta_I^{\vee} \qquad (12)$$

Linearization of Discretized Equations and Solution Procedure

If the non-linear Langmuir isotherm equation is used in the dimensionless storage term Θ_I in equations of the form (12), the resulting equations are non-linear in form. The Newton-Raphson technique is used to linearize the equations. The solution of the micropore transport equation, using the example of equation (12) for the Ith node, is as follows:

1) At each new iteration (ν+1) the approximations $\rho_{Di}^{(\nu+1)} = \rho_{Di}^{(\nu)} + \Delta\rho_{Di}^{(\nu)}$ and $\Theta(\rho_{Di}^{(\nu)}) + \dfrac{\partial\Theta(\rho_{Di}^{(\nu)})}{\partial\rho_{Di}}\Delta\rho_{Di}^{(\nu)}$ are substituted into equations of the form (12).

2) The resulting equations are of the form:
$$A_{I-1}\Delta\rho_{DiI-1}^{(\nu)} + \left\{B_I + \Theta'(\rho_{DiI}^{(\nu)})\right\}\Delta\rho_{DiI}^{(\nu)} + C_{I+1}\Delta\rho_{DiI+1}^{(\nu)} =$$
$$\Theta_I^{\nu} - \left\{\Theta_I^{(\nu)} + A_{I-1}\rho_{DiI-1}^{(\nu)} + B_I\rho_{DiI}^{(\nu)} + C_{I+1}\rho_{DiI+1}^{(\nu)}\right\}$$
or: $$A_{I-1}\Delta\rho_{DiI-1}^{(\nu)} + \left\{B_I + \Theta'(\rho_{DiI}^{(\nu)})\right\}\Delta\rho_{DiI}^{(\nu)} + C_{I+1}\Delta\rho_{DiI+1}^{(\nu)} = R_I$$

where R_I is the residual

3) The resulting set of linearized equations, with the coefficients forming a tridiagonal matrix, are solved using a direct solver routine. The resulting $\Delta\rho_{DiI}$ are then used in the latest approximation to ρ_{DiI}.

4) The above procedures are repeated until the residuals of the equations in procedure 2) are minimized.

References

1. Narasimhan, T.N., and Witherspoon, P.A. *Water Resour. Res.* 1976, **12**, 57

APPENDIX VIII - Model Verification

The numerical solution to equations (23)-(27) and (15)-(22) of Chapter 4, the unipore and bidisperse models, respectively, were verified through comparison with several available analytical solutions.

Unipore Model

The numerical unipore model solution was compared to the following analytical solution for diffusion in a sphere, subject to variable surface concentration (ϕ)[1]:

$$\frac{C}{C_o} = 1 - \frac{a}{r}\exp(-\beta t)\frac{\sin\left\{(\beta a^2/D)^{1/2} r/a\right\}}{\sin\left\{\beta a^2/D\right\}^{1/2}} - \frac{2\beta a^3}{\pi D r}\sum_{n=1}^{\infty}(-1)^n \frac{\exp(-Dn^2\pi^2 t/a^2)}{n(n^2\pi^2 - \beta a^2/D)}\sin\frac{n\pi r}{a}$$

where:

$$\phi(t) = C_o\left\{1 - \exp(-\beta t)\right\}$$

The initial concentration C_o of a sphere of radius a is assumed to be zero. The infinite series in the above equation was converged using procedures described in Press *et al.*[2] The solution was programmed in FORTRAN 77. The numerical and analytical solutions were compared for various values of $\beta a^2/D$ and C/C_o. Agreement between numerical and analytical solutions in all cases is excellent.

Bidisperse Model

The bidisperse model was compared to the analytical solution for macrosphere fluid phase concentration presented in Ruckenstein *et al.*[3] (equation 11):

$$\theta_a = 1 + \frac{4\pi}{\eta\beta}\sum_{k=1}^{\infty}\sum_{q=1}^{\infty}\frac{(-1)^k k \sin(k\pi\eta)\exp\left[-\alpha\xi_{qk}^2\tau\right]}{\xi_{qk}^2\left[\frac{\alpha}{\beta} + 1 + \cot^2\xi_{qk} - \left(1 - \frac{k^2\pi^2}{\beta}\right)\frac{1}{\xi_{qk}^2}\right]}$$

where ξ_{qk} are the roots of the transcendental equation

$$\beta\left(1 - \xi_{qk}\cot\xi_{qk}\right) + \alpha\xi_{qk}^2 = k^2\pi^2; \quad k = 1,2,3,\ldots,\infty.$$

$\theta_a = (C_a - C_{ao})/(C_{a\infty} - C_{ao})$, dimensionless macropore concentration,

$\alpha = \frac{R_a^2 D_i}{D_a R_i^2}$, dimensionless parameter

$\beta = \frac{3(1-\phi_a)\phi_i}{\phi_a} \frac{R_a^2 D_i}{D_a R_i^2}$, dimensionless parameter

$\tau = \frac{D_a t}{R_a^2}$, dimensionless time

ϕ = porosity

$\eta = \frac{r_a}{R_a}$, dimensionless macrosphere radial position

The analytical solution was programmed in FORTRAN and the roots of the transcendental equation were determined using the Bisection Method algorithm provided in 'Numerical Recipes in FORTRAN'[2]. The numerical and analytical solutions were compared for various values of α, α/β, and η. Agreement between the numerical and analytical solutions in all cases is good.

References

1. Crank, J. 'Mathematics of Diffusion', Oxford Press, London, 1975

2. Press, W.H., Teukolsky, S.A., Vettering, W.T., and Flannery, B.P. 'Numerical Recipes in FORTRAN: The Art of Scientific Computing', second edition, Cambridge University Press, Cambridge, 1994

3. Ruckenstein, E., Vaidyanathan, A.S., and Youngquist, G.R. *Chem. Eng. Sci.* 1971, 1305